UNIVERSITÁ DEGLI STUDI DI PADOVA

Dipartimento di Biologia

SCUOLA DI DOTTORATO DI RICERCA IN BIOSCIENZE E BIOTECNOLOGIE

INDIRIZZO BIOCHIMICA E BIOFISICA

CICLO XXV

Functional characterization of *At*TPK3 potassium channel of *Arabidopsis thaliana*

Direttore della Scuola: Ch.mo Prof. Giuseppe Zanotti

Coordinatore d'indirizzo: Ch.ma Prof.ssa Catia Sorgato

Supervisore: Ch.ma Prof.ssa Ildikò Szabò

Dottorando: Luca Carraretto

TABLE OF CONTENTS

DESCRIZIONE RIASSUNTIVA ED INTRODUZIONE AL PROGETTO DI DOTTORATO

Versione in italiano

Il mio progetto di dottorato si è focalizzato sulla caratterizzazione, dal punto di vista biochimico ed elettrofisiologico, di una proteina denominata TPK3 che è predetta di funzionare come canale selettiva per il potassio (K^+) ed essere localizzata nei cloroplasti nelle piante superiori,. Questa proteina appartiene alla famiglia dei canali TPK (da ***T**andem-**P**ore **K**$^+$ channels*) e mostra omologia di sequenza a un altro canale del K^+ studiato nello stesso nostro laboratorio, denominato *Syn*K (Zanetti *et al*., 2010), a localizzazione tilacoidale ed appartenente al *phylum* dei Cianobatteri. È stato dimostrato in più esperimenti che il canale *Syn*K è fondamentale per la regolazione della fotosintesi nei Cianobatteri, in considerazione del fenotipo fotosensibile mostrato dai mutanti per il gene *synk*. Visto la localizzazione predetta del TPK3, è stato ipotizzato in partenza che TPK3 potesse svolgere un ruolo simile nelle piante superiori. Finora nulla si conosceva sulle proprietà di TPK3, ne sui suoi ruoli fisiologici, ne su di un suo eventuale coinvolgimento nella fotosintesi nelle piante superiori; il lavoro contenuto nel progetto presentato ha cercato di chiarire alcuni aspetti salienti delle funzioni di TPK3.
Dopo studi di localizzazione subcellulare condotti con tecniche di biochimica e microscopia confocale, il canale TPK3 è stato espresso in *E. coli* per la successiva caratterizzazione elettrofisiologica in *bilayer* lipidico planare allo scopo di determinare la sua funzione come canale di K^+. L'assenza di mutanti commerciali per il gene *tpk3* ha necessitato la messa a punto del suo silenziamento tramite RNA *interference* del messaggero per la proteina suddetta, al fine di analizzarne i possibili ruoli fisiologici. Le piante silenziate risultanti, sottoposte a differenti condizioni di crescita, sono state studiate in vari esperimenti atti a determinarne vari parametri inclusi quelli fotosintetici.
Contemporaneamente allo studio del TPK3, quello di maggior rilievo nel mio dottorato, ho seguito anche altri due filoni di ricerca principali, riguardanti l'uno l'approfondimento delle funzioni di due membri dei Recettori di Glutammato vegetali (GluRs) e l'altro la caratterizzazione degli omologhi del recentemente identificato MCU (***M**itochondrial **C**alcium **U**niporter*) di Mammiferi. Nella presente tesi è inoltre incluso un manoscritto (Checchetto *et al*., 2012) per il quale ho collaborato nell'espressione eterologa del canale di K^+ calcio-dipendente (*Syn*CaK*)* di Cianobatteri.

English version

My Ph.D. project has focused on the characterization of TPK3, a putative channel selective for potassium (K^+) with a predicted chloroplast localization in higher plants, from biochemical, physiological and electrophysiological point of view. This protein belongs to the TPK channel family (from **T**andem-**P**ore **K**$^+$ channels) and displays amino acid sequence homology with another K^+ channel studied in our laboratory, called *Syn*K (Zanetti *et al*., 2010). *Syn*K shows thylakoid localization in Cyanobacteria. The *SynK* channel has been shown to be critical for photosynthetic performances in Cyanobacteria, given the photosensitive phenotype displayed by the mutants lacking the *Syn*K protein. Given the homology, we hypothesized that similarly, TPK3 might be involved in the regulation of photosynthetic processes in higher plants. So far, no information is available about the properties of TPK3, nor about its physiological roles, neither about its possible involvement in photosynthesis; the work presented in this thesis had the aim of clarifying some important aspects of the functions of TPK3.
Following subcellular localization studies carried out using biochemistry and confocal microscopy techniques, the TPK3 channel was expressed in *E. coli* cells for subsequent electrophysiological characterization in a planar lipid bilayer setup in order to prove its function as K^+ channel. The

unavailability of commercial mutants for *tpk3* gene required setting up of a silencing procedure *via* RNA interference of the messenger for the protein, in order to analyze the possible physiological roles of TPK3. The resulting silenced plants have been studied under different growth conditions to determine changes in physiology of the plants including their photosynthetic parameters.
In parallel with the TPK3 project, the most important part of my Ph.D., I also followed two other major areas of research: one concerning the study of the functions of two members of plant Glutamate Receptors (GluRs) and the other one concerning the characterization of the plant homologous of the recently identified MCU (**M**itochondrial **C**alcium **U**niporter) of mammals. This thesis also includes a manuscript (Checchetto *et al*., 2012) to which I contributed with the heterologous expression of a calcium-activated K^+ channel, *Syn*CaK, of Cyanobacteria.

Section 1

1. INTRODUCTION

The first ion channels have been studied and consequently to be the best known are those in connection with the nervous system, especially those involved in the generation and propagation of action potentials. However, now ion channels are also known to be involved in secretion, endocytosis, muscle contraction, synaptic transmission, ciliary control and fertilization. Ion channels have been found in Bacteria, Archaea and Eukaryotes, indicating deep evolutionary roots. For technical and historical reasons, studied channels are mainly those of the animal kingdom and prokaryotic ones. In this work will be discussed the characteristics of *At*TPK ion channels, glutamate receptors (*At*GluRs) and MCU channels (that are calcium channels) identified in higher plants (using *Arabidopsis thaliana* as a reference model). In particular, will be presented in detail *At*TPK3, that is a channel selective for potassium and is considered the hypothetical counterpart of another channel located in the chloroplast of Cyanobacteria. It becomes necessary a brief introduction of the potassium homeostasis and the regulation of its transport into cells, in particular of prokaryotic and plant cells. So we will outline the photosynthetic process and the importance of ion channels in the regulation of photosynthesis. For *At*GluRs and MCU, which characterization is still a work in progress, will be presented only general features.

1.1 The homeostasis of potassium (K^+) in cells

1.1.1 The K^+ ion and the electrochemical gradient

Potassium (K^+) is the most abundant ion present in the cytosol of the cells. *Escherichia coli*, for example, has a concentration of about 200 mM K^+ internal, while the standard growth medium for these bacteria (Luria-Bertani) contains K^+ at a concentration of about 7 mM (Kuo *et al*., 2003). This so high internal concentration is maintained even when the bacteria are grown in a minimal medium, containing submolar concentrations of K^+ (Schulz and Solomon, 1961). The enzymatic and metabolic processes of the cell are generally better adapted to such high internal concentrations. Unlike other cations, these concentrations of K^+ does not interfere with the structures and reactions of macromolecules such as DNA, RNA and proteins in aqueous solutions. The consequence of this abundance of K^+ and its counterions (glutamate, organic phosphates, etc.) is that it serves as the main osmolar component inside the cell. This and other neutral molecules, such as glycine and betaine, favor the entry of water through the lipid bilayer in the cytoplasm, in order to maintain the cell turgor that is necessary for the destruction of existing structures, so the material of new synthesis can be added during the growth. Because of this critical role, it is believed that has been evolved a feedback mechanism to adjust the internal concentration of K^+, depending on the total external osmolarity. The K^+ content in *E. coli* cells, for example, increases in a linear fashion from 200 to 1000 mM when the external osmolarity increases from 100 to 1200 mOsm (Epstein, 2003; Bakker, 1993). The lipid bilayer of membranes maintains the difference in K^+ concentration and the potential difference between the inside and the outside. The electrochemical gradient of K^+ through the membrane, expressed in terms of energy, is:

$$\Delta\mu K^+ = F\Delta\psi + RT \cdot \ln [K^+]_{in}/[K^+]_{out}$$

where $\Delta\psi$ is the membrane potential (for example, the electric potential of the cytoplasm respect to the external environment), F is the Faraday's constant, R is the gas constant and T is the absolute temperature. As we saw earlier, the inner concentration of K^+ ($[K^+]_{in}$) is greater than the outer one ($[K^+]_{out}$), but very often the cytoplasm is electrically negative. The membrane potential of *E. coli* grown aerobically, for example, is estimated to be between -94 and -157 mV when the external pH

is changed from 6.25 to 8.25 (Harold, 1996; Kashket, 1982). The electrical component $\Delta\psi$ therefore tends to bring K^+ into the cell, while the chemical component of the equation ($\ln [K^+]_{in}/[K^+]_{out}$) tends to carry it out. The K^+ can then be driven passively towards the inside or the outside of the cell depending on the relative importance of these two components in determining the driving force.

1.1.2 The movement of ions across cell membrane

The gradient of organic and inorganic ions through the membrane can be maintained thanks to the hydrocarbons of the lipid bilayer, as they make the membrane significantly impermeable to ions. In the absence of neutralizing counterions (NH_4^+, acetate, etc.), ions can pass through the membrane through the *lumen* or the pore of various membrane proteins. There are three categories of proteins that can regulate ion trafficking: the first two categories are constituted by carriers (ion pumps or exchangers), while the third consists of ion channels. The transporter proteins move ions against gradient with consumption of energy in terms of ATP hydrolysis (for pumps) or gradient of other ions (for exchangers, both simporters and antiporters). *E. coli*, for example, has 3 systems to import K^+ into the cell: Trk, Kdp and Kup (Epstein, 2003). The main system is Trk (Transporter of K^+), a constitutive low-affinity and high-speed system, energized by the proton driving force and ATP hydrolysis. The second one is Kdp (K^+-dependent growth), a high-affinity and low-speed system, inducible by the P-type ATPase pump. The third one, Kup, is apparently an alternative system to Trk, and it works mainly when cells are grown at low pH values (Trchounian and Kobayashi, 1999). There is also an efflux mechanism for K^+ in these cells, which includes KefB and KefC systems, that are apparently more similar to Na^+/H^+ and K^+/H^+ antiporters respect to K^+ channels. In *Synechocystis sp*. PCC 6803 genome were identified three transport systems for K^+: Ktr carrier, Kdp carrier and K^+ channels. Ktr system, a Na^+-dependent carrier, consisting of three subunits (KtrA, KtrB and KtrE), seems to be predominant among the systems of K^+ uptake in *Synechocystis* (Berry *et al*., 2003; Matsuda *et al*., 2004; Matsuda *et al*., 2006). Recent studies have suggested that this system is driven by a Ktr-ATPase and a Na^+/H^+ antiporter, which are considered the most responsible for the extrusion of Na^+ in *Synechocystis*. In addition, other membrane proteins could be involved in the formation of the proton gradient, as the extrusion induced by light of H^+ was observed in several Cyanobacteria (Matsuda *et al*., 2006). All these influx and efflux systems have not to be confused with K^+-selective channels, which are members of the third class of proteins that regulate the traffic of ions. Ion channels are different from the previous two classes of carriers, as a channel consists exclusively of an “open pore” through which ions can diffuse following their electrochemical gradient. Unlike β-barrels, which form the porins of the outer membrane of Gram-, subunits of ion channels of the plasma membrane are constituted by α-helices. These pores are often formed when the helices of different identical or similar subunits are put together to surround a passage for ions. The conformation of the pore allows these proteins to function in a completely different way than that of the pumps or exchangers. When a channel is opened, when membrane potential is equal to zero, the ions move passively according to the pre-existing concentration gradient, dissipating this ionic gradient. As discussed above, the membrane potential and the concentration gradient are the driving force ($\Delta\mu K^+$) and may have opposite effects on the direction of the flow of K^+ ions. Thus, the flow of K^+ through the channels is inbound or outbound from the cell depending on the balance of these two components. The functions of the passive fluxes of ions through the channels in Prokaryotes, however, is not yet well known. Many K^+ channels in animals are also able to maintain the rest membrane potential, or they can restore it quickly following a depolarization event. Other K^+ channels of animals regulate the resting membrane potential according to different stimuli. The K^+ channels are not generally suitable to conduct large amounts of ions in animals; there are evidence of this type of transport in plants (Kwak *et al*., 2001; Hirsch *et al*., 1998).

1.1.3 Ion channels

Ion channels are membrane proteins that form hydrophilic pores which facilitate the passage of ions across cell membranes: they participate in many biological processes, from the transmission of the excitatory signal to the modulation of behavior in mammals or of the swimming in Protozoa. They allow the flow of more than a million ions per second from one side to the other of a biological membrane.
Each ion channel presents its own particular behavior that distinguishes it: for each of them, it can be evaluated conductance, selectivity, kinetics, mechanism of activation and pharmacology, determining the typical properties of a channel. These properties, that will be now defined, can be detected through analysis of single channel or all the channels in a cell.
Electrical conductance (measured in Siemens): measures the ease with which is realized a current flow between two points; according to the Ohm's law, is defined for the conductors as the relationship between current and voltage difference through the conductor. The conductance is the reciprocal of resistance. In practice, each channel acts as a primary conductor in the membrane, which can have high (in the order of 1 nS) or low conductance (in the order of some pS).
Selectivity: ion channels are preferentially permeable to some ions and not for others. In general, there are no channels perfectly selective for a single ion. The channels most studied are those selective for K^+, sodium (Na^+), chloride (Cl^-) and calcium (Ca^{2+}): there are however also channels that do not have a particular selectivity, as well as those that are selective in general for the cations or anions without distinguish between them.
Kinetic: through a statistical analysis it is possible to evaluate the kinetic behavior of a channel, a fundamental property that is often used to determine the sensitivity of a channel to different stimuli. For example, an increase in the fraction of the overall time spent by the channel in the closed state as effect of a drug, implies the channel inhibition by the drug itself, that is then defined inhibitor; *vice versa*, the activators behave favoring the opened state. The probability of the opened state (P_O, open probability) is determined as the integral of the current that flows through all open channels during a certain recording time, divided by the number of active channels during the same period, divided by the current value that would pass through a single open channel during the same recording time. The probability of the closed state is, instead, $1 - P_O$. Another parameter is the average time of opening: it is calculated by dividing the sum of the duration of each opening by the number of opening events. To obtain the average time of closing, the sum of the closed intervals has to be divided by their number and by the number of channels.
Activation mechanism: the factors that modulate the activity of ion channels in the membrane may be of various nature (Figure 1). We can distinguish between channels activated by changes of membrane potential (voltage-gated), channels modulated by ligand (ligand-gated) and channels that open as a result of applying a tension on the membrane (stretch-activated). The ligand-gated channels can be modulated by various types of ligands, such as neurotransmitters, ions, nucleotides, G proteins.
Pharmacology: this term refers to a set of substances that act on a specific channel, reducing or increasing its activity. They are called inhibitors or activators of a channel: having a defined pharmacological framework can be very useful to modulate its activity or even identify a channel. To study the functioning of channels special tools are required, as the patch-clamp or the planar lipid bilayer: these techniques allow to measure the current which permeates through the ion channels at a given potential value, due to the passage of ions depending on their electrochemical gradient through open channels.

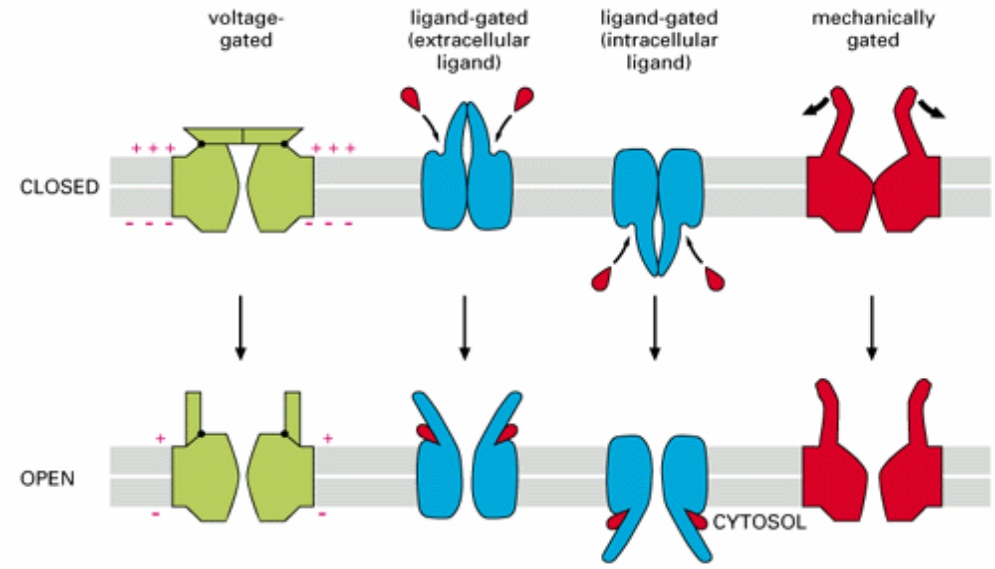

Figure 1 – Different activation mechanisms for ion channels (from the textbook "The essential of cell molecular biology", II edition, Alberts *et al.*, 2005).

1.2 General characteristics of K^+ channels

1.2.1 Basic structure and activity

K^+ channels are tetramers, generally consisting of identical subunits, even if animal channels consisting of hetero-tetramers made of similar subunits exist. These subunits are also called α-subunit being subunits that form the channel pore, to distinguish them from other associated auxiliary subunits (β, γ, etc…) which serve to regulate the main α-subunit. The core of the α-subunit of K^+ channels consists of two TM α-helices traditionally called TM1 and TM2 (TM: transmembrane helical segment), flanking a short helix that forms the pore (P: pore helix and filter loop) which contains the amino acid sequence defined K^+-filter. The simplest TM1-P-TM2 subunits is composed of only 94 amino acid residues encoded by a virus (PBCV-1) found in a green alga (*Chlorella*) which is a symbiont of a *Paramecium* (*Paramecium bursaria*) (Kang *et al.*, 2004). This TM1-P-TM2 structure (2TM) without additional peptide domains appears to be the minimum structure necessary for the permeation, the filtration and the opening. The crystallographic structure of the K^+ channel of *Streptomyces lividans*, KcsA (Figure 2), shows that the C-terminus end of the 4 2TM subunits converges towards the cytoplasm and occludes the ion passage (Doyle *et al.*, 1998; Zhou *et al.*, 2001). This convergence is also known as a gate which, in the crystallographic structure, is found in the closed conformation (Jiang, 2002). This structure with two transmembrane helices also exists in a class of channels called inward rectifyers (Kir) found in both Prokaryotes and Eukaryotes. Kir channels have an architecture similar to that of the KcsA channel, with small differences in the orientation of the helices and assembly (Kuo *et al.*, 2003). Instead, α-subunits of the type TM1-P1-TM2-TM3-P2-TM4, which form the K^+ channels with two pores, that have been found in animals and plants, have not been found in the genomes of prokaryotic and eukaryotic microbial organisms yet, in the case of these two pore channels (TPK), two subunits form a dimeric channel. It seems evident that these TPK subunits owe their origin to a phenomenon of gene duplication which allowed the formation of a $(\alpha\text{-}\alpha')_2$ type hetero-tetramer. Another structural motif common to α-subunits of K^+ channels is S1-S2-S3-S4-S5-S6-P (S: transmembrane helical segment) defined also 6TM type subunit. This structure is often called Shaker, a name due to a mutant of *Drosophila melanogaster*, which corresponds to the first cloned gene for K^+ channels (Papazian *et*

al., 1987; Tempel *et al*., 1987). In this design, the fragment P-S5-S6 maintains the same characteristics of the TM1-P-TM2 core, described previously. The helices S1-S2-S3-S4 act as controllers of the core, e.g. if they harbor positively charged amino acids in the S4 segment, such TM acts as voltage sensor. Different additional forms were discovered in studies of single-cell Eukaryotes such as ciliates and fungi. For example, the fungi have K^+ channels with 8 transmembrane segments (S1-S2-S3-S4-S5-P1-S6-S7-P2-S8) and the *Paramecium* has K^+ channels with 12TM pattern (S1-S2-S3-S4-S5-P1-S6-S7-S8-S9-S10-S11-S12-P2) (Ketchum *et al*., 1995; Zhou *et al*., 1995). As a direct consequence of being an "open pore", the activity of K^+ channels can be directly measured using radioactive isotopes or electrophysiological techniques, such as patch-clamp and planar lipid bilayer. The electrophysiological techniques allow to describe the particular behavior that distinguishes one channel from the other: for each one is possible, therefore, to evaluate conductance, selectivity, kinetics, mechanism of activation and pharmacology, as already mentioned above.

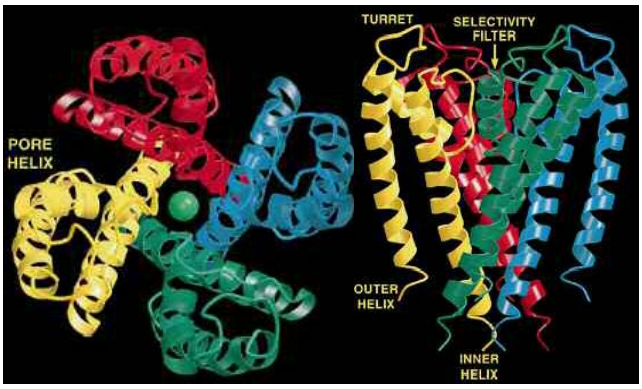

Figure 2 – 3D-structure of KcsA K^+ channel of *S. lividans*. Left: view from extracellular side. Right: normal view of left image. Green sphere represents K^+ ion (from Doyle *et al*., 1998).

1.2.2 The selectivity filter (K^+-filter) and its variants

The term "channel", as mentioned above, refers to the way that allows a passive flow of solutes. Channels are similar to enzymes in which there are sites that preferentially interact with specific molecules or ions. The K^+ channels in general have the filter region (Figure 3) separated from the region responsible for regulating opening and closing (gating). This has been verified at the atomic level thanks to the determination of the crystallographic structure of KcsA. The mechanism of filtration of ions in K^+ channels is highly efficient and discriminating at the same time. In contrast to enzymes which have a turnover rate of approximately 10^3 molecules of substrate per second, many types of channels have a higher speed, of 10^7 ions per second and, at the same time, maintain high selectivity. A K^+ channel can have a permeability ratio of 300 to 1 in favor of the K^+ with respect to Na^+. This seems at odds with the principles of binding energy of ions. The crystallographic structure of KcsA explained a part of this enigma (Figure 2). Each K^+ channel is formed by α-helices deriving from 4 separated subunits to enclose an aqueous center, which narrows in a selective filter of 2.0 Å in diameter near the cytoplasmic surface (Doyle *et al*., 1998; Zhou *et al*., 2001). The filter is characterized by the alignment of the carbonyl oxygens arranged horizontally, belonging to the canonical amino acid sequence TXGYGD for each of the 4 subunits. Pairs of these quartets of oxygens partially surround K^+ ions with greater efficiency compared to the eight oxygens of hydration of the sphere surrounding it in aqueous solution. The removal of the sphere of hydration requires a high energy cost, therefore, the selectivity filter is structured so as to perfectly mimic the sphere of hydration of a K^+ ion, minimizing the energy cost for each ion that enters or leaves the filter. Cations of different sizes, such as Na^+ and Ca^{2+}, require substantially

different energies for the passage. The structure, therefore, has allowed the understanding of the high selectivity to K^+ and the permeation rate similar to that by simple diffusion. In the three-dimensional structure of KcsA, the central filter is supported by 4 helices of the pore. Under the cone formed by the 4 helices there is a cavity filled with water, which is sealed from the cytoplasmic side by convergence of 4 TM2 helices when the channel is in the closed conformation. The TM2 helices also form the gate (Jiang *et al*., 2002). The canonical sequence of the selectivity filter, TXGYGD, shows small variations between described channels. In animal channels, for example, sometimes the tyrosine (Y) is replaced with phenylalanine (F) and this substitution is conservative because it preserves the aromatic group of the side chain that surrounds and supports the filter. In both the channel Kch of *E. coli* and KcsA of *S. lividans* this substitution retains the function of K^+ filtration (Kuo *et al*., 2003; Splitt *et al*., 2000). The GFG sequence is present in the selectivity filters of K^+ channels of some species of Bacteria, such as *Thermoplasma volcanium*, *Mycoplasma mobile*, *Magnetococcus sp*. MC1 and others. Another variant which is often found in the animal channels is the substitution of an aspartate residue (D) with a glutamate (E). Most likely this substitution is permitted, as maintains the negative charge. In Prokaryotes this variant was found only in (2TM)-KTN/RCK channels of many Cyanobacteria, some species of proteobacteria and a few species of other *phyla*.

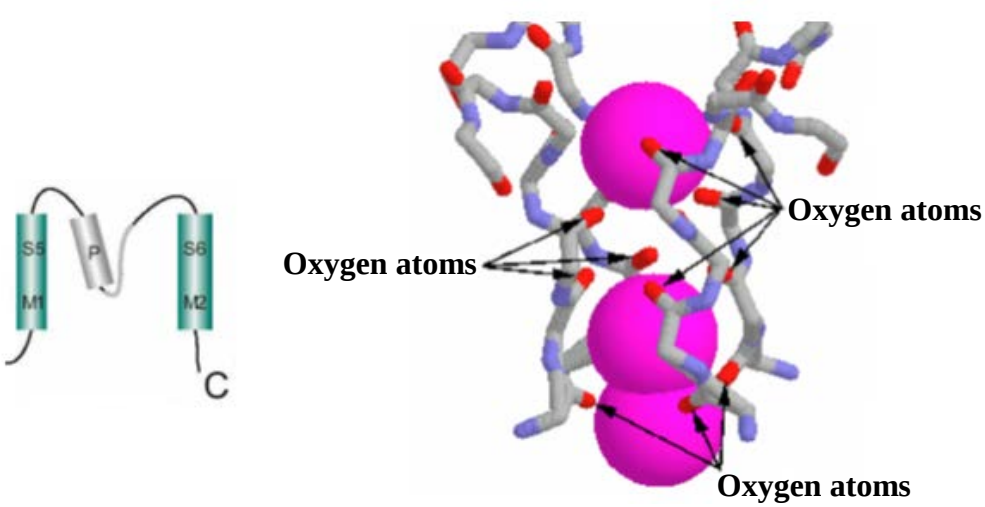

Figure 3 – Schematic representation and structure of TM1-P-TM2 motif and of the region containing the selectivity filter, typical of K^+ channels. K^+ is highlighted in pink in the selectivity filter. O_2 coordination atoms are also highlighted, they mimic the hydration sphere of the K^+ ion.

1.2.3 The mechanisms of regulation of opening/closing of channels

Channels are typically in the closed state, since the flow of ions through an open pore is unfavorable to cell metabolism. The tetramer can exist, therefore, in at least two conformations: closed and open (however, biophysical analysis have revealed that there are multiple states or open/closed so called sub-states). Both in MscL and KcsA, the conformational changes of the subunits during the opening of the channel show a mechanism similar to that of the aperture of a camera. Ion channels can be also considered as transducers which convert the binding energy of the ligand, the change in voltage, or the mechanical work into the opening of the ion channel, transducing the external signal (chemical, electrical or mechanical) into an electrical or chemical signal in the cytoplasm. The different physical/chemical parameters that open channels are the so-called stimuli. In general, in association with opening, the occurrence of an electric current through the channel due to a specific stimulus, a phenomenon called “channel activation” can be described. The term “activation” also indicates the increase in the probability of channel opening. For many channels, the current

decreases after the initial activation, even if the stimulus is maintained. This process is known as inactivation which must not be confused with the deactivation, the process by which the current disappears after removal of the stimulus. Many different additional molecular mechanisms were determined to describe the activation, inactivation and deactivation (Hille, 2001). Activation can depend on voltage, ligand binding and mechanical stimuli. In general, many proteins perceive the electric field through their amino acid residues. The voltage-dependent channels often show patterns of charged amino acids (in S1-S4 segments) and are particularly sensitive to changes in the membrane potential. The voltage sensor is a region of the channel enriched in electrical charges that can move in response to voltage changes, causing the opening or closing of the channel. The S4 helix of each subunit of different Shaker type channels contains a series of arginines (R) and lysines (K) regularly spaced by 2 residues, such as in the pattern shown here: RXXRXXRXXRXXKXXRXXKXX. This motif (or similar motifs with different number of charged residues) has been shown in many K^+ channels activated by voltage and has been shown that constitute the most important part of the voltage sensor. The positively charged residues at the N-terminus constitute another important part of the voltage sensor (Seoh *et al*., 1996). Many prokaryotic genomes contain genes that encode hypothetical K^+ channels of the Shaker type. Two of these genes have been successfully cloned and their activity as voltage-dependent K^+ channels has been demonstrated. The first of these is the KvAP channel of *Aeropyrum pernix*, which is a specific K^+ channel activated by depolarization, the second is MVP of *Methanocaldococcus jannaschii*, a channel selective for K^+ activated by hyperpolarization (Ruta *et al*., 2003; Sesti *et al*., 2003). As to class of the ligand-gated channels, their opening mechanism is very similar to that of the activation of an enzyme. The binding of a ligand, in fact, induces a change from the closed conformation (inactive) to the open one (active). Animal ion channels can be opened by different types of ligands, those located externally (glutamate, acetylcholine, protons) and those that are located internally (e.g. ATP, cyclic nucleotides, Ca^{2+}). Finally, the mechanical forces can be transmitted to the channels through the lipid bilayer to induce their opening. This type of mechanism has been found in the bacterial channels MscL, MscS and in some animal channels (Blount, 2003; Patel *et al*., 2001).

1.2.4 K^+ channels in Prokaryotes

Most of our knowledge on the structure and selectivity as well as gating mechanisms of ion channels is due to studies on prokaryotic channels. In the study of prokaryotic K^+ channels it is of interest that, in the genome of *E. coli* close to the *trp* operon sequence, there is an open reading frame (Kch) which was identified as a sequence that could conceptually give rise to a protein with the canonical sequence of the selectivity filter, similar to that of Shaker type K^+ channels of Eukaryotes (Milkman, 1994). Although the patch-clamp technique was successfully applied to the native membranes of *E. coli*, a specific electrical conductance of K^+ was not detected. The electrical activity of the prokaryotic K^+ channels has been successfully registered in 6 cases when the channel proteins were expressed in heterologous systems, such as *E. coli*, yeast, *Xenopus* oocytes, cultured mammalian cells or were reconstituted into artificial lipid membranes. However, the activity of prokaryotic K^+ channels in their native membranes has never been reported. The analysis of the information contained in gene sequences, currently provides information on the prevalence and variability of K^+ channel genes in Prokaryotes. To identify genes that encode for K^+ channels in the genomes, in fact, bioinformatic programs are used, such as BLASTP and TBLASTN of the NCBI website, which align the 270 totally or partially sequenced prokaryotic genomes. The translation product of the open reading frame that conceptually meets the following criteria is considered a counterpart of K^+ channels. As a first step, the sequence of the selectivity filter of Kch (TITTVGYGDITP) is used as a query in the alignment. Subsequently, the topology of the

sequences obtained, containing indifferently GYG or GFG, are examined using the pattern of hydropathicity to determine if the K^+-filter sequence is localized, as expected, towards the C-terminus fragment in a small hydrophobic fragment (the pore helix) between two 22-24 amino acids-long transmembrane helices (according to the TM1-P-TM2 motif). The most similar sequences, then, can be divided into 3 groups: those that have only two transmembrane segments that flank the pore region, called 2TM, and those that have 4 or 2 TM upstream of the core region, called respectively 6TM and 4TM. Among these K^+ channels, some include only the region of the TM helices, others also contain the extensions, both between the transmembrane helices and the N- and C-terminus. Homologues of 2TM channels without extensions to the terminals, which include the KcsA channel, are part of the core-type K^+-channels. Many of the counterparts of 6TM channels are also recognizable as they contain charged amino acid residues (arginine, lysine, histidine) in the S4 helix, giving to the channel the characteristic voltage-dependence for adjusting the opening. To determine the characteristics of the voltage-dependence, these sequences were aligned with ClustalX bioinformatic software. In this way those proteins that showed charged amino acids in the S4 segment were classified as voltage-dependent channels, while the remaining channels were classified as type "6TM core only" (Kuo *et al*., 2005). All homologues of 4TM/1P channels that have been found didn't show long amino acid sequences at the N- and C-terminus. This type of channel seems to be unique in prokaryotic cells. It has also been proposed that the pore segment and other different parts (such as, for example, the gate region) of α-subunit of K^+ channels may result from the association of two different peptides (whose genes are located in the same operon) (Kumanovics *et al*., 2002). Eukaryotic Kir homologous, the "glutamate receptors" and "cyclic nucleotides-binding channels" are all characterized by long peptide end chains, supporting the above hypothesis. A high number of 2TM and 6TM K^+ channels found have a domain named KTN (Rossmann fold or NAD-binding domain) or RCK (Regulating the Conductance of K^+), among which we find Kch and MthK (a channel of *Methanobacterium thermautotrophicum*), and are classified as "KTN/RCK domain channels" (Rossmann *et al*., 1974). Some 2TM channels have a long tail that is not homologous to any known type of domain, referred to as "unknown domain channels".

1.2.5 *Syn*K K^+ channel

A sequence of 234 amino acids which seems to encode a voltage-dependent K^+ channel, resembling members of the Shaker family has been identified in the proteome of *Synechocystis sp*. PCC6803, using bioinformatic programs (BLAST algorithm). The protein was named *Syn*K. The alignment was obtained between TMTTVGYGD motif, characteristic of the selectivity filter of K^+ channels, against the whole proteome of *Synechocystis*. The identified putative channel, according to the bioinformatic software Hierarchical Neural Network (HNN, by Qian and Sejnovski), consists of six transmembrane segments (S1 to S6) and a pore region (P between S5 and S6). The pore region contains the TLTTLGYGD motif, which is characteristic of the selectivity filter of K^+ channels (valine and leucine are similar amino acids). The predictions on the three-dimensional structure of the protein and the amino acid sequence alignment indicates a high similarity of the *Syn*K channel with the KvAP K^+ channel of *Aeropyrum pernix*, for which three-dimensional structure (obtained by crystallography and X-ray analysis) and activity *in vitro* (obtained using planar lipid bilayer technique) (Jiang *et al*., 2003; Ruta *et al*., 2003) are known. On the basis of the similarity between these two channels it is also proposed that the channel of *Synechocystis* is constituted by 4 monomers. In order to determine the functionality of the *Syn*K protein *in vitro*, its expression in a heterologous system and its analysis using electrophysiological techniques were carried out in our laboratory. In particular, we have chosen to express the protein in mammalian cells (CHO-K1) as its expression in *E. coli* has proved impossible due to the toxicity of the protein for bacteria. The

expression system used therefore was a transient transfection system in CHO-K1 cells, carried out with the system of the cationic lipids leading to the expression of the *Syn*K-EGFP fusion product. The presence of the fluorescent protein EGFP at the C-terminus of the protein has allowed us to monitor the expression and localization of the recombinant protein within CHO cells. The images obtained with fluorescence microscopy show that a part of the fusion product is localized in the plasma membrane of CHO-K1 cells (Zanetti, 2004, thesis). The immunoblot experiments with anti-EGFP, performed on total lysates of transfected cells, showed that a part of the protein was expressed with the molecular weight predicted for the fusion protein, 54 kDa (26 kDa for *Syn*K and 28 kDa for EGFP). The localization in the plasma membrane of mammalian cells of the fusion product *Syn*K-EGFP was a necessary condition to be able to perform the subsequent electrophysiological studies with the patch-clamp technique in the whole-cell configuration. This way, it was possible to determine the protein activity *in vitro*. Data obtained showed that the protein, in this system, mediated the efflux of K^+ ions outward from the cell (positive current, in accordance with the convention and illustrated as upward current) when positive, depolarizing potentials, were applied through the membrane and the intra- and extracellular concentrations of K^+ were 140 and 5 mM, respectively. *Syn*K shows homology to the higher plant channel TPK3, the subject of my work, however the evolutionary step linking the two proteins is not clear. Data suggest that *Syn*K may be an ancestor of *At*TPK3, a member of the tandem-pore potassium channel family in *Arabidopsis* (Mäser *et al*., 2001). When BLAST search is performed, *At*TPK3 results as the closest homolog of *Syn*K in the whole *Arabidopsis* genome and *vice versa*, according to Aramemnon. The evolutionary origin of eukaryotic tandem-pore channels is still vague but according to one hypothesis, 6TM prokaryotic PNBD-less potassium channels (like *Syn*K) might have given origin to TPK channels (Derst and Karschin, 1998). A conserved pore region feature (presence of YF residues) in both *Syn*K and plant TPK channels represents an additional point to an evolutionary link between the two proteins. Findings indicate the presence of *At*TPK3 protein in the thylakoid membrane (Zanetti *et al*., 2010). Independently of whether *Syn*K is the precursor of *At*TPK3 or not, this is the first thylakoid-located cation channel identified from molecular point of view in higher plants (in addition to proton-conducting F0/F1 ATP-ase). The thylakoid localization of this protein opens the way to functional characterization of this still putative channel.

1.2.6 *Syn*CaK K^+ channel

Recently a so-far uncharacterized putative potassium channel (NP_440478, encoded by the open reading frame *sll*0993) named *Syn*CaK was identified in *Synechocystis*. This protein shares sequence homology with *Mt*hK, a Ca^{2+}-activated K^+ channel of the archaeon *Methanobacterium thermoautotrophicum*. The structure of *Mt*hK in an open conformation has been determined (Jiang *et al.*, 2002). The *Mt*hK subunit has two transmembrane segments and one pore region (TM1-P-TM2), followed by an extension of approximately 200 amino acid residues which contains a region called the RCK (for Regulator of the Conductance of K^+) domain. RCK of *Mt*hK binds divalent cations, such as Ca^{2+} or Cd^{2+} (Jiang *et al.*, 2001, 2002). Various studies led to a model in which the channel is a heterooctamer, where the *Mt*hK transmembrane tetramer assembles with eight RCK domains: four covalently linked to the four TM2 helices and four additional ones assembled onto them at the cytoplasmic side. The physiological meaning of the activation of *Mt*hK with millimolar Ca^{2+} is unclear, since Ca^{2+} as a second messenger operates at micromolar concentrations in Eukaryotes, and the possible signaling roles of Ca^{2+} in Prokaryotes are still unclear.
*Syn*CaK resembles some of the electrophysiological activity properties of *Mt*hK: in fact, similarly to *Mt*hK, also *Syn*CaK could be activated by Ca^{2+}. Actually it was find an increased activity when changing the intracellular concentration from 0 to 10 mM Ca^{2+} in inside-out excised patches (Checchetto *et al*., 2012). The properties of the channel could not be studied in the whole-cell

configuration given that cells cannot withstand such a high intracellular Ca^{2+} concentration. However, in the same paper it was demonstrated that *Syn*CaK works as K^+ channel, in accordance with the bioinformatic predictions.

1.2.7 K^+ channels in plants

In plants evidence that K^+ plays an important role in a large number of functions such as the elongation of cells, movement of the stomata, regulation of gas exchange and transduction of various signals has been obtained during the last 30 years (Clarkson and Hanson, 1980; Zimmermann and Sentenac, 1999; Véry and Sentenac, 2003). Sequencing of the entire *Arabidopsis* genome has allowed the identification, by studies of sequence similarity with the animal channels, of 15 putative K^+ channels (Figure 6). These can be divided into three main groups, which take their names from their counterparts in animals: Shaker, KCO (or KCNK or TPK according to the new nomenclature) and Kir (Figure 4). In plants, as in animals, the activity of K^+ channels determines the electrical properties of the membranes. Their physiological function has been clarified through analysis of expression patterns and mutational analysis. Through the use of yeast mutants defective for K^+ uptake, in 1992 a French group has cloned from *Arabidopsis thaliana*, the first plant ion transport systems: KAT1 and AKT1 (Sentenac *et al*., 1992). Structural studies have shown that these inward rectifying channels, are structurally very similar to the animal Shaker K^+ channels.

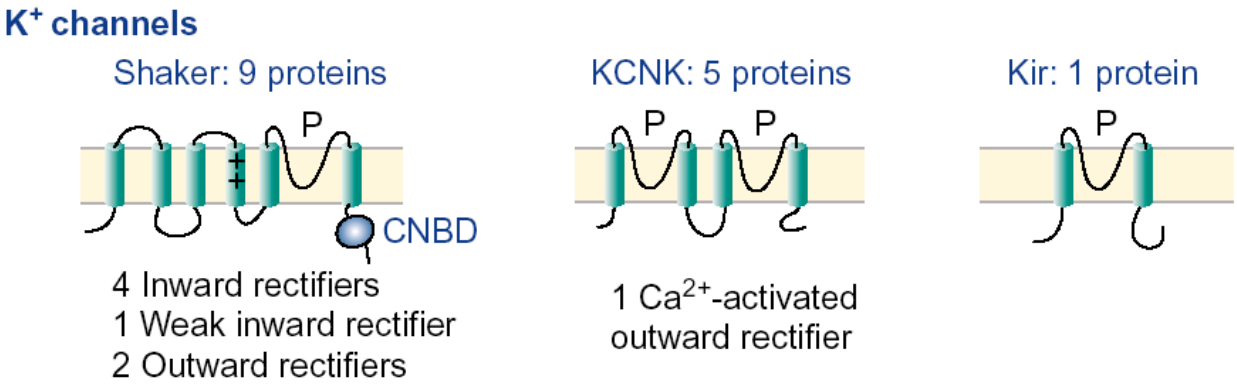

Figure 4 - Different families of putative K^+ channels in the *Arabidopsis* genome: *Shaker*, KCNK (or KCO) and Kir (++: positively-charged residues in the voltage sensor; CNBD: putative cyclic nucleotide binding domain; P: pore domain) (from Véry and Sentenac, 2002).

1.2.8 *Shaker* channels in plants

Shaker channels (Figure 5) in plants are similar to animal Shaker channels with six transmembrane segments. The better characterized channels in animals are those of the Kv family (Shaker voltage-dependent), both from a structural point of view and functional. The homology between plant and Kv channels is limited to the core and in particular to the pore region. The animal channels that are more similar to those of plants are the EAG Shaker channels (EAG, ELK, ERG, HCN and CNG). In plants, usually, the Shaker type channels show a shorter region (of about 60 residues) at the N-terminus domain, followed by a hydrophobic core composed of six transmembrane helices (S1 to S6, with the domain of the pore between S5 and S6), and a long cytoplasmic region. The fourth transmembrane segment contains positively charged amino acids (R and K) and is expected to act as voltage sensor. The highly conserved pore domain, containing the GYGD/E motif, is present between S5 and S6. The C-terminus region contains a putative binding site for cyclic nucleotides and, in most cases, an ankyrin repeat domain, potentially involved in protein-protein interactions

(Chérel, 2004). At the C-terminus there is the K_{HA} region (rich in hydrophobic and acid residues), which may be involved in tetramerization of the subunits. In addition to the α-subunit, plant Shaker channels can have β-subunits, the function of which in plants is currently uncertain. In *Arabidopsis*, for example, *kab1* genes, coding for proteins that are homologous to the animal Kv β-subunits have been identified. There is the possibility that the β-subunits are associated with other types of non-Shaker channels, such as those with outward rectification (as KCO and SKOR). As in animals, also plant inward rectifying α-subunit channels form homo- and hetero-tetramers. In plants, the composition of hetero-tetramers seems to be more determined by the expression of tissue-specific genes for channels rather than by the sequence. In *Arabidopsis* 9 proteins belonging to the Shaker family were characterized and divided into three subfamilies depending on their rectification properties: inward, outward and weakly inward rectifyer (Schachtman, 2000). Although the molecular mechanism that determines the rectification is not well understood yet, the experiments show that it can be due to an intrinsic process of gating, rather than to the locking part of Mg^{2+} ions, as occurs in animal inward rectifying channels. In KAT1, for example, inward rectification is due to the N-terminal region and to the first 4 transmembrane segments. The involvement of the N-terminus region in rectification is in contrast with what occurs in animal inward rectifying channels, in which the C-terminus region seems to be involved (Véry and Sentenac, 2002). In addition to Shaker channels with inward rectification, electrophysiological techniques have demonstrated the presence of Shaker channels with outward rectification, as SKOR. This channel is involved in the release of K^+ in the xylem. Shaker channels are expressed in different tissues. The available information suggests that these channels are involved in nutrition and regulating the osmotic state of the cell. A multidisciplinary approach, comprising the expression in heterologous systems, electrophysiological characterization and the production of knockout mutants, allowed to unravel the role of some Shaker channels. For example, AKT1 is an inward rectifyer channel found to be the major system for K^+ uptake in roots and mesophyll (Hirsch *et al*., 1998; Ivashikina *et al*., 2001; Dennison *et al*., 2001), while SPIK (Shaker Pollen Inward K^+ channel) is involved in K^+ uptake in pollen. Its activity is necessary for the correct development of pollen tubes (Mouline *et al*., 2001). KAT1, KAT2 and GORK (plant Shaker channel that functions as outward rectifyer) are expressed in guard cells (Nakamura *et al*., 1995; Pilot *et al*., 2001; Szyroky *et al*., 2001). *At*KC1 is expressed in peripheral root cells where it could play a role in K^+ uptake (Véry and Sentenac, 2003). Finally, analysis of mutants unraveled that AKT2 is involved in the control of membrane potential of phloem cells and in the transport of sucrose in the phloem (Deeken *et al*., 2002).

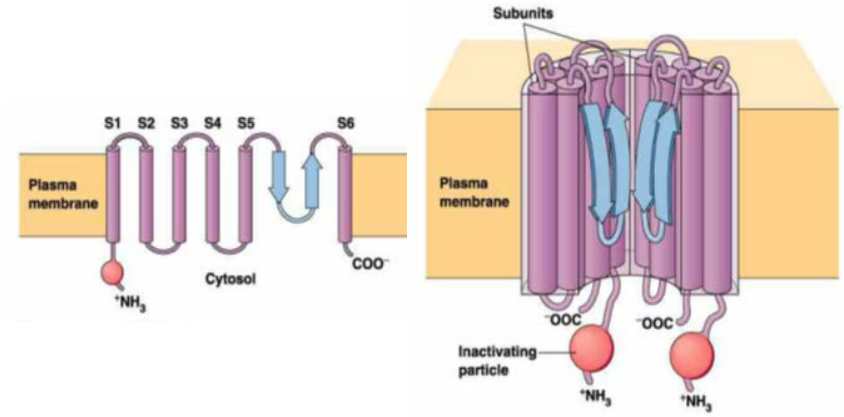

Figure 5 – Structure of a *Shaker* channel (© Addison Wesley Longman, Inc.).

1.2.9 Other K^+ channels in plants

Studies of sequence similarity with animal channels have led in *Arabidopsis* to the identification of

other gene families encoding K^+ channels, such as KCNK and Kir channels (K^+ inward rectifying). Plant KCNK channels have a hydrophobic core consisting of four transmembrane segments, containing two P domains and are devoid of the voltage sensor. In *Arabidopsis* five channels which have structural similarity with these animal channels were identified, three of which also have a binding site for Ca^{2+} at the level of the C-terminus region. Recent studies have demonstrated their activity in the vacuolar membrane (Schönknecht *et al*., 2002). The Kir channels were observed in root plasma membrane, they are characterized by a hydrophobic core consisting of only two segments and a transmembrane P domain (Véry and Sentenac, 2002). Reporter genes, used to study the localization of K^+ channels in plants, have demonstrated their presence at the level of different compartments such as the plasma membrane, the tonoplast and the Golgi apparatus of different tissues such as roots, leaves, seeds and flowers (Schachtman, 2000). For example, Shaker channels like *At*KC1, KAT1 and KAT2 are localized at hydathodes, trichomes, guard cells and roots (Jeanguenin *et al*., 2011), *At*KCO1 of *Arabidopsis thaliana* is expressed in leaves (at the level of vascular tissue and guard cells, in particular), in the root and a little bit in pollen grains (Czempinski *et al*., 2002).

1.2.10 TPK channels

In 2000 the *Arabidopsis* genome became available and were identified also 5 tandem-pore K^+ channels (*At*TPK1, 2, 3, 4 and 5) (Figure 6, violet panel). In an introductory insight into the role of TPK channels in plants, the genomes of 19 fully sequenced plants were screened for homologues of *Arabidopsis* TPK/KCO channels. TPK-coding sequences were identified in 12 genomes. Homologues of *A. thaliana At*KCO3 were only found in the related specie *A. lyrata*, suggesting that *At*KCO3 developed through a recent evolutionary event involving gene duplication followed by a partial deletion. In phylogenetic analysis, the *At*KCO3 protein clusters closely with *At*TPK2 and the corresponding proteins from *A. lyrata*. In algal genomes TPK family members were only detected in the two *Ostreococcus* species, although with distinct insertions/deletions that locate them outside the tree that groups TPK/KCO from land plants.

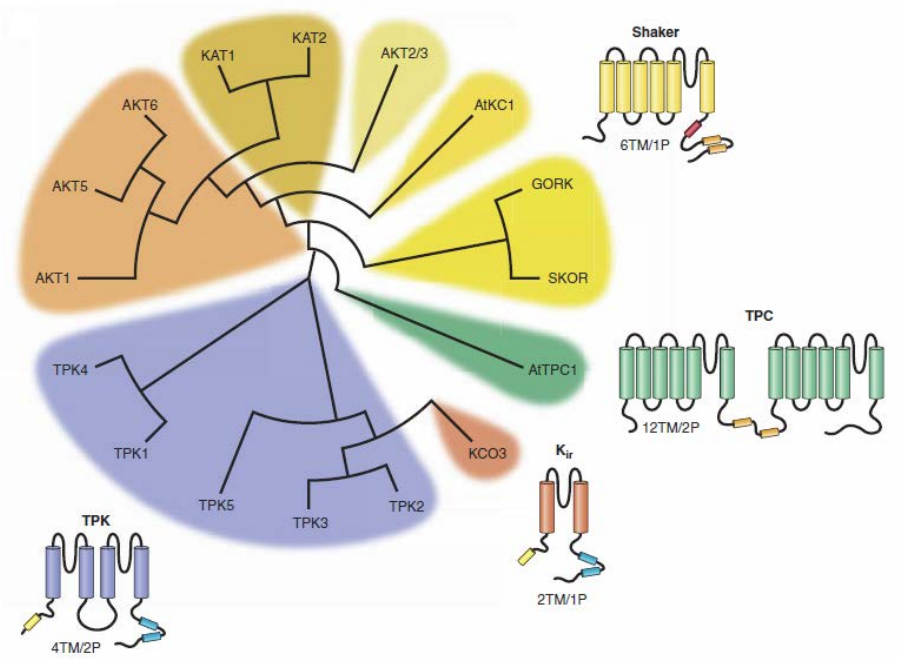

Figure 6 – Phylogenetic tree of the relationships between all *Arabidopsis thaliana* K^+ channels (15) and a non-selective cation channel (*At*TPC1). *At*TPK channels are positioned in the violet panel, the Kir like outsider *At*KCO3 channel is evidenced in red (modified from Hedrich, 2012).

1.2.11 Structural insights of TPK channels

Channels of the TPK family are characterized by a duplicated KcsA-like structure with four transmembrane domains and two-pore domains. TPK channels were proposed to form dimers consisting of two identical subunits (Voelker *et al*., 2006). Notably, both KCO3 and members of TPKs contain N-terminal binding sites for 14-3-3 proteins and putative Ca^{2+} binding EF hands in the cytosolic C-terminal parts, indicating that the channels can be regulated by similar biochemical mechanisms. The exception is represented by TPK4, which lacks these regulatory and protein interaction motifs (Czempinski *et al*., 1999; Becker *et al*., 2004). Another tandem-pore channel with structural analogies with TPK members is a channel of the vacuolar membrane, named TPC1 (Two-Pore Channel 1) showing a duplicated Shaker-like structure with a total of 12 transmembrane segments and two pore loops. TPC1 is a voltage-dependent channel (Peiter *et al*., 2005; Ranf *et al*., 2008) that mediates slow-activating (SV) currents through the tonoplast. The SV channel is ubiquitous in plants and is believed to play a role in cation homeostasis and Ca^{2+} signalling.

1.2.12 TPK channels interact with 14-3-3 proteins

In animals, the activity of two-pore channels has been shown to be regulated through an interaction with 14-3-3 proteins. Likewise, in plants 14-3-3 proteins interact with plasma membrane K^+ channels (Sottocornola *et al*., 2006). In barley radicle protoplasts, for example, Shaker-like outward-rectifying (K^+ out) and inward-rectifying (K^+ in) channels are under the control of 14-3-3 proteins, increasing the activity of K^+ in channels but decreasing that of K^+ out channels (Van den Wijngaard *et al*., 2005). Vacuolar channels are also regulated by 14-3-3 proteins; for example, 14-3-3 proteins down-regulate K^+ channel activity at the vacuolar membrane of barley mesophyll cells (de Boer, 2002). It was also demonstrated that HvTPK1, a barley homologue of *Arabidopsis* TPK1, interacts with 14-3-3 proteins (Sinnige *et al*., 2005). Similar results were obtained for *Arabidopsis* TPKs, indicating their interaction with 14-3-3 proteins *in vitro* and *in vivo*. As mentioned before, the cytosolic N-terminal regions of most TPKs exhibit a classical type I binding motif (RSXpS/TXP) for 14-3-3 proteins, with a serine or threonine residue acting as potential phosphorylation site. Phosphorylation of this residue appears to be a prerequisite for protein-protein interaction. In plant cells, *wt* TPK1 and GRF6 co-localize at the vacuolar membrane; this co-localization is lost when a mutant of TPK1 (S42A) is co-expressed with GRF6 (Latz *et al*., 2007). The protein interaction affects channel activity. Addition of 14-3-3 protein (GRF6) to TPK1-expressing yeast cells strongly increases TPK1 activity in a dose-dependent manner (Latz *et al*., 2007). However, the TPK/14-3-3 interaction appears not to influence protein targeting. By deleting the cytosolic N-terminal domain including the 14-3-3 binding site, TPK1 was still partially transported to the vacuolar membrane, but was mainly retained in the ER. When the N-terminal of TPK1 was replaced by that of TPK4, which lacks a 14-3-3 binding motif, the chimeric channel was clearly detected at the tonoplast, indicating that the N-terminal part including its 14-3-3 binding site is not essential for vacuolar targeting (Dunkel *et al*., 2008).

1.2.13 TPK channels: homomers or heteromers?

As said before, four P-domains are needed to form the permeation path, implying that functional K^+ channels can theoretically consist of a combination of the different structural elements. Very likely K^+ channels are formed by: two TPK channel α-subunits; or four KCO3 subunits. It might, however, also be possible that a TPK subunit combines with two KCO3 subunits. However, it is not necessarily true that a channel functions as a homomer formed by identical subunits (i.e., proteins of identical sequence and structure). For Shaker-like K^+ channels, it is well known that different α-

subunits have the potential to assemble into heteromeric channel complexes, consisting of proteins of different sequences but similar structures (Dreyer *et al*., 1997, 2004; Jeanguenin *et al*., 2008), and this process also occurs *in vivo* (Lebaudy *et al*., 2008). In contrast, for TPK and Kir-like channels, the informations about channel assembly are still elementary. However, important information became available through the application of optical methods (Lalonde *et al*., 2008). TPK and KCO3 channels were tagged with yellow and blue-shifted variants (YFP, CFP) of the green fluorescent protein (GFP), and the proximity of the two fluorescent proteins was measured using Fluorescence Resonance Energy Transfer (FRET). FRET analysis resulted in positive signals for TPK1, TPK5 and KCO3 homomeric subunit interactions, whereas FRET signals at background level were detected for heteromeric combinations (TPK1/TPK5; TPK1/KCO3; TPK5/KCO3). These background signals were interpreted as the result of dimer formation of the fluorophores at very high protein concentration (Voelker *et al*., 2006). Results obtained with FRET were completed by Bimolecular Fluorescence Complementation (BiFC) experiments. Split-YFP analysis of TPK1, TPK2, TPK5 and KCO3 indicated a clear vacuolar targeting of the channels when homomeric subunit combinations were tested. In contrast, expression of heteromeric protein combinations resulted in diffuse signals in non-target compartments (ER, cytosol) and, in part, in the vacuolar membrane, but a distinct signal exclusively associated with the vacuolar membrane was never observed. The fluorescence signal detected in heteromeric TPK/KCO3 combinations may result from an initial (unspecific) protein association due to high concentration in the ER and subsequent permanent coupling via the restored YFP attached to the channel subunits. Such erroneously assembled protein multimers may be recognized by the cellular quality control system, leading to degradation of the false protein complex on its way to the vacuole (Voelker *et al*., 2006). Both FRET and BiFC analysis strongly support the existence of homomeric TPK/KCO3 channels, specifically dimers in the case of TPK1 and TPK5, and tetramers in the case of KCO3. To date, there is no convincing evidence for the existence of heteromeric TPK/KCO3 channels. However, the results obtained so far do not fully exclude the possibility that TPK/KCO channel subunits may assemble into heteromeric channels *in vivo* (Voelker *et al*., 2006).

1.2.14 The putative physiological function of plant TPK channels

There is still a huge gap in knowledge about the physiological roles of TPK channels in plants. Therefore, some information can be obtained from the homologous channels in mammalians. Here, two-pore domain K^+ (K2P) channels are extensively distributed in the central nervous system and peripheral tissues. The crystallographic structure of one of K2P channels (TRAAK) was determined in 2012 (Brohawn *et al*., 2012). K2P channels are largely voltage-independent and generate well-modulated background K^+ currents across the plasma membrane. These channels act in concert with other membrane transporters and play key roles in fine-tuning of the resting membrane potential and cell excitability. Interestingly, the activity of K2P channels is strongly modulated by signalling molecules (for example, hormones, pH, O_2, CO_2, NOx, ROS) or physical factors, like temperature or pressure. Due to this physicochemical sensory function, K2P channels are primary targets for external or internal stimuli. Modulation of background K^+ currents can have a strong influence on the electrical properties of a cell. Inhibition of K2P channels, for instance, causes membrane depolarization. This, in turn, increases the electrical activity in excitable cells, improves sensitivity to other inputs and enhances Ca^{2+} entry to incite hormone and/or transmitter release from secretory cells or contraction in smooth muscle cells. Activation of K2P channels, in contrast, hyperpolarizes the membrane and reduces cell excitability and responsiveness. Based on analogy, it might therefore be speculated that plant TPKs are also targets of external and internal *stimuli* to fine-tune the electrical properties of the membrane (mostly the tonoplast) for specialized transport tasks.

1.2.15 Summary on TPK channels

Arabidopsis thaliana genome harbors six genes coding for putative voltage-independent K^+ channels but, till now, only for TPK1 and TPK4 are available detailed informations about their activity and physiological roles. TPK1 shows all the marks of the electrophysiologically well-characterized VK channel; it has voltage-independent gating, K^+ selectivity, a vacuolar localization and regulation by cytosolic Ca^{2+} and 14-3-3 proteins. There are many evidences that TPK1 is necessary and sufficient in vacuolar K^+ release, especially in guard cells (MacRobbie, 1998), where ABA-induced TPK1-mediated K^+ release from the vacuole is important in stomatal closure. This channel is also important during seed germination and in turgor-guided cell expansion in roots (Gobert *et al*., 2007). TPK4, the TPK channel of the plasma membrane, located in particular in the pollen tube membrane, is also voltage-independent and highly selective for K^+ ions. TPK4 is sensitive to external Ca^{2+} and to cytoplasmic acidification (Becker *et al*., 2004). It seems that this ion channel is able to integrate the properties of another plasma membrane K^+ channel, named SPIK1. In fact, SPIK1 has the opposite features described for TPK4 (SPIK1 is sensitive to external pH but not to external Ca^{2+}), so the coupling of these functions may regulate pollen tube membrane potential and physiology in a wide range of conditions (Becker *et al*., 2004). Functional data for TPK2, TPK3, TPK5 and KCO3 gene products are still missing (for TPK3 is presented, in the second section of this thesis, a submitted paper that describes, for the first time, the biochemical and electrophysiological characterization of this channel and its possible involvement in the regulation of photosynthesis in higher plants). Chimeric approaches in the TPK4 background involving the P-loops of different TPK channels, however, suggest that other members of the *Arabidopsis* TPK family act as K^+-selective channels (Voelker *et al*., 2010). The weak expression of genes coding for tonoplast ion channels and their partially tissue-specific expression domains are certainly problems that need to be solved in future experiments. Besides functional studies of TPK/KCO channels, a more detailed analysis of their structural features will provide valuable information about how they exercise their biological roles. The diacidic ER export motif present in TPK1 is conserved among its plant homologues, but is absent from other members of the TPK/KCO family, suggesting divergent targeting strategies. The targeting mechanisms of plant ion channels and tonoplast proteins in general still have to be clarified in detail. An essential milestone towards uncovering the physiological roles of tonoplast-located TPK, KCO or TPC subunits lies further in searching for the possibility of homo- or heteromeric channel formation and the possible interaction with other regulatory proteins under various environmental conditions. The different experimental approaches will further improve our understanding of transport processes across the vacuolar membrane, which encloses up to 90% of the cell volume.

1.3 Photosynthesis

The photosynthetic organisms use light energy for the production of reducing equivalents and energy necessary to organicate carbon. Photosynthesis is a very important biological process because it is capable of supporting life on Earth. It is a complicated process that requires the involvement of several protein complexes: in general, during the photosynthetic activity, the light energy is absorbed by the antennas (protein-pigment complexes) of photosystems and used for the reduction of CO_2 to carbohydrates. The entire process can be represented schematically by the following equation:

$$CO_2 + H_2O + \text{LIGHT} \longrightarrow CH_2O + O_2$$

where CH_2O is the carbohydrate formed.
Photosynthesis is divided into two main phases, the light phase and the dark phase (or assimilation) (Figure 7).

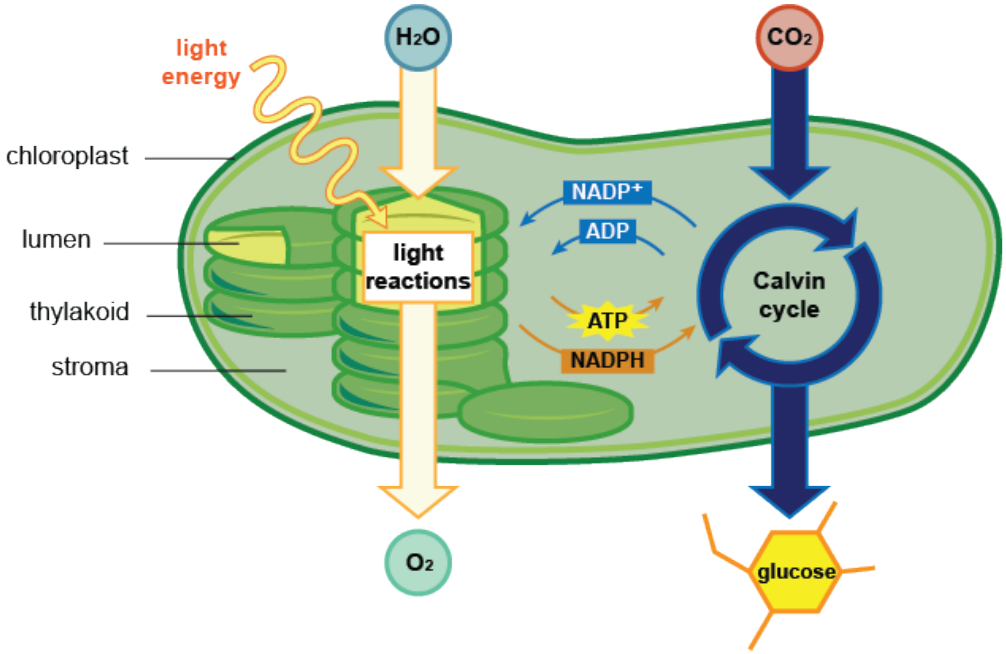

Figure 7 – Schematic representation of light phase and dark phase (C assimilation) in the photosynthetic process (http://www.shmoop.com/photosynthesis/inputs-architecture.html).

In the reactions of photosynthetic electron transport (light phase), solar energy energizes an electron in chlorophyll, making it able to move along a chain of redox reactions in the thylakoid membranes. This process of electron transport generates high energy electrons that can reduce the $NADP^+$ and at the same time determines a proton gradient across the membrane which is used for the synthesis of ATP. In the phase of assimilation NADPH and ATP are used, respectively, as a source of reducing equivalents and of energy for the reactions that determine the conversion of carbon dioxide into carbohydrates, in a series of reactions known as the Calvin cycle. The reactions of the light phase are performed by multi-protein complexes localized in the thylakoid membrane that, in photosynthetic Bacteria, is constituted by a "specialization" of the plasma membrane, while in plants is localized in the chloroplast, the intracellular organelle deputed to photosynthesis. The chloroplast is bounded by a double membrane: the inter-membrane space between the two membranes is greatly reduced, while the space delimited by the inner membrane, the stroma, is

much greater. The stroma contains the third system of membranes, the thylakoids. The continuous space inside the whole body of thylakoid membranes takes the name of *lumen*. In oxygenic photosynthetic organisms, like higher plants, algae and Cyanobacteria, the first phase of photosynthesis is carried out by protein complexes of the thylakoid membrane: the Photosystem II (PSII) and the relative antenna apparatus or Light Harvesting Complex (PSII-LHCII), cytochrome b_6f (cyt b_6f), Photosystem I (PSI) with its antenna (PSI-LHCI) and the ATP-synthase. The reactions of the dark phase takes place in the stroma of chloroplasts or in the cytoplasm in the lower organisms.

1.3.1 The chloroplasts: structure and function

The chloroplast (Figure 8) is an autonomous organelle, being a site of fundamental biosynthetic functions in plants. It is delimited by an envelope, composed of two independent lipid membranes, physically separating the internal environment of the plastid from the cytoplasm.

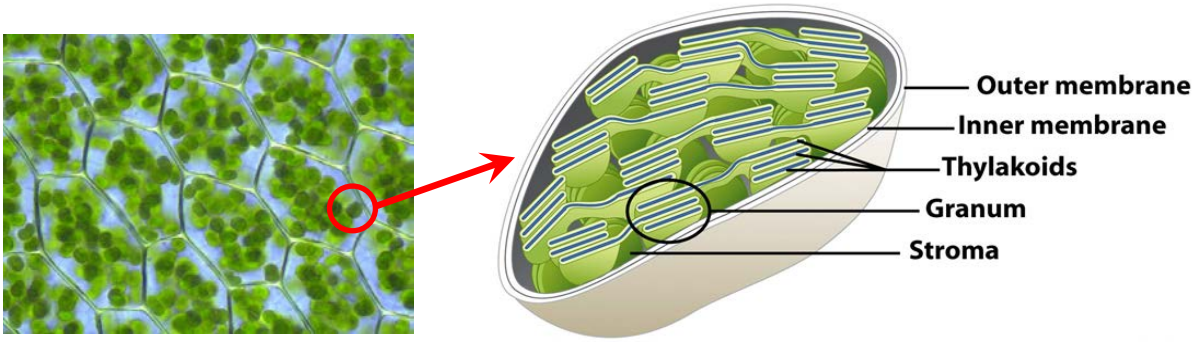

Figure 8 – Schematic representation of chloroplast structure and of its membrane composition (© Pearson Prentice Hall, Inc., modified).

Both membranes of the envelope are distinct in structure, function and biochemical properties, but at the same time they cooperate in several important physiological processes, such as the synthesis of lipids or the translocation of proteins in the chloroplast. The inner membrane delimits an aqueous space, called stroma: in this environment, there are the plastid genome, a complete apparatus for the transcription and translation, starch granules and lipid bodies. The stroma contains also a third membrane system, the thylakoids (collected in stacked tank structures, called *grana*, interconnected by stromal lamellae), which accommodate the protein complexes responsible for the photosynthetic process. As it is evident from electron microscope photographs (Figure 9), the outer and the inner membranes are extremely close to each other and run in parallel: only at the level of the contact sites these two membranes are joined. Chloroplasts are the sites of reduction and assimilation of carbon dioxide into carbohydrates, amino acids, fatty acids and terpenes. All these biosynthetic functions require the existence of different mechanisms for the selective transport through the membranes of the envelope, in order to provide to the cell carbohydrate and compounds, Fe, nitrogen and sulfur (Neuhaus *et al*., 2000). Chloroplasts require inorganic cations (K^+, Na^+, Mg^{2+}, Ca^{2+}, Mn^{2+} and Zn^{2+}), anions (NO_2^-, SO_4^{2-}, PO_4^{3-}) and a variety of organic intermediates of biosynthetic pathways, such as phosphoenolpyruvate, dicarboxylic acids, acetate, amino acids and ATP, to achieve correct function of their biosynthetic pathways.

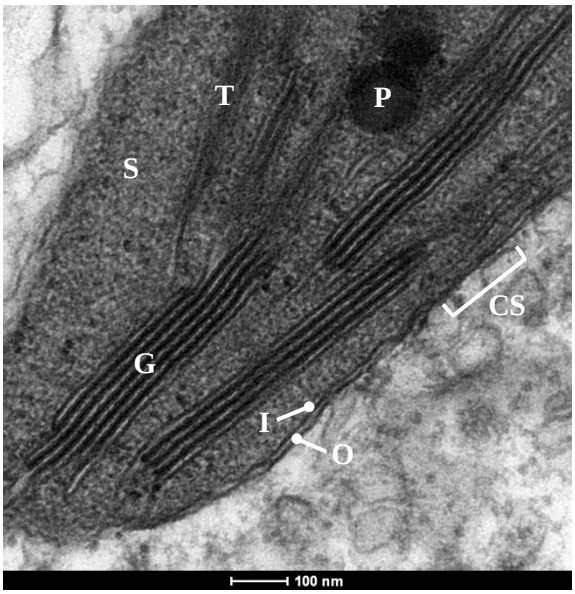

Figure 9 – TEM micrography of a region of a chloroplast (CS: contact site; T: thylakoids; G: *granum*; I: inner envelope; O: outer envelope; S: stroma; P: plastoglobule).

1.3.2 Photosystems

The Photosystems can be divided into two parts, one formed by the antenna (chlorophyll-protein complexes with light energy collection function) and the other consisting of the reaction centers with the dual function of electron transport chain and generation of proton gradient. The Photosystem I presents a set of pigments that are preferentially excited by light at a wavelength of 700 nm while the Photosystem II is energized more efficiently by light at a wavelength of 680 nm.

1.3.3 The "Z pattern"

In 1960 it was proposed by Hill and Bendall that the two Photosystems cooperate in determining the electrons' transfer from water to carbon dioxide. According to this model, called "Z pattern", the activity of the two coupled Photosystems allows to overcome the jump of redox potential existing between the water oxidation and reduction of $NADP^+$, not otherwise surmountable with the activity of a single Photosystem. The PSII, following the absorption of a photon, produces an oxidation potential sufficient to split water into oxygen and reducing equivalents transferred then to the cyt b_6f. When, instead, the PSI is energized, it produces the low redox potential necessary to reduce the $NADP^+$ to NADPH, via the ferredoxin. The two Photosystems are dipped in the thylakoid membrane and are connected by an electron carrier chain, the plastoquinone (PQ) and the plastocyanin (PC), and cofactors of the cyt b_6f complex (Figure 10). The primary event of the whole process is the excitation of PSII by light. In the excited state, PSII is able to extract an electron from the water, producing a molecule of oxygen every two molecules of water. This electron is ripped to replace the one given by excited PSII to cyt b_6f. The electron is then transferred through a chain of redox reactions, where each element of the path is reduced and then returns to the oxidized state by transferring the electron to the next element. The charge separation catalyzed by light at the level of the PSII and the PSI, simultaneously with electron transfer processes, generates a transmembrane proton gradient that feeds the phosphorylation of ADP to ATP by the ATP-synthase complex. This type of energy production in which the two Photosystems are involved is called non-cyclic phosphorylation, in opposition to the process of cyclic phosphorylation. In this latter process ATP is produced by generation of a proton gradient using only the cyt b6f complex and PSI. In this case the transferred electron does not originate from water, but from the PSI and is recycled to the same PSI.

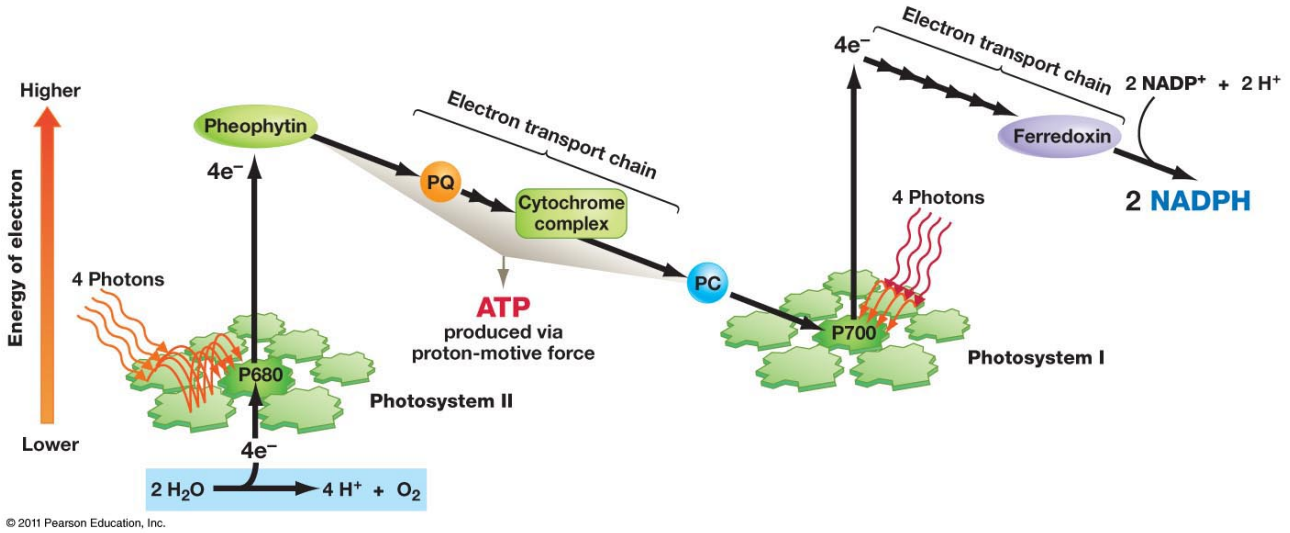

Figure 10 – The "Z pattern", representative of electron transfer and of various photosynthesis redox processes (© Pearson Education, Inc.).

1.3.4 Light absorption and electron transport

The fundamental event of photosynthesis consists in the absorption of light and in transfer of energy by pigment molecules. The photon absorption by a pigment causes the transition of an electron from the normal state to the excited, high-energy, singlet state. In the PSI and PSII the photon absorption by a pigment of the *antennae* is followed by a rapid transfer of excitation energy to the reaction center, where charge separation occurs. This initial event is stabilized and neutralized by subsequent redox reactions in the electron transfer chain. Optimized organization of the pigments of the antenna-proteins and cofactors in the reaction center allows to obtain a high capture efficiency and limits the loss of energy from other relaxation mechanisms. The antenna complex (LHC), moreover, allows the system to operate in a wide range of light intensities and wavelengths, thus increasing the overall efficiency. The key step for energy capture is the photo-induced charge separation between a primary donor (P) and a primary acceptor (A). Both in PSI and in PSII, the primary donors are chlorophyll molecules. After being excited by light, P becomes a powerful reducing agent (P*) and interacts with an acceptor (A) determining the primary event of the electron transfer:

$$P + A \xrightarrow{\text{Light}} P^* + A \longrightarrow P^* + A^-$$

The chlorophyll of PSII reaction center, called P680, is oxidized and the electron is transferred to the pool of plastoquinones. The P680 is reduced by the WOC complex (Water Oxidation Complex) with consequent oxygen production. Similar events, occurring at the PSI, result in the reduction of ferredoxin, and then of $NADP^+$ to produce NADPH, and the oxidation of plastocyanin or cytochrome c (cyt c) by the chlorophyll of the P700 reaction center. For both the PSI and PSII, inorganic and organic cofactors are used for the electron transfer. The process of electron transfer between PSI and PSII involves the cyt b_6f complex, a protein complex containing membrane-embedded cytochromes and iron-sulfur center, called Rieske. The cyt b_6f complex catalyzes the oxidation of plastoquinol and the reduction of plastocyanin or cyt c. At the same time, cyt b_6f complex pumps protons into the thylakoid *lumen*, generating a H^+ electrochemical gradient then used by ATP synthase to synthesize ATP. This complex is also involved in cyclic electron flow around PSI. The complex of PSII contains more than 20 different polypeptides and cofactors. The reaction center is formed by membrane proteins Dl and D2 and cyt b559, that is closely associated

with the internal *antennae*, consisting of complexes of chlorophyll a and CP47 and CP43 proteins. The PSII is completed with an external *antenna* (LHCII, Light Harvesting Complex II), consisting of chlorophyll a/b binding proteins. Associated with the reaction center, on the lumenal side, is also present the WOC complex, where takes place the photolysis of water molecules.

1.3.5 Ion channels of chloroplasts

The presence of ion channels in the membranes of chloroplasts has been known for many years thanks to the application of electrophysiological techniques, however in almost all cases the molecular identity of the proteins diving rise to these activities is unknown. There are numerous activities that have been attributed to various channels in different membranes of chloroplasts. Over the years, the different ionic conditions used by various authors and the limited pharmacology made it difficult to understand if all these activities described are due to different proteins, or if some activities correspond to those already described above. For example the channel of 1016 pS (in 100 mM KCl) described by Pottosin (1992) in the outer membrane could correspond to the channel of 730 pS (in 100/50 mM KCl) described by Muniz (1995). While taking account of these limitations, it can be assumed that there are a number of separate selective or non-selective channels. Most of these measurements were performed on chloroplasts of higher plants, when the genome of *Arabidopsis thaliana* was not sequenced completely yet, thus preventing an albeit hypothetical molecular identification of the relevant activities. A further complexity is given by the fact that organellar ion channels in mammals as well as in plants are encoded by nuclear genes, therefore limits in the accuracy of targeting prediction programs leads to the requirement of experimental evidences when it comes to determination of the localization of ion channels.

1.3.6 The role of ion channels in the regulation of photosynthesis

In the ‘70s a few studies suggested an important role for ion channels in the regulation of photosynthesis. Unfortunately, at that time, the pharmacology and genetics of the channels were still at the initial state, therefore it was not possible to use drugs, inhibitors or activators of specific channels. Furthermore, the molecular identity of plant channels was rather obscure because, with very few exceptions (Schulenburg *et al*., 1992), the use of more specific inhibitors has not been taken in consideration until the 80s. Nevertheless, there are old works (one of these is Deamer and Packer, 1969) from which the existence of chloride channels and cationic channels selective for K^+ and Mg^{2+}, proposed to play an important role in the regulation of photosynthesis emerged. In particular, it was suggested, that these channels might be involved in the electric counterbalance. During photosynthesis, a light-driven flux of protons from the stroma to the lumenal side of the thylakoid membrane occurs *via* photosytem PSII water splitting, plastoquinone reduction and cyt b_6f turnover. These processes lead to the formation of a pH gradient and to the development of a transmembrane electrical potential. Ion fluxes across thylakoid membranes might contribute to regulation of photosynthesis and respiration by modulating the electric component of the transthylakoid proton motive force (pmf, composed of osmotic component ΔpH and of electric component $\Delta\Psi$). Recent works indicate an approximate 50% contribution of the electric field to steady-state transthylakoid pmf in higher plants and eukaryotic algae (Cruz *et al*., 2005; Kramer *et al*., 2003). In higher plants, it has been postulated that the efflux of cations from the *lumen* toward the stroma or flux of anions in the opposite direction (Schönknecht *et al*., 1988; Barber *et al*., 1974) would permit dissipation of the transmembrane electrical potential while conserving the pH gradient (Checchetto *et al*., 2012). If this does not happen would develop a membrane potential, as in fact happens in the case of the mitochondrial membrane, where the effective permeability to various cations and anions is less than what is found in the thylakoid membrane. Also, the control of Ca^{2+}

levels in the chloroplast has become increasingly important as it has been proposed that Ca^{2+} can regulate the activity of key enzymes in the assimilation of CO_2 and the activity of the oxygen evolving complex (Brand and Becker, 1984; Grove and Brudvig, 1998; Loll *et al*., 2005).

1.4 Glutamate Ionotropic Receptors (iGluRs)

1.4.1 Animal ionotropic receptors

Ionotropic receptors are ion channels activated by the binding of their ligand: in animals, they mediate the majority of excitatory nerve transmission in the brain, but they also seem to have different functions outside of the nervous system, such as the secretion of insulin, bone resumption, cardiac pacemaking and tactile sensation (Ault and Hildebrand, 1993; Carlton *et al*., 1995; Chenu *et al*., 1998; Gill *et al*., 1998; Inagaki *et al*., 1995; Jorgensen *et al*., 1995; Patton *et al*., 1998; Weaver *et al*., 1996). They're also thought to be involved in learning and memory. Many of their failure are connected to several diseases, such as epilepsy, ischemic damage and are also implicated in pain perception (Dingledine *et al*., 1999). There are two classes of glutamate receptors: ionotropic and metabotropic ones. Ionotropic receptors are ion channels. Instead, metabotropic receptors activate G proteins: they have not their own channel, but possess transmembrane segments similar to those of receptors coupled to G proteins, but with an extracellular domain that is more similar to the domain for the binding of ligand in ionotropic receptors (O'Hara *et al*., 1993). In mammals more than 20 different ionotropic GluR subunits, encoded by 6 gene families have been identified; on the basis of activation by various agonists, ionotropic GluRs can be divided into three categories: kainate receptors, the AMPA (α-amino-3-hydroxy-5-methyl-4-isoxazole propionate) and NMDA (N-methyl-D-aspartate) (Figure 11). The kainate receptors are activated by seaweed toxin and glutamate: both induce a full activation and rapid desensitization (closure of the pore, although it is still tied to the agonist) for this class of iGluRs. AMPA receptors are activated and desensitized quickly and completely by AMPA and glutamate, but only partially by kainate. Finally, the NMDA receptors comprise two subtypes (NR1 and NR2), have a slow activation and desensitization, and need both glycine and glutamate for the complete activation, respectively bound to the NR1 and NR2 subunits. The ion selectivity is generally cationic in these receptors: Na^+ and K^+ permeate similarly; only Ca^{2+} permeates more in NMDA receptors. In addition to the described receptors, there are two orphan subunits in mammals (δ1 and δ2): they have a low amino acid identity (18-25%, Lomeli *et al*., 1993) with iGluR, they don't themselves form a channel, nor can modulate the activity of iGluR; mutation in a δ2 subunit, however, leads to neurological pathology associated with the "Lurcher" phenotype in mouse (Zuo *et al*., 1997; Kashiwabuchi *et al*., 1995). Finally, homologous of iGluR were cloned from Prokaryotes organisms (Chen *et al*., 1999; Kuner *et al*., 2003; Mayer *et al*., 2001), from various invertebrates (Schuster *et al*., 1991; Maricq *et al*., 1995) and plants (Lam *et al*., 1998; Davenport, 2002; Kang and Turano, 2003; Kim *et al*., 2001; Lam *et al*., 1998). In addition to the agonists discovered so far, numerous other modulators have been developed, displaying different efficiency and specificity (Brauner-Osborne *et al*., 2000), but none with a specificity directed to a single subunit. Despite pharmacological differences, all of glutamate ionotropic receptors share the same basic structure.

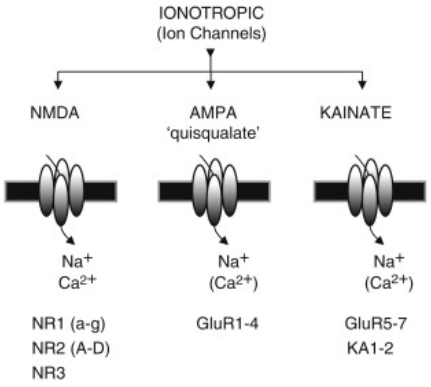

Figure 11 – Representation of various types of ionotropic iGluRs receptors (modified from Cryan and Kumlesh, 2008).

1.4.2 Structure of animal ionotropic glutamate receptors

The structure of ionotropic glutamate receptors (Figure 12) has the characteristic of being built in modules, with an extracellular N-terminus and a cytosolic C-terminus:

• Membrane portion: has four helices, three helices are transmembrane segments (M1, M3 and M4) the fourth is partially surrounded by the cytosolic side (M2), it participates in the formation of the pore because there are key residues for the control of permeability of these channels;
• ATD domain (amino-terminal domain): is involved in binding of modulators of many receptors and has been implicated in the modulation of desensitization in NMDA receptors (Krupp *et al*., 1998; Choi and Lipton, 1999; Fayyazuddin *et al*., 2000; Zheng *et al*., 2001); in non-NMDA, it seems to contribute to the assembly of the receptor (Ayalon and Stern-Bach, 2001);
• Ligand binding domain (LBD or S1S2 domain): has a structure of two lobes (S1 and S2), formed by different portions (the loop between helices M3-M4 and the portion between the helices and the M1 ATD domain);
• The flip/flop region: is an α-helical structure present on the opposite side with respect to the opening of S1S2 domain, which can exist in two different forms, or flip/flop (the result of alternative splicing, Sommer *et al*., 1990) and which may confer different properties of desensitization to receptors (Mosbacher *et al*., 1994);
• C-terminus domain: is the most variable portion of the receptors; may be a short sequence of 50 amino acids or an entire domain, capable of interacting with other proteins containing PDZ domains (domains of interaction between peptides, Bolton *et al*., 2000).

Regarding the ATD domain, there is no structural information, although sequence similarity suggests that it may be related to the LIVBP (leucine-isoleucine-valine binding protein, structure of two lobes, each with α-helices and a central β-core) and to the domains of the metabotropic receptors (O'Hara *et al*., 1993). In this case, this would suggest a bilobated structure for the ATD domain, though a specific ligand for this domain has not been identified yet. As already mentioned, the iGluR channels are activated by the binding of specific ligands: currently, crystallographic structures of S1S2 domains for numerous receptors, such as the iGluR2 (Armstrong *et al*., 1998; Armstrong and Gouaux, 2000; Högner *et al*., 2002, 2003; Jin and Gouaux, 2003; Jin *et al*., 2003; Lunn *et al*., 2003), GluR0 (Mayer *et al*., 2001) and NR1 (Furukawa and Gouaux, 2003), complexed with various agonists and antagonists are available. This has allowed to understand in greater detail the structure and the mechanism of function. The structures of the S1S2 domain of iGluR2 without

ligand and complexed with an antagonist and an agonist, partial or complete, have highlighted how the two lobes can be close to each other: this mechanism, called "Venus-flytrap", allows the complete closure of the two lobes as a result of the binding of a full agonist; on the contrary, in the ligand-free form the two lobes are open. Binding of an antagonist stabilizes the domain in this open form. The partial closure of the two lobes by partial agonists leads to an incomplete activity of the channel as well. In practice, the level of closure of the lobes differs not only between agonists and antagonists, but also between partial/total agonists (Armstrong and Gouaux, 2000). However, despite the many details of the S1S2 domain it is still unclear how the closure of the two lobes can result in the opening of the channel; according to some models (Armstrong and Gouaux, 2000; Mayer *et al*., 2001), closing the gap between the two lobes in a subunit would push the transmembrane domain of the same subunit off the pore axis, resulting in the opening. The binding of the agonist leads to the opening (middle part) through a conformational change that is transmitted by the S1S2 domain to the transmembrane pore domain. Subsequently, a slip of the subunits would allow the pore to close again, while the S1S2 domain remains in the closed conformation with the attached ligand (desensitization).

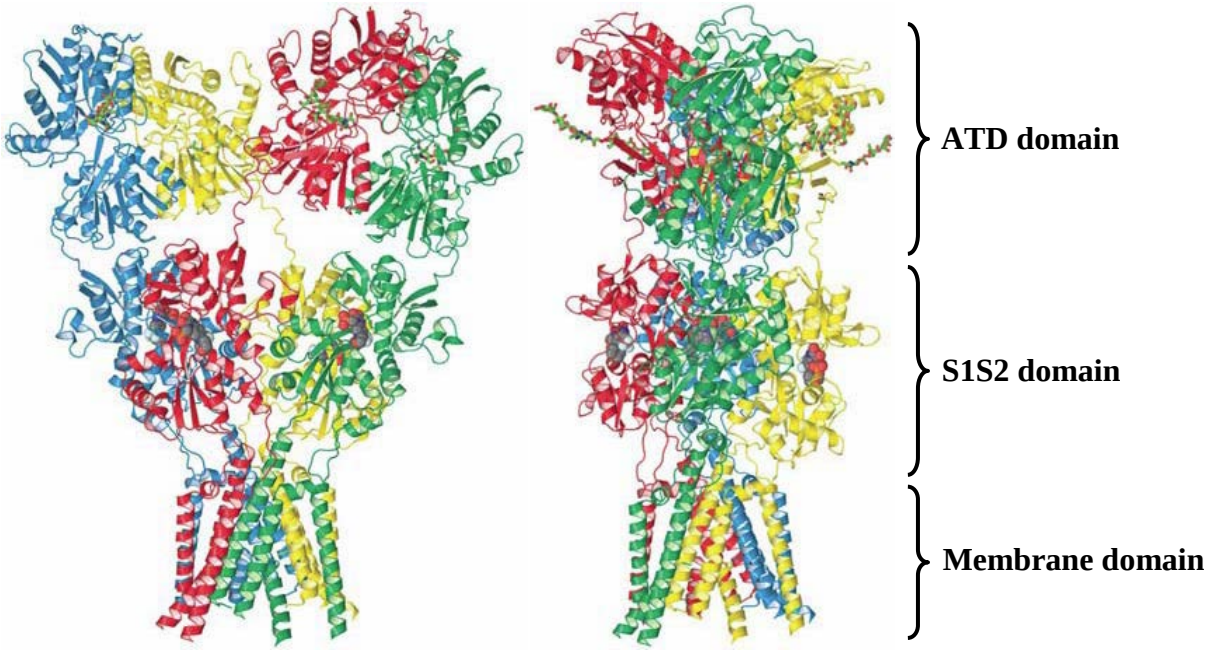

Figure 12 – 3D structure of a iGluR receptor (modified from Sobolevsky *et al*., 2009).

1.4.3 Stoichiometry and assembly

Despite the numerous studies on S1S2 domain, the spatial arrangement of the domains, as well as the structure of individual subunits, remains to be clarified. Even the proposed stoichiometry, i.e. a tetramer, was highly discussed. (Kuusinen *et al*., 1999; Ayalon and Stern-Bach, 2001; Rosenmund *et al*., 1998; Laube *et al*., 1998; Safferling *et al*., 2001). In 2001 the first evidence was provided on the assembly of tetrameric iGluRs (Ayalon and Stern-Bach, 2001) as dimers of dimers: tetramerization occurs primarily by an initial dimerization via ATD domain, these dimers then take part to a second dimerization mediated by S2 and/or the transmembrane domains. The AMPA and kainate channels are homo- or hetero-multimers, unlike the NMDA that are homo-multimers. In any case, the iGluR subunits can co-assemble with multiple subunits of the same family, giving different combinations. In addition, alternative splicing, RNA editing, and post-translational modifications may contribute to increase the variability of the structure of these channels.

1.4.4 Pore structure

The crystallographic structure of glutamate ionotropic receptors has been obtained only for the S1S2 domain: with regard to the pore, the structure can only be inferred through homology modeling softwares (Chohan *et al*., 2000) basing the analysis on a comparison with the structure of K^+ channels (Doyle *et al*., 1998; Jiang *et al*., 2002, 2003). When the transmembrane topology outlined (Wo *et al*., 1995; Wood *et al*., 1995), it became clear that there is a structural homology of the P-loop (the loop forming the pore) of K^+ channels with the pore of iGluR receptors: a consensus motif (tryptophan, phenylalanine, tryptophan, 8X, G, 3-5X, proline) has been identified that is common to the regions of the pore of the two channels. In the case of K^+ channels, however, this loop is inserted into the membrane from the extracellular side, while in the receptors is inserted from the cytosolic side, suggesting that receptors and K^+ channels have a similar structure, but reversed. Scanning mutagenesis experiments carried out on both channels confirmed their structural similarity: the accessibility of specific amino acids (cysteine, alanine and tryptophan) show a similar pattern for the two classes of channels (Kuner *et al*., 1996, 2001; Panchenko *et al*., 2001; Kurz *et al*., 1995; Pascual *et al*., 1995). In conclusion, the homology modeling and experimental evidences agree with a domain structure for receptors that similar to that of K^+ channels, but with inverted membrane topology. With regard to the M3 helix, this seems to have an important role in the gating: mutations in this helix (responsible for the "Lurcher" phenotype in mouse) convert for example the δ2 receptor in a constitutively active form (Zuo *et al*., 1997). Similar mutations are responsible for constitutively active forms in other receptors (Kohda *et al*., 2000). These data suggest that this helix is involved in gating, also because it is the most highly conserved transmembrane domain between the glutamate receptors; this domain also presents homologies with the helix positioned after the P-loop (Kuner *et al*., 2003) in K^+ channels: in these channels, two glycines positioned on this propeller, appear to be fundamental for the gating (Jiang *et al*., 2002), but mutations in glycines of M3 helix of glutamate receptors have no effects on gating (Sobolevsky *et al*., 2003), suggesting that, despite the structural similarity, the mechanism which regulates the opening/closing of these receptors is different from that of the K^+ channels.

1.4.5 Plant ionotropic glutamate receptors

In plants, the information for this class of channels is still limited and the first receptors in plants have been characterized only recently (Kim *et al*., 2001; Kang and Turano, 2003; Kang *et al*., 2004; Meyerhoff *et al*., 2005, Li *et al*., 2006). The discovery of these channels in plants became possible only after the complete sequencing of the genome of *Arabidopsis*: subsequent bioinformatic analysis have in fact identified 15 genes for putative K^+ channels, a gene for a channel similar to a voltage-dependent Ca^{2+} channel and 40 genes that encode for many cation-selective channels (Demidchik *et al*., 2002). Surprisingly, these 40 genes are correlated with ion channels already known and characterized in animals, but for which no physiological evidence had been detected in plants: these are cyclic nucleotide-binding dependent ion channels and ionotropic receptors for glutamate. The first group collects inward rectifying K^+ channels, whose opening is dependent on cyclic nucleotides (Leng *et al*., 1999, 2002). With regard to the iGluR receptors, sequence similarity searches have identified 20 genes in *Arabidopsis* that encode for putative receptors (Lacombe *et al*., 2001; Chiu *et al*., 2002). The first evidence on the existence of these channels in plants was obtained already in 1998 (Lam *et al*., 1998). Phylogenetic analysis of the *Arabidopsis* receptor genes has allowed to divide these into three distinct clades. This analysis is based on the current nomenclature of ionotropic receptors: for each clade is assigned a number X (from 1 to 3) and for the genes within a clade a growing number Y, so that any single gene may have a name *At*GluRX.Y. The identification of these 20 putative receptors in plants suggests that a primitive

signaling mechanism that would involve excitatory amino acids or similar small molecules existed before the divergence between animals and plants (Chiu *et al*., 2002).

1.4.6 Structure of plant ionotropic glutamate receptors

Plant receptors have a primary structure that is similar to that of the animal receptors with the highest amino acid sequence identity at the level of the ligand binding domain (S1S2 domain) and the transmembrane domain between the helices M1, M2 (P-loop) and M3. In particular, the M3 helix is the most conserved, although in plants lacking two residues (proline and lysine/arginine) highly conserved in animal receptors except in δ ones (δ1 and δ2 iGluRs). The most significant difference is in the M2 helix, that forms the pore: the unusual sequence of the pore therefore suggests a selectivity mechanism that is different from that of animals (Lam *et al*., 1998). Plant ionotropic receptors (Figure 13) therefore are hypothesized to occur with 4 transmembrane helices (M1-M4) of which the second is only partially in membrane, a ligand binding domain (formed by the two regions S1 and S2, separated by M1-M3 helices), and a long N-terminus domain of unclear function (possible role in the allosteric modulation of Ca^{2+} and other metabolites).

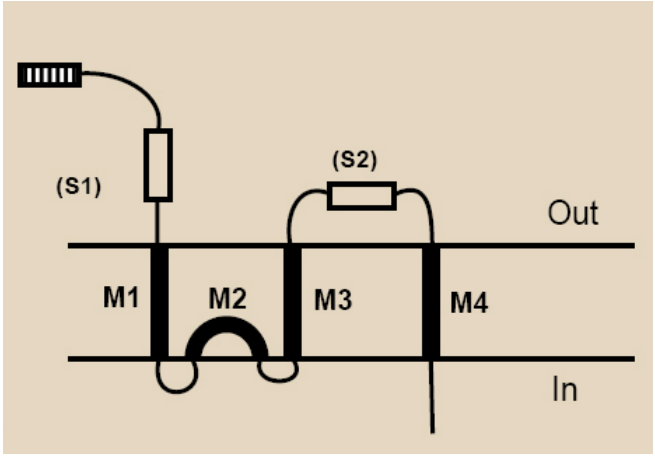

Figure 13 – Transmembrane topology of a plant iGluR receptor (modified from Lam *et al*., 1998).

1.4.7 Tissue-specific expression

Arabidopsis has a large family of receptors that may be involved in many functions. To understand if the three clades represent functionally distinct classes of proteins, the pattern of *m*RNA expression of all 20 genes must be examined. Since the receptors function as hetero-multimers, determining the specific tissue and cell type expression pattern, it will be maybe also possible to determine which gene products can potentially interact *in vivo*. This aspect is particularly interesting considering that the hetero-multimeric co-assembly can deeply influence the function of these proteins (Nitabach *et al*., 2001). By RT-PCR, it was possible to obtain the profile of *m*RNA expression of 20 genes in four different organs (Chiu *et al*., 2002), namely in leaf, root, flower and siliqua. The expression profiles show an overlap between the three clades: while the genes of clades I and III are expressed in a more ubiquitous manner, the genes of clade II are more specific for the roots. The three clades are not functionally distinct classes and may contain genes with similar functions *in vivo*. Five of nine clade II genes are expressed exclusively in roots suggesting that only this could be a functional class of receptors. In the same work, the expression of receptors in different cell lines was also evaluated the expression of receptors in different cell lines, preparing transgenic plants that express a construct with promoter/reporter gene.

1.4.8 Intracellular localization

Another much debated point is the intracellular localization, although the general idea is that they are mainly present in the plasma membrane. According bioinformatics softwares, most of the *Arabidopsis* receptors are directed towards the secretory pathway, which includes all the proteins processed in the endoplasmic reticulum and subsequently transported to the plasma membrane, to the tonoplast or to peroxisomes (Johnson and Olsen, 2001). Only two receptors seem to have a different target: they are the *At*GluR3.3 and *At*GluR3.4, whose predicted location are the mitochondria and chloroplasts, respectively. In 2011 was confirmed the subcellular localization for *At*GluR3.4 in chloroplasts and plasma membrane (Teardo *et al*., 2011). Also for another iGluR, *At*GluR3.5, is predicted a mitochondrial and plastidial localization (according to Aramemnon, http://aramemnon.botanik.uni-koeln.de/) for the two splicing variants detected. In the second section of this thesis is presented a submitted work regarding the splicing variants for *Atglr3.5* gene, responsible for its double-localization pattern.

1.4.9 Gating of plant ionotropic GLR channels by glutamate

A controversial point on the mechanism of receptor functioning in plant is the ability to bind glutamate or other agonists. The high similarity of S1S2 domain between plants and animals would suggest a dependence of these channels from their agonist: there are many evidences that confirm this point, but no direct evidence has been reported yet. The possibility that glutamate could open Ca^{2+}-permeable channels in the plasma membrane was initially assessed by measuring the concentration of cytosolic Ca^{2+} in transgenic plants that express aequorin, a Ca^{2+}-dependent luminescent protein (Knight *et al*., 1991). With this system, Dennison and Spalding (2000) have seen that the application of 1 mM glutamate in the growth medium of *Arabidopsis* leads to a rapid increase in the concentration of cytosolic Ca^{2+} and causes depolarization of the membrane of root cells. The addition of arginine, aspartate, D-glutamate or agonists of animal NMDA receptors and AMPA didn't give results comparable to those of glutamate, while pretreatment with La^{3+}, an inhibitor of Ca^{2+}-channels, prevents the increase of Ca^{2+} and the depolarization of the membrane. These effects are attributed to the activation of glutamate-dependent Ca^{2+} channels of the plasma membrane, although we cannot exclude that may be due to the activation of secondary flows of Ca^{2+} uptake as a result of glutamate. In similar experiments, exposure of root protoplasts of *Arabidopsis* to millimolar concentrations of glutamate induces an increase in non-selective cationic currents (Na^{+} and Ca^{2+}, Demidchik *et al*., 2004). In mesophyll cells of transgenic *Arabidopsis* plants (which express aequorin), the application of glutamate induces a depolarization of the membrane potential and dose-dependent Ca^{2+} transients (Meyerhoff *et al*., 2005): both responses to glutamate are also sensitive to inhibitors of ionotropic receptors. The capacity of glutamate to evoke Ca^{2+} transients is only an indirect evidence of the involvement of ionotropic receptors: currently, there are two works in which Ca^{2+} transients induced by glutamate are connected directly to a specific receptor. Qi *et al*. (2006) showed that the Ca^{2+} influx and membrane depolarization is missing in the *At*GluR3.3 gene knockout mutants. Finally, transgenic lines of *Arabidopsis*, overexpressing an ionotropic receptor of *Raphanus sativus* (radish), showed stronger transient changes in the concentration of cytosolic Ca^{2+} induced by glutamate if compared to wild-type plants (Kang *et al*., 2006). One aspect in the plants is the possibility that glutamate is not the only natural ligand: in fact, plant receptors resemble especially animal NMDA receptors. These, for their complete activation, need both glutamate and glycine. Always using transgenic plants that express aequorin, Dubos (2003) has shown that glutamate and glycine act synergistically to mediate Ca^{2+} flows and to adjust the hypocotyl elongation, phenomena both inhibited by DNQX, an inhibitor of ionotropic receptors. Although it has been suggested (Chiu *et al*., 1999) that some plant receptors can be

constitutively active (and therefore insensitive to agonists), it is nonetheless clear that glutamate acts on these channels leading to a whole series of responses ranging by variations in the concentration of Ca^{2+} in the regulation of various physiological processes. In support to this last statement, in Vincill *et al*., (2012) is reported that iGluR3.4 is activated by glutamate (and at least by other three structurally-different amino acids, like serine, glycine and asparagine) and shown high selectivity for Ca^{2+} ions in standard HEK cells patch clamp recording conditions.

1.4.10 Physiological roles

Glutamate has always been considered as an important molecule for signaling in animals, where it assumes the role of excitatory neurotransmitter. The glutamate signaling, initially deemed exclusive of animal systems, is becoming increasingly important in plants because of the broad phylogenetic distribution of ionotropic receptors. The presence of animal homologous receptors in plants, invertebrates and Prokaryote organisms leads us to believe that the role of glutamate as a signalling molecule has very ancient origins. Only recently, as we saw in the previous section, the first evidence of the physiological function of glutamate and ionotropic receptors appeared. However, much remains to understand about the physiological roles of these channels and their involvement in glutamate signaling. The ability of the iGluR receptors to form channels is still under discussion, as it is very difficult to clone and express them in heterologous system. In *E. coli*, the genes for the plant receptors encode proteins that cause an ion imbalance that is toxic. Problems of expression have also been seen with eukaryotic systems: toxicity of the channel, incorrect folding, post-translational modification or the need for several other subunits for the correct assembly of these channels are the main causes. Two cases of receptors expressed in *Xenopus* oocytes have been reported: the expression of *At*GluR3.7 gives rise to a non-selective cation channel permeable to Ca^{2+} and constitutively active; also the expression of *At*GluR3.4 in oocytes or HEK cells (Human Embryonic Kidney) leads to a voltage-dependent cationic current and insensitive to glutamate (Lacombe *et al*., 2001). In whole plants there are many indications that iGluR receptors may mediate ion fluxes, especially of Ca^{2+} through the plasma membrane, but the significance of these concentration changes is still unclear (Demidchik *et al*., 2004; Dubos *et al*., 2003; White *et al*., 2002; Dennison and Spalding, 2000, Meyerhoff *et al*., 2005). The functions attributed to date to iGluR receptors are based especially on pharmacological studies. The use of β-Methylamino-L-Alanine (BMAA), an agonist of mammalian iGluRs, was shown to inhibit *Arabidopsis* root growth and cotyledon opening, and to stimulate elongation of light-grown hypocotyls (Brenner *et al*., 2000). On the contrary, when *Arabidopsis* seedling were light-grown in a medium containing DNQX, an antagonist of iGluRs, a long-hypocotyl phenotype was detected, suggesting a possible role of iGluRs involvement in light-signal transduction (Lam *et al*., 1998). The intracellular distribution of glutamate is critical for its various roles (Davenport, 2002): in this context ionotropic receptors localized in endomembrane may signal local concentrations of nitrogen, N. In plants, in fact, the amino acid signalling has evolved in different directions to become important as a sensor for the N and the *ratio* N:C. For example, the presence of endogenous glutamine at high concentrations has been associated with a feedback inhibition of N uptake in the roots (Rawat *et al*., 1999; Zhuo *et al*., 1999). The key amino acids of the N assimilation, storage and long-distance transport are glutamate and glutamine (the first product of assimilation of N) and aspartate and asparagine (synthesized from glutamate and glutamine). Glutamate is synthesized in the cytosol, in the plastids and probably in mitochondria, and it works as an intermediate in the photorespiration cycle in peroxisomes. The contribution of the different organelles to N metabolism varies depending on the type of tissue, exposure to light and nutrient status in the plant: any receptor localized in internal membranal systems may then release Ca^{2+} from intracellular stores to change the expression of genes involved in the assimilation of N in response to different intracellular levels

of glutamate. More generally, Ca^{2+} transients may represent the first step in the process of transduction of environmental stimuli in physiological responses mediated by ionotropic receptors for glutamate. For example, using transgenic plants of tobacco which express aequorin in the chloroplasts, flow of Ca^{2+}, induced by stromal light-dark transition in plants were observed (Sai and Johnson, 2002). Alternatively, the ionotropic receptors may also function as glutamate-dependent channels for NH_4^+. NH_4^+ is absorbed by plant roots and is also the main intermediate in the assimilation of N (from the reduction of NO_3^-) and in its re-assumption during photorespiration, in the recirculation of proteins and seed germination. NH_4^+ is assimilated into amino acids for long-distance transport, but inside the cell it travels between the chloroplasts, the mitochondria and the cytosol during release and uptake, and then is retained within the vacuoles. Receptors localized in the plasma membrane or in endomembrane may participate in the transport of NH_4^+ between cells or between intracellular compartments in response to changes in the level of amino acids that signal the request for a greater assimilation or deposit of N (Davenport, 2002). Plants have then developed mechanisms that allow them to sense and respond to changes in the level of C and N: these mechanisms regulate the expression of genes and the activity of proteins involved in the transport and metabolism of these two elements, allowing the plant to optimize the use of energy resources (Dubos *et al*., 2005). In fact, sources of reduced N, as NH_4^+, glutamate or glutamine, negatively regulate the transcription and the activity of the transport systems of nitrates (Coruzzi *et al*., 2001). Furthermore, using an "antisense" strategy (Kang and Turano, 2003; Dubos *et al*., 2005), it has been shown that the receptor *At*GluR1.1 is involved in the perception of C:N *ratio*. The germination of anti-*At*GluR1.1 plants is inhibited by sucrose, but recovered in presence of NO_3^-: this receptor also regulates the accumulation of enzymes of the metabolism of C and N. Subsequently (Kang *et al*., 2004), it was seen that the same receptor regulates biosynthesis and signalling related to abscissic acid, suggesting that the *At*GluR1.1 receptor can integrate and regulate various aspects of the amount of C and N in order to ensure the normal development of the plant. Initially the receptors have been linked to photomorphogenesis (Lam *et al*., 1998; Brenner *et al*., 2000): *Arabidopsis* plants grown in a medium containing DNQX, a kainate receptor antagonist/AMPA, showed a phenotype similar to that of etiolated plants (hypocotyl elongation and low levels of chlorophyll) in a light pattern and in a dose-dependent manner. The same treatment does not cause any effect on plants grown in the dark, suggesting that the DNQX influenced the light signalling. As already mentioned, plant ionotropic receptors participate in the signalling of Ca^{2+}: in some cases, however, these channels may also affect its homeostasis. In *Arabidopsis* mutants that overexpress *At*GluR3.2 (Kim *et al*., 2001), the total content of Ca^{2+} does not change, but the plant requires three times more Ca^{2+} for optimal growth, suggesting that the distribution of Ca^{2+}, rather than the uptake, would be affected. Following the expression of the promoter it was seen that this receptor is present in star cells surrounding the vascular system of roots and shoots, giving to this receptor a role in Ca^{2+} discharging from the xylem. The author also proposed that overexpression of *At*GluR3.2 can interfere with the stoichiometry of hetero-multimers native receptor and reduce their ability to transport Ca^{2+}. Another aspect of the growth of a plant related with ionotropic receptors is the development of the roots: the main objective of the roots is to explore the soil to search water and nutrients. To achieve this goal, the roots are able to discriminate between the different nutrients, including those (such as NO_3^- and glutamate) that provide the same element (N) in different forms, and to modify their growth (Zhang *et al*., 1999; Linkohr *et al*., 2002; Filleur *et al*., 2005; Walch-Liu *et al*., 2006). At the molecular level the ability to distinguish NO_3^- and glutamate resides in the cells at the tip of roots: features of sensors for NO_3^- are not known, but for the glutamate ionotropic receptors are the best candidates (consider that almost all receptors are expressed in root, Chiu *et al*., 2002; Birnbaum *et al*., 2003). The application of exogenous glutamate to the roots shown specific and very evident effects in the development of the roots of *Arabidopsis* (Filleur *et al*., 2005; Walch-Liu *et al*., 2006): the growth of the primary root is strongly inhibited, and, in a second time,

also the secondary side. Altogether, the root is shorter and more branched. This effect is specific for this amino acid: aspartate, glutamine and glycine do not give the same effects, even at high concentrations. Furthermore, it was seen that the root responds to glutamate applied on the tip, but not in other parts: the cells of the root tip are then able to sense the presence of extracellular glutamate and to induce the reduction of the growth of the root itself. In line with these data is a work made of rice plants (*Oryza sativa*): an insertional mutant for *At*GluR3.1 receptor shown a phenotype with short roots, altered activity of root meristems and an increase in programmed cell death (Li *et al*., 2006). This receptor *At*GluR3.1 in rice plays a crucial role in the maintenance of cell division and in promoting the survival of cells of the root apical meristems. Finally, the presence of receptors in the roots was also associated with the response to toxic elements by the plant (Sivaguru *et al*., 2003): at radical level, the aluminum (Al) depolymerizes the cortical microtubules and depolarizes the plasma membrane. Through a pharmacological approach, it is shown that the response to Al may also depend on Ca^{2+} transients mediated by glutamate receptors: the advanced hypothesis is that the signalling in response to Al is started from an efflux of a ligand similar to glutamate through an Al-dependent anion channel and the subsequent binding of this ligand to glutamate ionotropic receptors.

1.5 MCU and calcium signalling

1.5.1 Ca^{2+} compartmentalization in plant cells

Plants respond to environmental changes, to quickly adapt their metabolism to the new external conditions. They react through different signal transduction pathways, but the most used for this purpose is the one that uses Ca^{2+} as a second messenger. In the cytoplasm of the cell, the Ca^{2+} concentration is maintained at levels much lower than the extra-cytoplasmic compartments (about 10000-fold difference) in order to not interfere with the phosphate metabolism; for this reason that ion must be compartmentalized. The compartmentalization occurs at the level of different organelles in plant cells and the maintenance of this difference in concentration leads to the generation of signals mediated by Ca^{2+}, in response to biotic and/or abiotic *stimuli* or stresses, thanks to the use of Ca^{2+} carriers or channels situated on cell membranes (Figure 14). In plant cells, as in those of animals, the compartments for the storage of Ca^{2+} ions are the endoplasmic reticulum and mitochondria; moreover, plant cell has the apoplast (the space between the cell walls) and the vacuole, the main retention compartment for Ca^{2+} in plants. In addition, calcium is accumulated also in chloroplasts where the major part of it becomes bound and only a small portion of calcium is free.

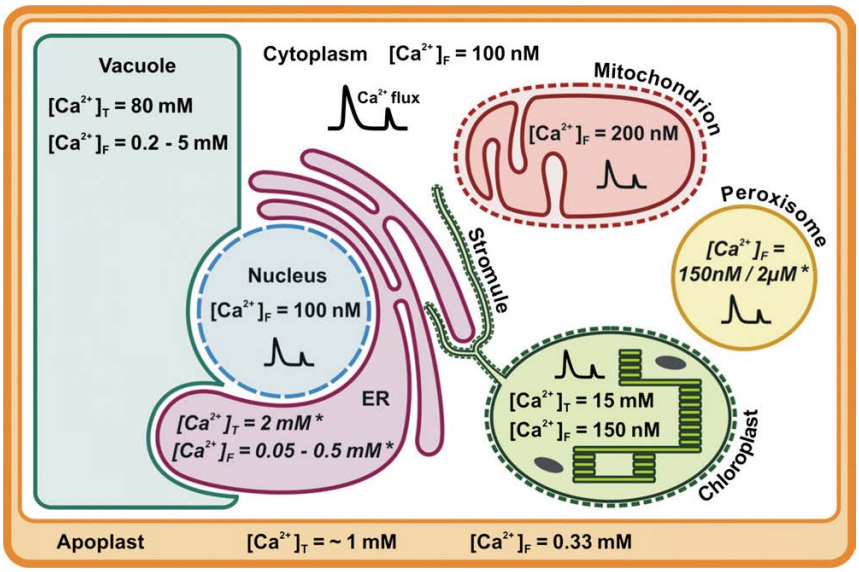

Figure 14 – Compartmentalization of Ca^{2+} in different cell organelles and its concentrations (from Stael *et al.*, 2012).

Vacuolar concentration of Ca^{2+} is comprised between 200 µM and 5 mM, to reach the maximum total Ca^{2+} (chelated and free) of 80 mM (Conn and Gilliham, 2010). A large amount of Ca^{2+} ions is chelated stably or is transiently bound to proteins, therefore not available to be used immediately in the signalling. In addition to the signalling, vacuolar Ca^{2+} can also regulate the activity of tonoplast channels or transporters (Peiter, 2011), like voltage-dependent Ca^{2+} channels that carry Ca^{2+} ions into the cytosol (Sanders *et al.*, 2002).

Little is known about endoplasmic reticulum and its use in plants as one of the main system for compartmentalization or for signalling usage of Ca^{2+}, given the lack, to date, of molecular information about ER ion channels involved in Ca^{2+} signaling. Some data concern the calreticulin, an ER protein capable of Ca^{2+} binding, important for regulating ion homeostasis in plants. Its overexpression in tobacco leads to greater retention of Ca^{2+} in ER, while its down-regulation in

Arabidopsis leads to a higher sensitivity to low concentrations of Ca^{2+} by the plant (Persson *et al*., 2001). From a comparison between Ca^{2+}-binding proteins in animals and plants, probably the calreticulin is the system of choice for the storage of Ca^{2+} in the ER (Nagata *et al*., 2004).
The apoplast is another major storage compartment for Ca^{2+}. It serves as a path for transfer of Ca^{2+} ions between the cells. The Ca^{2+} concentration must be strictly controlled, since at high concentrations does not allow the movement of stomata (Kim *et al*., 2010) with a resulting loss adjustment of gas exchanges; Ca^{2+} regulates also the rigidity of cell wall (Hepler, 2005).
In plants, the concentration of Ca^{2+} in mitochondria is approximately 200 nM (Logan and Knight, 2003), in the form of amorphous phosphate salt and ready to be released during the signalling (Chalmers and Nicholls, 2003; Starkov, 2010). In *Arabidopsis* mitochondria were observed different Ca^{2+} transients, due to responses to different types of stimuli (Logan and Knight, 2003). Some stimuli produce very similar Ca^{2+} gradients, for other ones Ca^{2+} flows represent a signature for that specific stimulus. So the mitochondria cannot be considered as simple reservoirs of Ca^{2+} available for signaling, but they may adjust their flows of Ca^{2+} to modulate a specific response.

1.5.2 MCU channels and mitochondrial calcium signalling

Mitochondrial Ca^{2+} uniporter (MCU) transports Ca^{2+} into mitochondria from confined areas at very high concentrations of cytosolic/ER Ca^{2+}. To date, various informations on the characteristics of MCU from bioenergetic experiments are available: 1) the ionic transport is drivenby the negative inner membrane potential, 2) it has low affinity for Ca^{2+}; 3) it is blocked by Lanthanides and ruthenium red. The molecular features of MCU have been described in several works (Perocchi *et al*., 2010; Baughman *et al*., 2011; De Stefani *et al*., 2011); in a study of integrated genomics and proteomics, a protein with EF-hand and targeted to the inner mitochondrial membrane has been found, and later it has been shown that it allows allows Ca^{2+}-dependent Ca^{2+} flow into the mitochondria. The protein has been called MICU1, but probably represents only the Ca^{2+} sensor (the regulator of MCU). Recently, a negative regulatory role has been proposed for MICU1, although direct, electrophysiological evidences are still missing (Mallilankaraman *et al*., 2012). Subsequent experiments, based on the characteristics and distribution of MICU1, as well as on search in the Mitocarta database, have identified a protein of about 40 kDa, identified as the Ca^{2+} channel called responsible for MCU activity. MCU consists of 2 transmembrane helices, connected by a loop containing the conserved amino acid sequence DIME (Figure 15).

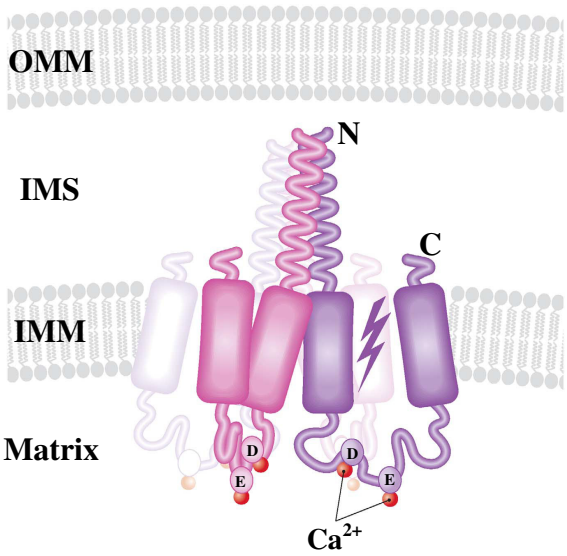

Figure 15 – Representation of MCU channel, according to De Stefani *et al.*, 2011. The amino acid residues D and E are responsible of Ca^{2+} selectivity (re-adapted from Drago *et al.*, 2011).

In *Arabidopsis thaliana* genome there are six genes encoding for putative proteins which show , homology to the mammalian MCU counterparts, sharing the transmembrane domains, the pore-loop domain and the conserved DVME signature sequence (Figure 16). It seems that *Arabidopsis* MCU isoforms are localized at the level of mitochondria, except for *At*5g66650, which seems to have a mitochondrial and plastidial dual localization (Schwacke *et al.*, 2003).

A

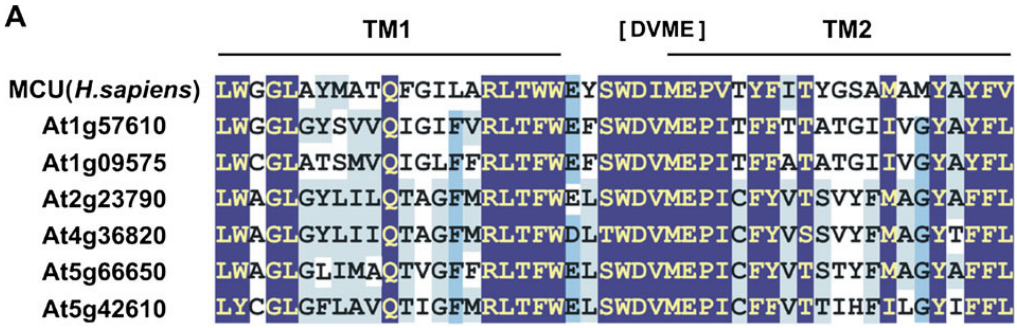

B

AGI	Aramemnon	Expression (Genevestigator)	ESTs (TAIR 10)
At1g57610 (5e-23)	mito (15.7)	low	18
At1g09575 (2e-20)	mito (20.1)	global	8
At2g23790 (1e-16)	mito (16.5)	flower	83
At4g36820 (3e-15)	mito (16.6)	low	46
At5g66650 (3e-13)	chloro (8.5)/mito (8.8)	guard cell/root	16
At5g42610 (3e-11)	mito (15.6)	low	10

Figure 16 – A) Sequence alignment for human MCU and the 6 *Arabidopsis* MCU isoforms. Identities are shown in violet.
B) The 6 *Arabidopsis* MCU isoforms, their predicted subcellular localization and tissues of expression (according to Genevestigator) (from Stael *et al.*, 2012).

2. REFERENCES

- **Alberts B., Bray D., Hopkin K., Johnson A., Lewis J., Raff M., Roberts K., Walter P. (2005)** – The essential of cell molecular biology. *Zanichelli, second edition*

- **Armstrong N., Sun Y., Chen G.Q., Gouaux E. (1998)** – Structure of a glutamate-receptor ligand-binding core in complex with kainate. *Nature vol. 395, 913-917*

- **Ault B., Hildebrand L.M. (1993)** – Activation of nociceptive reflexes by peripheral kainate receptors. *J. Pharmacol. Exp. Ther. 265, 927-932*

- **Ayalon G., Stern-Bach Y. (2001)** – Functional assembly of AMPA and kainate receptors is mediated by several discrete protein-protein interactions. *Nature vol. 31, 103-113*

- **Bakker E.P. (1993)** – In alkali cation transport systems in Prokaryotes. *CRC Press, Ann Arbor. Bakker, E.P., Ed., 205-224*

- **Barber J., Mills J.B., Nicolson J. (1974)** – Studies with cation specific ionophores show that within the intact chloroplast Mg^{2+} acts as the main exchange cation for H^{+} pumping. *FEBS Letters 49, 106-110*

- **Baughman J.M., Perocchi F., Girgis H.S., Plovanich M., Belcher-Timme C.A., Sancak Y., Bao X.R., Strittmatter L., Goldberger O., Bogorad R.L., Koteliansky V., Mootha V.K. (2012)** – Integrative genomics identifies MCU as an essential component of the mitochondrial calcium uniporter. *Nature vol. 476(7360), 341-345*

- **Becker D., Geiger D., Dunkel M., Roller A., Bertl A., Latz A., Carpaneto A., Dietrich P., Roelfsema M.R.G., Voelker C., Schmidt D., Mueller-Roeber B., Czempinski K., Hedrich R. (2004)** – *At*TPK4, an *Arabidopsis* tandem-pore K^{+} channel, poised to control the pollen membrane voltage in a pH- and Ca^{2+}-dependent manner. *PNAS vol. 101, No. 44, 15621-15626*

- **Becker D., Geiger D., Dunkel M., Roller A., Bertl A., Latz A., Carpaneto A., Dietrich P., Roelfsema M.R.G., Voelker C., Schmidt D., Mueller-Roeber B., Czempinski K., Hedrich R. (2004)** – *At*TPK4, an *Arabidopsis* tandem-pore K^{+} channel, poised to control the pollen membrane voltage in a pH- and Ca^{2+}-dependent manner. *PNAS vol. 101(44), 15621-15626*

- **Berry S., Esper B., Karandashova I., Teuber M., Elanskaya I., Rogner M., Hagemann M. (2003)** – Potassium uptake in the unicellular cyanobacterium *Synechocystis* sp. strain PCC 6803 mainly depends on a Ktr-like system encoded by slr1509 (*ntpJ*). *FEBS Letters 548, 53-58*

- **Birnbaum K., Shasha D.E., Wang J.Y., Jung J.W., Lambert G.M., Galbraith D.W., Benfey P.N. (2003)** – A gene expression map of the *Arabidopsis* root. *Science vol. 302, 1956-1960*

- **Blount, P. (2003)** – Molecular mechanisms of mechanosensation: big lessons from small cells. *Neuron 37, 731-734*

- **Bolton M.M., Blanpied T.A., Ehlers M.D. (2000)** – Localization and stabilization of ionotropic glutamate receptors at synapses. *Cell. Mol. Life Sci. 57, 1517-1525*

- **Brand J.J., Becker D.W. (1984)** – Evidence for direct roles of Ca^{2+} in photosynthesis. *J. Bioenerg. Biomembr. 16, 239-249*

- **Brauner-Osborne H., Egebjerg J., Nielsen E.O., Madsen U., Krogsgaard-Larsen P. (2000)** – Ligands for glutamate receptors: design and therapeutic prospects. *J. Med. Chem. 43, 2609-2645*

- **Brenner E.D., Martinez-Barboza N., Clark A.P., Liang Q.S., Stevenson D.W., Coruzzi G. (2000)** – *Arabidopsis* mutants resistant to S(+)-β-methyl-a,b-diaminopropionic acid, a cycad-derived glutamate receptor agonist. *Plant Physiology vol. 124, 1615-1624*

- **Brohawn S.G., Del Mármol J., MacKinnon R. (2012)** – Crystal structure of the human K2P TRAAK, a lipid- and mechano-sensitive K^+ ion channel. *Science vol. 335, 436-441*

- **Carlton S.M., Hargett G.L., Coggeshall R.E. (1995)** – Localization and activation of glutamate receptors in unmyelinated axons of rat labrous skin. *Neurosci. Lett. 197, 25-28*

- **Chalmers S., Nicholls D.G. (2003)** – The relationship between free and total calcium concentrations in the matrix of liver and brain mitochondria. *J. Biol. Chem. 278, 19062-19070*

- **Checchetto V., Formentin E., Carraretto L., Giacometti G.M., Szabò I., Bergantino E. (2013)** – Functional and physiological characterization of a calcium-dependent potassium channel from *Synechocystis* sp. PCC 6803 Cyanobacteria. *Submitted to Plant Physiology*

- **Checchetto V., Segalla A., Allorent G., La Rocca N., Leanza L., Giacometti G.M., Uozumi N., Finazzi G., Bergantino E., Szabò I. (2012)** – Thylakoid potassium channel is required for efficient photosynthesis in Cyanobacteria. *PNAS vol. 109(27), 11043-11048*

- **Chen G.Q., Cui C., Mayer M.L., Gouaux E. (1999)** – Functional characterization of a potassium-selective prokaryotic glutamate receptor. *Nature vol. 402, 817-821*

- **Chenu C., Serre C.M., Raynal C., Burt-Pichat B., Delmas P.D. (1998)** – Glutamate receptors are expressed by bone cells and are involved in bone resorption. *Bone vol. 22, 295-299*

- **Chérel I. (2004)** – Regulation of K^+ channel activities in plants: from physiological to molecular aspects. *Journal of Experimental Botany vol. 55, 337-351*

- **Chiu J., Brenner E.D., De Salle R., Nitabach M.N., Holmes T.C., Coruzzi G. (2002)** – Phylogenetic and expression analysis of the glutamate receptor-like gene family in *Arabidopsis thaliana*. *Mol. Biol. Evol. 19(7), 1066-1082*

- **Chiu J., De Salle R., Lam H.M., Meisel L., Coruzzi G. (1999)** – Molecular evolution of glutamate receptors: a primitive signaling mechanism that existed before plants and animals diverged. *Mol. Biol. Evol. 16(6), 826-838*

- **Chohan K.K., Wo Z.G., Oswald R.E., Sutcliffe M.J. (2000)** – Structural insights into NMDA ionotropic glutamate receptors via molecular modeling. *J. Mol. Model. 6, 16-25*

- **Choi Y.B., Lipton S.A. (1999)** – Identification and mechanism of action of two histidine residues underlying high-affinity Zn^{2+} inhibition of the NMDA receptor. *Neuron 23, 171-180*

- **Clarkson D.T., Hanson J.B. (1980)** – The mineral nutrition of higher plants. *Annual Reviews of plant Physiology 31, 239-298*

- **Conn S., Gilliham M. (2010)** – Comparative physiology of elemental distributions in plants. *Ann Bot. 105(7), 1081-1102*

- **Coruzzi G., Zhou L. (2001)** – Carbon and nitrogen sensing and signaling in plants: emerging "matrix effects". *Physiology and metabolism, 247-253*

- **Cruz J.A., Kanazawa A., Treff N., Kramer D.M. (2005)** – Storage of light-driven transthylakoid proton motive force as an electric field (*Deltapsi*) under steady-state conditions in intact cells of *Chlamydomonas reinhardtii*. *Photosynth. Res. 85, 221-233*

- **Cryan J.F., Kumlesh K. (2008)** – The glutamatergic system as a potential therapeutic target for the treatment of anxiety disorders. *Handbook of Anxiety and Fear vol. 17*

- **Czempinski K., Frachisse J.M., Maurel C., Barbier-Brygoo H., Mueller-Roeber B. (2002)** – Vacuolar membrane localization of the *Arabidopsis* two-pore channel KCO1. *The Plant Journal vol. 29(6), 809-820*

- **Czempinski K., Gaedeke N., Zimmermann S., Mueller-Roeber B. (1999)** – Molecular mechanisms and regulation of plant ion channels. *Journal of Experimental Botany 50, 955-966*

- **Davenport R. (2002)** – Glutamate receptors in plants. *Ann. Bot. 90, 549-557*

- **De Boer A.H. (2002)** – Plant 14-3-3 proteins assist ion channels and pumps. *Biochemical Society Transactions 30, 416-421*

- **De Stefani D., Raffaello A., Teardo E., Szabò I., Rizzuto R. (2011)** – A forty-kilodalton protein of the inner membrane is the mitochondrial calcium uniporter. *Nature vol. 476, 336-342*

- **Deamer D.W., Packer L. (1969)** – Light-dependent anion transport in isolated spinach chloroplasts. *Biochimica et Biophysica Acta vol. 172(3), 539-545*

- **Deeken R., Geiger D., Fromm J., Koroleva O., Ache P., Langenfeld- Heyser R., Sauer N., May S.T., Hedrich R. (2002)** – Loss of the AKT2/3 potassium channel affects sugar loading into the phloem of *Arabidopsis*. *Planta 216(2), 334-344*

- **Demidchik V., Davenport R.J., Tester M. (2002)** – Nonselective cation channels in plants. *Annual Reviews of Plant Physiology and Plant Molecular Biology 53, 67-107*

- **Demidchik V., Essah P.A., Tester M. (2004)** – Glutamate activates cation currents in the plasma membrane of *Arabidopsis* root cells. *Planta 219, 167-175*

- **Dennison K.L., Robertson W.R., Lewis B.D., Hirsch R.E.,. Sussman M.R., Spalding E.P. (2001)** – Functions of AKT1 and AKT2 potassium channels determined by studies of single and double mutants of *Arabidopsis. Plant Physiology vol. 127(3), 1012-1019*

- **Dennison K.L., Spalding E.P. (2000)** – Glutamate-gated calcium fluxes in *Arabidopsis. Plant Physiology vol. 124, 1511-1514*

- **Derst C., Karschin A. (1998)** – Evolutionary link between prokaryotic and eukaryotic K^+ channels. *J. Exp. Biol. 201, 2791-2799*

- **Dingledine R., Borges K., Bowie D., Traynelis S.F. (1999)** – The glutamate receptor ion channels. *Pharmacological reviews vol. 51, No. 1*

- **Doyle D.A., Morais Cabral J., Pfuetzner R.A., Kuo A., Gulbis J.M., Cohen S.L., Chait B.T., MacKinnon R. (1998)** – The structure of the potassium channel: molecular basis of K^+ conduction and selectivity. *Science vol. 280, 69-77*

- **Drago I., Pizzo P., Pozzan T. (2011)** – After half a century mitochondrial calcium in- and efflux machineries reveal themselves. *The EMBO Journal 30, 4119-4125*

- **Dreyer I., Antunes S., Hoshi T., Mueller-Roeber B., Palme K., Pongs O., Reintanz B., Hedrich R. (1997)** – Plant K^+ channel alpha-subunits assemble indiscriminately. *Biophysical Journal 72, 2143-2150*

- **Dreyer I., Poree F., Schneider A., Mittelstädt J., Bertl A., Sentenac H., Thibaud J.B., Mueller-Roeber B. (2004)** – Assembly of plant Shaker-like K_{out} channels requires two distinct sites of the channel alpha-subunit. *Biophysical Journal 87, 858-872*

- **Dubos C., Huggins D., Grant G.H., Knight M.R., Campbell M.M. (2003)** – A role for glycine in the gating of plant NMDA-like receptors. *The Plant Journal vol. 35, 800-810*

- **Dubos C., Willment J., Huggins D., Grant G.H., Campbell M.M. (2005)** – Kanamycin reveals the role played by glutamate receptors in shaping plant resource allocation. *The Plant Journal vol. 43, 348-355*

- **Dunkel M., Latz A., Schumacher K., Müller T., Becker D., Hedrich R. (2008)** – Targeting of vacuolar membrane localized members of the TPK channel family. *Molecular Plant vol. 1, No. 6, 938-949*

- **Epstein W. (2003)** – The roles and regulation of potassium in bacteria. *Progress in Nucleic Acid Research and Molecular Biology 75, 293-320*

- **Fayyazuddin A., Villarroel A., Le Goff A., Lerma J., Neyton J. (2000)** – Four residues of the extracellular N-terminal domain of the NR2A subunit control high-affinity Zn^{2+} binding to NMDA receptors. *Neuron 25, 683-694*

- **Filleur S., Walch-Liu P., Gan Y., Forde B.G. (2005)** – Nitrate and glutamate sensing by plant roots. *Biochemical Society Transactions 33, part I*

- **Furukawa H., Gouaux E. (2003)** – Mechanisms of activation, inhibition and specificity: crystal structures of the NMDA receptor NR1 ligand-binding core. *The EMBO Journal 22, 2873-2885*

- **Gill S.S., Pulido O.M., Mueller R.W., McGuire P.F. (1998)** – Molecular and immunochemical characterization of the ionotropic glutamate receptors in the rat heart. *Brain Res. Bull. 46, 429-434*

- **Gobert A., Isayenkov S., Voelker C., Czempinski K., Maathuis F.J.M. (2007)** – The two-pore channel *TPK1* gene encodes the vacuolar K^+ conductance and plays a role in K^+ homeostasis. *PNAS vol. 104(25), 10726-1073*

- **Grove G.N., Brudvig G.W. (1998)** – Calcium binding studies on photosystem II using a Ca^{2+}-selective electrode. *Biochemistry 37, 1532-1539*

- **Harold F.M. (1996)** – *In Escherichia coli and Salmonella ASM Press, Washington D.C. USA. Neidhardt F.C., Ed., 1, 283-306*

- **Hedrich R. (2012)** – Ion channels in plants. *Physiol. Rev. 92, 1777-1811*

- **Hepler P.K (2005)** – Calcium: a central regulator of plant growth and development. *Plant Cell vol. 17(8), 2142-2155*

- **Hille B. (2001)** – Ion channels of excitable membranes. *Sinauer Associates, Inc., Sunderland, MA, p. 814*

- **Hirsch R.E., Lewis B.D., Spalding E.P., Sussman M.R. (1998)** – A role for the AKT1 potassium channel in plant nutrition. *Science vol. 280, 918-921*

- **Hogner A., Greenwood J.R., Liljefors T., Lunn M.L., Egebjerg J., Larsen I.K., Gouaux E., Kastrup J.S. (2003)** – Competitive antagonism of AMPA receptors by ligands of different classes: Crystal structure of ATPO bound to the GluR2 ligand-binding core, in comparison with DNQX. *J. Med. Chem. 46, 214-221*

- **Hogner A., Kastrup J., Jin R., Liljefors T., Mayer M., Egebjerg J., Larsen I., Gouaux E. (2002)** – Structural basis for AMPA receptor activation and ligand selectivity: crystal structures of five agonist complexes with the GluR2 ligand-binding core. *J. Mol. Biol. 322, 93-109*

- **Inagaki N., Kuromi H., Gonoi T., Okamoto Y., Ishida H., Seino Y., Kaneko T., Iwanaga T., Seino S. (1995)** – Expression and role of ionotropic glutamate receptors in pancreatic islet cells. *FASEB J. 9, 686-691*

- **Ivashikina N., Becker D., Ache P., Meyerhoff O., Felle H.H., Hedrich R., Dennison K.L., Robertson W.R., Lewis B.D., Hirsch R.E., Sussman M.R., Spalding E.P. (2001)** – K^+

channel profile and electrical properties of *Arabidopsis* root hairs. *FEBS Letters 508(3), 463-469*

- **Jeanguenin L., Alcon C., Duby G., Boeglin M., Chérel I., Gaillard I., Zimmermann S., Sentenac H., Véry A.A. (2011)** – *At*KC1 is a general modulator of *Arabidopsis* inward Shaker channel activity. *The Plant Journal vol. 67, 570-582*

- **Jeanguenin L., Lebaudy A., Xicluna J., Alcon C., Hosy E., Duby G., Michard E., Lacombe B., Dreyer I., Thibaud J.B. (2008)** – Heteromerization of *Arabidopsis* Kv channel alpha-subunits: data and prospects. *Plant Signaling & Behavior 3, 622-625*

- **Jiang Y., Lee A., Chen J., Cadene M., Chait B.T., MacKinnon R. (2002[1])** – Crystal structure and mechanism of a calcium-gated potassium channel. *Nature vol. 417, 515-522*

- **Jiang Y., Lee A., Chen J., Cadene M., Chait B.T., MacKinnon R. (2002[2])** – The open pore conformation of potassium channels. *Nature vol. 417, 523-526*

- **Jiang Y., Lee A., Chen J., Ruta V., Cadene M., Chait B.T., MacKinnon R. (2003[1])** – X-ray structure of a voltage-dependent K^+ channel. *Nature vol. 423, 33-41*

- **Jiang Y., Pico A., Cadene M., Chait B.T., MacKinnon R. (2001)** – Structure of the RCK domain from the *E. coli* K-channel and demonstration of its presence in the human BK channel. *Neuron 29, 593-601*

- **Jiang Y., Ruta V., Chen J., Lee A., MacKinnon, R. (2003[2])** – The principle of gating charge movement in a voltage-dependent K^+ channel. *Nature vol. 423, 42-48*

- **Jin R., Banke T.G., Mayer M.L., Traynelis S.F., Gouaux E. (2003)** – Structural basis for partial agonist action at ionotropic glutamate receptors. *Nat. Neurosci. 6, 803-810*

- **Jin R., Gouaux E. (2003)** – Probing the function, conformational plasticity, and dimer-dimer contacts of the GluR2 ligand-binding core: studies of 5-substituted willardiines and GluR2 S1S2 in the crystal. *Biochemistry 42, 5201-5213*

- **Johnson T.L., Olsen L.J. (2001)** – Building new models for peroxisome biogenesis. *Plant Physiology vol. 127, 731-739*

- **Jorgensen M., Tygesen C.K., Andersen P.H. (1995)** – Ionotropic glutamate receptors focus on non-NMDA receptors. *Pharmacol. Toxicol. 76, 312-319*

- **Kang J., Mehta S., Turano F.J. (2004)** – The putative glutamate receptor 1.1 (*At*GLR1.1) in *Arabidopsis thaliana* regulates abscisic acid biosynthesis and signaling to control development and water loss. *Plant Cell Physiol. 45(10), 1380-1389*

- **Kang J., Turano F.J. (2003)** – The putative glutamate receptor 1.1 (*At*GLR1.1) functions as a regulator of carbon and nitrogen metabolism in *Arabidopsis thaliana*. *PNAS vol. 100, 6872-6877*

➢**Kang M., Moroni A., Gazzarrini S., Di Francesco D., Thiel G., Severino M., Van Etten J.L. (2004)** – Small potassium ion channel proteins encoded by chlorella viruses. *PNAS vol. 101, 5318-5324*

➢**Kang S., Kim H.B., Lee H., Choi J.Y., Heu S., Oh C.J., Kwon S.I., An C.S. (2006)** – Overexpression in *Arabidopsis* of a plasma membrane-targeting glutamate receptor from small radish increases glutamate-mediated Ca^{2+} influx and delays fungal infection. *Mol. Cells vol. 21, No. 3, 418-427*

➢**Kashiwabuchi N., Ikeda K., Araki K., Hirano T., Shibuki K., Takayama C., Inoue Y., Kutsuwada T., Yagi T., Kang Y. (1995)** – Impairment of motor coordination, Purkinje cell synapse formation, and cerebellar long-term depression in GluR mutant mice. *Cell 81, 245-252*

➢**Kashket E.R. (1982)** – Stoichiometry of the H^+-ATPase of growing and resting aerobic *Escherichia coli*. *Biochemistry 21, 5534-5538*

➢**Ketchum K.A., Joiner W.J., Sellers A.J., Kaczmarek L.K., Goldstein S.A. (1995)** – A new family of outwardly rectifying potassium channel proteins with two pore domains in tandem. *Nature vol. 376, 690-695*

➢**Kim S.A, Kwak J.M., Jae S.K., Wang M.H., Nam H.G. (2001)** – Overexpression of the *At*GluR2 gene encoding an *Arabidopsis* homolog of mammalian glutamate receptor impairs calcium utilization and sensitivity to ionic stress in transgenic plants. *Plant Cell Physiol. 42(1), 74-84*

➢**Kim T.H., Böhmer M., Hu H., Nishimura N., Schroeder J.I. (2010)** – Guard cell signal transduction network: advances in understanding abscisic acid, CO_2, and Ca^{2+} signaling. *Annual Reviews of Plant Biology 61, 516-591*

➢**Knight M.R., Campbell A.K., Smith S.M., Trewavas A.J. (1991)** – Transgenic plant aequorin reports the effects of touch and cold-shock and elicitors on cytoplasmic calcium. *Nature vol. 352, 524-526*

➢**Kohda K., Wang Y., Yuzaki M. (2000)** – Mutation of a glutamate receptor motif reveals its role in gating and delta2 receptor channel properties. *Nat. Neurosci. 3, 315-322*

➢**Kramer D.M., Cruz J.A., Kanazawa A. (2003)** – Balancing the central roles of the thylakoid proton gradient. *Trends Plant Sci. 8, 27-32*

➢**Kreimer G., Melkonian M., Holtum J.A.M., Latzko E. (1985)** – Characterization of calcium fluxes across the envelope of intact spinach chloroplasts. *Planta 166, 515-523*

➢**Krupp J.J., Vissel B., Heinemann S.F., Westbrook G.L. (1998)** – N-terminal domains in the NR2 subunit control desensitization of NMDA receptors. *Neuron 20, 317-327*

➢**Kumanovics A., Levin G., Blount, P. (2002)** – Family ties of gated pores: evolution of the sensor module. *FASEB J. 16, 1623-1629*

➢**Kuner T., Beck C., Sakmann B., Seeburg P.H. (2001)** – Channel-lining residues of the AMPA receptor M2 segment: Structural environment of the Q/R site and identification of the selectivity filter. *J. Neurosci. vol. 21, 4162-4172*

➢**Kuner T., Seeburg P.H., Guy H.R. (2003)** – A common architecture for K^+ channels and ionotropic glutamate receptors? *Trends in Neuroscience vol. 26, No. 1*

➢**Kuner T., Wollmuth L.P., Karlin A., Seeburg P.H., Sakmann B. (1996)** – Structure of the NMDA receptor channel M2 segment inferred from the accessibility of substituted cysteines. *Neuron 17, 343-352*

➢**Kuo M.M.C., Haynes W.J., Loukin S.H., Kung C., Saimi Y. (2005)**. Prokaryotic K^+ channels: from crystal structures to diversity. *FEMS Microbiology Reviews, 29 961-985*

➢**Kuo M.M.C., Saimi Y., Kung C. (2003)** – Gain-of-function mutations indicate that Escherichia coli Kch forms a functional K^+ conduit *in vivo*. *The EMBO Journal 22(16), 4049-4058*

➢**Kurz L.L., Zuhlke R.D., Zhang H.J., Joho R.H. (1995)** – Side-chain accessibilities in the pore of a K^+ channel probed by sulfhydryl-specific reagents after cysteine scanning mutagenesis. *Biophys. J. 68, 900-905*

➢**Kuusinen A., Abele R., Madden D.R., Keinänen K. (1999)** – Oligomerization and ligand-binding properties of the ectodomain of the AMPA receptor subunit GluRD. *J. Biol. Chem. 274, 28937-28943*

➢**Kwak J.M., Murata Y., Baizabal-Aguirre V.M., Merrill J., Wang M., Kemper A., Hawke S.D., Tallman G., Schroeder J.I. (2001)** – Dominant negative guard cell K^+ channel mutants reduce inward-rectifying K^+ currents and light-induced stomatal opening in *Arabidopsis*. *Plant Physiology vol. 127, 473-485*

➢**Lacombe B., Becker D., Hedrich R., De Salle R., Hollmann M., Kwak J.M., Schroeder J.I., Le Novère N., Nam H.G., Spalding E.P., Tester M., Turano F.J., Chiu J., Coruzzi G. (2001)** – The identity of plant glutamate receptors. *Science vol. 292, No. 5521, 1486-1487*

➢**Lalonde S., Ehrhardt D.W., Loqué D., Chen J., Rhee S.Y., Frommer W.B. (2008)** – Molecular and cellular approaches for the detection of protein-protein interactions: latest techniques and current limitations. *The Plant Journal vol. 53, 610-635*

➢**Lam H.M., Chiu J., Hsieh M.H., Meisel L., Oliveira I.C., Shin M., Coruzzi G. (1998)** – Glutamate receptor genes in plants. *Nature vol. 396, 125-126*

➢**Latz A., Becker D., Hekman M., Müller T., Beyhl D., Marten I., Eing C., Fischer A., Dunkel M., Bertl A., Rapp U.R., Hedrich R. (2007)** – TPK1, a Ca^{2+}-regulated *Arabidopsis* vacuole two-pore K^+ channel is activated by 14-3-3 proteins. *The Plant Journal vol. 52, 449-459*

➢**Laube B., Kuhse J., Betz H. (1998)** – Evidence for a tetrameric structure of recombinant NMDA receptors. *J. Neurosci. 18, 2954-2961*

➢**Lebaudy A., Hosy E., Simonneau T., Sentenac H., Thibaud J.B., Dreyer I. (2008)** – Heteromeric K^+ channels in plants. *The Plant Journal vol. 54, 1076-1082*

➢**Leng Q., Mercier R.W., Hua B.G., Fromm H., Berkowitz G.A. (2002)** – Electrophysiological analysis of cloned cyclic nucleotide-gated ion channels. *Plant Physiology vol. 128, 400-410*

➢**Leng Q., Mercier R.W., Yao W., Berkowitz G.A. (1999)** – Cloning and first functional characterization of a plant cyclic nucleotide-gated cation channel. *Plant Physiology vol. 121, 753-761*

➢**Li J., Zhu S., Song X., Shen Y., Chen H., Yu J., Yi K., Liu Y., Karplus V.J., Wu P., Deng X.W. (2006)** – A rice glutamate receptor-like gene is critical for the division and survival of individual cells in the root apical meristem. *Plant Cell vol. 18, 340-349*

➢**Linkohr B.I., Williamson L.C., Fitter A.H., Leyser H.M.O. (2002)** – Nitrate and phosphate availability and distribution have different effects on root system architecture of *Arabidopsis*. *The Plant Journal vol. 29, 751-760*

➢**Logan D.C., Knight M.R., (2003)** – Mitochondrial and cytosolic calcium dynamics are differentially regulated in plants. *Plant Physiology vol. 133(1), 21-24*

➢**Loll B., Gerold G., Slowik D., Voelter W., Jung C., Saenger W., Irrgang H.D. (2005)** – Thermostability and Ca^{2+} binding properties of wild type and heterologously expressed PsbO protein from cyanobacterial Photosystem II. *Biochemistry 44, 4691-4698*

➢**Lomeli H., Sprengel R., Laurie D.J.., Kohr G, Herb A., Seeburg P.H., Wisden W. (1993)** – The rat delta-1 and delta-2 subunits extend the excitatory amino acid receptor family. *FEBS Letters 315, 318-322*

➢**Lunn M.L., Hogner A., Stensbol T.B., Gouaux E., Egebjerg J., Kastrup J.S. (2003)** – Three-dimensional structure of the ligand-binding core of GluR2 in complex with the agonist (S)-ATPA: implications for receptor subunit selectivity. *J. Med. Chem. 46, 872-875*

➢**MacRobbie E.A.C. (1998)** – *Philos. Trans. R. Soc. Lond. B. 353, 1475-1488*

➢**Mallilankaraman K., Doonan P., Càrdenas C., Chandramoorthy H.C., Müller M., Miller R., Hoffman N.E., Gandhirajan R.K., Molgò J., Birnbaum M.J., Rothberg B.S., Mak D.D., Foskett J.K., Madesh M. (2012)** – MICU1 is an essential gatekeeper for MCU-mediated mitochondrial Ca^{2+} uptake that regulates cell survival. *Cell 151, 630-644*

➢**Maricq A.V., Peckol E., Driscoll M., Bargmann C.I. (1995)** – Mechanosensory signalling in *C. elegans* mediated by the GLR-1 glutamate receptor. *Nature vol. 378, 78-81*

➢**Mäser P., Thomine S., Schroeder J.I., Ward J.M., Hirschi K., Sze H., Talke I.N., Amtmann A., Maathuis F.J.M., Sanders D., Harper J.F., Tchieu J., Gribskov M.,**

Persans M.W., Salt D.E., Kim S.A., Guerinot M.L. (2001) – Phylogenetic relationships within cation transporter families of *Arabidopsis*. *Plant Physiology vol. 126, 1646-1667*

- **Matsuda N., Kobayashi H., Katoh H., Ogawa T., Futatsugi L., Nakamura T., Bakker E.P., Uozumi N. (2004)** – Na^+-dependent K^+ uptake Ktr system from the cyanobacterium *Synechocystis* sp. PCC 6803 and its role in the early phases of cell adaptation to hyperosmotic shock. *J. Biol. Chem. 279, 54952-54962*

- **Matsuda N., Uozumi N. (2006)** – Ktr-mediated potassium transport, a major pathway for potassium uptake, is coupled to a proton gradient across the membrane in *Synechocystis* sp. PCC 6803. *Biosci. Biotechnol. Biochem. 70, 273-275*

- **Mayer M.L., Olson R., Gouaux E. (2001)** – Mechanisms for ligand binding to GluR0 ion channels: crystal structures of the glutamate and serine complexes and a closed APO state. *J. Mol. Biol. 311, 815-836*

- **Meyerhoff O., Muller K., Roelfsema M.R., Latz A., Lacombe B., Hedrich R., Dietrich P., Becker D. (2005)** – *At*GLR3.4, a glutamate receptor channel-like gene is sensitive to touch and cold. *Planta 222, 418-427*

- **Milkman R. (1994)** – An *Escherichia coli* homologue of eukaryotic potassium channel proteins. *PNAS vol. 91, 3510-3514*

- **Mosbacher J., Schoepfer R., Monyer H., Burnashev N., Seeburg P.H., Ruppersberg J.P. (1994)** – A molecular determinant for submillisecond desensitization in glutamate receptors. *Science vol. 266, 1059-1062*

- **Mouline K., Véry A.A., Gaymard F., Boucherez J., Pilot G., Devic M., Bouchez D., Thibaud J.B., Sentenac H. (2002)** – Pollen tube development and competitive ability are impaired by disruption of a Shaker K^+ channel in *Arabidopsis*. *Genes Dev. 16(3), 339-350*

- **Muniz J.J., Pottosin I.I., Sandoval L. (1995)** – Patch clamp study of vascular plant chloroplasts: ion channels and photocurrents. *J. Bioenerg. Biomembr. 27, 249-258*

- **Nagata T., Iizumi S., Satoh K., Ooka H., Kawai J., Carninci P., Hayashizaki Y., Otorno Y., Muramaki K., Matsubara K., Kikuchi S. (2004)** – Comparative analysis of plant and animal calcium signal transduction element using plant full-length *c*DNA data. *Mol. Biol. Evol. 21, 1855-1870*

- **Nakamura R.L., McKendree W.L. Jr, Hirsch R.E., Sedbrook J.C., Gaber R.F., Sussman M.R. (1995)** – Expression of an *Arabidopsis* potassium channel gene in guard cells. *Plant Physiology vol. 109(2), 371-374*

- **Neuhaus H.E., Wagner R. (2000)** – Solute pores, ion channels, and metabolite transporters in the outer and inner envelope membranes of higher plant plastids. *Biochimica et Biophysica Acta vol. 1465, 307-323*

- **Nitabach M.N., Llamas D.A., Araneda R.C., Intile J.L., Thompson I.J., Zhou Y.I., Holmes T.C. (2001)** – A mechanism for combinatorial regulation of electrical activity:

potassium channel subunits capable of functioning as Src homology 3-dependent adaptors. *PNAS vol. 98, 705-710*

- **O'Hara P.J., Sheppard P.O., Thogersen H., Venezia D., Haldeman B.A., McGrane V., Houamed K.M., Thomsen C., Gilbert T.L., Mulvihill E.R. (1993)** – The ligand-binding domain in metabotropic glutamate receptors is related to bacterial periplasmic binding proteins. *Neuron 11, 41-52*

- **Panchenko V.A., Glasser C.R., Mayer M.L. (2001)** – Structural similarities between glutamate receptor channels and K^+ channels examined by scanning mutagenesis. *J. Gen. Physiol. vol. 117, 345-360*

- **Papazian D.M., Schwarz T.L., Tempel B.L., Jan Y.N., Jan L.Y. (1987)** – Cloning of genomic and complementary DNA from Shaker, a putative potassium channel gene from *Drosophila*. *Science vol. 237, 749-753*

- **Pascual J.M., Shieh C.C., Kirsch G.E. and Brown A.M. (1995)** – K^+ pore structure revealed by reported cysteines and inner and outer surfaces. *Neuron 14, 1055-1063*

- **Patel A.J., Lazdunski M., Honore E. (2001)** – Lipid and mechano-gated 2P domain K^+ channels. *Current Opinion in Cell Biology 13, 422-427*

- **Patton A.J., Genever P.G., Birch M.A., Suva L.J., Skerry T.M. (1998)** – Expression of an N-methyl-D-aspartate-type receptor by human and rat osteoblasts and osteoclasts suggests a novel glutamate signaling pathway in bone. *Bone vol. 22, 645-649*

- **Peiter E., Maathuis F.J., Mills L.N., Knight H., Pelloux J., Hetherington A.M., Sanders D. (2005)** – The vacuolar Ca^{2+}-activated channel TPC1 regulates germination and stomatal movement. *Nature vol. 434, 404-408*

- **Perocchi F., Gohil V.M., Girgis H.S., Bao X.R., McCombs J.E., Palmer A.E., Mootha V.K. (2010)** – MICU1 encodes a mitochondrial EF hand protein required for Ca^{2+} uptake. *Nature vol. 476, 291-296*

- **Persson S., Wyatt S.E., Love J., Thompson W.F., Robertson D., Boss W.F. (2001)** – The Ca^{2+} status of the endoplasmic reticulum is altered by induction of calreticulin expression in transgenic plants. *Plant Physiology vol. 123(3), 1092-1104*

- **Pilot G., Lacombe B., Gaymard F., Cherel I., Boucherez J., Thibaud J.B., Sentenac H. (2001)** – Guard cell inward K^+ channel activity in *Arabidopsis* involves expression of the twin channel subunits KAT1 and KAT2. *J. Biol. Chem. 276(5), 3215-3221*

- **Pottosin I.I. (1992)** – Single channel recording in the chloroplast envelope. *FEBS Letters 308, 87-90*

- **Qi Z., Stephens N.R., Spalding E.P. (2006)** – Calcium entry mediated by GLR3.3, an *Arabidopsis* glutamate receptor with a broad agonist profile. *Plant Physiology vol. 142, 963-971*

- **Ranf S., Wunnenberg P., Lee J., Becker D., Dunkel M., Hedrich R., Scheel D., Dietrich P. (2008)** – Loss of the vacuolar cation channel, *At*TPC1, does not impair Ca^{2+} signals induced by abiotic and biotic stresses. *The Plant Journal vol. 53, 287-299*

- **Rawat S.R., Silim S.N., Kronzucker H.J., Siddiqi M.Y., Glass A.D.M. (1999)** – *At*AMT1 gene expression and NH_4^+ uptake in roots of *Arabidopsis thaliana*: evidence for regulation by root glutamine levels. *The Plant Journal vol. 19, 143-152*

- **Rosenmund C., Stern-Bach Y., Stevens C.F. (1998)** – The tetrameric structure of a glutamate receptor channel. *Science vol. 280, 1596-1599*

- **Rossmann M.G., Moras D., Olsen K.W. (1974)** – Chemical and biological evolution of a nucleotide-binding protein. *Nature vol. 250, 194-199*

- **Ruta V., Jiang Y., Lee A., Che J., MacKinnon R. (2003)** – Functional analysis of an archeobacterial voltage-dependent K^+ channel. *Nature vol. 422, 180-185*

- **Safferling M., Tichelaar W., Kummerle G., Jouppila A., Kuusinen A., Keinanen K., Madden D.R. (2001)** – First images of a glutamate receptor ion channel: oligomeric state and molecular dimensions of GluRB homomers. *Biochemistry 40, 13948-13953*

- **Sai J., Johnson C.H. (2002)** – Dark-stimulated calcium ion fluxes in the chloroplast stroma and cytosol. *Plant Cell vol. 14, 1279-1291*

- **Sanders D., Pelloux J., Brownlee C., Harper J.F. (2002)** – Calcium at the crossroads of signaling. *Plant Cell vol.14 (supplement), s401-s417*

- **Schachtman D.P. (2000)** – Molecular insights into the structure and function of plant K^+ transport mechanisms. *Biochimica et Biophysica Acta vol. 1465, 127-139*

- **Schönknecht G., Hedrich R., Junge W., Raschke K. (1988)** – A voltage dependent chloride channel in the photosynthetic membrane of higher plant. *Nature vol. 336, 589-592*

- **Schönknecht G., Spoormaker P., Steinmeyer R., Brüggeman L., Ache P., Dutta R., Reintanz B., Godde M., Hedrich R., Palme K. (2002)** – KCO1 is a component of the slow-vacuolar (SV) ion channel. *FEBS Letters 511(1-3), 28-32*

- **Schulenburg P., Schwarz M., Wagner R. (1992)** – Inhibition of chloroplast ATPase by the K^+ channel blocker a-dendrotoxin. *Eur. J. Biochem. 210, 257-267*

- **Schultz S.G., Solomon A.K. (1961)** – Cation transport in *Escherichia coli*. I. Intracellular Na and K concentrations and cation movement. *J. Gen. Physiol. vol. 45, 355-369*

- **Schuster C.M., Ultsch A., Schloss P., Cox J.A., Schmitt B., Betz H. (1991)** – Molecular cloning of an invertebrate glutamate receptor subunit expressed in *Drosophila* muscle. *Science vol. 254, 112-114*

- **Schwacke R., Schneider A., Van der Graaff E., Fischer K., Catoni E., Desimone M., Frommer WB, Flugge UI, Kunze R. (2003)** – ARAMEMNON, a novel database for *Arabidopsis* integral membrane proteins. *Plant Physiology vol. 131, 16-26*

- **Sentenac H., Bonneaud N., Minet M., Lacroute F., Salmon J.M., Gaymard F., Grignon C., Schönknecht G., Spoormaker P., Steinmeyer R., Brüggeman L., Ache P., Dutta R., Reintanz B., Godde M., Hedrich R., Palme K. (1992)** – Cloning and expression in yeast of a plant potassium ion transport system. *Science vol. 256(5057), 663-665*

- **Seoh S.A., Sigg D., Papazian D.M., Bezanilla F. (1996)** – Voltage-sensing residues in the S2 and S4 segments of the Shaker K^+ channel. *Neuron 16, 1159-1167*

- **Sesti F., Rajan S., Gonzalez-Colaso R., Nikolaeva N., Goldstein S.A. (2003)** – Hyperpolarization moves S4 sensors inward to open MVP, a methanococcal voltage-gated potassium channel. *Nat. Neurosci. 6, 353-361*

- **Sinnige M.P., Ten Hoopen P., Van den Wijngaard P.W.J., Roobeek I., Schoonheim P.J., Mol J.N.M., De Boer A.H. (2005)** – The barley two-pore K^+ channel HvKCO1 interacts with 14-3-3 proteins in an isoform specific manner. *Plant Science 169, 612-619*

- **Sivaguru M., Pike S., Gassmann W., Baskin T.I. (2003)** – Aluminium rapidly depolymerizes cortical microtubules and depolarizes the plasma membrane: evidence that these responses are mediated by a glutamate receptor. *Plant Cell Physiol. 44(7), 667-675*

- **Sobolevsky A.I., Rosconi M.P., Gouaux E. (2009)** – X-ray structure, symmetry and mechanism of an AMPA-subtype glutamate receptor. *Nature vol. 462, 745-758*

- **Sobolevsky A.I., Yelshansky M.V. and Wollmuth L.P. (2003)** – Different gating mechanisms in glutamate receptor and K^+ channels. *J. Neurosci. 23, 7559-7568*

- **Sommer B., Keinanen K., Verdoorn T.A., Wisden W., Burnashev N., Herb A., Kohler M., Takagi T., Sakmann G., Seeburg P.H. (1990)** – Flip and flop: a cell-specific functional switch in glutamate-operated channels of the CNS. *Science vol. 249, 1580-1584*

- **Sottocornola B., Visconti S., Orsi S., Gazzarrini S., Giacometti S., Olivari C., Camoni L., Aducci P., Marra M., Abenavoli A., Thiel G., Moroni A. (2006)** – The potassium channel KAT1 is activated by plant and animal 14-3-3 proteins. *J. Biol. Chem. 281, 35735-35741*

- **Splitt H., Meuser D., Borovok I., Betzler M., Schrempf H. (2000)** – Pore mutations affecting tetrameric assembly and functioning of the potassium channel KcsA from *Streptomyces lividans. FEBS Letters 472, 83-87*

- **Stael S., Wurzinger B., Mair A., Mehlmer N., Vothknecht U.C., Teige M. (2012)** – Plant organellar calcium signalling: an emerging field. *Journal of Experimental Botany vol. 63, No. 4, pp.1525-1542*

- **Starkov A.A. (2010)** – The molecular identity of the mitochondrial Ca^{2+} sequestration system. *FEBS Journal 277, 3652-3663*

- **Szyroki A., Ivashikina N., Dietrich P., Roelfsema M.R., Ache P., Reintanz B., Deeken R., Godde M., Felle H., Steinmeyer R., Palme K., Hedrich R. (2001)** – KAT1 is not essential for stomatal opening. *PNAS vol. 98(5), 2917-2921*

- **Teardo E., Formentin E., Segalla A., Giacometti G.M., Marin O., Zanetti M., Lo Schiavo F., Zoratti M., Szabò I. (2011)** – Dual localization of plant glutamate receptor *At*GLR3.4 to plastids and plasma membrane. *Biochimica et Biophysica Acta, Bioenergetics, vol. 1807, issue 3, 359-367*

- **Tempel B.L., Papazian D.M., Schwarz T.L., Jan Y.N., Jan L.Y. (1987)** – Sequence of a probable potassium channel component encoded at Shaker locus of *Drosophila. Science vol. 237, 770-775*

- **Trchounian A., Kobayashi H. (1999)** – Kup is the major K+ uptake system in Escherichia coli upon hyper-osmotic stress at a low pH. *FEBS Letters 447, 144-148*

- **Van den Wijngaard P.W., Sinnige M.P., Roobeek I., Reumer A., Schoonheim P.J., Mol J.N., Wang M., De Boer A.H. (2005)** – Abscisic acid and 14-3-3 proteins control K channel activity in barley embryonic root. *The Plant Journal vol. 41, 43-55*

- **Véry A.A., Sentenac H. (2002)** – Cation channels in the *Arabidopsis* plasma membrane. *Trends Plant Sci. 7, 168-175*

- **Véry A.A., Sentenac H. (2003)** – Molecular mechanisms and regulation of K^+ transport in higher plants. *Annual Reviews of Plant Biology 54, 575-603*

- **Vincill E.D., Bieck A.M., Spalding E.P. (2012)** – Ca^{2+} conduction by an amino acid-gated ion channel related to glutamate receptors. *Plant Physiology vol. 159, 40-46*

- **Voelker C., Schmidt D., Mueller-Roeber B., Czempinski K. (2006)** – Members of the *Arabidopsis At*TPK/KCO family form homomeric vacuolar channels *in planta*. *The Plant Journal vol. 48, 296-306*

- **Walch-Liu P., Liu L.H., Remans T., Tester M., Forde B.G. (2006)** – Evidence that L-glutamate can act as an exogenous signal to modulate root growth and branching in *Arabidopsis thaliana*. *Plant and Cell Physiology 47(8), 1045-1057*

- **Weaver C.D., Yao T.L., Powers A.C., Verdoorn T.A. (1996)** – Differential expression of glutamate receptor subtypes in rat pancreatic islets. *J. Biol. Chem. 271, 12977-12984*

- **White P.J., Bowen H.C., Demidchik V., Nichols C., Davies J.M. (2002)** – Genes for calcium-permeable channels in the plasma membrane of plant root cells. *Biochimica et Biophysica Acta vol. 1564, 299-309*

- **Wo Z.G., Oswald R.E. (1995)** – Unraveling the modular design of glutamate gated ion channels. *Trends in Neuroscience vol. 18, 161-168*

- **Wood M.W., Van Dongen H.M.A., Van Dongen A.M.J. (1995)** – Structural conservation of ion conduction pathways in K^+ channels and glutamate receptors. *PNAS vol. 92, 4882-4886*

- **Zanetti M., Teardo E., La Rocca N., Zulkifli L., Checchetto V., Shijuku T., Sato Y., Giacometti G.M., Uozumi N., Bergantino E., Szabò I. (2010)** – A novel potassium channel in photosynthetic Cyanobacteria. *PLoS One, vol. 5, issue 4*

- **Zhang H.M., Jennings A., Barlow P.W., Forde B.G. (1999)** – Dual pathways for regulation of root branching by nitrate. *PNAS vol. 96, 6529-6534*

- **Zheng F., Erreger K., Low C.M., Banke T., Lee C.J., Conn P.J., Traynelis S.F. (2001)** – Allosteric interaction between the amino terminal domain and the ligand binding domain of NR2A. *Nat. Neurosci. 4, 894-901*

- **Zhou X.L., Vaillant B., Loukin S.H., Kung C., Saimi Y**. **(1995)** – YKC1 encodes the depolarization-activated K^+ channel in the plasma membrane of yeast. *FEBS Letters 373, 170-176*

- **Zhou Y., Morais-Cabral J.H., Kaufman A., MacKinnon R. (2001)** – Chemistry of ion coordination and hydration revealed by a K^+ channel-Fab complex at 2.0 Å resolution. *Nature vol. 414, 43-48*

- **Zhuo D., Okamoto M., Vidmar J.J., Glass A.D.M. (1999)** – Regulation of a putative high-affinity nitrate transporter (Nrt2;1At) in roots of *Arabidopsis thaliana*. *The Plant Journal vol. 17, 563-568*

- **Zimmermann S., Sentenac H. (1999)**. Plant ion channels: from molecular structures to physiological functions. *Curr. Opin. Plant Biol. 2, 477-482*

- **Zuo J., De Jager P.L., Takahashi K.A., Jiang W., Linden D.J., Heintz N. (1997)** – Neurodegeneration in Lurcher mice caused by mutation in δ2 glutamate receptor gene. *Nature vol. 388, 769-773*

Section 2

*At*TPK3 project

A thylakoid-located two-pore potassium channel regulates photosensitivity in higher plants.

Luca Carraretto[1], Elide Formentin[1], Enrico Teardo[1], Martino Tomizioli[2], Vanessa Checchetto[1], Tomas Morosinotto[1], Giorgio Mario Giacometti[1], Giovanni Finazzi[2], Ildikò Szabò[1]

[1]Department of Biology, University of Padua
[2]Centre National Recherche Scientifique, Unité Mixte Recherche 5168, Laboratoire Physiologie Cellulaire et Végétale, F-38054 Grenoble, France

Correspondence to: I. Szabò (ildi@civ.bio.unipd.it) and G. Finazzi (Finazzi@cnrs.fr)

ABSTRACT

Photosynthetic organisms have developed different strategies to cope with excessive light intensity which may cause severe photoinhibition. In the present work we define a novel component of the thylakoid membrane which contributes to the regulation of transmembrane proton gradient, the two-pore potassium channel TPK3. We show that recombinant TPK3 gives rise to a calcium- and proton-sensitive, potassium-selective channel activity in electrophysiological experiments. Localization of TPK3 in chloroplasts and in stromal lamellae in the Arabidopsis model plant is indicated by fluorescence microscopy and biochemistry. Arabidopsis, stably silenced for TPK3, displayed enhanced anthocyanin accumulation, reduced growth and altered thylakoid membrane organization, already at moderate growth light intensity. The capacity of the silenced lines to build a ΔpH and consistently, to increase its non-photochemical quenching when shifted from low to higher light, was lower than in the wt Col0. Our results thus provide a genetic proof for an important role of a thylakoid-located potassium channel in regulation of photosensitivity.

Under submission to Plant Cell

INTRODUCTION

TPK channels (for Tandem-Pore K^+ Channels) are the plant counterparts of animal leak TWIK/TREK channels (Enyedi and Czirjak, 2010). The first plant TPK member, TPK1, was identified by *in silico* searches and was later proposed to contribute to the vacuolar VK conductance (Schönknecht *et al*., 2002, but see Bihler *et al*., 2005) in terms of activation properties, ion selectivity and Ca^{2+} sensitivity (Czempinski *et al*., 1997; 2002). Characterization of transgenic plants showed that TPK1 has a function in intracellular K^+ homeostasis, affecting germination, seedling growth and stomatal movement (Gobert *et al*., 2007). In addition to TPK1, the only other plant TPK channel electrophysiologically characterized by far is TPK4 which is targeted to the plasma membrane, where it establishes a voltage-independent K^+ channel. Hyperpolarizing as well as depolarizing membrane voltages elicited instantaneous K^+ currents, which were blocked by extracellular Ca^{2+} and cytoplasmic protons (Becker *et al*., 2004). TPK4 operates as a so-called "open rectifier" exhibiting saturating currents at depolarizing membrane potentials. Although reminiscent of the

rectification properties of animal Kir channels, the molecular mechanism of rectification in TPK4 is currently unknown.
So far the biophysical properties and physiological roles of the other *Arabidopsis* vacuolar TPK channels (Voelker *et al*., 2006, Dunkel *et al*., 2008), TPK2, TPK3, and TPK5, remain unknown (Voelker *et al*., 2010). In order to characterize functional domains of these vacuolar TPKs, domain-swapping experiments with TPK4 and vacuolar TPKs have recently been performed. Employing TPK channels of *A*. *thaliana* for pore-domain swapping experiments, the second pore of TPK4 by the second pore of all other TPKs and that of the one-pore channel KCO3 was replaced (Marcel *et al*., 2010). The obtained results indicated that the vacuolar TPK2, TPK3 and TPK5 are potassium channels with a similar selectivity and instantaneous activity as TPK4. The prediction of a single Ca^{2+} binding EF-hand in TPK2 and TPK3 suggest a regulation of TPK2/3 by Ca^{2+} similarly to that of TPK1. However, nor the biophysical characteristics of TPK3 homomeric channel, neither its physiological functions have been determined up to now.
We have recently reported detection of *At*TPK3, a putative two-pore potassium channel protein with relatively high probability of targeting to chloroplast, in isolated thylakoid membrane obtained from *Arabidopsis* plants, by using a specific monoclonal antibody, 3A8 (Zanetti *et al*., 2010). Given that these plants were not manipulated genetically, possible overexpression-induced mistargeting can be excluded.
In the present work we describe the successful expression of TPK3 in *E*. *coli*, its purification and the biophysical characteristics of the channel studied in planar lipid bilayer experiments. Furthermore, we determined the physiological role of TPK3 by using silenced plants.

RESULTS AND DISCUSSION

In order to confirm the subcellular localization of TPK3 channel also in intact leaves, we used *At*TPK3-DsRed2 fusion protein and visualized DsRed2 fluorescence in agro-infiltrated *Arabidopsis* leaves. Co-localization with chloroplasts was proved by merging DsRed2 image and chlorophyll autofluorescence (Fig. 1A). Further, we studied localization of the protein in leaves from *wt Col0* plants: immunoblotting with specific monoclonal anti-TPK3 antibody revealed this protein in the lamellae fraction (Fig. 1B). Western blots using specific antibodies against markers of districts of the thylakoid membrane confirm lack of cross-contamination of the purified fractions (e.g. PSI component PsaD, PSII internal antennae CP43, HMA1 Cu-ATPase and KARI ketol-acid reductoisomerase).
Next, in order to investigate whether *At*TPK3 gives rise to channel activity, the protein was expressed, purified and studied in electrophysiological planar lipid bilayer (BLM) experiments. *At*TPK3 was expressed in fusion with N-terminal His_6 TAG in *E*. *coli*. As illustrated in Fig. 2A, the anti-His_6 TAG antibody recognized a 51 kDa band only in the cells transfected with pET28a carrying the *tpk3* gene and only following induction of expression with IPTG. The observed apparent molecular weight is in good agreement with the predicted one (54 kDa) indicating that the protein does not undergo degradation in this expression system. Bacteria expressing the proteins were used for subsequent purification of the protein. As shown in Fig. 2B, the eluted protein was recognized by three different antibodies: anti-His_6 TAG antibody, a specific monoclonal antibody raised against TPK3 and a general antibody able to recognize the highly conserved selectivity filter region of all potassium channels. The same band was recognized in the eluted fraction and in *A*. *thaliana* thylakoids (Fig. S1). Given

that all three antibodies recognize the same protein of 51 kDa, strongly indicating successful purification of *At*TPK3, we used the eluted protein fraction for functional analysis.
The purified protein was added to artificial planar bilayer to study its channel activity. Fig. 3. shows representative current traces recorded at +80 and -80 mV under symmetrical potassium gluconate solution (A) and the current-voltage relationship recorded under the same conditions, yielding a slope conductance of 35 pS and a slight rectification (B). Channel activity required calcium, in accordance with the EF-hand present in the protein. In particular, calcium induced an increase of the open probability as observable in the current traces as well as the amplitude histograms in Fig. 4. In order to study the selectivity of the observed activity, asymmetrical ionic conditions were used (500 mM KCl on the *cis* side, while 100 mM KCl on the *trans* side of the chamber). Fig. 5 illustrates the channel activity at various potentials and the single channel current-voltage (i-V) curve. Under these ionic conditions a reversal potential of -40,6 mV is expected for a perfectly selective potassium channel. The observed value of -26 mV in our experiments indicates a P_K/P_{Cl} value of approx. 4. In accordance with the selectivity of the channel for potassium, we observed activity with 30-35 pS also in potassium gluconate solution where gluconate is used as an impermeant anion (Fig. 5A and B). Interestingly, the channel adopted a half conductance state in several experiments (Fig. 5B). Next, we studied the effect of classical potassium channel inhibitors on TPK3 activity. As shown in Fig. 6A, barium added to the *cis* side was able to cause a fast block of the activity already at 5 mM concentration, while tetraethylammonium did not affect activity even at 100 mM concentration added to both sides (Fig. 6B). Given that *At*TPK1 can be activated by protons and proton concentration changes in the *lumen* and in the stroma during photosynthesis, we investigated the effect of protons on *At*TPK3 activity. As shown in Fig. 6C, the open probability of the channel increased upon acidification of the *cis* compartment as indicated by an increased current level in the amplitude histogram.
In order to investigate the physiological role of *At*TPK3, plants lacking the channel protein were obtained. Given that T-DNA insertion lines are not available in current seed banks (Zanetti *et al*., 2010), we constructed silenced *Arabidopsis* lines. Silencing was obtained using a strategy consisting in floral-dip-mediated transformation of *wt Col0* plants with *Agrobacterium tumefaciens* carrying a pBIN Rolc plasmid containing a kanamycin resistance cassette and a 200 bp-long sequence equivalent to the 5'-UTR region of the TPK3 messenger RNA, linked to an antisense sequence of the same portion of *m*RNA (Molesini *et al*., 2009). Fig. 7A illustrates that in 3 independent lines successful silencing was obtained, while in 3 other lines *m*RNA coding for TPK3 was still detectable. Selection of silenced plants was obtained on kanamycin-containing agar plate (Fig. S2). The successful silencing was further confirmed by Western blot using the specific monoclonal anti-TPK3 antibody on thylakoids isolated from *wt Col0* plants as well as from a pool of the silenced plants lacking TPK3 transcripts (Fig. 7B). This result further confirmed, also by biochemical means, the presence of TPK3 in thylakoids.
Plants effectively lacking the *At*TPK3 channel protein were cultured under different conditions to visualize any phenotype. *wt Col0* and silenced seedlings, grown on agar plate, did not show any difference in germination (Fig. S3). Plants grown in soil and cultured under a light regime of LD 12:12 photoperiod at 40 µmol m^{-2} s^{-1} photons intensity showed no difference with respect to *wt Col0* (Fig. 8A). However, when light intensity was increased to 90 µmol m^{-2} s^{-1} photons during growth, the silenced plant showed a decreased rosette size with respect to *wt Col0* (Fig. 8A and B). Examples of rosettes from one representative experiment are shown in Fig. 8A. Difference in growth was statistically significant (for rosette size) and was reproduced other 5 times. Furthermore, the silenced plants cultured under this condition were reproducibly characterized by an altered pigmentation due to accumulation of

anthocyans (Fig. 8A and Fig. 8C). No significant differences could be observed in the content of other photosynthetic pigments (Table I). Please note that plants transformed with the same strategy but not successfully silenced, did not show significant difference with respect to *wt Col0* (Fig. S4), indicating that the silencing construct itself was not responsible for the observed phenotype. Given the thylakoid location of *At*TPK3 and the light-dependent phenotype, we investigated the ultrastructure of TPK3-less plants and highlighted a dramatic change in the organization of the thylakoids. In particular, membranes in *grana* regions were not stacked in all three silenced lines, but only in those cultured at 90 µmol m^{-2} s^{-1} photons light intensity (Fig. 9A). These data further confirm that the silencing construct was not determining the phenotype, rather, the higher light intensity caused its appearance.
The observed thylakoid disorganization might *a priori* result from an altered overall photosystem composition. Therefore we've tested the intactness and relative quantity of the photosynthetic complexes using non-denaturing Deriphat PAGE (e.g. Teardo *et al*., 2007). No differences could be observed indicating that the lack of the channel itself did not have an impact on PSI/PSII complex organization (Fig. 9B). On the other hand, such an altered thylakoid structure is expected to affect photosynthetic efficiency in TPK3-less plants. In accordance, chlorophyll fluorescence measurements of variable/maximal fluorescence, a parameter related to efficiency of charge separation at Photosystem II, highlighted that this value was significantly lower in silenced plants cultured at 90 µmol m^{-2} s^{-1} photons (Fig. 9C). The observed light-sensitive phenotype as well as the decrease of Fv/Fm values might *a priori* be due to degradation of some PSII components. Thus, we investigated the protein content for some of the main components of PSI, PSII, ATP synthase and cyt b_6f complexes (Fig. S5), revealing no gross alterations.
In oxygenic photosynthesis, light drives photosynthesis mostly via linear photosynthetic electron transfer, which occurs via the in-series activity of the two photosystems (PS). This process generates an electrochemical proton gradient ($\Delta\mu_{H^+}$ or pmf), which is used to produce ATP, which is used along with the reducing power (NADPH) for proper carbon assimilation in Benson-Bassham Calvin cycle. Moreover, generation of the electrochemical proton gradient is required for proper stress response, because it modulates capacity to dissipate excess light as heat via NPQ (Szabò *et al*., 2005). This term describes thermal dissipation of absorbed energy that occurs in the pigment-containing proteins of Photosystem II (PSII), and is controlled by *lumen* acidification via its activation of the xanthophyll cycle (XC) and of the NPQ effector PsbS. To see if TPK3 could be involved in the modulation of the pmf *in vivo*, and in the plant acclimation capacity, we compared *wt Col0* and mutant lines grown at 40 µmol m^{-2} s^{-1} photons and at higher light intensity (90 µmol m^{-2} s^{-1} photons). While no difference were found at the lower intensity a clear phenotype was seen at 90 µmol m^{-2} s^{-1} photons, where TPK3 as displayed enhanced antocyanin accumulation, a partially chlorotic phenotype and a reduced growth capacity (Fig. 8). We therefore investigated their ability to build a pmf in the light taking advantage of the relationship existing between the $\Delta\mu_{H^+}$ and the electrochromic shift (ECS). This signal stems from a change in the absorption spectrum of specific pigments embedded in the thylakoids upon exposure to the electric field component of the $\Delta\mu_{H^+}$ (Witt, 1979). Upon illumination with continuous light, the ECS signal can be used to assess the absolute size of the proton motive force, and that of its two components, $\Delta\Psi$ and ΔpH though the utilization of the "Dark Induced Relaxation Kinetics" (DIRK) approach (Kramer and Sacksteder 1998; Kanazawa and Kramer, 2002; Cruz *et al*., 2001, 2004). In particular, when the light is switched off during steady state photosynthesis, a fast decay is seen, which reflects H^+ leak through the ATP synthase (g_{H^+}), and is followed by a slower inversion of the ECS. This signal has been interpreted in terms of the transient inversion of the membrane potential due

to a difference in the relaxation rates of the ΔpH and ΔΨ. The faster relaxation rate of the electric component of the pmf, due to the low dielectric constant of the thylakoid membranes (Vredenberg, 1976), the high H^+ buffering capacity of the lumen (Junge and McLaughlin, 1987), and the slow rate of charge redistribution along the membranes (Cruz *et al*., 2001) leads to a membrane potential depolarisation until a negative value is attained, which is proportional to the size of the steady state ΔpH. Again, no differences were found between the two genotypes at low light while at higher light both the size of the pmf, as well as the proton conductivity of the membranes (g_{H^+}) were reduced in the mutant (Fig. 10A). Moreover, as judged by the extent of the inversion of the ECS, its capacity to build a ΔpH was lower in silenced plants as than in the *wt Col0* (Fig. 10B). Consistent with this conclusion, while the *wt Col0* was able to increase its NPQ capacity when shifted from low to higher light, NPQ remained lower in the mutant despite of the fact that its xanthophyll cycle capacity was the same (Fig. 10A and Table I). This lower capacity to dissipate thermally the absorbed energy could be one of the elements responsible for the enhanced photosensitivity observed in *tpk3*-silenced plants. In both cases, infiltration of mutant and *wt Col0* leaves with a solution containing saturating concentration of the ionophore nigericin (which exchanges H^+ with K^+ and therefore collapses the ΔpH without affecting the ΔΨ) removed all the differences measured though the ECS spectroscopy (g_{H^+}, ECS inversion), confirming that they related to differences in the ΔpH.
The above experiments were performed on plants acclimated to different light intensities from the beginning of germination. To further confirm the photosensitive phenotype of the TPK3-knock-down plants, we treated the plants with high, 1500 $\mu molm^{-2}\ s^{-1}$ photons intensity for the indicated times and observed a dramatic decrease in Fv/Fm value in the silenced plants with respect to *wt Col0*, where an initial decrease was followed by recovery (Fig. 11A). Also in these samples however, degradation of the PSII component known to be principally affected during photoinhibition, i.e. D1, was not significantly higher than in *wt Col0* plants (Fig. 11B and S6). Furthermore, addition of lincomycin, which inhibits protein synthesis and therefore D1 turnover, prevented recovery of the Fv/Fm value in both *wt Col0* and silenced plants to a similar extent, indicating that the observed photoinhibitory phenotype was probably not due to the damage of recovery mechanisms in the silenced plants (Fig. S7).
In summary, this is the first work demonstrating by genetic means the importance of a thylakoid-located channel in the regulation of photosynthesis in higher plants.

MATERIALS AND METHODS

Heterologous expression of *tpk3*

tpk3 gene was expressed in C41(DE3) *E. coli* cells. These cells were transformed with *tpk3* gene in pET28a vector (*in frame* with a His_6 TAG at the N-terminus): 100 ng of DNA were used to transform competent cells by heat shock. After transformation, cells were selected on LB kanamycin plates (50 μg/mL) overnight at 37°C. Next day a single colony was picked up and inoculated in 5 mL of liquid LB medium supported with kanamycin (50 μg/mL) and grown overnight at 37°C in constant agitation (180 rpm).
On the third day 2 mL of the pre-inoculum were inoculated in 98 mL of fresh liquid LB medium with kanamycin (50 μg/mL); bacteria were grown in constant agitation at 37°C until the OD_{600} reached a value between 0.900 and 1.000. 0.7 mM IPTG (Sigma-Aldrich®) and 10 mM $BaCl_2$ (to guarantee a better growth of cells) was added to bacteria, grown at 37°C for a maximum of 19 hours.

Bacteria were collected at various times (0, 1, 3, 5, 19 hours after induction) by centrifugation at 6000 *g* for 10 minutes, 4°C (Allegra™ 25R, Beckman Coulter; TS-5.1-500 swinging bucket rotor, Beckman Coulter) and stored at -20°C.

Purification of *At*TPK3

Cells collected by centrifugation were resuspended in sonication buffer (250 mM NaCl, 25 mM TRIS, pH 8.0) added with protease inhibitors (1 µg/mL leupeptine and pepstatine) and then processed by sonication (cells were sonicated in ice to avoid heating in 6 cycles of 10 seconds each with 15 seconds of pause between cycles). After sonication, sample was centrifuged at 15000 *g* for 30 minutes, 4°C (5417R centrifuge, Eppendorf), to separate membrane fraction (pellet) from soluble fraction (supernatant).

Pellet was resuspended in 2.5% decyl-β-D-maltopyranoside solution (Sigma-Aldrich®) in sonication buffer and solubilized for 3 hours at room temperature in constant agitation. After a centrifugation at 15000 *g* for 30 minutes, 4°C (5417R centrifuge, Eppendorf), were obtained 2 fractions: a pellet from detergent treatment (called P_D) and a supernatant from detergent treatment (called S_D).

S_D was loaded on a Ni resin (HIS-Select® Nickel Affinity Gel, Sigma-Aldrich®) in a batch configuration and put in agitation at room temperature for 1 hour. After 3 washes in equilibration buffer (50 mM sodium phosphate, pH 8.0, 300 mM sodium chloride), *At*TPK3 was eluted from the resin in 3 consecutive steps with 250 mM imidazole solution (Sigma-Aldrich®) in equilibration buffer.

All the fractions were collected and tested in SDS-PAGE analysis.

SDS-PAGE and Western blot analysis

To test the presence of the channel and the district of accumulation in bacteria we performed an SDS-PAGE protein separation followed by a Western blot and immunodetection with anti-His_6 TAG antibody (Sigma-Aldrich®). Whole cells, pellet, supernatant from sonication treatment and (after verifying the localization of channel) other fractions collected were solubilized in SB buffer (300 mM TRIS/HCl pH 6.8, 11,5% w/v SDS, 50% w/v glycerol, 500 mM DTT, 0,1% w/v blue bromophenol) and loaded in a 10% acrylammide-6 M urea gel. After separation, proteins were transferred overnight on a PVDF membrane (BioTrace® PVDF Membrane, VWR).

Immunodetection of His_6-TPK3 was performed as reported: membrane was blocked in 10% milk solution in TBS buffer (10 mM TRIS pH 7.4, 150 mM NaCl), incubated for 2 hours with anti-His_6 TAG antibody diluted 1:1000 in TTBS buffer (10 mM TRIS pH 7.4, 150 mM NaCl, 0.05% v/v Tween 20), washed 6 times for 5 minutes each with TTBS buffer, incubated with HRP-conjugated secondary antibody (diluted 1:10000 in TTBS buffer), washed 6 times for 5 minutes each with TTBS buffer and then exposed to HRP substrate (SuperSignal® West Pico, Thermo Scientific) for 5 minutes in agitation. Signal was detected with autoradiography films (Amersham Hyperfilm ECL™, GE Healthcare).

Activity of *At*TPK3 in planar lipid bilayer

Planar lipid bilayer experiments were carried out to determine electrophysiological activity of *At*TPK3 as previously described (e.g. Teardo et al, 2011; De Stefani et al, 2011). It was used an asolecitin solution in decane/chloroform with a 100:1 ratio *per* mg of lipids. A membrane of 150 mV/pF was constructed between 2 compartments (*cis*/*trans*) and 3 mL of K gluconate (250 mM K gluconate, 10 mM HEPES, pH 7.4, 5 mM EDTA for calcium test; 250 mM K

gluconate, 10 mM HEPES, pH 7.4, 100 µM $CaCl_2$ for pH test) were added in *cis* and *trans* compartments.
Defined volumes of $CaCl_2$ 1 M (or H_3PO_4 2% v/v, to obtain defined concentrations of free calcium/pH) were added alternatively in both compartments to test the possible modulation of the channel.

Subcellular localization of *At*TPK3
The subcellular localization of *At*TPK3 channel was studied by agroinfiltration of *Arabidopsis thaliana wt Col0* plant leaves with a suspension of *Agrobacterium tumefaciens* carrying pGREAT-DsRed2 vector with *tpk3* gene in the MCS.

***A. tumefaciens* strain, transformation and preparation for agroinfiltration**
A. tumefaciens GV3101 strain, carrying the pSoup vector, was used for transformation of plants. This strain was transformed with pGREAT vector containing *tpk3* gene *in frame* with DsRed2 sequence, and used for the infiltration of *A. thaliana* 4-weeks-old plants leaves.
A. tumefaciens was transformed using the freeze-thaw method as described in Jyothishwaran *et al.*, 2007, and then plated in LB agar medium (10 g/L Tryptone, 5 g/L yeast extract, 10 g/L NaCl, 15 g/L Bacto-agar) with antibiotics.
Two days before infiltration, a single colony of transformed *A. tumefaciens* grown on agar plates was inoculated in 5 mL of YEP liquid medium (10 g/L Bacto-Tryptone, 10 g/L yeast extract, 5 g/L NaCl, pH 7.0) supplemented with specific antibiotics. Bacterial culture was incubated for 2 days at 30°C at 180 rpm on an orbital shaker.
After 48 hours, 2 mL of culture were transferred to Eppendorf tubes and pelleted by centrifugation at 3000 *g* for 5 min at room temperature (5417R centrifuge, Eppendorf). Bacterial pellet was resuspended in 1 mL of induction medium (10.5 g/L K_2HPO_4, 4.5 g/L KH_2PO_4, 1 g/L $(NH_4)_2SO_4$, 0.5 g/L Na citrate, 1 g/L glucose, 4 g/L glycerol, 1 mM $MgSO_4$, 10 mM MES, pH 5.6) and then transferred in 3 mL of induction medium supplemented with 100 µM acetosyringone (Sigma-Aldrich®) and grown for 6 hours at 30°C. Bacteria were pelleted at 3000 *g* for 5 minutes at room temperature (5417R centrifuge, Eppendorf), resuspended in infiltration medium (10 mM $MgSO_4$, 10 mM MES, pH 5.6) to a final OD_{600} of 0.400 and supplemented with 200 µM acetosyringone. This suspension was used for infiltration.

Agroinfiltration of *Arabidopsis thaliana* leaves
Agroinfiltration was conducted by infiltration of agrobacterial suspension in infiltration medium into intercellular spaces of fingernail-sized leaves of 4-weeks-old plants.
Plants used were kept in constant darkness for at least 16 hours before infiltration and without water supply. Leaves were infiltrated in the late afternoon in the abaxial side, using a needleless plastic syringe. Plants were then transferred in a growth room with controlled climatic conditions and tested for transformation after 4 days.

Confocal microscopy for infiltrated leaves *in planta*
Infiltrated leaves were observed after 4 days with the confocal microscope Leica TCS SP5 II (Leica Microsystems) mounted on a Leica DMI6000 CS inverted microscope with automated programmable scanning stage and motorized lens turret.
The images were collected with the Leica Application Suite software (LAS AF, Leica Microsystems). For the excitation of chlorophyll was used an Ar laser (wavelength: 488 nm) and, for DsRed2, a HeNe laser (wavelength: 543 nm); for fluorescence emission were used

Leica pre-setted filters ("Leica EGFP", 500-520 nm; "Leica DsRed", 570-620 nm; "Chlorophyll", 680-720 nm).

Post-transcriptional silencing of *tpk3* gene

Because of the unavailability of commercial mutants to permit the study of *tpk3* gene function was decided to silence the gene by a post-transcriptional system based on *si*RNA. Stable silenced plants were obtained with the floral dip method. Inflorescence of *wt Col0* plants were immerged in a suspension of *A. tumefaciens* carrying pBIN RolC vector (Molesini *et al*., 2009). Seeds collected from these plants were spread on $MS^{-1/2}$ plates added with kanamycin (50 µg/mL), because of the presence of a kan resistance cassette in the silencing construct. Plants grown on kanamycin were transferred to Jiffy-7® substrate (Jiffy Group), grown and tested for silencing by *m*RNA extraction.

Test of silencing success

Plants grown on kanamycin plates were tested for post-transcriptional silencing of *tpk3* gene by *m*RNA extraction. *m*RNA was extracted from a single leaf of each 4 weeks-old *wt Col0* (controls) and putative silenced plant, to verify the presence/absence of *tpk3* messenger. Leaves were collected and immediately frozen in liquid nitrogen and pulverized. 1 mL of TRIzol® (Invitrogen) was added to the powder, then mixed vigorously for 5 minutes and centrifuged for 5 minutes at 14000 rpm at room temperature (5417R centrifuge, Eppendorf). Supernatant was transferred in new Eppendorf tubes, were added 200 µL of chloroform and the samples were mixed for 5 minutes, then left at room temperature for 10 minutes. After a centrifugation at 13000 rpm for 5 minutes (5417R centrifuge, Eppendorf) and the recovery of the clear supernatant were added 0.7 volumes of isopropanol and the samples were mixed and kept at -20°C for 10 minutes. After a centrifugation at 14000 rpm for 10 minutes (5417R centrifuge, Eppendorf) were done 2 washes with 70% v/v ethanol solution, followed by RNA quantification. 5 µg of total RNA were used for DNase treatment and subsequent retrotranscription; after retrotranscription the final volume of *c*DNA was brought to 100 µL with ddH_2O and 5 µL of each sample was used for PCR analysis.

Test of photosynthetic efficiency of silenced plants

Silenced plants were tested by PAM analysis (WALZ Dual PAM 100, Heinz Walz, GmbH) to determine their photosynthetic efficiency (e.g. Teardo *et al*., 2010). It were determined parameters like Fv/Fm, ETR(II) and NPQ after dark adaptation of 20 minutes.

Growth conditions

Experiments were carried out on 4 to 12 week old *wt Col0* (control) and silenced *tpk3* lines. All genotypes were grown on Jiffy-7® substrate (Jiffy Group) in a phytotron at two different light intensities, 40 and 90 µmol m^{-2} s^{-1} photons, with a 12 hours photoperiod at 20°C and a 65% relative humidity. Plant was dark-adapted for at least 1 hour prior to taking measurements. For visualization of photosynthetic phenotype in silenced plants, *wt Col0* (controls) and silenced lines tested seeds were spread on Jiffy-7® substrate (Jiffy Group) and grown in 2 different irradiation conditions (40 and 90 µmol m^{-2} s^{-1} photons, respectively "low" and "high" light conditions) in the same humidity conditions and photoperiod (70% RH, LD 12:12).

Transmission Electron Microscopy (TEM) on leaves of silenced plants

wt Col0 (controls) and silenced lines leaves were collected from 4-weeks-old plants and processed for TEM analysis.

Leaf samples were collected at midday and fixed overnight in 2.5% v/v glutaraldehyde solution in 100 mM sodium cacodylate pH 7.2, 4°C. Were done 3 washes of 7 minutes each in 100 mM sodium cacodylate pH 7.2 and a post-fixation in a 1% OsO_4 solution in 100 mM sodium cacodylate pH 7.2, 4°C in the dark for 1 hour. The de-hydration of samples was conducted through a graded ethanol series (25, 50, 70, 95, 100% v/v in ddH_2O) in 3 steps of 15 minutes for each concentration, followed by 3 steps of 15 minutes each in propylene oxide (the first one at 4°C, the other two at room temperature). The impregnation of samples was done at 45°C in 3 steps of 1 hour each with Epon resin solutions in propylene oxide (Sigma-Aldrich®) with different resin:propylene oxide proportions (1:3 for the first step, 1:1 for the second step, 3:1 for the third step), followed by 2 steps of 1 hour each in pure Epon resin (Sigma-Aldrich®) at 37°C. The polymerization was carried out putting samples in an heater for 3 days at different temperatures from day to day (day 1: 37°C; day 2: 45°C; day 3: 60°C). Samples were cut in 80 nm slices with the Ultrotome V ultramicrotome (LKB). Sections were collected on copper support grids and then contrasted with an uranyl acetate saturated solution in 100% ethanol for 15 minutes followed by an incubation in a 1% w/v lead citrate solution in 100% ethanol for 7 minutes. Samples were observed with the Tecnai G^2 Spirit Transmission Electron Microscope (Fei™ Electron Microscopes), operating at 100 kV.

Isolation of thylakoids and test for photosystems proteins

Thylakoids from *wt Col0* and *tpk3*-silenced plants (in low and high light conditions) were isolated to test the amount of photosystems' proteins.

Leaves were ground with a pestle in liquid nitrogen to obtain a fine powder, then homogenized with B1 buffer (400 mM sodium chloride, 200 mM magnesium chloride, 0.5% milk, 20 mM tricine/KOH pH 7.8, 2 mM benzamidine, 1 mM β-amino caproic acid). Homogenate was then filtered through a nylon muslin and collected in a tube, then centrifuged at 1200 *g* for 12 minutes, 4°C (5417R centrifuge, Eppendorf). After discarding the supernatant, chloroplast pellet was gently resuspended in B2 hypotonic solution (15 mM sodium chloride, 5 mM magnesium chloride, 20 mM tricine/KOH pH 7.8, 2 mM benzamidine, 1 mM β-amino caproic acid), to break the chloroplast envelope. Samples were centrifuged at 4000 *g* for 12 minutes, 4°C (5417R centrifuge, Eppendorf), to obtain a pellet composed of thylakoid membranes. After a wash of pellet in B2 buffer and a second centrifugation at 6000 *g* for 12 minutes, 4°C (5417R centrifuge, Eppendorf), thylakoids were resuspended in B4 buffer (400 mM sorbitol, 15 mM sodium chloride, 5 mM magnesium chloride, 20 mM HEPES/KOH pH 7.5).

Thylakoids were diluted in 80% acetone, chlorophyll concentration was measured spectroscopically (Porra, 1974).

Differential amounts of thylakoids (as µg of chlorophyll or total proteins) were loaded in SDS-PAGE gel, then were performed a Western blot and immunodetection with antibodies specific for photosystems proteins (D1, D2, LHC, etc...), as reported in "*SDS-PAGE and Western blot analysis"* section.

Biochemical characterization of TPK3 localization

For immunoblot analyses, leaves were harvested and chloroplast fractions were purified according to Salvi *et al*., (2011).

The fractions collected were solubilized in SB buffer, loaded in a 12% acrylammide-6 M urea gel and transferred on a nitrocellulose membrane (Whatman, Germany). In the Western blot analyses each fraction contained 6 µg of proteins.
Replicate filters were incubated with antibodies specific for different marker proteins (anti-HMA1, anti-PsaD, anti-KARI and anti-CP43) and a specific antibody for the interested channel (anti-TPK3). Signals were detected using the Enhanced Chemiluminescence Western Blotting Kit (GE HEALTHCARE, UK). anti-HMA1 1:1000, anti-PsaD 1:3000 , anti-KARI 1:15000, anti-CP43 1:10000 and anti-TPK3 1:1.

Spectroscopic measurements
Spectroscopic measurements were performed on intact leaves with a flash spectrophotometer (JTS-10, BioLogic France).
The induction of NPQ was determined sing the (Fm-Fm')/Fm' formula (Bilger and Bjorkman, 1991), where Fm is the maximum fluorescence emission in the dark (Q_A reduced) while Fm' is the maximum emission measured upon steady state illumination. Changes in the pmf were evaluated form signals reflecting membrane potential changes (ECS) at 520-545 nm to deconvolute the ECS signal from redox changes associated with the cytochrome b_6f complex. A white LED source filtered through appropriate interference filters. The photodiodes were protected from actinic light by a BG 39 filter.
At the beginning of each experiment, fluorescence parameters (Fv/Fm) were measured to verify the physiological status of the plant.

FIGURE LEGENDS

Figure 1. TPK3 is located to stromal *lamellae* thylakoid membrane.
A) Localization of *At*TPK3 in chloroplasts of infiltrated leaves. Left panel: chlorophyll signal; middle panel: DsRed2 signal; right panel: merged image. Yellow arrows show the *At*TPK3-DsRed2 fluorophore in chloroplasts, white arrow shows non-transformed chloroplasts. **B)** Localization of TPK3 in *Arabidopsis thaliana* leaves. *Lamellae* (L), BBY (BBY), margin (M), thylakoids (TH), chloroplasts (CHL), stroma (S), envelope (E) and thylakoids (THY) fractions were isolated from *Arabidopsis thaliana wt Col0* leaves. Purity of the employed fractions was tested using antibodies against proteins known to be mostly localized in the grana inner part (BBY) and margins (PSII, CP43) or in the stroma *lamellae* (PSI, PsaD) (Albertsson, 2001), in the chloroplast envelope (HMA1)(Segneurin-Berny *et al*., 2006) or in the stroma (Kari) (Dumas *et al*., 1994).

Figure 2. Expression and purification of *At*TPK3 protein from *E. coli*.
A) Expression of *At*TPK3 in *E. coli* C41(DE3) cells, Western blot and immunodetection with anti-His_6 TAG antibody (T: entire bacteria; P: pellet after sonication; S: supernatant after sonication). The first set represents bacteria transformed with empty pET28a vector and induced for 19 hours, as negative control. The other 4 sets represent bacteria transformed with pET28a*::tpk3* vector and induced for 0, 1, 3 and 5 hours. IPTG used for induction was added at final concentration of 700 mM to cell culture at OD_{600} = 0,800. **B)** Purification of *At*TPK3, Western blot and immunodetection with anti-His_6 TAG antibody, 3A8 monoclonal serum and anti-KPORE antibody (D-T P: detergent-treated pellet after sonication; SDT: supernatant from detergent treatment; FT: column flow-through; W_{EB}: column wash with

equilibration buffer; W_I: column wash with 5 mM imidazole; E1, E2, E3: elution fractions in 250 mM imidazole). *At*TPK3 is showed by arrows.

Figure 3. Recombinant TPK3 induces channel activity in planar lipid bilayer.
A) Representative current traces recorded at the indicated voltages in symmetrical 250 mM K gluconate solution in the presence of 100 μM calcium. Amplitude histograms were obtained from 100 second-long traces and were fitted using the Origin 6.1 program set.
B) Single channel i-V curve obtained from different experiments (N = 5). Mean current ±SD are shown. Fitting revealed a chord conductance of 35 pS.

Figure 4. Calcium-sensitivity of TPK3 activity.
Activity was recorded as in Fig. 3, before and following the addition of calcium to the *cis* side resulting in the indicated calcium concentrations.

Figure 5. TPK3 is selective for potassium.
A) Upper part: representative traces recorded in asymmetrical KCl solution at the indicated voltages (*cis*: 500 mM KCl; *trans*: 100 mM KCl). Lower part: i-V curve obtained from 2 different experiments. **B)** Exemplificative current trace showing transitions to half-conductance sub-state recorded at +100 mV.

Figure 6. Pharmacological characterization of TPK3 activity.
Addition of barium **(A)** to the *cis* side resulted in fast block of the activity, while TEA^+, even at 50 mM does not reduce activity **(B)**. **C)** decrease of pH from 7.4 to 6.5 increased activity as observable from the amplitude histograms.

Figure 7. Stable silencing of *tpk3* gene results in lack of TPK3 protein in thylakoids.
A) PCR on *c*DNA retro-transcribed from total *m*RNA extracted from *wt Col0* and 6 putative silenced lines for *tpk3* messenger. The band corresponding to *tpk3* messenger is clearly shown in *wt Col0* plant and in *tpk3*- #4, #5 and #6 (non-silenced lines, n-s.l.). In *Arabidopsis* lines called *tpk3*- #1, #2 and #3 the *m*RNA is not present (silenced lines, s.l.). Below there is the amplification of *actin* as control (1st lane: molecular markers). **B)** Western blot and immunodetection with 3A8 monoclonal serum of thylakoid fractions of *wt Col0* and *tpk3*-silenced lines. Total protein amount *per* lane is 200 μg. *At*TPK3 and ATP-synthase bands are shown by arrows. ATP-synthase was used as loading control.

Figure 8. Plants lacking TPK3 display reduced growth and increased photosensitivity.
A) The «macroscopic» phenotype of *wt Col0* and *tpk3*-silenced plants, in «low» light conditions (40 μmol m^{-2} s^{-1} photons) and «high» light conditions (90 μmol m^{-2} s^{-1} photons). *tpk3*-silenced plants in high light conditions shown a clear photosynthetic phenotype respect to *wt Col0* in all irradiation conditions and *tpk3*-silenced plants in low light conditions. **B)** Comparison between rosette dimension of *wt Col0* and *tpk3*-silenced plants. At 40 μmol m^{-2} s^{-1} photons there are no significative differences in rosette diameter, whereas at 90 μmol m^{-2} s^{-1} photons rosette dimension is reduced (N = 5 plants *per* genotype). **C)** Antocyanin absorbance value/x μg of isolated thylakoid. Antocyanin content was measured as described in Stettler *et al*., (2009).

Figure 9. Lack of TPK3 results in altered thylakoid membrane organization in plants cultured at 90 μmol m^{-2} s^{-1} photons.
A) The «microscopic» phenotype of *wt Col0* and *tpk3*-silenced lines. Micrographies show chloroplasts of *wt Col0* and *tpk3*-silenced 6-weeks-old plants in «low» light conditions (40 μmol m^{-2} s^{-1} photons) and «high» light conditions (90 μmol m^{-2} s^{-1} photons). Chloroplasts of *wt Col0*, in all irradiation conditions, were normal and showed good thylakoids and *grana* (like *tpk3*-silenced plants in low light conditions), whereas *tpk3*-silenced plants in high light conditions showed abnormal thylakoid structures and no *grana*. **B)** Deriphat-PAGE of *wt Col0* and *tpk3*-silenced thylakoids for visualizing entire photosynthetic complexes. No differences can be detected between samples (30 mg of chlorophyll *per* lane loaded). **C)** Comparison between Fv/Fm values of *wt Col0* and *tpk3*-silenced plants grown in 40 and 90 μmol m^{-2} s^{-1} photons. Only for plants grown in high light conditions are shown significative differences (N = 9 plants *per* genotype).

Figure 10. Functional characterization of *wt Col0* and *tpk3*$^{-}$ plants under low and moderate light intensities.
A) Upper panel: visible phenotype of *wt Col0* and mutant plants grown at 40 and 90 μmol m^{-2} s^{-1} photons. Middle panel: H^+ conductivity of the ATP synthase (g_{H^+}) in the presence and absence of the H^+/K^+ exchanger nigericin. Proton permeability was evaluated form the decay of the ECS signal upon dark adaptation of leaves exposed to 1100 μmol m^{-2} s^{-1} photons. ($g_{H^+} = 1/\tau$) after fitting the decay kinetics with a single exponential (see following figure); fitting the traces with two exponential did not improve the quality of the fit; data ±s.e. (N = 4-10). Lower panel: NPQ capacity; NPQ was estimated according to the formula Fm-Fm'/Fm' (Bilger and Bjorkman, 1991); maximum NPQ capacity was estimated upon exposure to saturating light for 10 minutes using a fluorescence imaging device). Data ±s.e. (N = 20-25). Deconvolution of ECS signals **(B)** revealed a decreased proton conductance and NPQ in silenced plants. Data are from 24 curves obtained with all three silenced lines.

Figure 11. Strong photoinhibition is associated with lack of TPK3.
A) Time trend of Fv/Fm values for *wt Col0* and *tpk3*-silenced lines, after photoinhibition treatment. Plants were conditioned in «low» light conditions (40 μmol m^{-2} s^{-1} photons) for 1 hour and then exposed to 1500 μmol m^{-2} s^{-1} photons from 0 to 24 hours. Fv/Fm values were collected at 0, 1, 2, 3, 4, 5, 6, 8 and 24 hours of photoinhibition treatment and after a 20 minutes dark adaptation (N = 25 plants *per* genotype). **B)** Western blot on total extracts of *wt Col0* and 2 of the 3 *tpk3*-silenced lines and immunodetection with anti-D1 (strip 1) and anti-PsaA (strip 2). Arrows indicate proteins recognized by the antibodies. Total extracts were made after 1 hour of irradiance at 40 μmol m^{-2} s^{-1} as control (Time: 0 hours PI) and after 6 hours of photoinhibitory treatment (Time: 6 hours PI). 2 plants *per* genotype were tested.

SUPPLEMENTARY FIGURE LEGENDS

Figure S1. Western blot and immunodetection with 3A8 monoclonal serum of thylakoid fraction and E_1 elution fraction.
*At*TPK3 is showed by arrows (200 μg of protein loaded).

Figure S2. Selection of seeds on kanamycin plates. Only transgenic seeds can give rise to silenced plants.

Figure S3. Agar-plate germinated 2-weeks-old seedlings of *wt Col0*, silenced (s.l.) and non-silenced (n-s.l.) lines for *tpk3* messenger.
For all the genotypes, no differences in germination were observed.

Figure S4. Comparison of phenotypes between *wt Col0* and silenced and non-silenced plants.
Silenced line (for example, is shown *tpk3*$^{-}$ #1) has the already described phenotype, with reduced rosette diameter and brown leaves. Non-silenced lines (*tpk3*$^{-}$ #4, #5 and #6) are very similar to *wt Col0* ones. All plants were grown at 90 μmol m^{-2} s^{-1} photons.

Figure S5. Western blot and immunodetection with antibodies specific for proteins of the photosysnthetic apparatus.
1st strip: D1, 0,1 μg of chlorophyll loaded; 2nd strip: D2, 1 μg of chlorophyll loaded; 3rd strip: LHCII, 0,5 μg of chlorophyll loaded; 4th strip: cytochrome f, 5 μg of chlorophyll loaded; 5th strip: *Atp*B, 1 μg of chlorophyll loaded; 6th strip: PsaA, 5 μg of chlorophyll loaded.

Figure S6. Densitometry dataset for Western blot of Fig. 11B. Values represent the intensity *per* mm^2 of all bands quantified for *wt Col0* controls and 2 of the 3 *tpk3*-silenced lines. 2 plants *per* genotype were tested.

Figure S7. Lincomycin treatment of *wt Col0* and *tpk3*$^{-}$ #1 and #2 lines. All the lines behavior similarly before and after the antibiotic treatment, suggesting the absence of turnover problems for photosystems' proteins.

REFERENCES

Albertsson P.A. (2001) A quantitative model of the domain structure of the photosynthetic membrane. *Trends Plant Sci. 6, 349-354*

Becker D., Geiger D., Dunkel M., Roller A., Bertl A., Latz A., Carpaneto A., Dietrich P., Roelfsema M.R., Voelker C., Schmidt D., Mueller-Roeber B., Czempinski K., Hedrich R. (2004) *At*TPK4, an *Arabidopsis* tandem-pore K^+ channel, poised to control the pollen membrane voltage in a pH- and Ca^{2+}-dependent manner. *Proc. Natl. Acad. Sci. USA 101, 15621-15626*

Bihler H., Eing C., Hebeisen S., Roller A., Czempinski K., Bertl A. (2005) TPK1 is a vacuolar ion channel different from the slow vacuolar cation channel. *Plant Physiology 139, 417-424*

Bublitz G.U., Boxer S.G. (1997) Stark spectroscopy: applications in chemistry, biology, and materials science. *Annu. Rev. Phys. Chem. 48, 213-242*

Checchetto V., Segalla A., Allorent G., La Rocca N., Leanza L., Giacometti G.M., Uozumi N., Finazzi G., Bergantino E., Szabò I. (2012) Thylakoid potassium channel is required for efficient photosynthesis in Cyanobacteria. *Proc. Natl. Acad. Sci. USA 109: 11043-11048*

Cruz J.A., Sacksteder C.A., Kanazawa A., Kramer D.M. (2001) *Biochemistry 40, 1226-1237*

Czempinski K., Zimmermann S., Ehrhardt T., Mueller-Roeber B. (1997) New structure and function in plant K^+ channels: KCO1, an outward rectifier with a steep Ca^{2+} dependency. *EMBO J. 16, 2565-2575*

Czempinski K., Frachisse J.M., Maurel C., Barbier-Brygoo H., Mueller-Roeber B. (2002) Vacuolar membrane localization of the *Arabidopsis* "two-pore" K^+ channel KCO1. *Plant Journal 29, 809-820*

De Stefani D., Raffaello A., Teardo E., Szabò I., Rizzuto R. (2011) A forty-kilodalton protein of the inner membrane is the mitochondrial calcium uniporter. *Nature 476, 336-340*

Dumas R., Cornillon-Bertrand C., Guigue-Talet P., Genix P., Douce R., Job D. (1994) Interactions of plant acetohydroxy acid isomeroreductase with reaction intermediate analogues: correlation of the slow, competitive, inhibition kinetics of enzyme activity and herbicidal effects. *Biochem. J. 301, 813-820*

Dunkel M., Latz A., Schumacher K., Müller T., Becker D., Hedrich R. (2008) Targeting of vacuolar membrane localized members of the TPK channel family. *Mol. Plant. 1, 938-949*

Enyedi P., Czirják G. (2010) Molecular background of leak K^+ currents: two-pore domain potassium channels. *Physiol. Rev. 90, 559-605*

Gobert A., Isayenkov S., Voelker C., Czempinski K., Maathuis F.J. (2007) The two-pore channel TPK1 gene encodes the vacuolar K^+ conductance and plays a role in K^+ homeostasis. *Proc. Natl. Acad. Sci. USA 104, 10726-10731*

Genty B., Briantais J.M., Baker N.R. (1989) *Biochim. Biophys. Acta 990, 87-92*

Junge W., McLaughlin S. (1987) The role of fixed and mobile buffers in the kinetics of proton movement. *Biochim. Biophys. Acta 890, 1-5*

Junge W., Witt H.T. (1968) *Nature 222, 5198-5199*

Jyothishwaran G., Kotresha D., Selvaraj T., Srideshikan S.M., Rajvanshi P.K., Jayabaskaran C. (2007) A modified freeze-thaw method for efficient transformation of *Agrobacterium tumefaciens. Curr. Sci. 93, 770-772*

Kanazawa A., Kramer D.M. (2002) *Proc. Natl. Acad. Sci. USA 99, 12789-12794*

Kramer D.M., Sacksteder C.A., Cruz J.A. (1999) *Photosynth Res. 60, 151-163*

Marcel D., Müller T., Hedrich R., Geiger D. (2010) K^+ transport characteristics of the plasma membrane tandem-pore channel TPK4 and pore chimeras with its vacuolar homologs. *FEBS Lett. 584, 2433-2439*

Molesini B., Pandolfini T., Rotino G.L., Dani V., Spena A. (2009) Aucsia gene silencing causes parthenocarpic fruit development in tomato. *Plant Physiol. 149, 534-48*

Porra R.J., Grimme L.H. (1974) A new procedure for the determination of chlorophylls a and b and its application to normal and regreening *Chlorella*. *Anal. Biochem. 57, 255-267*

Schönknecht G., Spoormaker P., Steinmeyer R., Bruggemann L.I., Ache P., Dutta R., Reintanz B., Godde M., Hedrich R., Palme K. (2002) KCO1 is a component of the slow-vacuolar (SV) ion channel. *FEBS Lett. 511, 28-32*

Salvi D., Moyet L., Seigneurin-Berny D., Ferro M., Joyard J., Rolland N. (2011) Preparation of envelope membrane fractions from *Arabidopsis* chloroplasts for proteomic analysis and other studies. *Methods Mol. Biol. 775, 189*

Seigneurin-Berny D., Gravot A., Auroy P., Mazard C., Kraut A., Finazzi G., Grunwald D., Rappaport F., Vavasseur A., Joyard J., Richaud P., Rolland N. (2006) HMA1, a new Cu-ATPase of the chloroplast envelope, is essential for growth under adverse light conditions. *J. Biol. Chem. 281, 2882-2892*

Stettler M., Eicke S., Mettler T., Messerli G., Hörtensteiner S., Zeeman S.C. (2009) Blocking the metabolism of starch breakdown products in *Arabidopsis* leaves triggers chloroplast degradation. *Mol. Plant 2, 1233-1246*

Szabó I., Bergantino E., Giacometti G.M. (2005) Light and oxygenic photosynthesis: energy dissipation as a protection mechanism against photo-oxidation. *EMBO Rep. 6, 629-634*

Teardo E., Formentin E., Segalla A., Giacometti G.M, Marin O., Zanetti M., Lo Schiavo F., Zoratti M., Szabò I. (2011) Dual localization of plant glutamate receptor *At*GLR3.4 to plastids and plasmamembrane. *Biochim. Biophys. Acta 1807, 359-367*

Teardo E., Segalla A., Formentin E., Zanetti M., Marin O., Giacometti G.M., Lo Schiavo F., Zoratti M., Szabò I. (2010) Characterization of a plant glutamate receptor activity. *Cell Physiol. Biochem. 26, 253-262*

Voelker C., Schmidt D., Mueller-Roeber B., Czempinski K. (2006) Members of the *Arabidopsis At*TPK /KCO family form homomeric vacuolar channels *in planta*. *Plant Journal 48, 296-306*

Voelker C., Gomez-Porras J.L., Becker D., Hamamoto S., Uozumi N., Gambale F., Mueller-Roeber B., Czempinski K., Dreyer I. (2010) Roles of tandem-pore K^+ channels in plants - A puzzle still to be solved. *Plant Biol. (Stuttg) 1, 56-63*

Vredenberg W.J. (1976) Electrostatic interactions and gradients between chloroplast compartments and cytoplasm, in Barber, J. (ed) the intact chloroplast. *Elsevier/North Holland Biomedical Press, Amsterdam, The Netherlands pp. 53-87*

Witt H.T. (1979) *Biochim. Biophys. Acta 505, 355-427*

Zanetti M., Teardo E., La Rocca N., Zulkifli L., Checchetto V., Shijuku T., Sato Y., Giacometti G.M., Uozumi N., Bergantino E., Szabò I. (2010) A novel potassium channel in photosynthetic Cyanobacteria. *PLoS One 5, e10118*

*At*TPK3 project figures

Figure 1

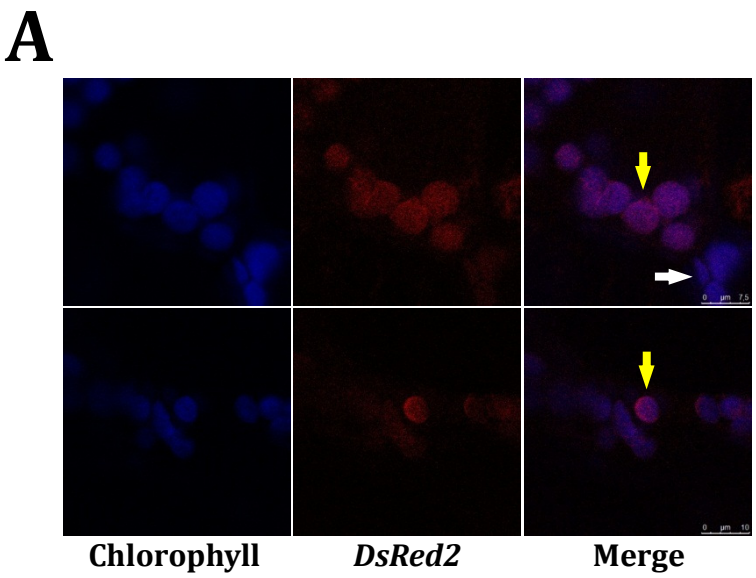
A
Chlorophyll
DsRed2
Merge

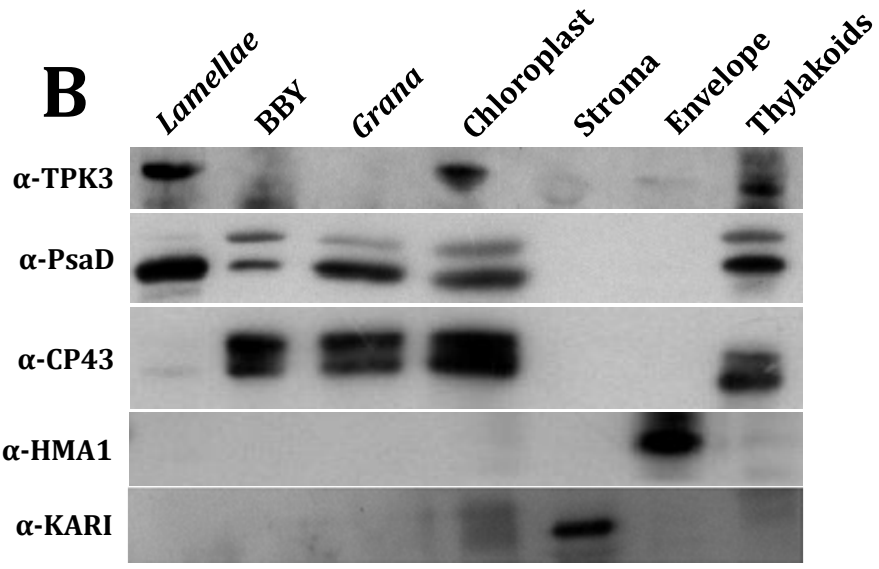
B
Lamellae
BBY
Grana
Chloroplast
Stroma
Envelope
Thylakoids
α-TPK3
α-PsaD
α-CP43
α-HMA1
α-KARI

Figure 2

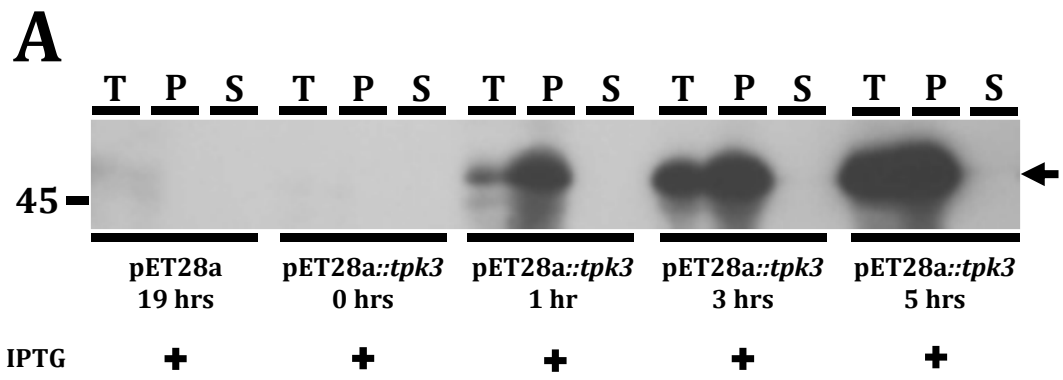
A
T P S T P S T P S T P S T P S
45
pET28a
19 hrs
pET28a::tpk3
0 hrs
pET28a::tpk3
1 hr
pET28a::tpk3
3 hrs
pET28a::tpk3
5 hrs
IPTG
+ + + + +

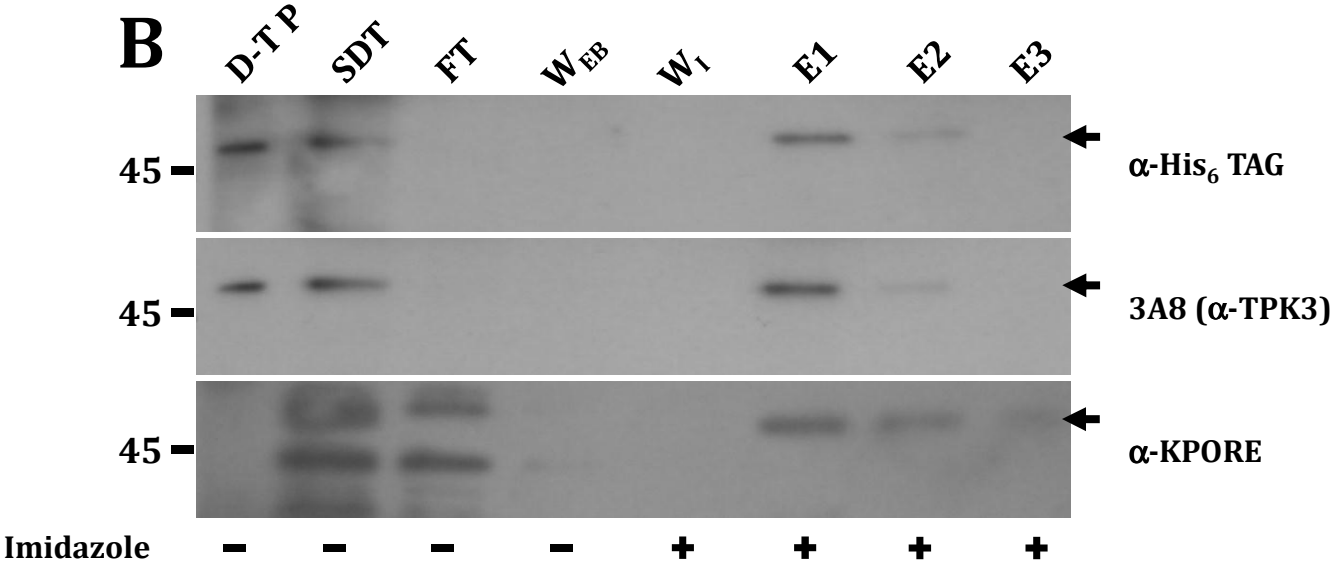
B
D-T P
SDT
FT
W EB
W 1
E1
E2
E3
45
45
45
α-His6 TAG
3A8 (α-TPK3)
α-KPORE
Imidazole
- - - - + + + +

Figure 3

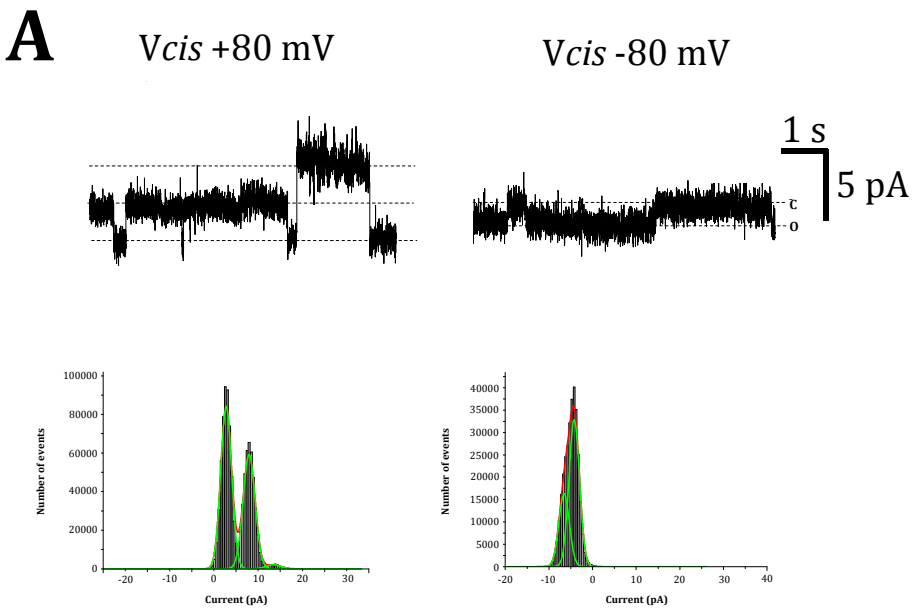
A
Vcis +80 mV
Vcis -80 mV
1 s
5 pA
c
o
Number of events
Current (pA)
Number of events
Current (pA)

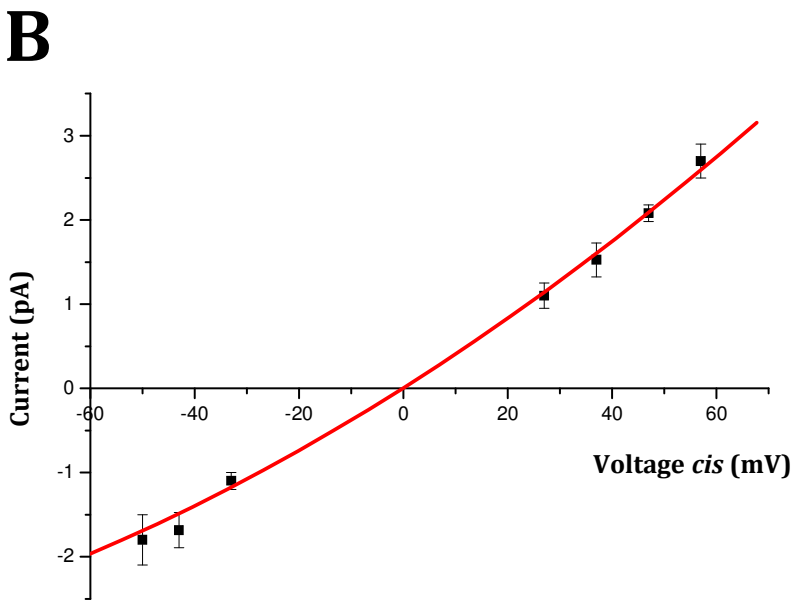
B
Current (pA)
Voltage cis (mV)

Figure 4

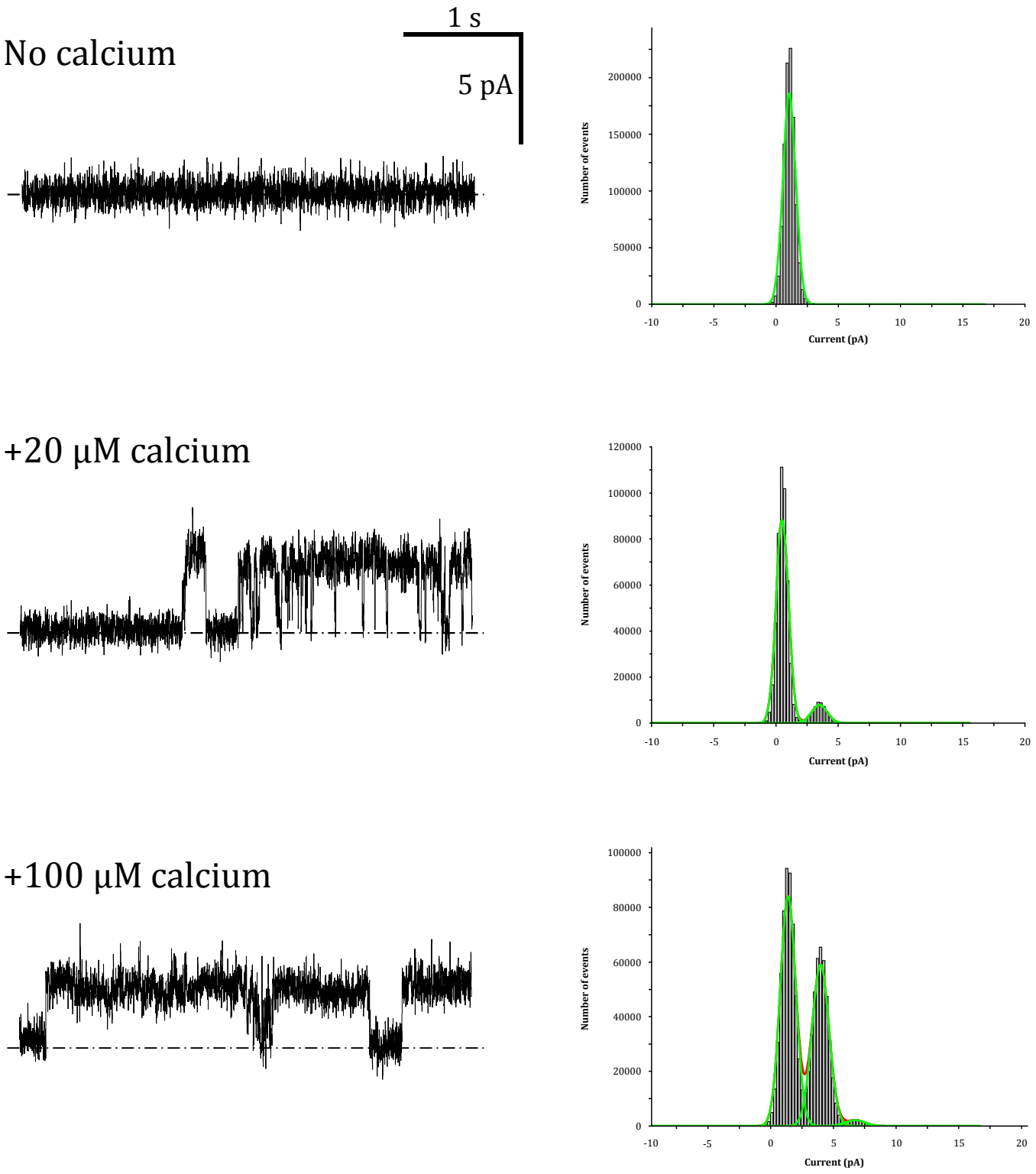
No calcium
1 s
5 pA
Number of events
Current (pA)
+20 µM calcium
Number of events
Current (pA)
+100 µM calcium
Number of events
Current (pA)

Figure 5

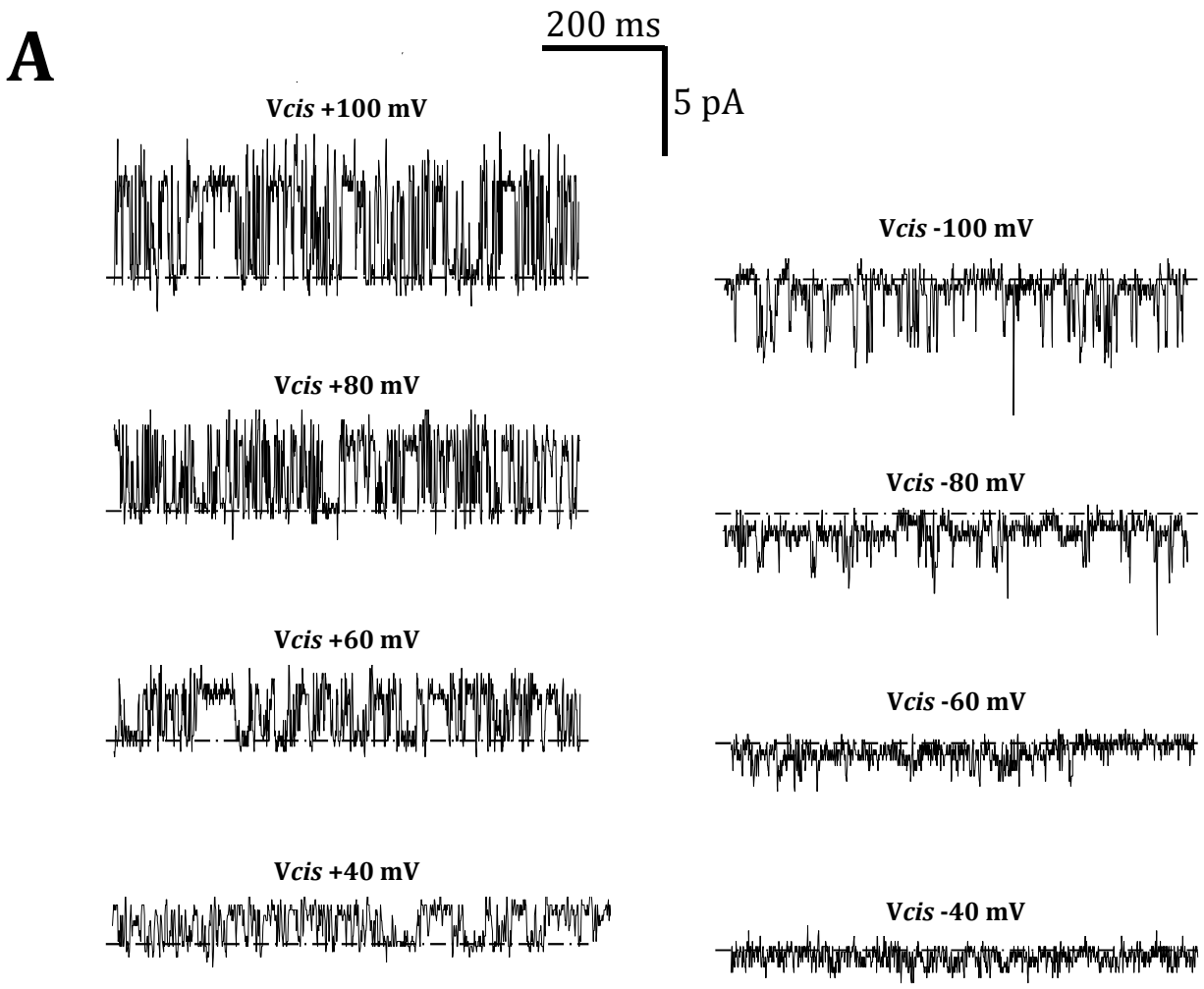
A
200 ms
5 pA
Vcis +100 mV
Vcis -100 mV
Vcis +80 mV
Vcis -80 mV
Vcis +60 mV
Vcis -60 mV
Vcis +40 mV
Vcis -40 mV

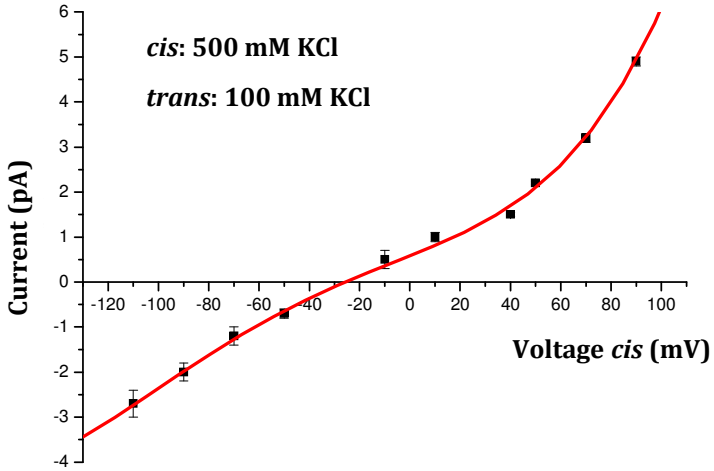
cis: 500 mM KCl
trans: 100 mM KCl
Current (pA)
Voltage cis (mV)
6
5
4
3
2
1
0
-1
-2
-3
-4
-120
-100
-80
-60
-40
-20
0
20
40
60
80
100

Figure 5

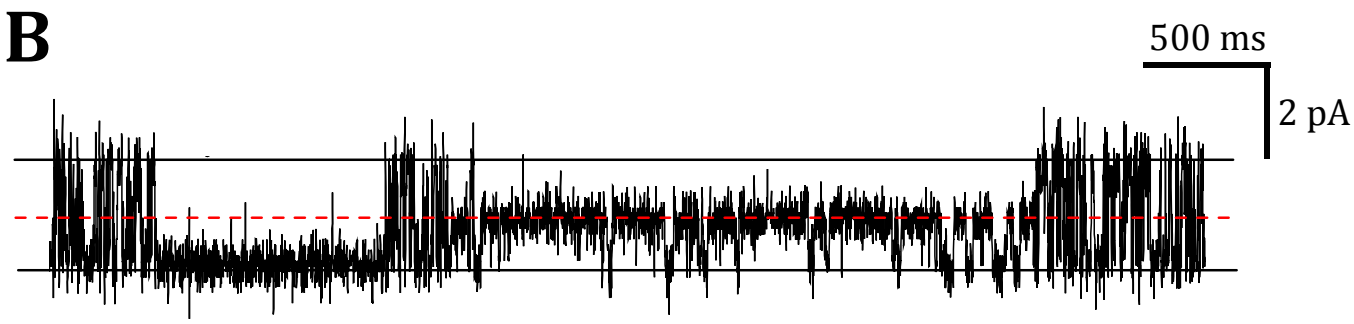

Figure 6

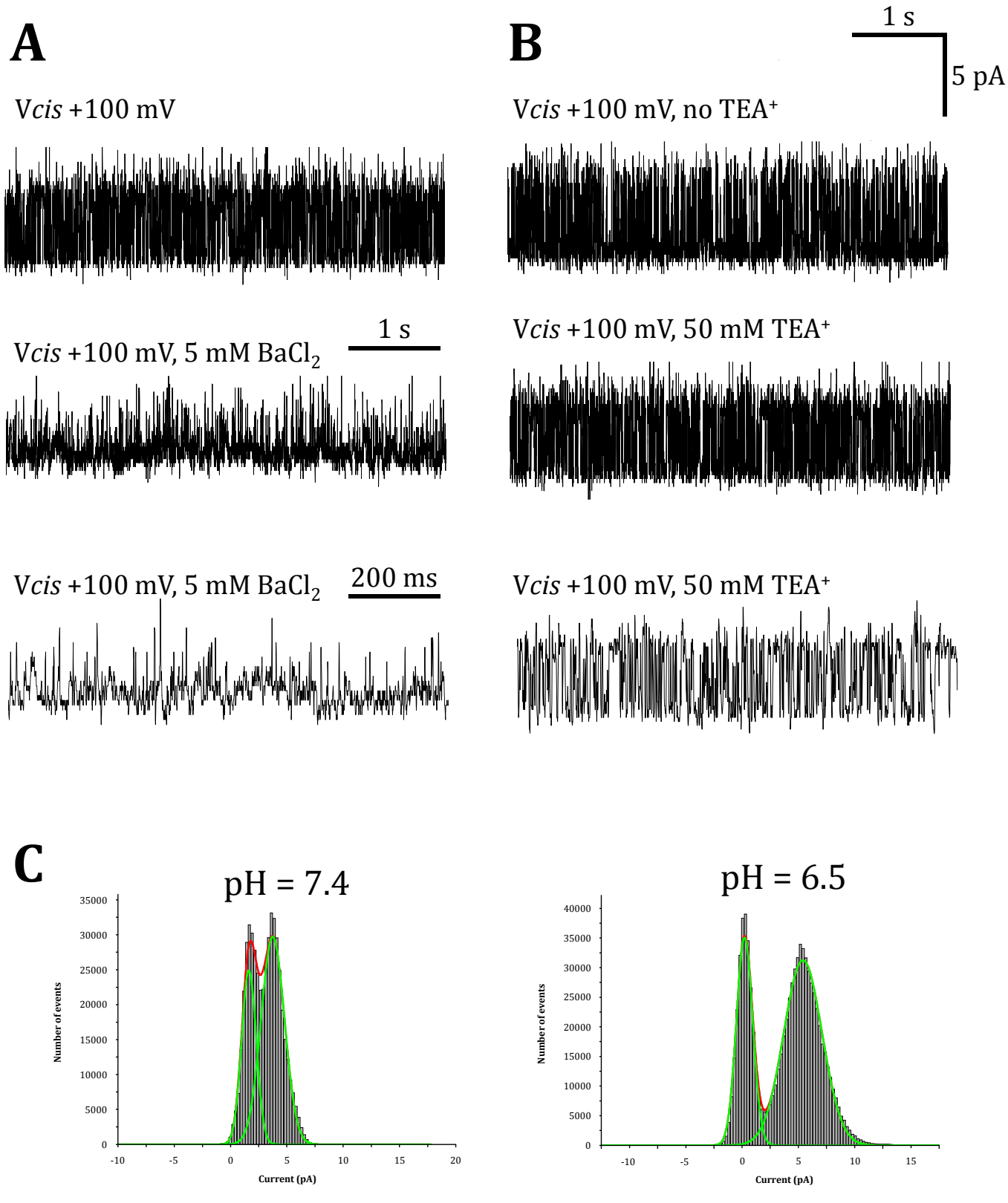
A
B
1 s
5 pA
Vcis +100 mV
Vcis +100 mV, no TEA+
Vcis +100 mV, 5 mM BaCl2
1 s
Vcis +100 mV, 50 mM TEA+
Vcis +100 mV, 5 mM BaCl2
200 ms
Vcis +100 mV, 50 mM TEA+

C
pH = 7.4
pH = 6.5
Number of events
Current (pA)
Number of events
Current (pA)

Figure 7

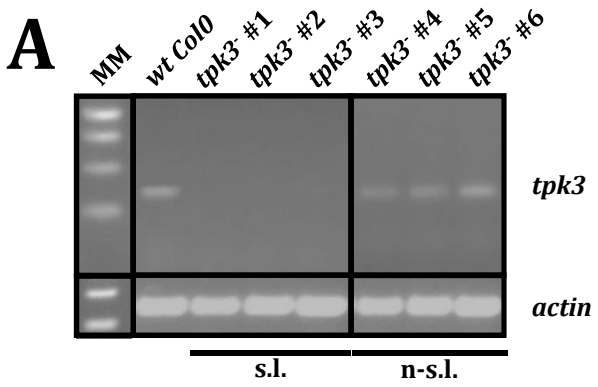
A
MM
wt Col0
tpk3- #1
tpk3- #2
tpk3- #3
tpk3- #4
tpk3- #5
tpk3- #6
tpk3
actin
s.l.
n-s.l.

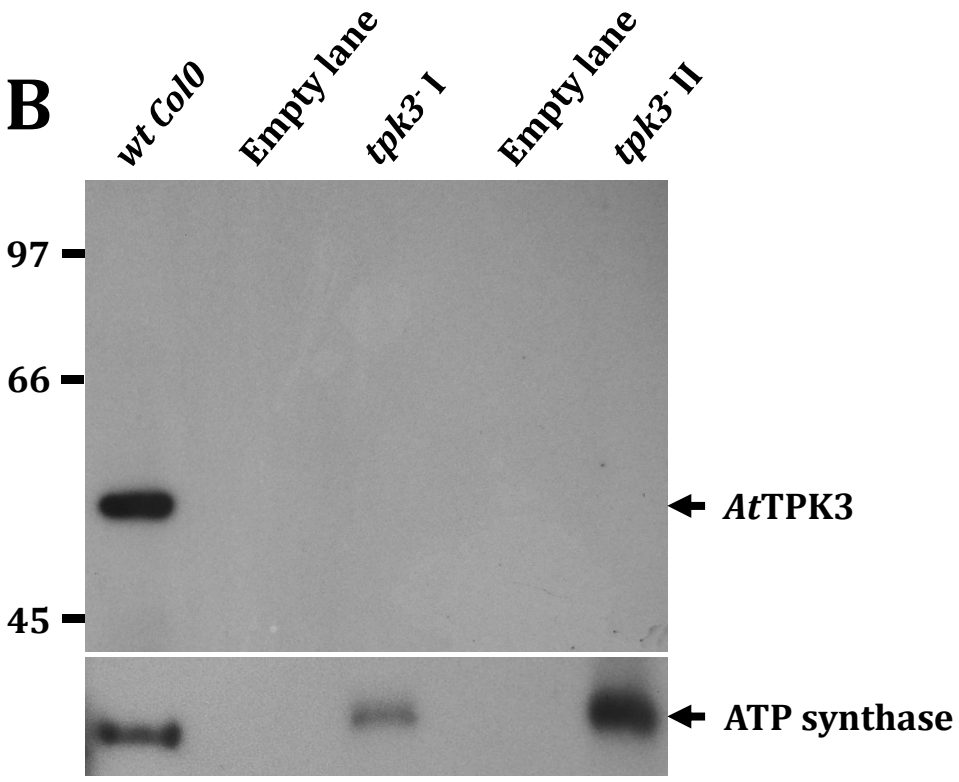
B
wt Col0
Empty lane
tpk3- I
Empty lane
tpk3- II
97
66
45
AtTPK3
ATP synthase

Figure 8

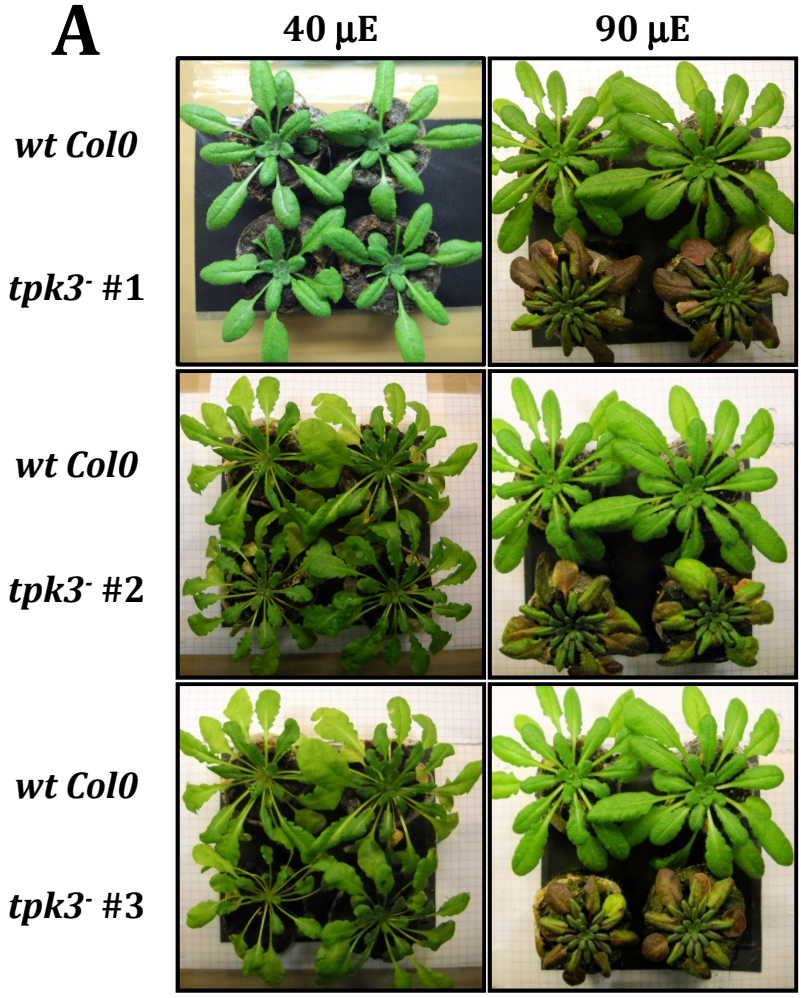

Figure 8

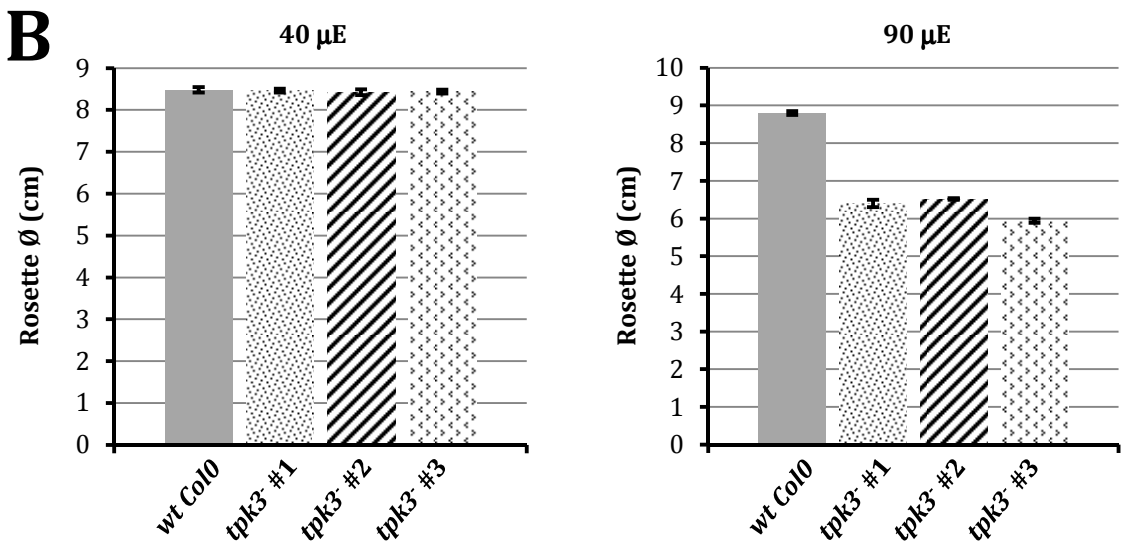
B
40 µE
Rosette Ø (cm)
0
1
2
3
4
5
6
7
8
9
wt Col0
tpk3- #1
tpk3- #2
tpk3- #3
90 µE
Rosette Ø (cm)
0
1
2
3
4
5
6
7
8
9
10
wt Col0
tpk3- #1
tpk3- #2
tpk3- #3

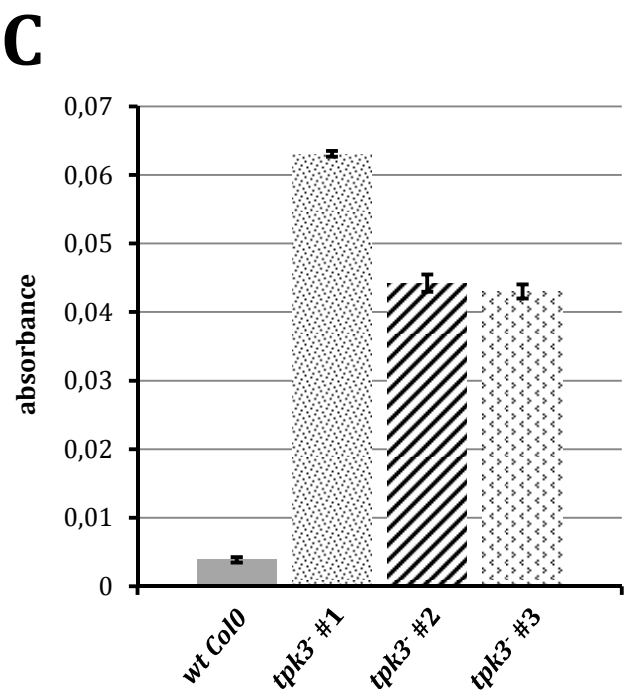
C
absorbance
0
0,01
0,02
0,03
0,04
0,05
0,06
0,07
wt Col0
tpk3- #1
tpk3- #2
tpk3- #3

Figure 9

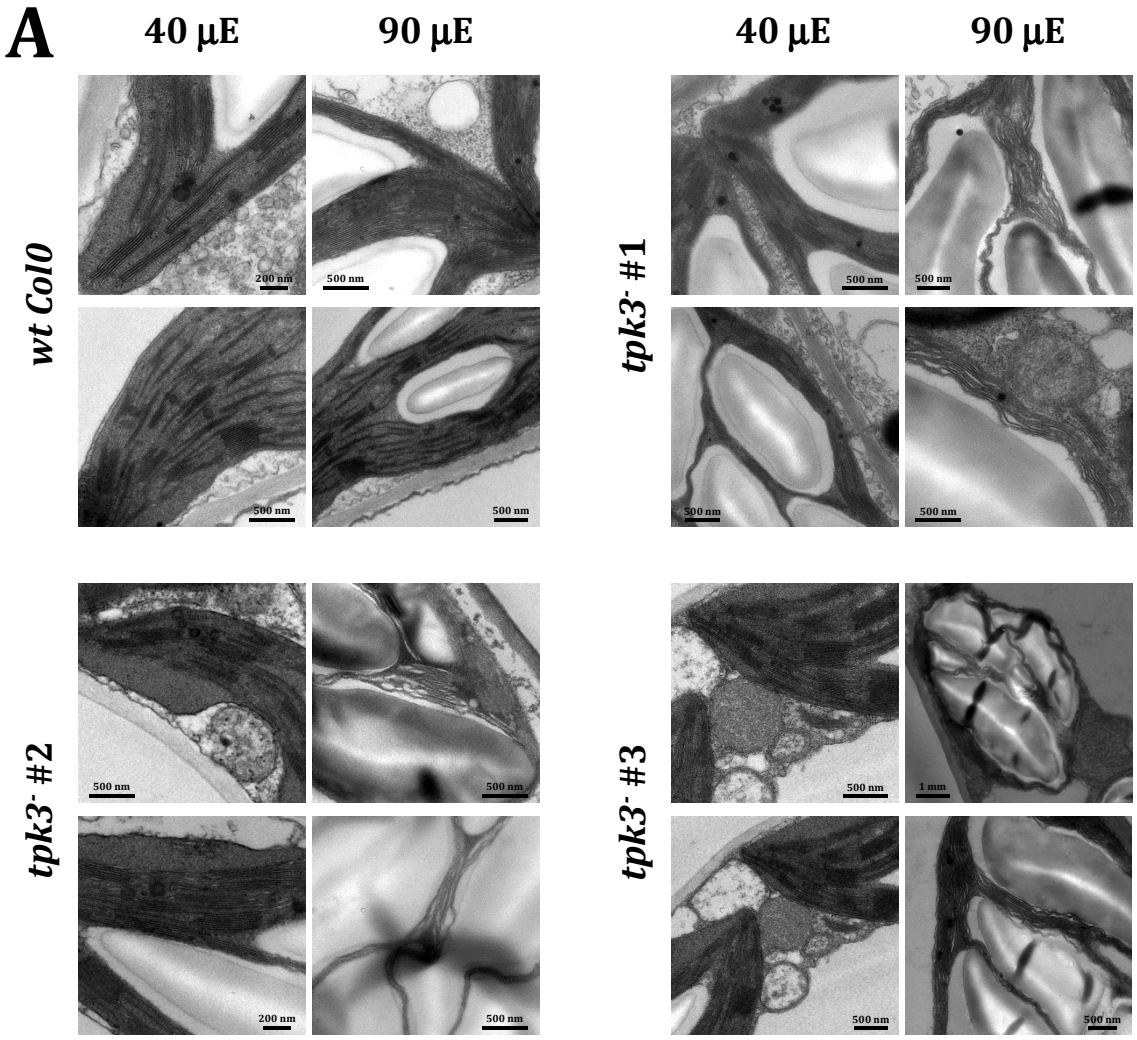
A
40 µE
90 µE
40 µE
90 µE
wt Col0
tpk3- #1
tpk3- #2
tpk3- #3
200 nm
500 nm
1 mm

Figure 9

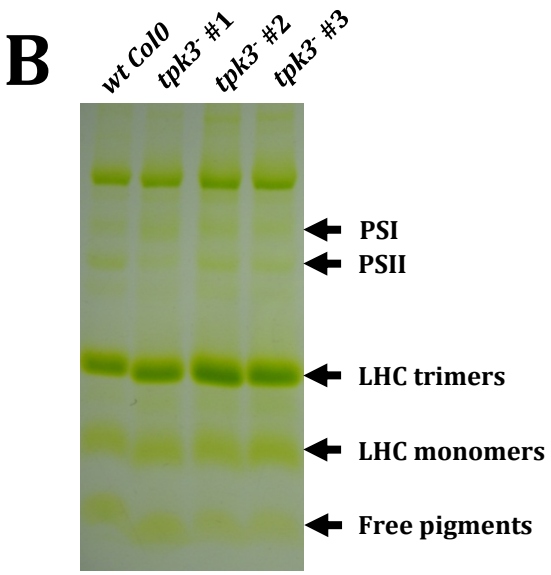
B
wt Col0
tpk3- #1
tpk3- #2
tpk3- #3
PSI
PSII
LHC trimers
LHC monomers
Free pigments

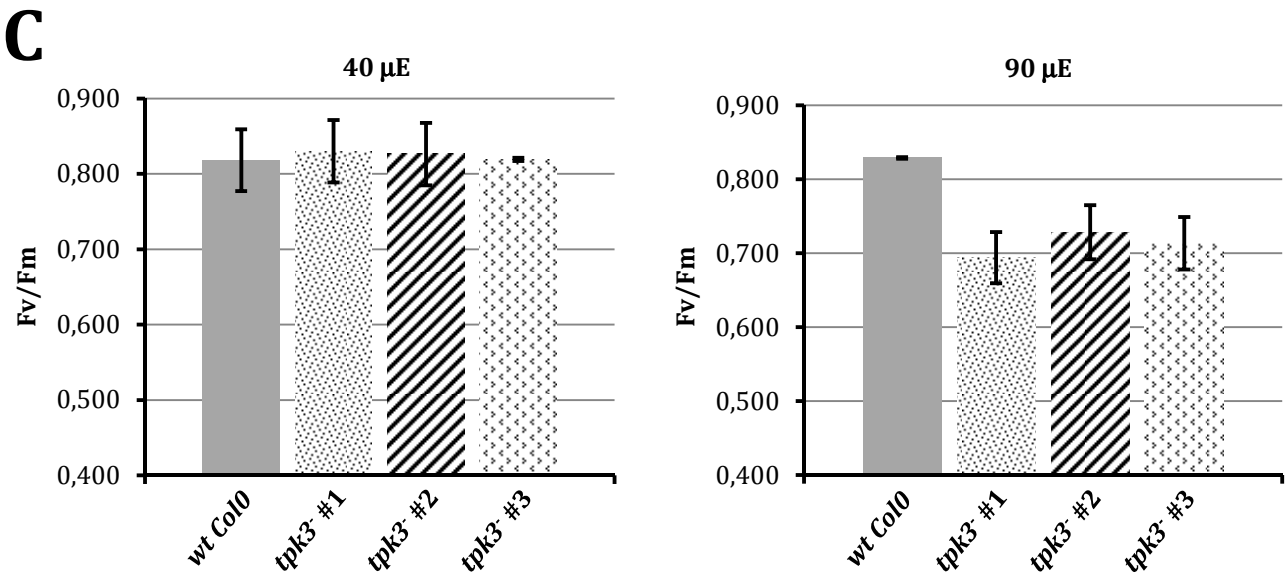
C
40 µE
90 µE
Fv/Fm
0,900
0,800
0,700
0,600
0,500
0,400
wt Col0
tpk3- #1
tpk3- #2
tpk3- #3

Figure 10

A

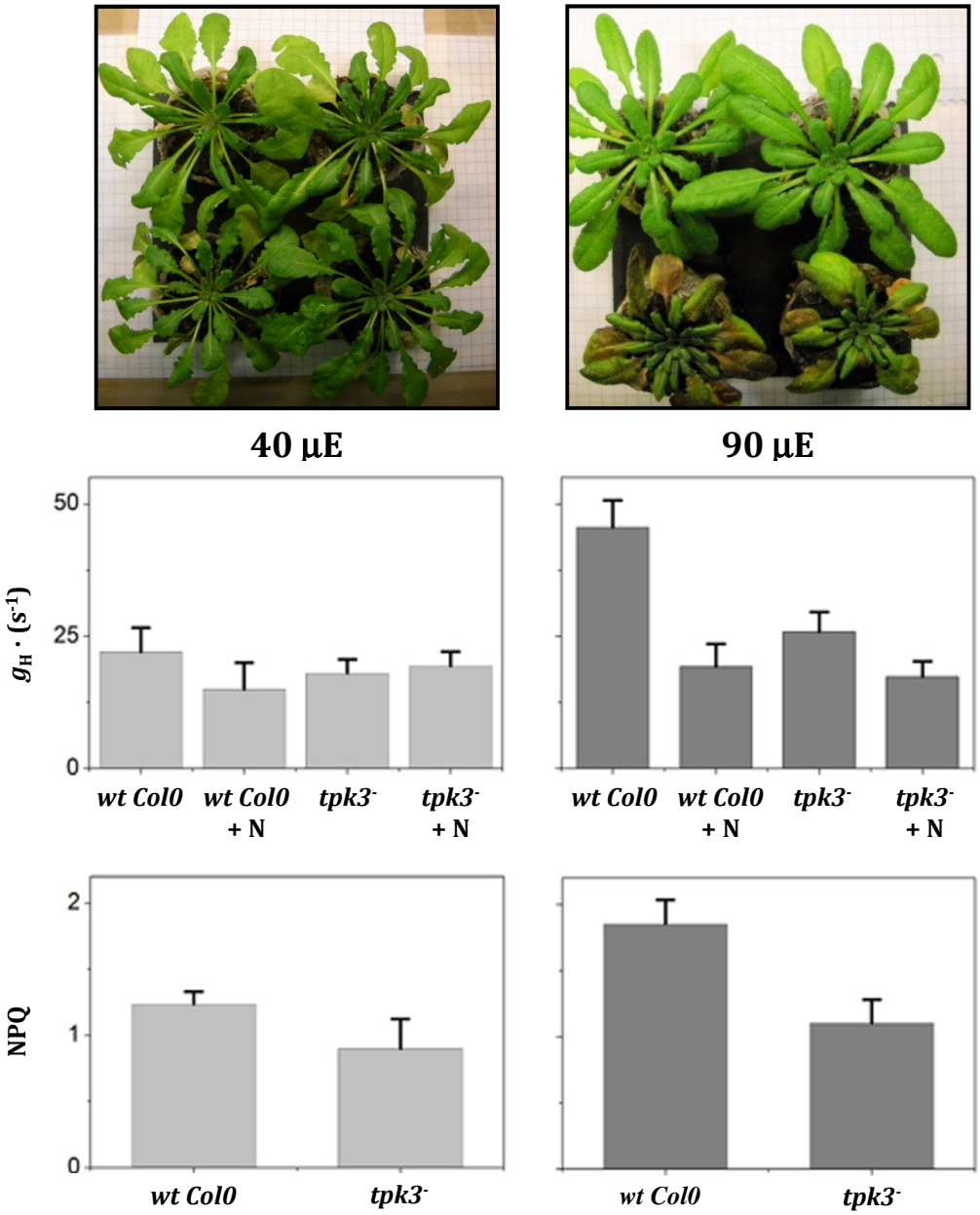
40 µE
90 µE
$g_H \cdot (s^{-1})$
50
25
0
wt Col0
wt Col0 + N
tpk3-
tpk3- + N
NPQ
2
1
0
wt Col0
tpk3-

Figure 10

B

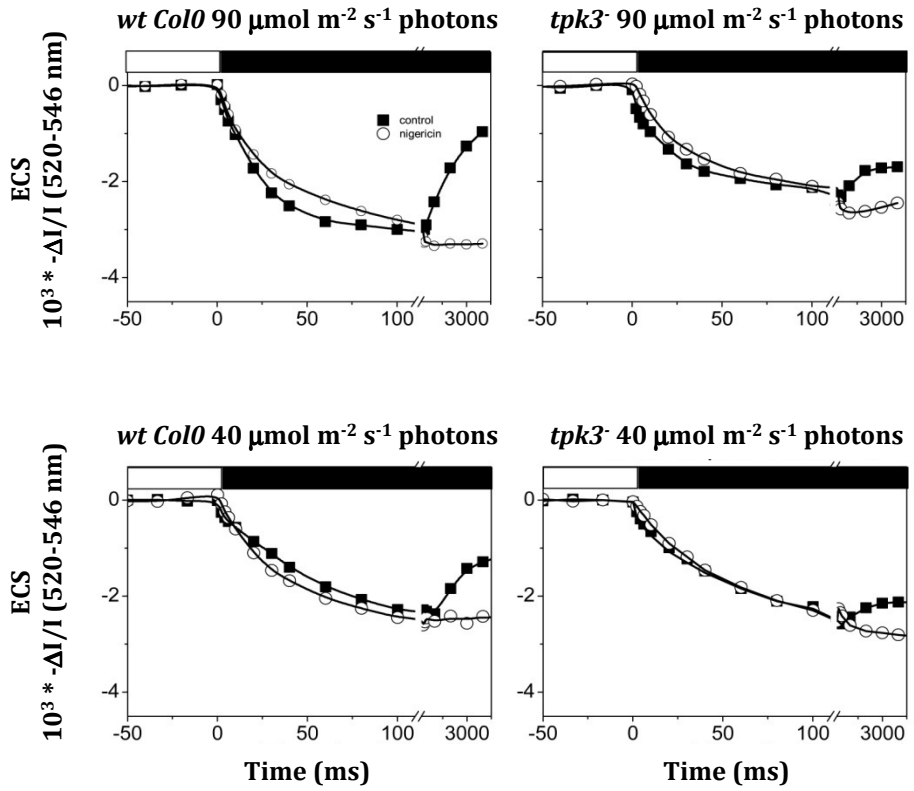
wt Col0 90 µmol m-2 s-1 photons
tpk3- 90 µmol m-2 s-1 photons
wt Col0 40 µmol m-2 s-1 photons
tpk3- 40 µmol m-2 s-1 photons
ECS
10³ * -ΔI/I (520-546 nm)
control
nigericin
0
-2
-4
-50
0
50
100
3000
Time (ms)

Figure 11

A

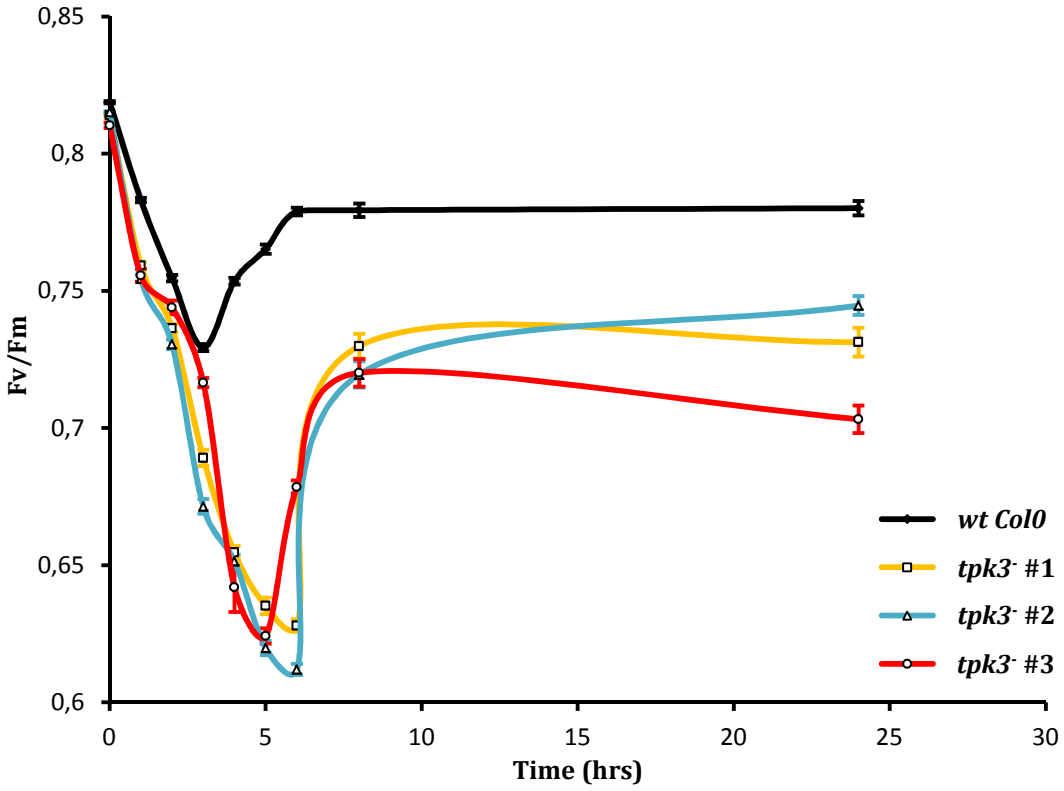
0,85
0,8
0,75
0,7
0,65
0,6
Fv/Fm
0
5
10
15
20
25
30
Time (hrs)
wt Col0
tpk3- #1
tpk3- #2
tpk3- #3

B

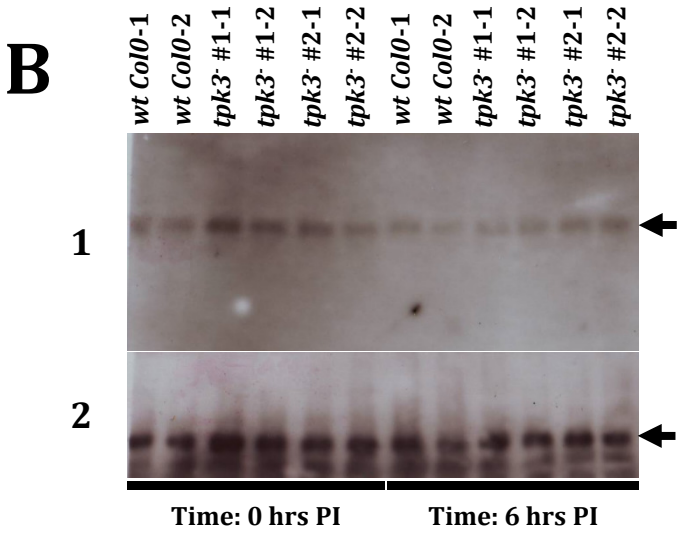
wt Col0-1
wt Col0-2
tpk3- #1-1
tpk3- #1-2
tpk3- #2-1
tpk3- #2-2
wt Col0-1
wt Col0-2
tpk3- #1-1
tpk3- #1-2
tpk3- #2-1
tpk3- #2-2
1
2
Time: 0 hrs PI
Time: 6 hrs PI

Tables

Table I

Irradiance	**40 µE**				**90 µE**			
Genotype	*wt Col0*	*tpk3*$^{-}$ #1	*tpk3*$^{-}$ #2	*tpk3*$^{-}$ #3	*wt Col0*	*tpk3*$^{-}$ #1	*tpk3*$^{-}$ #2	*tpk3*$^{-}$ #3
Pigment								
Neoxantin	3,08 ± 0,31	4,47 ± 0,04	4,69 ± 0,13	3,55 ± 0,34	5,19 ± 0,30	4,55 ± 0,36	5,43 ± 0,51	4,64 ± 0,06
Violaxantin	1,71 ± 0,27	3,21 ± 0,29	3,98 ± 0,79	2,58 ± 0,21	3,81 ± 0,16	4,43 ± 0,47	5,07 ± 0,25	4,89 ± 0,29
Anteraxantin	0,07 ± 0,04	0,20 ± 0,00	0,15 ± 0,07	0,05 ± 0,04	0,12 ± 0,00	0,16 ± 0,07	0,17 ± 0,10	0,21 ± 0,00
Lutein	12,5 ± 2,39	11,6 ± 0,71	15,8 ± 0,50	13,0 ± 0,37	17,1 ± 1,01	16,9 ± 0,53	17,2 ± 1,41	16,4 ± 0,34
b-chlorophyll	10,1 ± 0,86	8,66 ± 0,35	11,7 ± 0,68	9,60 ± 0,10	13,2 ± 0,14	11,3 ± 0,26	11,5 ± 0,16	10,1 ± 0,44
a-chlorophyll	29,4 ± 0,16	23,5 ± 1,93	38,6 ± 2,36	27,9 ± 2,38	43,8 ± 3,69	30,2 ± 3,05	33,9 ± 2,66	26,7 ± 2,46
β-carotene	5,71 ± 0,38	3,35 ± 0,21	3,66 ± 0,33	3,37 ± 0,97	3,83 ± 0,23	5,27 ± 1,44	3,20 ± 0,14	3,89 ± 0,13

Supplementary figures

Figure S1

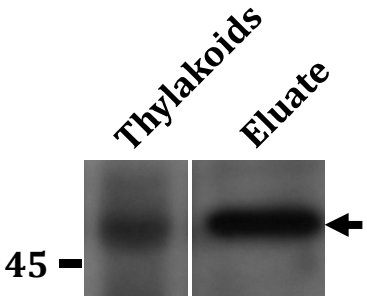

Figure S2

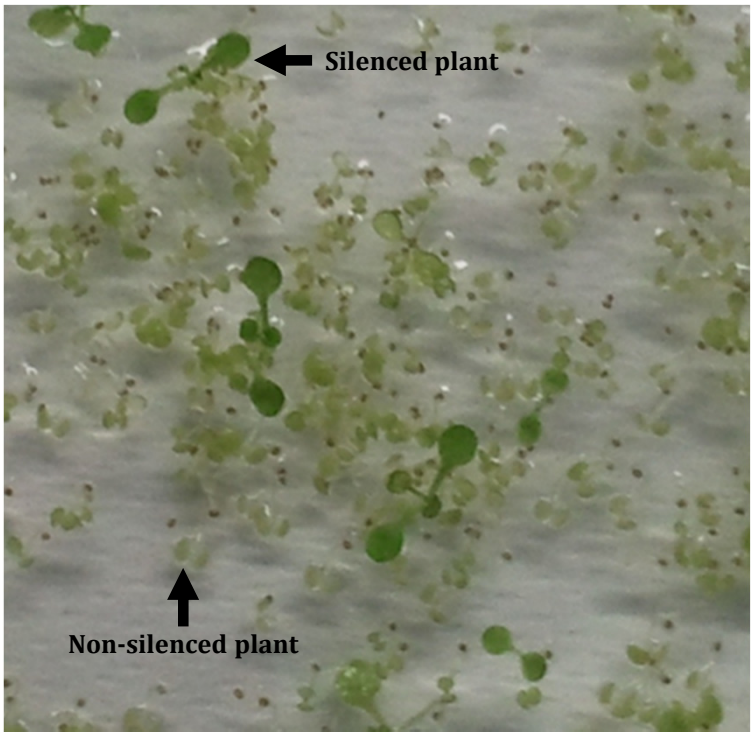

Figure S3

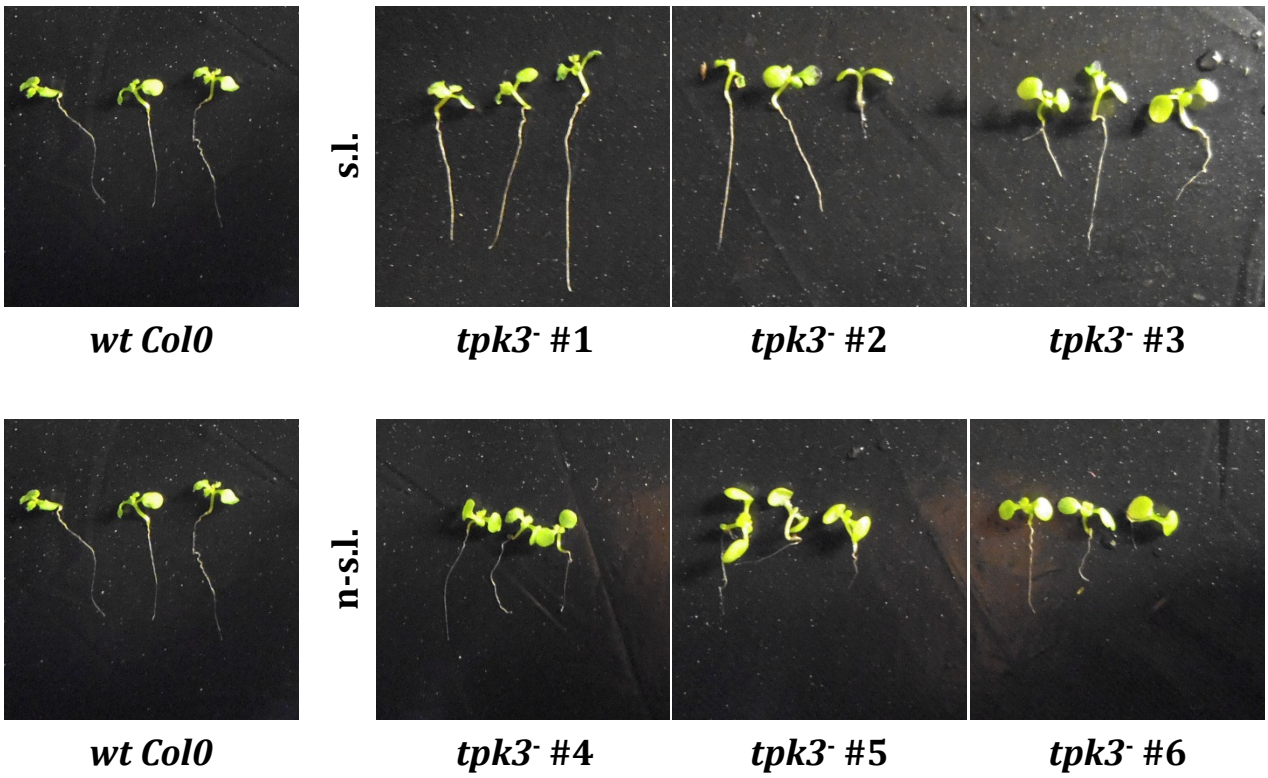

Figure S4

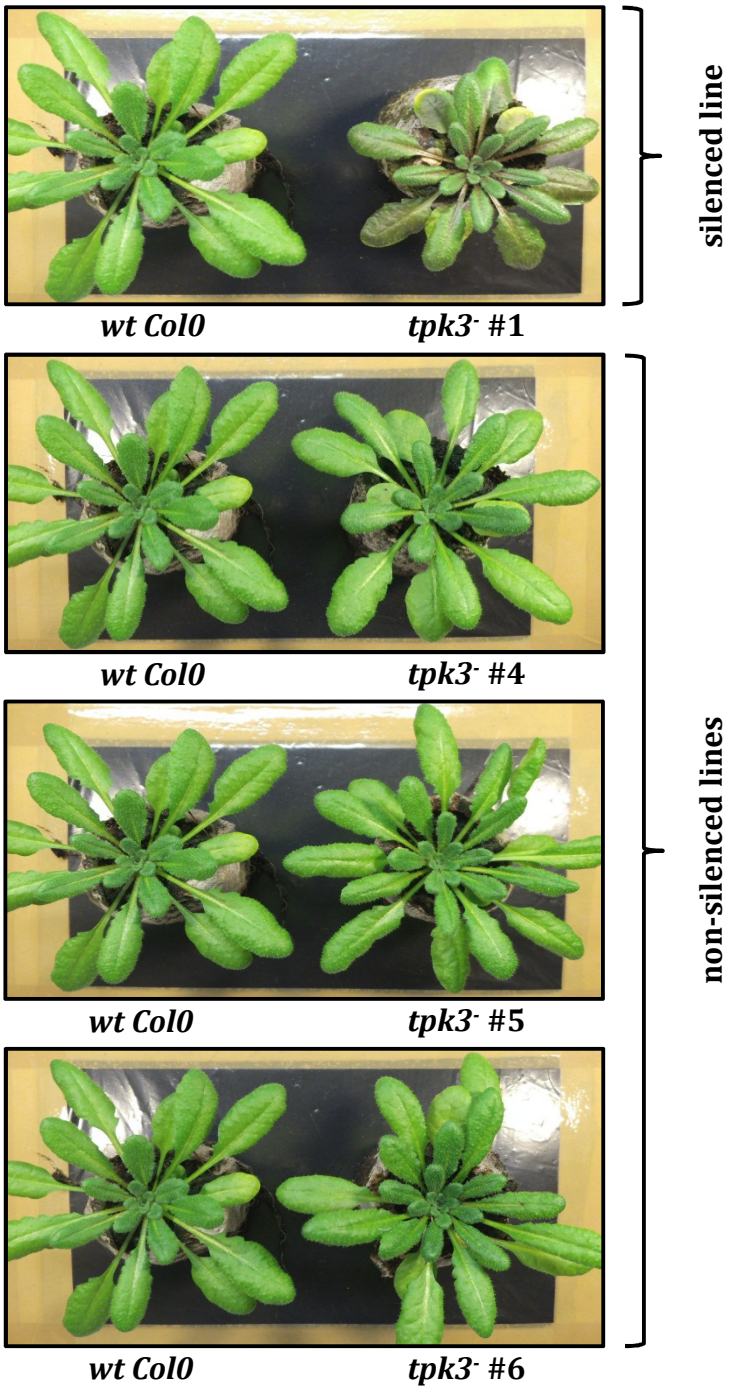
silenced line
wt Col0
tpk3- #1
wt Col0
tpk3- #4
non-silenced lines
wt Col0
tpk3- #5
wt Col0
tpk3- #6

Figure S5

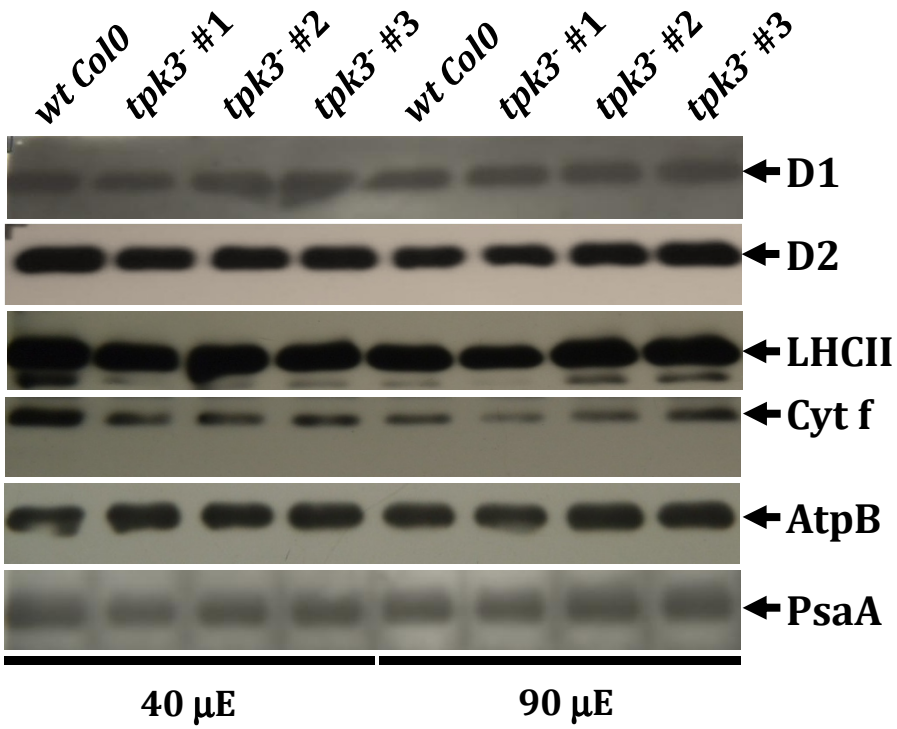
wt Col0
tpk3- #1
tpk3- #2
tpk3- #3
wt Col0
tpk3- #1
tpk3- #2
tpk3- #3
D1
D2
LHCII
Cyt f
AtpB
PsaA
40 µE
90 µE

Figure S6

Photoinhibition time	Genotype	Densitometry value for D1 protein
0 hours	*wt Col0*-1	278,52
	wt Col0-2	249,67
	tpk3^{-} #1-1	229,78
	tpk3^{-} #1-2	226,78
	tpk3^{-} #2-1	258,67
	tpk3^{-} #2-2	266,85
6 hours	*wt Col0*-1	229,18
	wt Col0-2	239,06
	tpk3^{-} #1-1	244,71
	tpk3^{-} #1-2	245,82
	tpk3^{-} #2-1	269,30
	tpk3^{-} #2-2	291,31

Figure S7

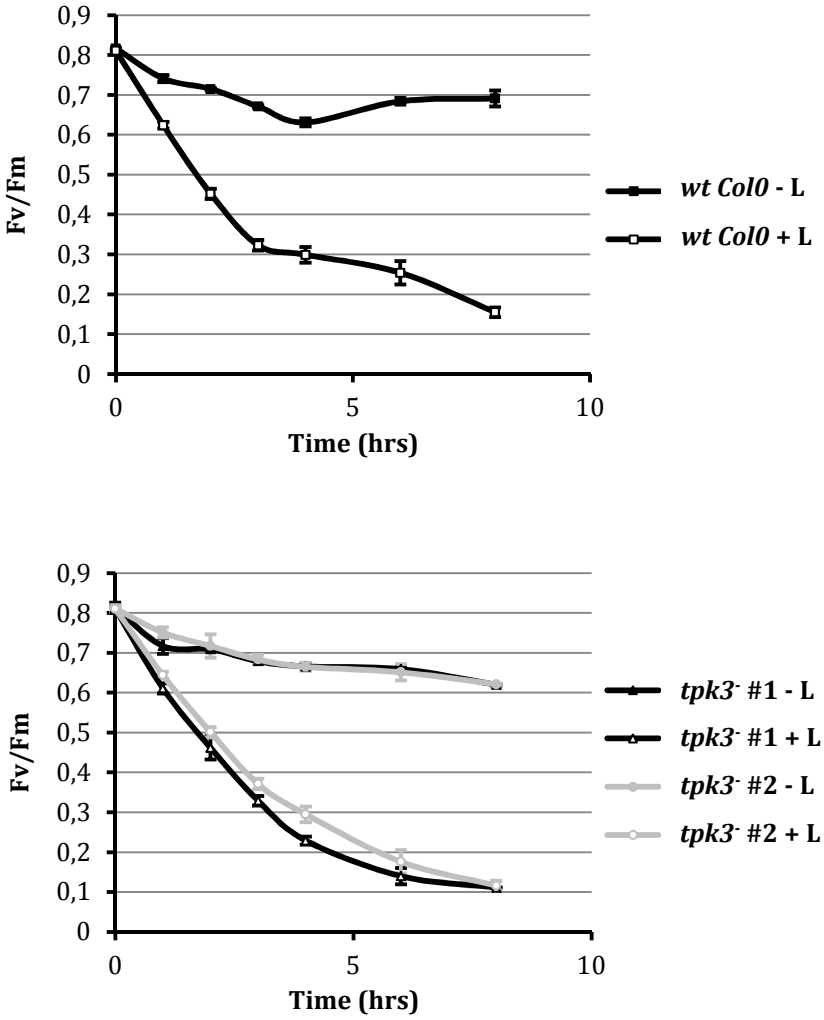
0,9
0,8
0,7
0,6
0,5
0,4
0,3
0,2
0,1
0
Fv/Fm
0
5
10
Time (hrs)
wt Col0 - L
wt Col0 + L
tpk3- #1 - L
tpk3- #1 + L
tpk3- #2 - L
tpk3- #2 + L

iGLRs project

Alternative splicing-mediated mitochondrial targeting of a plant glutamate receptor, GLR3.5.

Enrico Teardo, Luca Carraretto, Elide Formentin° and Ildikò Szabò°

Department of Biology, University of Padua, 35121 Padua, Italy

° These authors share last authorship

Correspondence should be sent to: ildi@civ.bio.unipd.it

ABSTRACT

There are twenty genes in plants encoding for putative glutamate receptors. For most of these receptors neither their channel-forming and/or physiological function nor their localization within the plant cells are known and up to now only one member was found in intracellular membrane, namely in chloroplast. Here we report an unexpected dual localization of one member of the subfamily 3, GLR3.5. This glutamate receptor is transcribed in two splice variants, one of which harbours an N-terminal peptide predicted to target the protein to the mitochondria. Using a novel pGREAT vector designed for expression of fusion proteins in plants, we located the G3.5v1-DsRed2 to mitochondria in Arabidopsis plants, while the other splicing variant product was detected in chloroplasts. Importantly, GLR3.5 was found also in mitochondria isolated from non-manipulated wt Col0 plants by Western blot. In accordance with mitochondrial localization of GLR3.5v1, two independent lines of knockout mutant plants displayed a strikingly altered mitochondrial ultrastructure. Our data thus identify for the first time a mechanism leading to dual, organellar targeting of two products of the same gene and identifies the first bona fide cation channel in plant mitochondria from molecular point of view.

Under submission to EMBO reports

INTRODUCTION

In vertebrates, ionotropic glutamate receptors (iGluRs) are ligand-gated cation channels that mediate the majority of the excitatory neurotransmission in the central nervous system. Mammalian iGluRs are grouped into four subfamilies according to pharmacological properties and sequence similarities: α-amino-3-hydroxy-5- methyl-4 isoxazole propionate (AMPA) receptors, kainate (KA) receptors, N-methyl-D-aspartate (NMDA) receptors, and delta receptors.

In the model plant *Arabidopsis thaliana*, 20 genes encoding homologues of animal iGluRs have been identified (Lam *et al*., 1998). According to phylogenetic analyses, the *A. thaliana* glutamate receptor homologues can be subdivided into three separate subgroups (Chiu *et al*., 1999; Chiu *et al*., 2002). Clear-cut evidence for channel-forming capability by plant iGLRS has been obtained only recently, and only for *At*GLR3.4 expressed in a heterologous system. The authors studies with transgenic plants suggested roles of members of the plant GLR family in Ca^{2+} fluxes (*At*GLR2) (Kim *et al*., 2001), coordination of mitotic activity in the root apical meristem (Li *et al*., 2006), regulation of abscisic acid biosynthesis and water balance (*At*GLR1.1) (Kang and Turano, 2003; Kang *et al*., 2004), carbon/nitrogen sensing (*At*GLR1.1)

(Kang and Turano, 2004) and resistance against fungal infection (Kang *et al*., 2006). Application of antagonists and agonists of animal iGluRs revealed that plant GLRs might be involved in regulation of root growth and branching (Walch-Liu *et al*., 2006), in light signal transduction (Lam *et al*., 1998; Brenner *et al*., 2000), and the response to aluminium (Sivaguru *et al*., 2003). In various cell types of plants, the agonists glutamate and glycine induced depolarisation and a rise in intracellular Ca^{2+} concentration that were inhibited by blockers of non-selective cation channels (NSCCs) and by antagonists of animal iGluRs (Dennison and Spalding, 2000; Dubos *et al*., 2003; Meyerhoff *et al*., 2005; Krol *et al*., 2007). Furthermore, glutamate-activated cation currents in patch-clamped root protoplasts were inhibited by NSCC blockers such as La^{3+} and Gd^{3+} (Demidchik *et al*., 2004). Therefore, it was proposed that plant iGLRs can form Ca^{2+}-permeable NSCCs, are inhibited by animal iGLR antagonists and contribute to the shaping of plant Ca^{2+} signalling (McAinsh and Pittman, 2009).

Studies using *At*GLR3.3 mutant plants showed that intracellular Ca^{2+} rise and membrane depolarization induced by glutamate in *Arabidopsis* hypocotyls and root cells are correlated with the presence of *At*GLR3.3 (Qi *et al*., 2006; Stephens *et al*., 2008). However, most plant iGLRs, when expressed in heterologous system, do not give rise to any current (oocytes) or are toxic for host cells (e.g. in mammalian cells) (Davenport, 2002). Recently, in order to examine whether *At*GLR homologues possess functional ion channel domains, Tapken and Hollmann (Tapken and Hollmann, 2008) transplanted the pore loop together with the two adjacent intracellular loops of 17 *At*GLR subunits into two rat iGluR subunits and tested the resulting chimaeric receptors for ion channel activity in the heterologous expression system *Xenopus oocyte*. They showed that *At*GLR1.1 and *At*GLR1.4 have functional ion pore domains. The *At*GLR1.1 pores are permeable to Na^+, K^+, and Ca^{2+} and are blocked by the non-specific cation channel blocker La^{3+} (Tapken and Hollmann, 2008).

Various localization prediction tools suggest that some of the plant iGLRs might have chloroplast and mitochondrial targeting sequences. However, no experimental evidence has been presented up to now concerning a possible intracellular localization of iGLRs. In general, determination of the subcellular localization of a protein is an important step toward understanding its function. We have recently reported localization of GLR3.4 to the inner chloroplast membrane (Teardo *et al*., 2011), which was also shown to harbour a DNQX-sensitive, calcium-permeable channel activity (Teardo *et al*., 2010). No other studies addressed eventual subcellular localization of other putative glutamate receptors.

In the present study we show that an isoform of GLR3.5 is efficiently targeted to mitochondria. Functional expression of the channel in this organelle is indicated by the fact that its lack in knockout plants leads to a dramatically altered ultrastructure of mitochondria.

RESULTS

Cloning of the two splicing variants of *Atglr3.5*

The *Arabidopsis* glutamate receptor *At*GLR3.5 is encoded by the *At*2g32390 gene that is transcribed in two splice variants, NM_128798 (isoform 1) and NM_001036387 (isoform 2) (sequence similarity is shown in Fig. 1), corresponding to the genes *At*2g32390.1 and *At*2g32390.2 respectively. Although recently a third gene model has been created in the TAIR10 version of the *Arabidopsis* genome database, only two isoforms have been demonstrated to be expressed so far (i.e. is found in EST database): AF170494 and AY495449. At the protein level, the isoform 1 (NP_565743.1) shows a putative signal peptide for the localization into the mitochondria that is missing in the isoform 2 (NP_001031464.1) (Aramemnon database: http://aramemnon.uni-koeln.de). Interestingly, both isoforms of

*Atglr*3.5 shows homology to cyanobacterial receptors (Table I). The predicted MWs are 100,9 kDa and 98,1 kDa for the full-length and the processed forms, respectively, for the isoform predicted to localize to mitochondria. The second, shorter form which may be targeted to chloroplasts has predicted MWs of 95,5 and 86,6 kDa for the full-length and the processed forms, respectively, according to ChloroP. To confirm the predicted localization of the two isoforms to the respective organelles, a previously described antibody against amino acids 933-947 of GLR3.5 (anti-933/947 antibody) was used, which, *a priori* may recognize also *At*GLR3.5 given that this latter protein displays a stretch of amino acids identical to those in the peptide used for immunization. By using the above antibody, we were able to visualize an approximately 85 kDa band in both isolated chloroplasts and mitochondria in the *wt Col0* plants. While the chloroplast preparation was not contaminated by mitochondria (no cytochrome c was present), the mitochondria preparation contained PsaA of Photosystem I. Nevertheless, the 85 kDa band in the mitochondria could not be merely due to contamination by the chloroplasts. We have previously shown that GLR3.4 in isolated chloroplasts was recognized indeed at 85 kDa, given that *At*GLR3.4-less chloroplasts lacked this band. In order to answer the question whether the 85 kDa band in the mitochondria contains *At*GLR3.5, we first checked if recombinant *At*GLR3.5 could be recognized by the anti-933/947 antibody. Fig. 2 illustrates that this is indeed the case: *At*GLR3.5 was successfully expressed using an *in vitro* transcription-translation system and was specifically recognized by the used antibody. Next, we've checked whether the 85 kDa band is present in mitochondria from mutant plants lacking *At*GLR3.5 (see below). The clear lack of this band in the knockout plants indicates that *At*GLR3.5 is located to mitochondria.

In order to prove localization of GLR3.5 in mitochondria, we isolated the *c*DNAs corresponding to transcripts NM_128798 and NM_001036387 from leaf RNA by RT-PCR using primers listed in Table 1. As the sequence recognized by the primer, corresponding to the beginning of CDS of isoform 1, is present also at the 5' UTR of isoform 2 transcript, the PCR product resulted in a pool of the two *c*DNAs. In order to discriminate between the two isoforms, we designed a primer spanning the 8 nucleotides in position 150-158 of the isoform 2 that are missing in the isoform 1. This primer has been used to find the clones containing the isoform 2 and eliminate them. We also observed that the isoform 1 was more abundant than the isoform 2. In fact, 9 clones to 10 harboured the isoform 1 *c*DNA (data not shown). This might be due to a tissue specificity of the two transcripts: in fact while microarray data suggest a ubiquitous expression profile for *At*2g32390 gene throughout the plant (eFP browser at www.arabidopsis.org), a previous work assigned the highest expression level in roots by qRT-PCR. We actually don't know if this difference is accountable to the diverse techniques or to the different probe used.

Two constructs, pGREAT- DsRed2-N1 and pGREAT- EGFP- N1, based on the backbone of the pGreen0029 binary vector and the T-DNA cassette of pSAT6 series, have been designed for "in planta" expression of fusion proteins. First the *Age*I restriction site has been inserted upstream of the *Kpn*I site in the MCS of pGreen0029 to obtain pGreen0029mut; then the "35S dual promoter-MCS-DsRed2-35S terminator" cassette from pSAT6-DsRed2-N1 vector has been cloned between *Age*I-*Not*I sites in the pGreen0029mut to obtain pGREAT-DsRed2-N1 vector. The EGFP coding region has been sub-cloned from pSAT6-EGFP-N1 vector between *BamH*I and *Not*I sites. Finally, the coding sequences of the two isoforms have been cloned into the above mentioned vectors (pGREAT-*g3.5v1::*DsRed2/EGFP and pGREAT-*g3.5v2::*DsRed2/EGFP) and transformed into *Arabidopsis* mesophyll protoplasts or into *A. tumefaciens* strain GV3101 for subsequent *Arabidopsis* leaf agroinfiltration.

*At*GLR3.5 isoform 1 is located in mitochondria

The analysis of the subcellular localization of the two isoforms in mesophyll protoplasts (Fig. 3) by confocal microscopy revealed the presence of the fluorescence signal in small highly mobiles structures into the cytoplasm for G3.5v1-DsRed2 fusion protein. The co-localization of the fluorescence red signal with that of the mitochondrial marker β-GFP demonstrated the localization of the long isoform in mitochondria.

The second isoform seems to be located in chloroplasts, as we can appreciate from the overlay between the red signal due to the fusion protein and the blue signal due to the chlorophyll into the chloroplasts. Moreover, a faint and uniform fluorescence can be noticed at the plasma membrane. To further confirm the subcellular plastidial location of *At*GLR3.5 splicing variant 2, confocal microscopy was used in a homologous expression system. *Arabidopsis* cultured cells were transformed with a plasmid encoding predicted signal peptide of *At*GLR3.5 splicing variant 2 in fusion with YFP (Green-G3.5SP*::*YFP). N-terminal signal peptides have been shown to be necessary and sufficient for chloroplast targeting of various proteins (e.g. Chen *et al*., 2004; Zybailov *et al*., 2008). Chloroplast stroma-targeted soluble fluorescent amylase (Green-TR-BAMY*::*GFP) was used as positive control (Fig. 4) and was present in plastids and stromules. The *At*GLR3.5 fusion protein was clearly located in plastids and stromules (Fig. 4).

Knockout mutants harbour mitochondria with altered ultrastructure

Two knockout homozygous mutant lines have been purchased from NASC stock center: N656359 (SALK_035264C, *atglr3.5-1*) and N661846 (SALK_023880C, *atglr3.5-2*). Both lines have been tested first for kanamycin resistance and then for T-DNA insertion (Fig. S1) and lack of *At*2g3290 gene expression.

We investigated the ultrastructure of mitochondria in 6 weeks old plants by TEM and we observed that some mitochondria are less electron-dense, swollen and lack the cristae (Fig. 5). A similar pattern has been observed during senescence. This phenotype is more evident in 6 weeks old plants and can explain the accelerated senescence observed after flowering. Importantly, the altered mitochondrial ultrastructure is observable in both independent mutant lines while, for comparison, *At*GLR3.4-less mitochondria were as those of *wt Col0*. No evident alterations are noticeable for chloroplasts or plasma membrane were the isoform 2 is located. This might be due to the presence of other members of the GLR family as the *At*GLR3.4 that has a similar subcellular localization and might compensate for the lost function.

DISCUSSION

The results shown a dual targeting of *At*GLR3.5, when studied in a homologous system. Although we do not know the reason of dual targeting, possible explanations can be put forward. For example, it has been reported that several members of the cytochrome P450 family (CYP) are targeted to both the ER and mitochondrial compartments (Anandatheerthavarada *et al*., 1999; Robin *et al*., 2001). Dual targeting of CYP apoproteins to the ER and to mitochondria is modulated by an amino-terminal bipartite signal, which includes an ER targeting sequence followed by a cryptic mitochondrial targeting sequence. Activation of the cryptic signal is mediated through post-translational modification. The relative affinities of the targeting signals to the ER versus mitochondria for this protein are regulated through cellular cAMP levels and phosphorylation of an internal site. By analogy, it can be hypothesized that effective targeting of *At*GLR3.4 depends on e.g. cAMP levels, which may vary from cell to cell in *Arabidopsis* cell culture as well as in a plant. Targeting may also depend on other kind of post-translational modifications or partnership. The chloroplast

proteome has been shown to contain N-glycosylated proteins that are transported though the endoplasmic reticulum (ER) to chloroplasts (Villajero *et al*., 2005) and direct contact as well as biochemical interactions between ER and chloroplast membrane systems have been demonstrated (Moreau *et al*., 1998; Xu *et al*., 2003). Concerning *At*GLR3.5, which has a clear mitochondrial targeting in the splicing variant 1 but less clear in splicing variant 2, it can be mentioned that several proteins are targeted to both mitochondria and chloroplasts because they have an ambiguous signal that can be recognized by both import systems (Silva-Filho, 2003). Dual targeting by ambiguous signals appears to be achieved by combining distinct targeting instructions in a single N-terminal peptide (Karniely and Pines, 2005). In mammalian system, several ion channels are located in multiple membranes within the cell (e.g. Siemen *et al*., 1999; Shoshan-Barmatz and Israelson, 2005; Köttgen *et al*., 2005; Szabò *et al*., 2008).

MATERIALS AND METHODS

Plant material

A. thaliana plants used for the experiments were grown in a growth room with controlled climatic conditions (photoperiod: LD 12:12; relative humidity: 70%; night temperature: 18,0°C; day temperature: 20,0°C). Protoplasts were collected from *wt Col0* ecotype plants; for the agroinfiltration experiments were used *wild-type Col0* and β-GFP plants for co-localization studies.

Seeds of *Arabidopsis thaliana* ecotype Columbia were sterilized, incubated for 3 days at 4°C in the dark and allowed to germinate in Murashige and Skoog medium (Murashige and Skoog, 1962) (Duchefa, The Netherlands) solid medium (0.8% plant agar, Duchefa) supplemented with 30 g/L sucrose in a growth chamber (24°C, 8/16 hours light/dark photoperiod, 70% RH). Seedlings were picked and grown in soil in a growth chamber (22˚C, 8/16 hours light/dark photoperiod, 70% RH). Rosette leaves from two weeks old plants were harvested and immediately powdered in liquid nitrogen for total RNA extraction.

Shoots of 5 days old seedlings were transferred on MSR2 medium (MS salts, 4.5 mg/L nicotinic acid, 10.9 mg/L thiamine HCl, 9.5 mg/L pyridoxal HCl, 200 mg/L KH_2PO_4, 0.5 g/L malt extract, 30 g/L sucrose, 1 mg/L 6-benzyl-aminopurine, 2 mg/L 2,4-dichlorophenoxyacetic acid, pH 5.7) for callus regeneration and cell cultures preparation. Cell lines were maintained in a growth chamber shaking at 80 rpm and sub-cultured weekly at 1.5/50 (v/v) in MSR2 medium.

Purification of chloroplasts

Chloroplasts were isolated on a discontinuous (10/40/75%) Percoll gradient (Prombona *et al*., 1988) in order to separate intact chloroplast. Chlorophyll concentration was measured after washing out Percoll.

Cloning and analysis

Total RNA was extracted from 100mg of powdered leaves using the TRIzol reagent (Gibco brl., Germany). After treatment with RNase-free DNase I (Ambion Ltd., UK), first strand *c*DNA was synthesized starting from 5μg of total RNA using the PowerScript™ Reverse Transcriptase (Clontech, USA).

Atglr3.5 signal peptide (SP) *c*DNA was isolated by RT-PCR using primers designed on the first 300 nucleotides of a splicing variant of the *Arabidopsis At*2g32390 gene (NP_001031464.1) and cloned into the pGreen0029 vector (28) fused to the YFP at the *Nco*I site: forward primer

5'-ATCCCATGGATCATATGGGAGCTTTGCAGCTAAT-3' and reverse primer 5'-ATCCCATGGCCATATGATCACCTAATACAGATATT-3'.

Sequence analysis

Bioinformatics analysis were performed using ChloroP and TargetP tools (http://www.cbs.dtu.dk/services), PCLRv_0.9 (http://andrewschein.com/pclr/) as well as BlastP (http://www.ncbi.nih.gov).

Subcellular localization

The *Atglr3.5SP c*DNAs were fused to YFP and cloned into the pGreen0029 vector (28). The pGreen-*Atglr3.4::YFP* and pGreen-*Atglr3.5SP::YFP* constructs were transformed in *Arabidopsis* (ecotype Columbia) cell protoplasts to follow the intracellular localization of YFP. The signal peptide of *Arabidopsis* thioredoxin-regulated β-amylase (TR-BAMY; *At*3g23920), fused to YFP (pGreen-*TR-BAMY::YFP*) has been used as positive control (29).

Protoplast isolation and transformation

Protoplasts of cultured *Arabidopsis* cells have been isolated and transformed following the Bregante *et al*. (30) protocol with some modifications. Briefly, 2 mL (packaged volume) of 5 days old suspension cultured cells have been washed once in K3 medium (3/1 v/v) (0.4 M sucrose, 1.67 mM xylose, 5 mM $CaCl_2$, 3 mM NH_4NO_3, 1X Gamborg B5 salts, 1X Kao and Michayluk organic acids, 5 μM α-naphthalene-acetic acid, 4.4 μM 6-benzyl-aminopurine, pH 5.8 and filter sterilized) and incubated 4 hours at 25°C in the dark at 80 rpm in plasmolyzation buffer (4/1 v/v) ($MS^{-½}$, 0.5 M mannitol, 13.5 mM $CaCl_2$, 44 μM 6-benzyl-aminopurine, pH 5.8 and filter sterilized) containing 0.5% macerozyme R10 (Yakult Pharmaceutical, Japan) and 1% cellulase Onozuka R10 (Yakult Pharmaceutical, Japan) (filter sterilized). Then protoplasts have been filtrated through 170 μm and 50 μm nylon meshes and centrifuged 5 minutes at 100 *g* at RT. The filtered protoplasts were washed three times with W5 solution (4/1 v/v) (154 mM NaCl, 5 mM KCl, 125 mM $CaCl_2$, 5 mM glucose, pH 5.8 and filter sterilized) and centrifuged 5 minutes at 100 *g* then resuspended in an appropriate volume of MaCa buffer (0.5 M mannitol, 20 mM $CaCl_2$, 0.1% w/v 2-[N-morpholino]ethanesulfonic acid (MES), pH 5.8 and filter sterilized) to obtain a final concentration of 10^6 protoplasts/mL.

For the Polyethylene-glycol (PEG) mediated transformation, 15 μg of plasmid's DNA (7 μg for positive control) were added to $3.0 \cdot 10^5$ protoplasts and mixed with an equal volume of PEG solution (40% w/v PEG4000, 0.4 M mannitol, 0.1 M $Ca(NO_3)_2$, pH 8 and filter sterilized). The protoplast suspension was gently mixed and left in the dark for 30 minutes at RT. The PEG was washed out with 5 mL of W5 solution then protoplasts were collected by 5 minutes centrifugation at 100 *g* and resuspended in 2 mL of K3 solution. The protoplasts were incubated at 20°C in the dark for at least 16 hours before the microscopy analysis.

***A. tumefaciens* strain, transformation and preparation for agroinfiltration**

A. tumefaciens GV3101 strain, carrying the pSoup vector, was used for transformation of plants. This strain was transformed with pGREAT vector containing *Atglr3.5v1* gene *in frame* with DsRed2 sequence, and used for the infiltration of *A. thaliana* 4-weeks-old plants leaves.

A. tumefaciens was transformed using the freeze-thaw method as described in Jyothishwaran *et al*., 2007, and then plated in LB agar medium (10 g/L Tryptone, 5 g/L yeast extract, 10 g/L NaCl, 15 g/L Bacto-agar) with antibiotics.

Two days before infiltration, a single colony of transformed *A. tumefaciens* grown on agar plates was inoculated in 5 mL of YEP liquid medium (10 g/L Bacto-Tryptone, 10 g/L yeast

extract, 5 g/L NaCl, pH 7.0) supplemented with specific antibiotics. Bacterial culture was incubated for 2 days at 30°C at 180 rpm on an orbital shaker.
After 48 hours, 2 mL of culture were transferred to Eppendorf tubes and pelleted by centrifugation at 3000 *g* for 5 min at room temperature. Bacterial pellet was resuspended in 1 mL of induction medium (10.5 g/L K_2HPO_4, 4.5 g/L KH_2PO_4, 1 g/L $(NH_4)_2SO_4$, 0.5 g/L Na citrate, 1 g/L glucose, 4 g/L glycerol, 1 mM $MgSO_4$, 10 mM MES, pH 5.6) and then transferred in 3 mL of induction medium supplemented with 100 μM acetosyringone (Sigma-Aldrich®) and grown for 6 hours at 30°C. Bacteria were pelleted at 3000 *g* for 5 minutes at room temperature, resuspended in infiltration medium (10 mM $MgSO_4$, 10 mM MES, pH 5.6) to a final OD_{600} of 0.400 and supplemented with 200 μM acetosyringone. This suspension was used for infiltration.

Agroinfiltration of *Arabidopsis thaliana* leaves
Agroinfiltration was conducted by infiltration of agrobacterial suspension in infiltration medium into intercellular spaces of fingernail-sized leaves of 4-weeks-old plants.
Plants used were kept in constant darkness for at least 16 hours before infiltration and without water supply. Leaves were infiltrated in the late afternoon in the abaxial side, using a needleless plastic syringe. Plants were then transferred in a growth room with controlled climatic conditions and tested for transformation after 4 days.

Confocal microscopy for protoplasts
Transformed protoplasts were observed after a maximum of 24 hours with the confocal scanning system Radiance 2000 (Bio-Rad) mounted on a Nikon Eclipse E600 optical microscope. The images were collected with the LaserSharp 2000 software (Bio-Rad). For the excitation of GFP and chlorophyll was used an Ar laser (wavelength: 488 nm) and, for DsRed2, a HeNe laser (wavelength: 543 nm); for fluorescence emission was used a HQ515/30 filter coupled with a 500 DCLP dichroic mirror.
Confocal microscope analyses were performed using a Nikon PCM2000 (Bio-Rad, Germany) laser scanning confocal imaging system with an excitation wavelength of 488nm and detection at 530/560nm or 515/530nm for YFP and GFP respectively. The images acquired from the confocal microscope were processed using the software Corel Photo-Paint (Corel Corporation, Dallas, TX, USA).

Confocal microscopy for infiltrated leaves *in planta*
Infiltrated leaves were observed after 4 days with the confocal microscope Leica TCS SP5 II (Leica Microsystems) mounted on a Leica DMI6000 CS inverted microscope with automated programmable scanning stage and motorized lens turret.
The images and videos were collected with the Leica Application Suite software (LAS AF, Leica Microsystems). For the excitation of GFP and chlorophyll was used an Ar laser (wavelength: 488 nm) and, for DsRed2, a HeNe laser (wavelength: 543 nm); for fluorescence emission were used Leica pre-setted filters ("Leica EGFP", 500-520 nm; "Leica DsRed", 570-620 nm; "Chlorophyll", 680-720 nm).

Transmission Electron Microscopy (TEM) on leaf samples
A TEM investigation on leaf samples was carried out to understand if the mutations in GluR genes were able to modify the mitochondrial and/or plastidial ultrastructure.
Leaf samples were collected at midday and fixed overnight in 2.5% v/v glutaraldehyde solution in 100 mM sodium cacodylate pH 7.2, 4°C. Were done 3 washes of 7 minutes each in 100 mM sodium cacodylate pH 7.2 and a post-fixation in a 1% OsO_4 solution in 100 mM sodium cacodylate pH 7.2, 4°C in the dark for 1 hour. The de-hydration of samples was

conducted through a graded ethanol series (25, 50, 70, 95, 100% v/v in ddH_2O) in 3 steps of 15 minutes for each concentration, followed by 3 steps of 15 minutes each in propylene oxide (the first one at 4°C, the other two at room temperature). The impregnation of samples was done at 45°C in 3 steps of 1 hour each with Epon resin solutions in propylene oxide (Sigma-Aldrich®) with different resin:propylene oxide proportions (1:3 for the first step, 1:1 for the second step, 3:1 for the third step), followed by 2 steps of 1 hour each in pure Epon resin (Sigma-Aldrich®) at 37°C. The polymerization was carried out putting samples in an heater for 3 days at different temperatures from day to day (day 1: 37°C; day 2: 45°C; day 3: 60°C). Samples were cut in 80 nm slices with the Ultrotome V ultramicrotome (LKB) equipped with a diamond blade. Sections were collected on copper support grids and then contrasted with an uranyl acetate saturated solution in 100% ethanol for 15 minutes followed by an incubation in a 1% w/v lead citrate solution in 100% ethanol for 7 minutes. Samples were observed with a Tecnai G^2 Spirit Transmission Electron Microscope (Fei™ Electron Microscopes), operating at 100 kV.

Protein extraction and precipitation, cellular fractionation, SDS-PAGE and Western blot
A week after infiltration, leaves were collected and frozen immediately in liquid nitrogen. We made a total protein extract, grinding leaves in a mortar with buffer A (50 mM TRIS/Acetate pH 7.5, 250 mM sorbitol, 2 mM EGTA, 2 mM DTT) added with protease inhibitor (1 μg/mL leupeptine and pepstatine, 20 μM PMSF). The mush was filtered with a nylon membrane (Ø: 250 μm) and collected in eppendorf tubes. A little volume of total extract was tested for the presence of DsRed2 protein. 100 μL of total extract was precipitated in a -20°C chilled 5:4 chloroform:methanol solution on ice in agitation for 20 minutes. Sample was centrifuged at 15000 *g* for 20 minutes, 4°C (5417R centrifuge, Eppendorf) and the pellet was solubilized in SB buffer (300 mM TRIS/HCl pH 6.8, 11,5% w/v SDS, 50% w/v glycerol, 500 mM DTT, 0,1% w/v blue bromophenol) for SDS-PAGE analysis.
The remaining total extract was centrifuged at 10000 *g* for 10 minutes, 4°C (5417R centrifuge, Eppendorf) and the resulting supernatant loaded in ultracentrifuge (Optima™ LE-80K Ultracentrifuge, Beckman Coulter) at 100000 *g* for 30 minutes, 4°C (70 Ti fixed-angle rotor, 8 x 39 mL, Beckman Coulter) to collect organelles (pellet). Pellet was resuspended in 300 μL of buffer B (10 mM Tricine/KOH pH 7.5, 5% w/v sucrose, 1 mM EGTA, 2 mM EDTA) and loaded at the top of a 11 mL continuous 15-45% sucrose gradient (10 mM Tricine/KOH pH 7.5, 1 mM EGTA, 2 mM EDTA, 15 and 45% w/v sucrose). Sample was ultracentrifuged at 77000 *g* for 19 hours, 4°C, in a swinging rotor (SW 41 Ti swinging bucket rotor, 6 x 13.2 mL, Beckman Coulter); all the gradient was collected in separated 450 μL fractions.
Fractions from 3 to 20 (in order from the top) were solubilized in SB buffer and then loaded in a 7.5%, 6 M urea SDS-PAGE gel. After separation, proteins were blotted overnight on PVDF membrane (BioTrace® PVDF Membrane, VWR).

FIGURE LEGENDS

Figure 1. DNA sequence of the two GLR3.5 isoforms.
Nucleotide sequences are shown.

Figure 2. Anti-933-947 antibody localizes *At*GLR3.5 to mitochondria.
Western blots using specific antibody on isolated chloroplasts and mitochondria from *wt Col0* and knockout plants as well as on the channel expressed *in vitro*.

Figure 3. Subcellular localization of the two GLR3.5 isoforms.

Two series of images are shown for the expression of the two constructs, pGREAT-35s-*glr3.5v1::*DsRed2 and pGREAT-35S-*glr3.5v2*::EGFP, in 4 weeks old *Arabidopsis* leaves. **Upper panel:** the isoform1-DsRed2 fusion protein is located in highly motile structures that look like mitochondria. **Lower panel:** the isoform2-EGFP fusion protein is detectable in chloroplasts, as demonstrated by the co-localization of the chlorophyll signal. Bar: 20 μm.

Figure 4. Subcellular localization of *At*GLR3.5 to chloroplast is guided by signal peptide. Subcellular localization of *At*GLR3.5SP-YFP and TR-BAMY-GFP (positive control) fusion proteins expressed in *Arabidopsis* (*wt Col0*) cell protoplasts. Images came from non-autofluorescent protoplasts. **(A-C)** GFP signal detected in protoplasts transformed with the pGreen-*TR-BAMY::GFP* construct. Arrows indicate plastids and stromules. **(H-J)** YFP signal detected in protoplasts transformed with the pGreen-*Atglr3.5SP::YFP* construct. The protein is located in plastids. Higher magnification of protoplasts and stromules are showed for each construct in **(C)**, **(G)** and **(J)**. pl, plastids; pm, plasma membrane; st, stromule. Bar: 10 μm.

Figure 5. TEM micrographies of mitochondria of *wt Col0* plants and GLR mutants.
Upper panel: *wt Col0* mitochondria in whole cell (left) and in detail (right). **Central panel**: mitochondria of GLR3.5 N656359 mutants: organelles appear empty, without *cristae*. **Lower panel**, left: also in GLR3.5 N661846 mutants mitochondria appear more empty respect to *wt Col0* ones; thylakoids in chloroplast are intact. Right: in GLR3.4 N579842 mutants (control) mitochondria are intact, like in *wt Col0* plants.

REFERENCES

Anandatheerthavarada H.K., Biswas G., Mullick J., Sepuri N.B., Otvos L., Pain D., Avadhani N.G. (1999) Dual targeting of cytochrome P4502B1 to endoplasmic reticulum and mitochondria involves a novel signal activation by cyclic AMP-dependent phosphorylation at SER128. *EMBO J. 18, 5494-5504*

Bregante M., Yang Y., Formentin E., Carpaneto A., Schroeder J., Gambale F., Lo Schiavo F., Costa A. (2008) KDC1, a carrot Shaker-like potassium channel, reveals its role as a silent regulatory subunit when expressed in plant cells. *Plant Mol. Biol. 66, 61-72*

Brenner E.D., Martinez-Barboza N., Clark A.P., Liang Q.S., Stevenson D.W., Coruzzi, G. (2000) *Arabidopsis* mutants resistant to S(+)-β-methyl-α,β- diaminopropionic acid, a cycad-derived glutamate receptor agonist. *Plant Physiol. 124, 1615-1624*

Chen M.H., Huang L.F., Li H., Chen Y.R., Yu S.M. (2004) Signal peptide-dependent targeting of a rice α-amylase and cargo proteins to plastids and extracellular compartments of plant cells. *Plant Physiol. 135, 1367-1377*

Chiu J.C., Brenner E.D., De Salle R., Nitabach M.N., Holmes T.C., Coruzzi G. (2002) Phylogenetic and expression analysis of the glutamate-receptor-like gene family in *Arabidopsis thaliana*. *Mol. Biol. Evol. 19, 1066-1082*

Chiu J., De Salle R., Lam H.M., Meisel L., Coruzzi G. (1999) Molecular evolution of glutamate receptors: a primitive signaling mechanism that existed before plants and animals diverged. *Mol. Biol. Evol. 16, 826-838*

Davenport R. (2002) Glutamate receptors in plants. *Annals of Botany 90, 549-557*

Demidchik V., Essah P.A., Tester M. (2004) Glutamate activates cation currents in the plasma membrane of *Arabidopsis* root cells. *Planta 219, 167-175*

Dennison K.L., Spalding E.P. (2000) Glutamate-gated calcium fluxes in *Arabidopsis*. *Plant Physiol.* 124, 1511-1514

Dubos C., Huggins D., Grant G.H., Knight M.R., Campbell M.M. (2003) A role for glycine in the gating of plant NMDA-like receptors. *Plant J. 35, 800-810*

Jyothishwaran G., Kotresha D., Selvaraj T., Srideshikan S.M., Rajvanshi P.K., Jayabaskaran C. (2007) A modified freeze-thaw method for efficient transformation of *Agrobacterium tumefaciens. Curr. Sci. 93, 770-772*

Kang S., Kim H.B., Lee H., Choi J.Y., Heu S., Oh C.J., Kwon S.I., An C.S. (2006) Overexpression in *Arabidopsis* of a plasma membrane-targeting glutamate receptor from small radish increases glutamate-mediated Ca^{2+} influx and delays fungal infection. *Mol. and Cells, 21, 418-427*

Kang J., Mehta S., Turano F.J. (2004) The putative glutamate receptor 1.1 (*At*GLR1.1) in *Arabidopsis thaliana* regulates abscisic acid biosynthesis and signaling to control development and water loss. *Plant Cell Physiol. 45, 1380-1389*

Kang J., Turano F.J. (2003) The putative glutamate receptor 1.1 (*At*GLR1.1) functions as a regulator of carbon and nitrogen metabolism in *Arabidopsis thaliana*. *Proc. Natl. Acad. Sci. USA, 100, 6872-6877*

Karniely S., Pines O. (2005) Single translation-dual destination. *EMBO Reports 6, 420-425*

Kim S. A., Kwak J.M., Jae S.K., Wang M.H., Nam H.G. (2001) Overexpression of the AtGluR2 gene encoding an *Arabidopsis* homolog of mammalian glutamate receptors impairs calcium utilization and sensitivity to ionic stress in transgenic plants. *Plant Cell Physiol. 42, 74-84*

Köttgen M., Benzing T., Simmen T., Tauber R., Buchholz B., Feliciangeli S., Huber T.B., Schermer B., Kramer-Zucker A., Höpker K., Simmen K.C., Tschucke C.C., Sandford R., Kim E., Thomas G., Walz G. (2005) Trafficking of TRPP2 by PACS proteins represents a novel mechanism of ion channel regulation. *EMBO J. 24, 705-716*

Krol E., Dziubinska H., Trebacz K., Koselski M., Stolarz M. (2007) The influence of glutamic and aminoacetic acids on the excitability of the liverwort *Conocephalum conicum*. *J. Plant Physiol. 164, 773-784*

Lam H.M., Chiu J., Hsieh M.H., Meisel L., Oliveira I.C., Shin M., Coruzzi G. (1998) Glutamate-receptor genes in plants. *Nature 396, 125-126*

Li J., Zhu S., Song X., Shen Y., Chen H., Yu J., Yi K., Karplus V.J., Wu P., Deng X.W. (2006) A rice glutamate receptor-like gene is critical for the division and survival of individual cells in the root apical meristem. *Plant Cell 18, 340-349*

McAinsh M.R., Pittman J.K. (2009) Shaping the calcium signature. *New Phytol. 181, 275-294*

Meyerhoff O., Müller K., Roelfsema M.R.G., Latz A., Lacombe B., Hedrich R., Dietrich P., Becker D. (2005) *At*GLR3.4, a glutamate receptor channel-like gene is sensitive to touch and cold. *Planta 222, 418-427*

Moreau P., Bessoule J.J., Mongrand S., Testet E., Vincent P., Cassagne, C. (1998) Lipid trafficking in plant cells. *Prog. Lipid Res. 37, 371-391*

Prombona A., Ogihara Y., Subramanian A.R. (1988) Cloning and identification of ribosomal protein genes in chloroplast DNA. *Methods Enzymol. 164, 748-761*

Qi Z., Stephens N.R., Spalding, E.P. (2006) Calcium entry mediated by GLR3.3, an *Arabidopsis* glutamate receptor with a broad agonist profile. *Plant Physiol. 142, 963-971*

Robin M.A., Anandatheerthavarada H.K., Fang J.K., Cudic M., Otvos L., Avadhani N.G. (2001) Mitochondrial targeted cytochrome P450 2E1 (P450 MT5) contains an intact N terminus and requires mitochondrial specific electron transfer proteins for activity. *J. Biol. Chem. 276, 24680-24689*

Shoshan-Barmatz V., Israelson A. (2005) The voltage-dependent anion channel in endoplasmic/sarcoplasmic reticulum: characterization, modulation and possible function. *J. Membr. Biol. 204, 57-66*

Siemen D., Loupatatzis C., Borecky J., Gulbins E., Lang F. (1999) Ca^{2+}-activated K^{+} channel of the BK-type in the inner mitochondrial membrane of a human glioma cell line. *Biochem. Biophys. Res. Commun. 257, 549-554*

Silva-Filho M.C. (2003) One ticket for multiple destinations: dual targeting of proteins to distinct subcellular locations. *Curr. Opin. Plant Biol. 6, 589-595*

Sivaguru M., Pike S., Gassmann W., Baskin T.I. (2003) Aluminum rapidly depolymerizes cortical microtubules and depolarizes the plasma membrane: evidence that these responses are mediated by a glutamate receptor. *Plant Cell Physiol. 44, 667-675*

Stephens N.R., Qi Z., Spalding E.P. (2008) Glutamate receptor subtypes evidenced by differences in desensitization and dependence on the GLR3.3 and GLR3.4 genes. *Plant Physiol. 146, 529-538*

Szabò I., Bock J., Grassmè H., Soddemann M., Wilker B., Lang F., Zoratti M., Gulbins E. (2008) Mitochondrial potassium channel Kv1.3 mediates Bax-induced apoptosis in lymphocytes. *Proc. Natl. Acad. Sci. USA 105, 14861-14866*

Tapken D., Hollmann M. (2008) *Arabidopsis thaliana* glutamate receptor ion channel function demonstrated by ion pore transplantation. *J. Mol. Biol. 383, 36-48*

Teardo E., Formentin E., Segalla A., Giacometti G.M., Marin O., Zanetti M., Lo Schiavo F., Zoratti M., Szabò I. (2011) Dual localization of plant glutamate receptor *At*GLR3.4 to plastids and plasma membrane. *Biochim. Biophys. Acta 1807(3), 359-367*

Teardo E., Segalla A., Formentin E., Zanetti M., Marin O.,Giacometti G.M., Lo Schiavo F., Zoratti M., Szabò I. (2010) Characterization of a plant glutamate receptor activity. *Cell Physiol. Biochem. 26(2), 253-262*

Villajero A., Burén S., Larsson S., Déjardin A., Monné M., Rudhe C., Karlsson J., Jansson S., Lerouge P., Rolland N., Von Heijne G., Grebe M., Bako L., Samuelsson G. (2005) Evidence for a protein transported through the secretory pathway en route to the higher plant chloroplast. *Nature Cell Biol. 7, 1224-1231*

Walch-Liu P., Liu L.H., Remans T., Tester M., Forde B.G. (2006) Evidence that L-glutamate can act as an exogenous signal to modulate root growth and branching in *Arabidopsis thaliana*. *Plant Cell Physiol. 47, 1045-1057*

Xu C., Fan J., Riekhof W., Froehlich J.E., Benning C. (2003) A permease-like protein involved in ER to thylakoid transfer in *Arabidopsis. EMBO J. 22, 2370-2379*

Zybailov B., Rutschow H., Friso G., Rudella A., Emanuelsson O., Sun Q., Van Wijk K.J. (2008) Sorting signals, N-terminal modifications and abundance of the chloroplast proteome. *PloS One 3, 1-19*

iGLRs project figures

Figure 1


CLUSTAL 2.1 multiple sequence alignment
NM_128798.1 ATGGGATTTTTCGTGATGATTAGAGATGTTTCCATGGGATTTATGCTCCTATGTATTTCT 60
NM_001036387.1 ----------
NM_128798.1 GCTTTGTGGGTTTTGCCAATACAAGGTGCTGGTAGAGAAAGTTTCTCAAGAAACTCTTCT 120
NM_001036387.1 ----------
NM_128798.1 TCTTCTTCTCTGCCAAGCTCTGTAAACGTTGGAGCTCTGTTTACTTATGATTCTTTCATT 180
NM_001036387.1 ----------ATGATTCTTTCATT 14
NM_128798.1 GGAAGAGCGGCCAAACTTGCGTTTGTGGCGGCCATTGAAGACATTAATGCTGACCAGAGT 240
NM_001036387.1 GGAAGAGCGGCCAAACTTGCGTTTGTGGCGGCCATTGAAGACATTAATGCTGACCAGAGT 74
NM_128798.1 ATCCTCAGGGGCACCAAGCTTAATATTGTCTTCCAGGACACTAATTGCAGTGGATTTGTT 300
NM_001036387.1 ATCCTCAGGGGCACCAAGCTTAATATTGTCTTCCAGGACACTAATTGCAGTGGATTTGTT 134
NM_128798.1 GGCACCATGGGAGCT--------AATGGAGAACAAGGTGGTTGCAGCCATTGGTCCACAA 352
NM_001036387.1 GGCACCATGGGAGCTTTGCAGCTAATGGAGAACAAGGTGGTTGCAGCCATTGGTCCACAA 194
NM_128798.1 TCTTCAGGAATTGGTCACATAATCTCCCATGTAGCTAATGAGCTTCATGTACCTTTCTTG 412
NM_001036387.1 TCTTCAGGAATTGGTCACATAATCTCCCATGTAGCTAATGAGCTTCATGTACCTTTCTTG 254
NM_128798.1 TCATTTGCAGCAACGGACCCGACTCTTTCTTCGCTTCAATACCCTTATTTCCTTCGTACC 472
NM_001036387.1 TCATTTGCAGCAACGGACCCGACTCTTTCTTCGCTTCAATACCCTTATTTCCTTCGTACC 314
NM_128798.1 ACACAGAATGATTACTTCCAGATGAATGCAATCACGGATTTTGTATCCTATTTTCGATGG 532
NM_001036387.1 ACACAGAATGATTACTTCCAGATGAATGCAATCACGGATTTTGTATCCTATTTTCGATGG 374
NM_128798.1 AGAGAAGTTGTTGCGATCTTTGTGGATGATGAGTATGGTAGGAATGGAATATCTGTATTA 592
NM_001036387.1 AGAGAAGTTGTTGCGATCTTTGTGGATGATGAGTATGGTAGGAATGGAATATCTGTATTA 434
NM_128798.1 GGTGATGCTTTAGCCAAGAAACGTGCCAAGATCTCTTACAAGGCTGCATTTCCACCTGGT 652
NM_001036387.1 GGTGATGCTTTAGCCAAGAAACGTGCCAAGATCTCTTACAAGGCTGCATTTCCACCTGGT 494
NM_128798.1 GCAGATAATAGCTCAATCAGTGATTTATTGGCTTCTGTTAATCTGATGGAATCTCGCATC 712
NM_001036387.1 GCAGATAATAGCTCAATCAGTGATTTATTGGCTTCTGTTAATCTGATGGAATCTCGCATC 554
NM_128798.1 TTTGTTGTTCATGTGAATCCTGATTCGGGTTTAAACATATTCTCTGTCGCCAAATCTCTT 772
NM_001036387.1 TTTGTTGTTCATGTGAATCCTGATTCGGGTTTAAACATATTCTCTGTCGCCAAATCTCTT 614
NM_128798.1 GGAATGATGGGAAGTGGCTATGTCTGGATCACTACTGATTGGCTTCTTACAGCTTTGGAT 832
NM_001036387.1 GGAATGATGGGAAGTGGCTATGTCTGGATCACTACTGATTGGCTTCTTACAGCTTTGGAT 674
NM_128798.1 TCCATGGAACCGTTGGATCCCAGAGCTTTGGATCTCTTGCAAGGAGTGGTTGCATTTCGT 892
NM_001036387.1 TCCATGGAACCGTTGGATCCCAGAGCTTTGGATCTCTTGCAAGGAGTGGTTGCATTTCGT 734
NM_128798.1 CATTACACACCTGAGAGTGACAACAAGAGACAGTTTAAAGGAAGATGGAAAAACCTTAGA 952

Figure 1


NM_001036387.1 CATTACACACCTGAGAGTGACAACAAGAGACAGTTTAAAGGAAGATGGAAAAACCTTAGA 794
NM_128798.1 TTCAAGGAGAGTCTAAAAAGTGATGATGGCTTCAATTCTTACGCGCTGTATGCTTACGAT 1012
NM_001036387.1 TTCAAGGAGAGTCTAAAAAGTGATGATGGCTTCAATTCTTACGCGCTGTATGCTTACGAT 854
NM_128798.1 TCTGTTTGGTTGGTAGCTCGCGCTCTCGATGTTTTCTTCAGCCAAGGCAATACAGTGACT 1072
NM_001036387.1 TCTGTTTGGTTGGTAGCTCGCGCTCTCGATGTTTTCTTCAGCCAAGGCAATACAGTGACT 914
NM_128798.1 TTCTCTAATGATCCAAGTCTGAGGAATACCAACGATAGCGGCATTAAGCTATCAAAACTT 1132
NM_001036387.1 TTCTCTAATGATCCAAGTCTGAGGAATACCAACGATAGCGGCATTAAGCTATCAAAACTT 974
NM_128798.1 CACATTTTCAATGAAGGGGAGAGGTTCTTGCAGGTCATTCTTGAGATGAATTATACAGGT 1192
NM_001036387.1 CACATTTTCAATGAAGGGGAGAGGTTCTTGCAGGTCATTCTTGAGATGAATTATACAGGT 1034
NM_128798.1 CTGACTGGACAAATCGAGTTTAATTCAGAGAAAAACCGGATTAATCCAGCCTACGACATT 1252
NM_001036387.1 CTGACTGGACAAATCGAGTTTAATTCAGAGAAAAACCGGATTAATCCAGCCTACGACATT 1094
NM_128798.1 CTGAACATAAAAAGTACAGGTCCACTGAGAGTTGGATACTGGTCGAATCATACAGGTTTC 1312
NM_001036387.1 CTGAACATAAAAAGTACAGGTCCACTGAGAGTTGGATACTGGTCGAATCATACAGGTTTC 1154
NM_128798.1 TCAGTCGCGCCTCCAGAGACATTATACTCTAAGCCTTCAAACACATCTGCAAAAGACCAA 1372
NM_001036387.1 TCAGTCGCGCCTCCAGAGACATTATACTCTAAGCCTTCAAACACATCTGCAAAAGACCAA 1214
NM_128798.1 CGTCTTAATGAGATCATATGGCCAGGGGAAGTAATAAAGCCACCTCGGGGTTGGGTTTTC 1432
NM_001036387.1 CGTCTTAATGAGATCATATGGCCAGGGGAAGTAATAAAGCCACCTCGGGGTTGGGTTTTC 1274
NM_128798.1 CCTGAAAATGGAAAGCCGCTGAAAATCGGGGTGCCTAACCGTGTAAGCTACAAAAACTAT 1492
NM_001036387.1 CCTGAAAATGGAAAGCCGCTGAAAATCGGGGTGCCTAACCGTGTAAGCTACAAAAACTAT 1334
NM_128798.1 GCTTCTAAGGACAAGAACCCGCTTGGTGTTAAAGGCTTTTGCATCGACATCTTTGAAGCT 1552
NM_001036387.1 GCTTCTAAGGACAAGAACCCGCTTGGTGTTAAAGGCTTTTGCATCGACATCTTTGAAGCT 1394
NM_128798.1 GCGATTCAATTGCTTCCATATCCCGTTCCACGTACTTATATACTATATGGGGACGGGAAG 1612
NM_001036387.1 GCGATTCAATTGCTTCCATATCCCGTTCCACGTACTTATATACTATATGGGGACGGGAAG 1454
NM_128798.1 AAAAATCCTTCATATGACAATCTCATAAGTGAAGTTGCTGCAAATATTTTCGATGTAGCT 1672
NM_001036387.1 AAAAATCCTTCATATGACAATCTCATAAGTGAAGTTGCTGCAAATATTTTCGATGTAGCT 1514
NM_128798.1 GTTGGGGATGTTACCATCATTACAAACAGAACCAAGTTTGTAGATTTCACGCAGCCATTT 1732
NM_001036387.1 GTTGGGGATGTTACCATCATTACAAACAGAACCAAGTTTGTAGATTTCACGCAGCCATTT 1574
NM_128798.1 ATAGAATCAGGGCTTGTGGTGGTAGCTCCAGTGAAGGGGGCCAAGTCTAGTCCTTGGTCC 1792
NM_001036387.1 ATAGAATCAGGGCTTGTGGTGGTAGCTCCAGTGAAGGGGGCCAAGTCTAGTCCTTGGTCC 1634
NM_128798.1 TTCTTGAAGCCATTCACTATAGAGATGTGGGCTGTGACCGGTGCCCTTTTTCTCTTTGTT 1852
NM_001036387.1 TTCTTGAAGCCATTCACTATAGAGATGTGGGCTGTGACCGGTGCCCTTTTTCTCTTTGTT 1694
NM_128798.1 GGAGCCGTCATCTGGATTCTTGAACATCGATTTAACGAAGAATTCCGCGGACCTCCTAGG 1912
NM_001036387.1 GGAGCCGTCATCTGGATTCTTGAACATCGATTTAACGAAGAATTCCGCGGACCTCCTAGG 1754

Figure 1


NM_128798.1 CGTCAAATCATTACAGTCTTCTGGTTTAGCTTCTCAACAATGTTCTTCTCTCACAGGGAG 1972
NM_001036387.1 CGTCAAATCATTACAGTCTTCTGGTTTAGCTTCTCAACAATGTTCTTCTCTCACAGGGAG 1814
NM_128798.1 AATACGGTGAGCACGTTGGGAAGGTTTGTGCTACTCGTATGGTTATTTGTGGTTCTAATC 2032
NM_001036387.1 AATACGGTGAGCACGTTGGGAAGGTTTGTGCTACTCGTATGGTTATTTGTGGTTCTAATC 1874
NM_128798.1 ATCAACTCAAGCTACACAGCCAGTCTCACTTCAATCCTCACCGTTCAACAGCTAACATCT 2092
NM_001036387.1 ATCAACTCAAGCTACACAGCCAGTCTCACTTCAATCCTCACCGTTCAACAGCTAACATCT 1934
NM_128798.1 CGGATAGAAGGAATGGACACTTTAATAGCAAGCAACGAACCCATTGGAGTCCAAGATGGT 2152
NM_001036387.1 CGGATAGAAGGAATGGACACTTTAATAGCAAGCAACGAACCCATTGGAGTCCAAGATGGT 1994
NM_128798.1 ACCTTTGCGTGGAAATTTCTGGTCAATGAACTTAACATAGCTCCATCAAGAATCATTCCG 2212
NM_001036387.1 ACCTTTGCGTGGAAATTTCTGGTCAATGAACTTAACATAGCTCCATCAAGAATCATTCCG 2054
NM_128798.1 CTTAAAGACGAAGAAGAATATCTCTCTGCTCTTCAACGTGGTCCCAGAGGCGGTGGCGTG 2272
NM_001036387.1 CTTAAAGACGAAGAAGAATATCTCTCTGCTCTTCAACGTGGTCCCAGAGGCGGTGGCGTG 2114
NM_128798.1 GCAGCCATTGTCGACGAGCTTCCTTACATTAAAGCTCTCTTGTCAAACAGCAACTGCAAG 2332
NM_001036387.1 GCAGCCATTGTCGACGAGCTTCCTTACATTAAAGCTCTCTTGTCAAACAGCAACTGCAAG 2174
NM_128798.1 TTTCGAACAGTTGGACAGGAATTCACTCGGACAGGCTGGGGATTTGCGTTCCAGAGAGAC 2392
NM_001036387.1 TTTCGAACAGTTGGACAGGAATTCACTCGGACAGGCTGGGGATTTGCGTTCCAGAGAGAC 2234
NM_128798.1 TCTCCTCTAGCTGTGGACATGTCGACAGCGATCCTGCAACTGGCTGAAGAAGGAAAACTC 2452
NM_001036387.1 TCTCCTCTAGCTGTGGACATGTCGACAGCGATCCTGCAACTGGCTGAAGAAGGAAAACTC 2294
NM_128798.1 GAGAAAATCCGCAAGAAATGGCTTACCTACGACCACGAATGTACAATGCAGATTTCAGAT 2512
NM_001036387.1 GAGAAAATCCGCAAGAAATGGCTTACCTACGACCACGAATGTACAATGCAGATTTCAGAT 2354
NM_128798.1 ACAGAAAACTATCAAATATCGGTACAGAGTTTCTGGGGACTCTTCCTAATATGTGGCGTC 2572
NM_001036387.1 ACAGAAAACTATCAAATATCGGTACAGAGTTTCTGGGGACTCTTCCTAATATGTGGCGTC 2414
NM_128798.1 GTTTGGTTCATTGCACTCACACTCTTCTGCTGGAAAGTTTTCTGGCAATACCAACGGTTA 2632
NM_001036387.1 GTTTGGTTCATTGCACTCACACTCTTCTGCTGGAAAGTTTTCTGGCAATACCAACGGTTA 2474
NM_128798.1 AGACCAGAAGAGAGTGATGAAGTACAGGCGAGGAGCGAGGAGGCTGGTTCTTCTAGAGGG 2692
NM_001036387.1 AGACCAGAAGAGAGTGATGAAGTACAGGCGAGGAGCGAGGAGGCTGGTTCTTCTAGAGGG 2534
NM_128798.1 AAAAGTTTGAGAGCAGTGAGTTTCAAGGATTTGATCAAAGTTGTTGATAAGAGAGAAGCA 2752
NM_001036387.1 AAAAGTTTGAGAGCAGTGAGTTTCAAGGATTTGATCAAAGTTGTTGATAAGAGAGAAGCA 2594
NM_128798.1 GAGATTAAGGAGATGCTTAAGGAGAAGAGCAGTAAGAAACTCAAAGATGGCCAAAGTTCA 2812
NM_001036387.1 GAGATTAAGGAGATGCTTAAGGAGAAGAGCAGTAAGAAACTCAAAGATGGCCAAAGTTCA 2654
NM_128798.1 GCTGAGAATTCGCAGTCGAAAGATCACGAAACTCCACAGTGA 2854
NM_001036387.1 GCTGAGAATTCGCAGTCGAAAGATCACGAAACTCCACAGTGA 2696

Figure 2

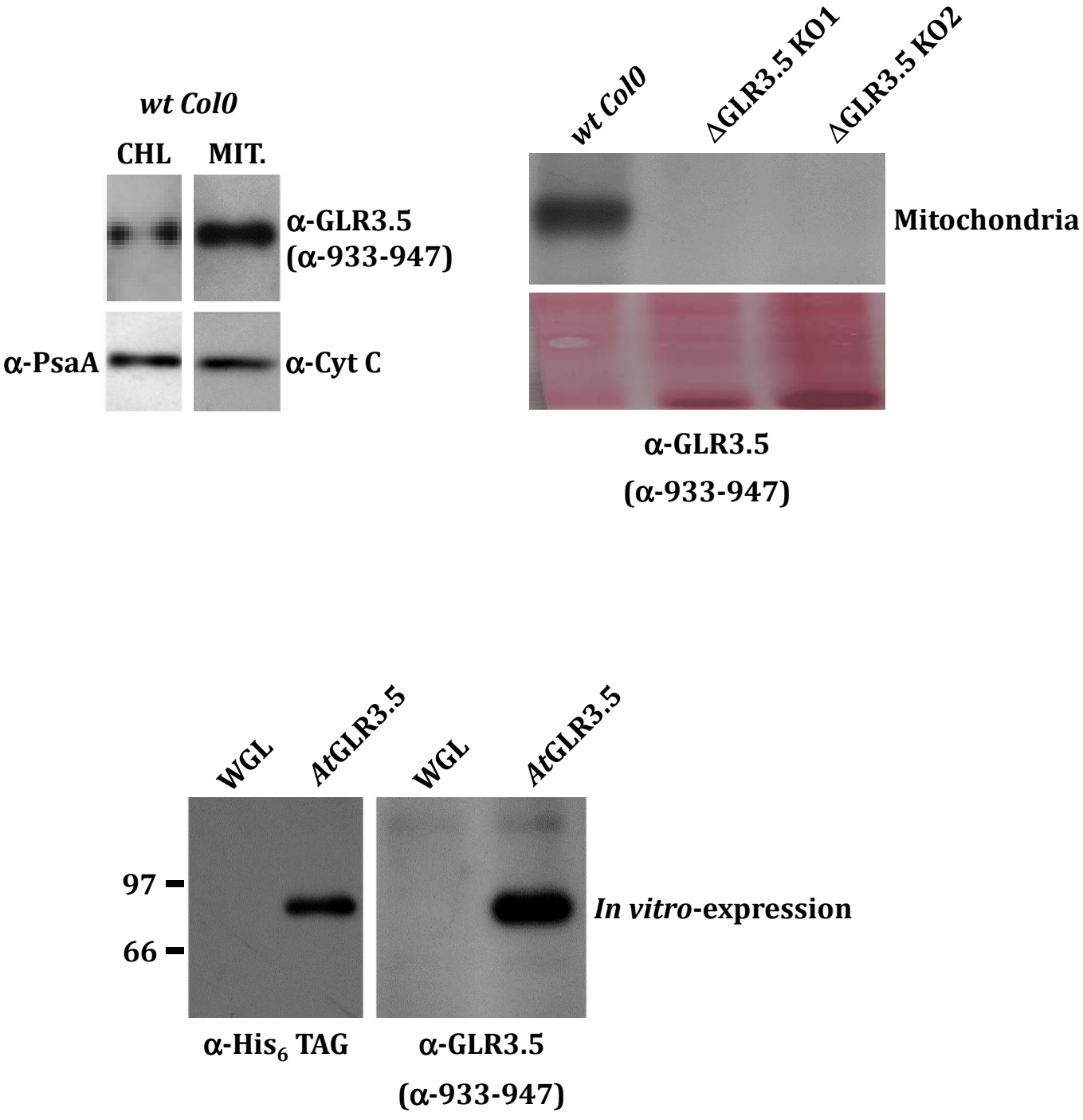
wt Col0
CHL
MIT.
α-GLR3.5
(α-933-947)
α-PsaA
α-Cyt C
wt Col0
ΔGLR3.5 KO1
ΔGLR3.5 KO2
Mitochondria
α-GLR3.5
(α-933-947)
WGL
AtGLR3.5
WGL
AtGLR3.5
97
66
In vitro-expression
α-His6 TAG
α-GLR3.5
(α-933-947)

Figure 3

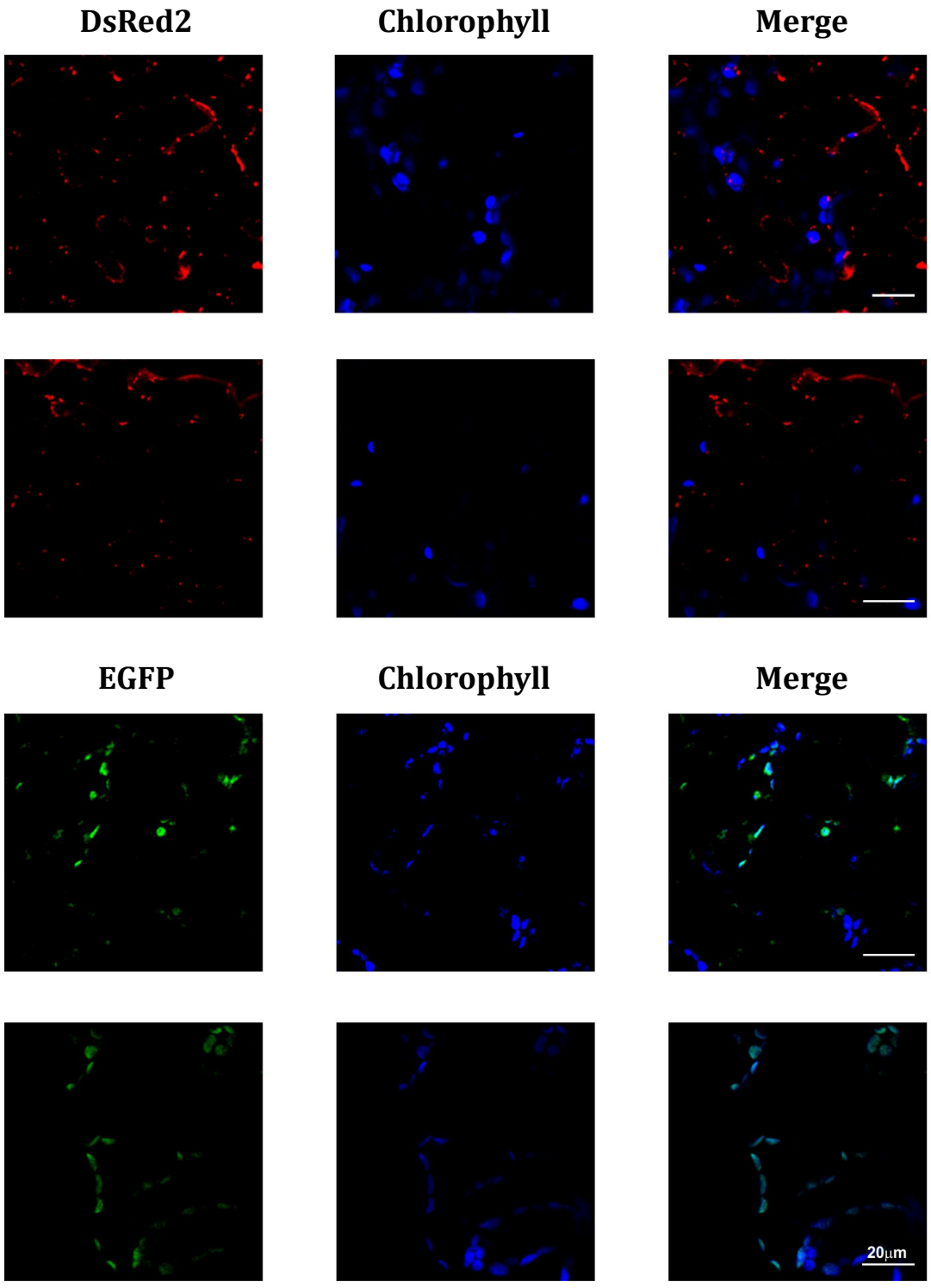
DsRed2
Chlorophyll
Merge
pGREAT-35S::g3.5v1::DsRed2
EGFP
Chlorophyll
Merge
pGREAT-35S::g3.5v2::EGFP
20μm

Figure 4

TR-BAMY-GFP

_At_GLR3.5SP-YFP

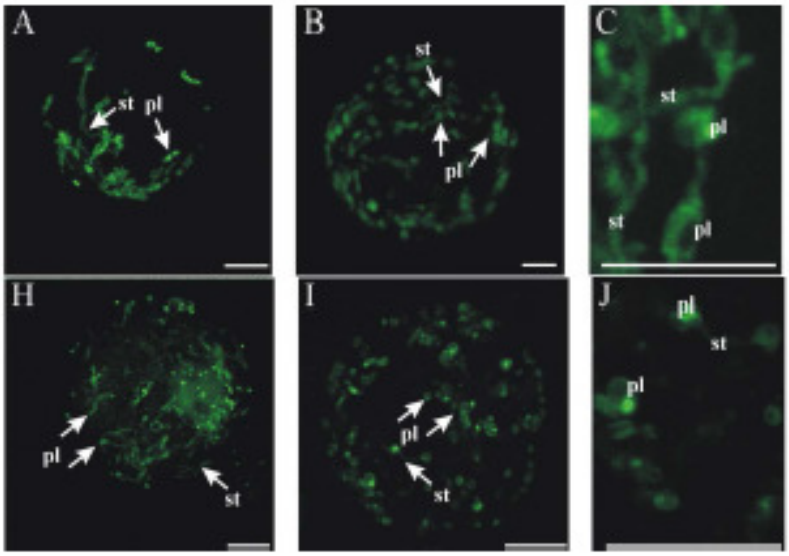

Figure 5

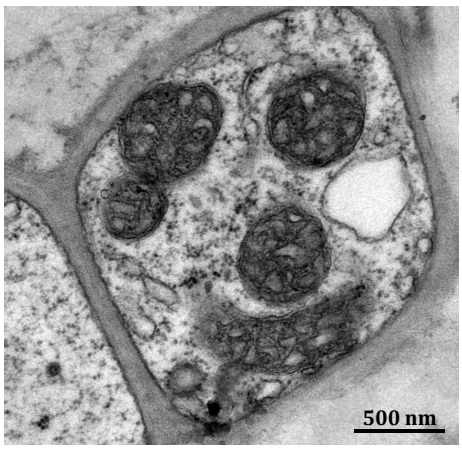

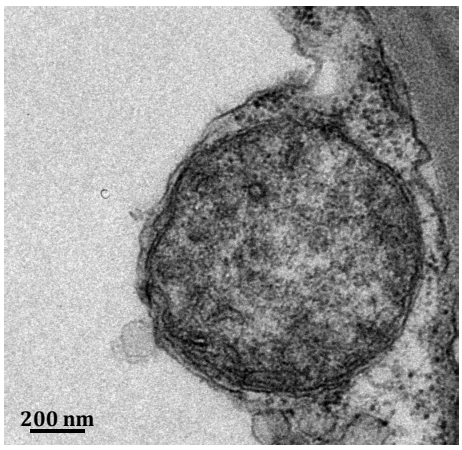

wt Col0

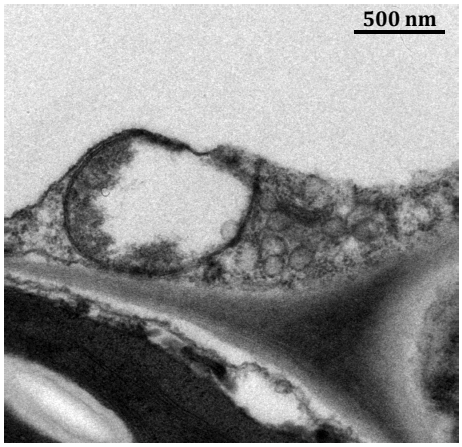

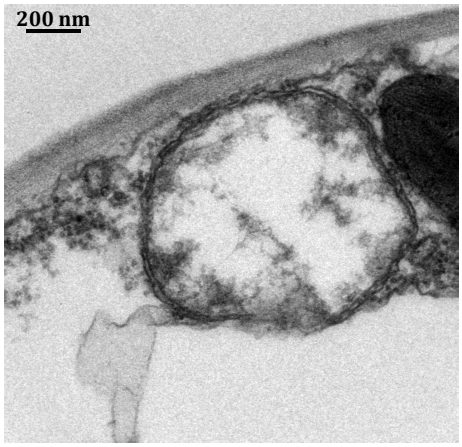

ΔGLR3.5 N656359

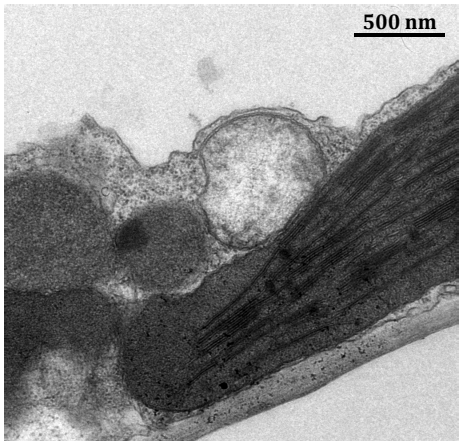

ΔGLR3.5 N661846

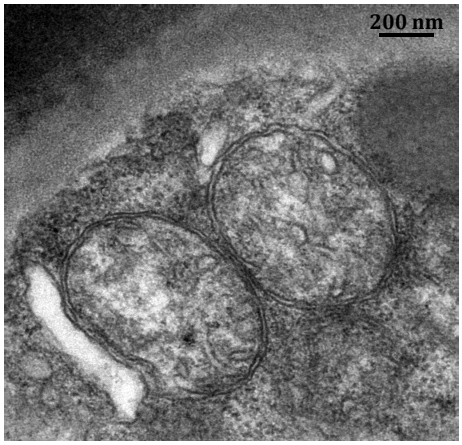

ΔGLR3.4 N579842 (C^-)

Tables

Table I

Table 1
AtGluR3.4, AtGluR3.5 and cyanobacterial glutamate receptors share sequence similarity

	AtGluR3.5 (At2g32390)
Synechocystis sp. PCC 6803 GluR0, slr 1257 (gi 1652933)	3×10^{-06} 73/294 (24%)
Nostoc punctiforme PCC 73102 GluRG2 (gi 23126603)	4×10^{-09} 73/291 (25%)
Magnetospirillum magnetotacticum MS-1 GluRG3 (gi 46202027)	5×10^{-09} 74/327 (22%)

Aminoacid sequences of GLRs channels (GI: Accession Nos. in NCBI data bank) were compared pairwise by BLASTP algorithm (www.ncbi.nih.gov). E values: number of hits expected to be found by chance. % of identity is shown and length of aligned sequence reported in brackets. Similarity is considered to be of higher degree when E value is lower and percentage of identity is higher over a longer region.

*Syn*CaK project

Functional characterization and determination of the physiological role of a calcium-dependent potassium channel from *Synechocystis* sp. PCC 6803 cyanobacteria.

Vanessa Checchetto, Elide Formentin, Luca Carraretto, Anna Segalla, Giorgio Mario Giacometti, Ildikò Szabò*, Elisabetta Bergantino*

Department of Biology, University of Padua

*These authors share last authorship

Correspondence should be sent to:
I.S. e-mail: ildi@civ.bio.unipd.it; E.B.: elisabetta.bergantino@unipd.it

ABSTRACT

Despite the important achievement of the high-resolution structures of several prokaryotic channels, current understanding of their physiological roles in bacteria themselves is still far from complete. We have identified a putative two transmembrane domain-containing channel (SynCaK) in the genome of the freshwater cyanobacterium Synechocystis sp. PCC 6803, a model photosynthetic organism. SynCaK displays significant sequence homology to MthK, a Ca^{2+}-dependent potassium channel isolated from M. thermoautotrophicum and to some members of two-pore potassium channels of higher plants. Expression of SynCaK in fusion with EGFP in mammalian Chinese Hamster Ovary (CHO) cells' plasma membrane gave rise to a calcium-activated, potassium-selective activity in patch clamp experiments. In cyanobacteria, Western blotting of isolated membrane fractions located SynCaK mainly to the plasma membrane. In order to understand its physiological function, a SynCaK-deficient mutant of Synechocystis sp. PCC 6803 (ΔSynCaK) has been obtained. Although the potassium content in the mutant organisms was comparable to that observed in wild-type, ΔSynCaK was characterized by a depolarized resting membrane potential as determined by a potential-sensitive fluorescent probe. Growth of the mutant under various conditions revealed that lack of SynCaK does not impair growth under osmotic or salt stress, that SynCaK is not involved in the regulation of photosynthesis. Instead, its lack conferred an increased resistance to the heavy metal zinc, an environmental pollutant. Our findings thus indicate that SynCaK is a functional channel and identify the physiological consequences of its deletion in cyanobacteria.

Submitted to Plant Physiology

Keywords: Ion transport; Cyanobacteria, potassium transport, calcium-dependent potassium channel.

INTRODUCTION

Detailed structural and mechanistic data that now exist for many prokaryotic channels, but their physiological roles remain largely unclear (Martinac *et al.*, 2008). This is especially true for potassium channels. Potassium (K^+) is the most abundant cation in organisms and in general it plays a crucial role in the survival and development of cells, by regulating enzyme activity and tuning electrochemical membrane potential. Potassium channels in prokaryotes have been hypothesized to contribute to the setting of membrane potential rather than to high-affinity potassium uptake, normally achieved thanks to specific ATP-dependent potassium transporters (Kuo *et al.*, 2005). K^+ channel genes are found in almost every prokaryotic genome that has been sequenced, but in most of the few studies where their deletion was obtained, no specific phenotype has been observed. For example, deletion of KcsA in *Streptomyces lividans* or deletion of the 6-TM KCh in *E. coli* did not produce obvious phenotype, suggesting either functional redundancy or that these channels are only required in case of rather specific environmental stresses. Gain of function (GOF) Kch mutants however failed to grow in millimolar added K^+ but not Na^+ (Kuo *et al.*, 2003) and external H^+ suppressed the GOF phenotype, supporting the hypothesis that KCh might function to regulate membrane potential. However, a clear-cut role of prokaryotic potassium channels by genetic deletion was demonstrated only in a few cases.

Synechocystis sp. PCC 6803 harbors an intracellular membrane system, the thylakoids, where both photosynthesis and respiration take place; it can grow in the absence of photosynthesis if a suitable carbon source such as glucose is provided, it is spontaneously transformable and able to integrate foreign DNA into its genome by homologous recombination. In the present work we have identified in *Synechocystis* a so-far uncharacterized putative potassium channel (NP_440478, encoded by the open reading frame *sll*0993) with sequence homology to *Mt*hK, a Ca^{2+}-activated K^+ channel of the archaeon *Methanobacterium thermoautotrophicum*. The structure of *Mt*hK in an open conformation has been determined (Jiang *et al.*, 2002). The *Mt*hK subunit has two transmembrane segments and one pore region (TM1-P-TM2), followed by an extension of approximately 200 amino acid residues which contains a region called the RCK (for regulator of the conductance of K^+) domain. RCK of *Mt*hK binds divalent cations, such as Ca^{2+} or Cd^{2+} (Jiang *et al.*, 2001, 2002). Various studies led to a model in which the channel is a hetero-octamer, where the *Mt*hK transmembrane tetramer assembles with eight RCK domains: four covalently linked to the four TM2 helices and four additional ones associated at the cytoplasmic side. The physiological meaning of the activation of *Mt*hK with millimolar Ca^{2+} (Jiang *et al.*, 2002) is unclear, since Ca^{2+} as a second messenger operates at micromolar concentrations in eukaryotes, and the possible signaling roles of Ca^{2+} in prokaryotes are still unclear. Another RCK-containing K^+ channel from the archaeon *Thermoplasma volcanium*, *Tv*oK, has also been cloned and reconstituted into planar lipid bilayers for functional analyses (Parfenova *et al.*, 2007). The channel, with a proposed hetero-octameric structure and displaying 160-pS conductance was also found to be activated by millimolar Ca^{2+}.

Here we report evidence that, similarly to *Mt*hK, also *Syn*CaK can be activated by calcium. Furthermore we show localization of the protein in cyanobacteria and describe a phenotype associated with the lack of the channel in *Syn*CaK-less mutant *Synechocystis* cells.

RESULTS

Predicted structural features of the *Syn*CaK channel

A search in the non-redundant protein database at the National Center for Biotechnology Information, using the W-BLAST algorithm and the amino acid sequence (T-X-G-[Y-F]-G-[D-E]) as query, revealed in *Synechocystis* sp. PCC 6803 a protein classified as a putative potassium channel (NP_440478). Until now, there is no experimental evidence about the function of this protein but bioinformatic analysis underlines a sequence homology with *Mt*hK, a calcium dependent potassium channel from the archeon *Methanobacterium thermoautophicum* (Jiang *et al.*, 2002) (Fig. 1). *In silico* analysis of the primary sequence of NP_440478, denominated *Syn*CaK, indicates that the protein contains two membrane spanning segments, a recognizable K^+ channel selectivity filter signature sequence with only conservative substitutions, and a regulatory sequence for K^+ conductance (RCK), similarly to *Mt*hK (Fig. 1 and Fig. S1). The RCK region contains two conserved domains, TrkA-N and TrkA-C, which occur in many potassium channels and transporters (Durrel *et al.*, 1999). TrkA-N contains an alternating βαβαβ Rossmann-fold motif, which may bind to nicotinamide adenine dinucleotide (NAD) or reduced NAD (NADH), thereby may mediate conformational switches (Roosild *et al.*, 2002). Since TrkA-N and TrkA-C are also present in the *Mt*hK channel, a similarity in domain organization between *Mt*hK and *Syn*CaK is probable. Structural studies of *Mt*hK revealed the presence of an octameric gating ring, composed of eight intracellular ligand-binding RCK domains. Binding of Ca^{2+} to RCK has been shown to regulate the gating ring conformation that in turn leads to the opening and closing of the channel (Jiang *et al*., 2002).

Expression and functional analysis of *Syn*CaK in CHO cells

To prove that *Syn*CaK forms a calcium-sensitive potassium channel, as expected, we used heterologous expression in mammalian cells, followed by electrophysiological analysis. Such approach has been successfully applied by various groups for the study of prokaryotic and even viral channels. To verify the plasma membrane localization of the channel protein expressed in Chinese Hamster Ovary (CHO) cells, a pre-requisite for the analysis of protein function by patch-clamp, *Syn*CaK was expressed in fusion with EGFP (*Syn*CaK-EGFP), a red-shifted variant of wild-type GFP which has been optimized for brighter fluorescence and higher expression in mammalian cells. Targeting of the channel to the plasma membrane (PM) was tested by examining co-localization of EGFP with a specific plasma membrane fluorescent dye (FM 4-64). Figure S2 shows fluorescence microscopy analysis of transfected CHO cells indicating that at least a part of the fusion protein reaches the PM. In the inside-out excised patch configuration *Syn*CaK-EGFP-transfected cells displayed an ion channel activity, however only in the presence of Ca^{2+} in the bath in the millimolar range. Fig. 2A upper traces show representative consecutive current traces recorded with the voltage ramp indicated after addition of 2 mM calcium to the cytoplasmic face, i.e. to the bath (N = 15). Cells transfected with the control vector encoding only for EGFP did not display any current at different potentials under the same ionic conditions (N = 50) (Fig. 2A, lower trace). These experiments were conducted in potassium gluconate, allowing to state that the slightly rectifying channel we observe is permeable to potassium, given that gluconate does not permeate across chloride channels in CHO cells. Channel conductance was 45 ± 7 pS at positive voltages while at negative voltages we observed 29±9 pS. To further prove the selectivity of *Syn*CaK, we performed experiments under asymmetric ionic conditions with Na gluconate in the pipette and K gluconate in the bath always in the presence of 2 mM calcium (N = 7). The observed

reversal potential (-77 ± 12 mV) is close to the predicted reversal potential for a perfectly selective potassium channel (value of -87 mV, as calculated from Nernst equation). Figure 2B shows a representative current trace under these conditions and show channel activity on an extended time scale as well. To further prove that the observed channel activity was due to *Syn*CaK, patch clamp experiments were performed also with cells expressing the mutant *Syn*CaKF68A-EGFP fusion protein: the introduced single point mutation did not alter PM targeting (Fig. S3) but changed a very conserved amino acid of the pore region which in general is essential for potassium conduction; K^+ channels with GAGD sequence are known to be expressed, but are unable to conduct a current (e.g. Heginbotham *et al.*, 1994). The mutant protein did not give rise to channel activity, even at 10 mM calcium (N = 5). Given the presence of the RCK domain in *Syn*CaK, its sequence similarity to the calcium-activated *Mt*hK, and the observation that the channel was not active in the absence of calcium, we finally tested channel activity at 10 mM Calcium (Fig. 2C). *Syn*CaK activity was increased when cytoplasmic calcium concentration was increased to 10 mM. In summary, these data indicate that *Syn*CaK indeed is able to function as calcium-activated potassium channel, and in accordance with reports on *Mt*hK, a high calcium concentration in the mM range is required for full activation (Jiang *et al.*, 2002).

Localization of *Syn*CaK channel in *Synechocystis* membranes

To determine the subcellular localization of *Syn*CaK, a specific antibody was raised against 15 amino acids of the protein. First, we tested for the specificity of the antibody by expressing *Syn*CaK in *E. coli*. Fig. S4 shows that the antibody recognized a 43 kDa protein only in transfected *E. coli* where expression was induced by IPTG, proving that the antibody indeed recognizes the recombinant protein. In whole cyanobacteria cell extracts, the antibody recognized three bands (see Fig. 4C), including a band with the predicted MW of the monomer, i.e. 40,5 kDa. Subfractionation of cyanobacteria was performed as previously described (Zanetti *et al.*, 2010) and revealed the presence of an approx. 41 kDa protein in the plasma membrane (PM) (Fig. 3A). We could also observe a fainter 41 kDa band in the thylakoid fraction (TH), whose intensity was consistent with residual contamination during purification of the fractions. Indeed, the plasma membrane marker NrtA was found also in the isolated thylakoid, indicating contamination of thylakoid by PM. *Vice versa*, CP43, a protein of Photosystem II, which is present only in the TH membrane (Zanetti *et al.*, 2010), was not revealed in our experiment in the PM fraction (Fig. 3B). Thus, the presence of *Syn*CaK in the PM cannot be due to contamination by thylakoids, while the observed band in thylakoids is most likely due to contamination by PM. A protein with approx. 45 kDa weight was also strongly recognized in the soluble fraction, indicating unspecific cross-reaction of our antibody. For this reason, our attempts to localize the protein also by electron microscopy did not give reliable results (not shown).

***Syn*CaK-less mutant is characterized by altered membrane potential and resistance to zinc**

Synechocystis sp. PCC 6803 is capable to integrate exogenous DNA into its genome (present in a dozen of copies) by homologous recombination, thus allowing targeted gene replacement. Almost the entire ORF *sll*0993, encoding the *Syn*CaK potassium channel, was substituted by a kanamycin resistance cassette (Figure 4A). Knock-out mutants were recovered after ten rounds of sub-cloning and complete segregation was verified by PCR on purified genomic DNA. Sites of insertion of the Kan^R cassette and correctness of flanking regions (ORFs *sll*0994 and *slr*1022) were verified by sequencing the products of amplification. Fig. 4B shows that,

according to PCR analyses, no wild-type DNA molecules were retained in the final clones In accordance, the absence of the 41 kDa band in the mutant confirmed the lack of *Syn*CaK protein expression (Fig. 4C). Therefore the produced mutant was suitable for further studies to evaluate the physiological role played by *Syn*CaK in this photosynthetic organism.

In most microorganisms, high affinity K^+ uptake occurs through ATP-dependent transport systems and indeed in *Synechocystis* the KtrB transporter was shown to prevalently mediate K^+ uptake (Matsuda *et al.*, 2006). However, at higher concentrations of K^+, uptake could *a priori* be mediated through K^+-selective channels due to the very negative membrane potential (about -200 mV). In fact, KirBac6.1 has recently been proposed to contribute to such low affinity K^+ uptake in *Synechocystis* (Paynter *et al.*, 2010) In the case of *Syn*CaK, no significant difference could be observed in the potassium content between wild-type and Δ*Syn*CaK organism, as determined by atomic absorption spectroscopy, indicating that the channel does not normally contribute to K^+ uptake (Fig. S5). Next, we checked whether growth deficiency could be observed in the mutant with respect to wild-type under various conditions, typically used to characterize cyanobacterial transporter mutants, including increasing light intensity (Fig. S6), salt stress at 100 mM KCl, osmotic stress with 0.5 M sorbitol, lack of glucose, alkaline external pH (pH 10) and 10 mM calcium in the growth medium (Fig. S7). None of these conditions evidenced any significant difference in growth, indicating that this channel is not involved in protection against osmotic and alkaline stress and is not indispensable for phototrophic growth. Involvement of the channel in the regulation of photosynthesis was further excluded by analysis of chlorophyll fluorescence using PAM. No differences in Fv/Fm (variable fluorescence/ maximal fluorescence) were revealed between wild-type and mutant organisms indicating that photosynthetic efficiency was not dependent on the presence of the channel (not shown).

Proton pumping and sodium-motive force are crucial in determining the resting membrane potential in bacteria, but K^+ gradient across the cell membrane is also expected to contribute to membrane potential, since intracellular K^+ is rather high (from 200 and 700 mM depending on species). At the very negative membrane potential in bacteria, a strong driving force allows flux of potassium ions through channels. Given the very small capacitance of the cytoplasmic membrane of bacterial cells, only a very small number of ions flowing through an ion channel would be sufficient to cause a substantial change in the resting membrane potential (Martinac *et al.*, 2008). To test the hypothesis that the lack of *Syn*CaK might alter the membrane potential, we used the ratiometric fluorescent cyanine dye 5,59,6,69-tetrachloro-1,19,3,39-tetraethylbenzimidazolocarbocyanine iodide (JC-1), efficiently exploited to measure very negative membrane potentials in mitochondria and bacteria (Novo *et al.*, 1999). JC-1 is a cationic dye that exhibit potential-dependent accumulation in bacteria, indicated by a fluorescence emission shift from green (~525 nm) under blue light excitation, to red (~590 nm) under green light excitation. Consequently, membrane depolarization is indicated by a decrease in the red/green fluorescence intensity ratio. The potential-sensitive color shift is due to concentration dependent formation of red fluorescent J-aggregates. Our measurements, shown in Fig. 5, suggest that the ratio between green versus red forms of the dye is significantly different between wild-type and mutant cells, indicating a depolarized membrane potential in the mutants. The ratio of green to red fluorescence is dependent only on the membrane potential and not on other factors such as size, shape, and density that may influence single-component fluorescence signals (see JC-1 data sheet of Invitrogen). The use of fluorescence JC-1 ratio detection therefore allowed us to make comparative measurements of membrane potential. The exact extent of depolarization cannot be estimated by any of the currently used methodologies to our knowledge.

According to the current hypotheses, most microbial channels might be called to function upon peculiar environmental stresses. Zn is an essential metal but is toxic at high concentrations. Zrt-Irt-like proteins (ZIPs) represent a major route for entry of zinc ions into prokaryotic cells and a recent work demonstrated that bacterial ZIP is a selective electro-diffusional channel (Lin *et al.*, 2010)). Thus, ZIPB facilitates passive zinc uptake driven by zinc concentration gradients and electrical driving force. Instead, ZitB was proposed to act as an efflux pump, since its overexpression increased zinc tolerance and reduced zinc uptake in *E. coli* (Grass *et al*., 2001). ZitB function depends on K^+ and H^+ fluxes (Guffanti *et al*., 2002) and indeed this molecule was identified as Zn^{2+}/H^+ antiporter (Chao and Fu, 2004). In light of these reports, we tested whether the *Syn*CaK strain, having a decreased membrane potential might become more resistant to zinc. The concentrations tested were in the range of the EC_{50} for the acute toxicity of Zn^{2+} in the cyanobacteria *Anabena* (Barran-Berdon *et al.*, 2010). Results of Fig. 6A demonstrate that increasing concentration of Zinc compromised growth of the wild-type cyanobacteria, in accordance with results of toxicology studies (Zeng and Wang, 2011). *Syn*CaK-less organisms were more resistant with respect to wild-type cells. Resistance to Zn^{2+} was observed also in cells cultured in liquid medium for two independent *Syn*CaK-less mutant clones, confirming that the phenotype is indeed related to the lack of the channel (Fig. 6B).

DISCUSSION

In the present work we have identified a new putative channel in the genome of *Synechocystis*, demonstrated that it functions as potassium channel, constructed a knock-out strain and identified a growth condition under which the mutant shows a clear phenotype. Our results suggest that *Syn*CaK might be involved in the regulation of membrane potential in cyanobacteria and its lack confers an increased resistance to Zn^{2+}, an environmental pollutant. A function related to ion homeostasis has been elucidated only in the case of very few bacterial ion channels. Mechanosensitive channels serve for fast release of osmolytes and ions in bacteria challenged with osmotic stress (e.g. Berrier *et al.*, 1992; Martinac *et al.*, 2008) and MscL was proposed to mediate also calcium efflux in cyanobacteria (Nazarenko *et al.*, 2003). The bacterial ClC are implicated in proton equilibrium maintenance (Iyer *et al.*, 2002), Kch K^+ channel of *Helicobacter pylori* has been shown to play an essential role for the ability of this organism to colonize the murine gut and to play an important role in K^+ uptake at low [K^+] (Stringl *et al.*, 2007). In a recent study, a K^+-dependent slight growth defect was observed when the cyanobacterial homologue of KirBac6.1 was deleted from *Synechocystis,* suggesting that KirBac might contribute to low affinity uptake of K^+ (Paynter *et al.*, 2010). A cyclic nucleotide-gated channel, when expressed in *E. coli*, rendered the cells sensitive to external potassium (Kuo *et al.*, 2007). Finally, a recent study from our laboratory provided genetic evidence that the voltage-dependent 6TM channel *Syn*K, located in thylakoid membranes in *Synechocystis* (Zanetti *et al.*, 2010), is required for efficient photosynthesis. In particular, the lack of the channel led to an altered partitioning of the proton motive force across thylakoids between the electric and the osmotic component. As a consequence, the *Syn*K-less mutant showed high photosensitivity (Checchetto *et al.*, 2012). In summary, evidence is accumulating on the physiological role of bacterial ion channels. Furthermore, in some cases, evolutionary conserved channels play a role in ion homeostasis in higher organisms as well. For example, mechanosensitive channel homologs in plastids have recently been shown to protect these organelles from hypoosmotic stress (Veley *et al.*, 2012). As to *Syn*CaK, it shows the highest

homology among all potassium channels in *Arabidopsis* to *At*TPK1, a two-pore potassium channel (e value: 8e-06, sequence identity: 35%). This latter channel, although having chloroplast targeting sequence, is located in the vacuolar membrane, where it has a role in intracellular K^+ homeostasis, thereby affecting seedling growth at different K^+ levels (Gobert *et al.*, 2007). The homology to the PM-targeted *At*TPK4 is also considerable (e value: 7e-06, identity: 35%). Interestingly, *Syn*CaK shows 43% identity (with an e value of 2e-04) to two putative TPK channels from *Zea mays*. *Syn*CaK, a 2 TM protein might *a priori* be the precursor of these higher plant 4TM TPK channels, however the localization of these proteins within the plant cells is not fully consistent with this idea. Whether the putative homologs of *Syn*CaK in *Arabidopsis* indirectly contribute to Zn^{2+} homeostasis also in plants is an open question and might worth future investigation.

As to the channel activity of *Syn*CaK, it resembles some of the properties of *Mt*hK, a calcium-dependent potassium channel. In particular, *Mt*hK has been shown to function also at low calcium concentration but its open probability sharply increased upon addition of calcium up to 25 mM in bilayer experiments to the internal side (Jiang *et al.*, 2002). In accordance, Zadek and colleagues observed activation by calcium in the millimolar range. In the case of *Syn*CaK, we also find an increased activity when augmenting the intracellular concentration to 10 mM calcium in inside-out excised patches. The properties of the channel could not be studied in the whole-cell configuration given that cells cannot withstand such a high intracellular calcium concentration. The conductance of the *Mt*hK channel was 200 pS in 150 mM KCl at -100 mV when reconstituted into an artificial bilayer (Jiang *et al.*, 2002). In another report, the chord conductance was 240 pS at -200 mV in 200 mM KCl (Zadek and Nimigaen, 2006). In both reports a strong rectification was observed, probably due to a fast block by calcium or to an electrostatic screening effect. However, when expressed in *E. coli* cytoplasmic membrane, *Mt*hK displayed an inward rectification and approximately 50 pS conductance in 150 mM KCl (Kuo *et al.*, 2007). *Syn*CaK, when expressed in CHO cells, displays a slight rectification and 45pS conductance at positive voltages. The reason for the lack of strong rectification is not clear. *Mt*hK was shown to be inhibited by Charybdotoxin (ChTx) (e.g. Jiang *et al.*, 2002; Zadek and Nimigaen, 2006). ChTx inhibit activity by binding to the pore region of the channel which faces the extracellular solution (in our experimental set-up facing the pipette). A more detailed electrophysiological/pharmacological characterization is beyond the scope of the present manuscript which aimed at defining the physiological function of such channel. In any case, we show that the overall behavior of *Syn*CaK is compatible with this protein being a calcium activated potassium-selective channel.

Cyanobacteria are the most abundant photosynthetic organisms on Earth. They share a wide range of genes in common with plants, since they are the likely ancestor of chloroplast according to the endosymbiontic hypothesis. Thus, information about stress responses in cyanobacteria might also facilitate to understand how plant cells cope with environmental challenges. Zn^{2+} has been reported to be toxic to plants as well and might impair photosynthesis (Sagardoy *et al.*, 2010), although Zn^{2+} uptake systems in the chloroplasts have not been identified (Nouet *et al.*, 2011). In general, photosynthetic organisms are increasingly challenged by heavy metals, which cannot be degraded. In this respect it is interesting to note that cyanobacteria are also suitable for biosensor and/or bioremediation applications. In the case of *Syn*CaK-less mutant, our tentative explanation for its increased resistance to Zinc derives from the observed depolarized cytoplasmic potential, which in turn can cause a decreased electrical gradient for Zn^{2+} uptake and might instead favor Zn^{2+} efflux. However, our results do not exclude other possible explanations. Unfortunately, the exact mechanisms leading to Zn^{2+} resistance in cyanobacteria are still not completely understood and both

decreased (Zeng and Wang, 2011) or increased Zn^{2+} accumulation/compartmentalization have been proposed to lead to resistance toward this heavy metal. In any case, active regulation of Zn^{2+} transport rather than genetic adaptation has been proposed to be the most important mechanism for Zn^{2+} detoxification (Zang *et al*., 2009). Earlier studies showed that metal efflux was an important mechanism to regulate the intracellular metal content in bacteria (Hassler *et al*., 2005; Nies, 2003). Furthermore, the internal metals were found to be partitioned in different subcellular compartments and to be sequestered by metallothioneins (Turner and Robinson, 1995), which may affect the tolerance capability (Wang and Rainbow, 2004; Wang and Wang, 2008). Our attempts to reveal a large difference in Zn^{2+} content as determined by atomic absorption spectroscopy were unsuccessful (not shown), The situation is further complicated by the fact that our knowledge on the physiological function of potassium channels in bacteria is very limited, so it cannot be excluded that they have an impact e.g. on signaling pathways, on enzyme activity, on redox state and on proliferation, similarly to animal cells. Thus, the lack of *Syn*CaK may impact on Zn^{2+} homeostasis by a more indirect way. In conclusion, further advance in the field is necessary to understand the exact mechanism by which *Syn*CaK regulates tolerance to Zn^{2+}.
In summary, our work demonstrates that *Syn*CaK works as potassium channel, in accordance with the bioinformatic predictions. Furthermore, we highlight the role of *Syn*CaK in regulating membrane potential, a hypothesis forwarded long ago concerning the function of prokaryotic potassium channels but, to our knowledge not proved by far by genetic means. *Syn*CaK, although contributing to the maintenance of membrane potential, does not compromise survival of Cyanobacteria and apparently is not involved in protection from various stresses.

MATERIALS AND METHODS

Construction of p*Syn*CaK-EGFP vectors

The *Syn*CaK gene was amplified by PCR from genomic DNA and cloned into pEGFP-N1 vector (Clontech). Primers were designed to introduce a *Hind*III site at the initiation codon and a *BamH*I site abolishing the stop codon, so that the gene could be expressed as fusions to the N-terminus of EGFP (*Syn*CaK::EGFP). The *Hind*III-*BamH*I restriction fragment of PCR product was introduced into the pEGFP-N1 multiple cloning site, to give plasmid p*Syn*CaK-EGFP. The single point mutation F68A was obtained by using the QuikChange II Site Directed Mutagenesis Kit (Stratagene), to obtain plasmid pF68A*Syn*CaK*::*EGFP. The recombinant construct was then verified by DNA sequencing. The wild-type and mutant fusion proteins *Syn*CaK-EGFP were expressed in Chinese Hamster Ovary (CHO) cells and used in electrophysiological analysis, the mutant form being used as negative control.

CHO cell culture and transfection

CHO cells were maintained at 37°C, 5% CO_2 in culture medium (DMEM, 10% fetal bovine serum, 1% penicillin/streptomycin and 1% non-essential amino acids). Cells were treated by standard trypsinization at 70-80% confluence. Culture medium was changed every 2 or 3 days to maintain good growth condition. One day prior to transfection, the cells were trypsinized and counted; confluent layers of cells were grown on coverslips and were transiently transfected with lipofectamine 2000 (Invitrogen) according to the manufacturer's instructions. Cells were transfected with 0,5 μg of DNA.

Confocal microscopy
After transfection (48 hours), CHO cells were incubated with FM® 4-64 dye (Invitrogen), a dye specific for plasma membrane, and analyzed using a Nikon PCM2000 (Bio-Rad, Germany) confocal microscope. We prepared a working staining solution of 5 µg/mL dye in ice-cold HBSS (Invitrogen). The coverslip with the cells was washed once in HBSS and immersed in the ice-cold staining solution for 30 seconds. After removal from the staining solution, cells were then mounted on glass slides and observed with a laser-scanning confocal microscope. Fluorescence filters set was: excitation 488 nm for EGFP and 543 nm for FM 4-64; emission 515/530 for EGFP and 570 long pass for FM 4-64. Observations were made with a Plan Apo 63X oil immersion objective with a numerical aperture of 1.4. Image analysis was done with the ImageJ bundle software (http://rsb.info.nih.gov/ij/).

Patch clamp analysis
Patch clamp experiments were performed in inside-out patch configuration on control or transfected CHO cells as previously described (Szabò *et al.*, 2000). Bath solution: 150 mM K gluconate, 10 mM KCl, 2 mM $CaCl_2$, 10 mM HEPES, pH 7.2 if not otherwise specified. Pipette solution: 150 mM Na-gluconate, 1 mM $CaCl_2$, and 10 mM HEPES, pH 7.2. Transmembrane voltages were applied and currents were monitored using an EPC-7 amplifier (HEKA-List). Pulse protocol was applied and data analysis was performed using the pClamp8 program set (Axon). The pipette resistance was 2-5 MegaOhm. Data were low pass-filtered with an eight-pole Bessel filter with a cut-off frequency of 0.5 kHz and analyzed off-line.

Production of anti-*Syn*Cak antibody
Anti-*Syn*CaK antibody was produced against the synthetic peptide EQKVIERLADHYILC, corresponding to a specific sequence of *Syn*CaK, by Agrisera (Sweden).

Cyanobacterial strains and growth conditions and isolation of plasma membrane, soluble and thylakoid membrane fractions from *Synechocystis*
Strains were cultured in BG11 medium (Ono & Murata, 1982) supplemented with 20 mM TES-KOH (pH 8.2) (referred to as BG11). The mutant strain grows in BG11 containing 50 µg/ml kanamycin at 30°C under continuous illumination (20 µmol m^{-2} s^{-1} photons) with rotary shaking. Growth on agar plate was obtained under the indicated conditions. Cyanobacteria cells were fractionated as described in Zanetti *et al.*, (2010).

Determination of chlorophyll and protein concentration
Pigments were extracted with 100% (v/v) methanol (Lichtenthaler, 1987). The extracts were mixed, and the concentration of *chlorophyll a* was measured according to the method described by MacKinney (1941). Total protein concentration was determined by the bicinchoninic acid (BCA) protein assay.

SDS-polyacrylamide electrophoresis (SDS-PAGE) and Western blotting
The electrophoretic separation of proteins in denaturing polyacrylamide gels was carried out as previously described (Bergantino *et al.*, 2003). For immunodetection, proteins were transferred onto a PVFD membrane. The membranes were incubated with diluted primary antibody (1:2500 for *Syn*CaK, 1:2000 for anti-His_6 TAG) in blocking solution for 2 hours at RT. HRP-conjugated goat anti-rabbit antibody was used as secondary antibody. Proteins were visualized with ECL Western Blot Detection Kit (Pierce).

Expression in *E. coli*

*Syn*CaK gene was amplified by PCR and cloned into pEGFP-N1 vector (Clontech). This construct was used as template in two separate PCRs with primers C-G_FOR (5'-ATTAATTGTGGGCCCGATGGGG-3') and pEGFP_Crick (5'-GACACGCTGAACTTGTGG-3'), or pEGFP_Watson (5'-TGTACGGTGGGAGGTCTA-3') and C-G_ REV (5'-CCCCATCGGGCCCACAATTAAT-3'), and high fidelity polymerase (Finnzyme). A following overlapping PCR was performed using VC7 (5'- CGAGCTCAAGCCCATGGGATTGG-3', inserting a *Nco*I site) and CV8 (5'-GACCGGTGGCTCGAGATGGTTTTT-3', inserting a *Xho*I site) and both previous amplimers as template. The PCR product and the expression plasmid pET28a(+) were digested with *Nco*I and *Xho*I, and ligated with T4 ligase. The resulting clone pET28a(+)-*Syn*CaK was subjected to DNA sequencing and espressed in C41(DE3) cells (Miroux and Walker, 1996). For protein expression, 1 mL pre-culture from one freshly transformed colony was grown overnight and used to inoculate 25 mL LB medium containing 50 µg/mL kanamycin at 37°C. Culture was grown under continuous shaking to A_{600} = 1, expression was induced by 0.7 mM IPTG, then culture was divided and further grown for 24 hours. Aliquots of cells equal to A_{600} = 1 were harvested at different times for each culture. Samples were centrifuged at 14000 *g* for 3 minutes, recovered pellets were solubilized in Laemmli loading buffer (Laemmli, 1970). Yield of expression was evaluated by Western blot using specific antibodies: anti-His_6 TAG (SIGMA) and anti-*Syn*CaK (Agrisera).

Determination of potassium concentration in cell extracts and culture medium

K^+ concentration was determined by atomic absorption spectroscopy with a model Analyst 100 spectrophotometer (PerkinElmer Life), in using an acetylene/air burner for flame analyses. Cell suspensions of 50 mL were centrifuged (5000 rpm, 10 minutes). The pellet was resuspended in a final volume of 2 ml with water and then treated with 1 ml of nitric acid overnight at 80°C. After the incubation, the potassium concentration was measured. The amount of K^+ was normalized to the chlorophyll concentration of the respective cultures.

Production of a *Syn*CaK-less *Synechocystis* mutant

Forward VC9 (5'-GGGCTGTCCATCGCTGTCGGGGT-3') and reverse CV10 (5'-ACGCCCCCGGCCAGACCCTT-3') primers were used to generate a PCR product including the part of the sll0994, the sll0993 and the slr1022 open reading frames. The *Sma*I_FOR (5'-TGGGCGATCGCCCGGGAAGCAAG-3') and *Sma*I_REV (5'-TGGCGGTGAGAATCCCGGGCTGTTCGAG-3') nested primers, both introducing a restriction site *Sma*I, were used in combination with primers Mut22_REV (5'-TGGGATTGGGATCCCATGGGGGACACCCATT-3') and Mut33_FOR (5'-CCCCCATGGGATCCCAATCCCATCCTAAA-3') with the VC9/CV10 amplimer as template in two separate amplifications, generating two PCR products (604 and 619 bp long respectively). Oligonucleotides Mut22_REV and Mut33_FOR had been projected with overlapping 5' extension containing a *Bam*HI restriction site. The two fragments were purified from agarose gel and used together as template in an amplification with primers *Sma*I_FOR and *Sma*I_REV. The single, 1202 bp long, obtained fragment was introduced in the pGEM®-T Easy vector (Promega). A kanamycin-resistance cassette (Kan^R), derived by *Bam*HI digestion from plasmid pUC4K, was cloned into the unique *Bam*Hi site of the latter plasmid, to give the final plasmid p*Syn*CaKKO_20. In the new plasmid, the entire insert was completely sequenced to verify that no undesired mutation had been introduced. Lastly, the new plasmid was used to transform wild-type *Synechocystis* sp. PCC 6803 (Zang, Liu, Liu, Arunakumara, and Zhang, 2007). Transformants were selected by screening for antibiotic-resistance on BG11 plates

containing 10 μg/mL kanamycin. After repeated subcloning steps, complete segregation of recombinant chromosomes in mutant strain was tested by PCR with primers: VC9, CV10, DISP2-rev (5'-ATAAATGGGCTCGCGATAATGTCGG-3') and DISP3-for (5'-CCGTCAAGTCAGCGTAATGCTCTGC-3').

Membrane potential analysis in *Synechocystis*

The dye JC-1 (5,5',6,6'-tetrachloro-1,1',3,3'-tetraethylbenzimidazolcarbocyanine iodide; Molecular Probes, Germany) was used to label cyanobacteria in transmembrane potential dependent manner. A stock solution of JC-1 was prepared at a concentration 1.5 mM in dimethyl sulfoxide (Sigma) and stored at -20°C. Fresh staining solution (7.5 □M) was prepared each time before application by diluting the stock solution in a buffer containing 1 mM $CaCl_2$, 1 mM $MgCl_2$, and 10 mM N-(2-hydroxyethyl) piperazine-N'-(2-ethanesulfonic acid) (HEPES) at pH 7.2 (Simeonova *et al.*, 2004) and added 1:1 to suspension cultured cyanobacteria (OD_{600} = 0.5). After 10 minutes of incubation in the dark the cells were imaged by using a Leica LCS-SP5 confocal microscopy (Leica Microsystems, Heidelberg, Germany). Observations were made with a Plan Apo 63X oil immersion objective with a numerical aperture of 1.4. The filters set was: for the green fluorescent monomers, excitation at 488 nm and emission at 515/545 nm; for the red fluorescent J-aggregates, excitation at 543 nm and emission at 560/590nm; the chlorophyll was detected at 680/720 nm. In order to eliminate the bleed through of the chlorophyll signal into the green emission range, we imaged the cells in sequential mode, using one laser at a time. The laser power was 30% for the 488 nm line and 70% for the 543 nm line. ImageJ software was used to analyse the fluorescence of the dye. ROIs (Region Of Interest) of the same shape and area have been used.

FIGURE LEGENDS

Figure 1. Predicted primary structure of *Syn*CaK.

ClustalW alignment of *Syn*CaK amino acid sequence (accession number NP_440478) with that of potassium channel protein *Mt*hK of *Methanobacterium thermoautotrophicum* (accession number O27564). The highly conserved selectivity filter of potassium channels (TXXTGFGE) is highlighted with a box.

Figure 2. *Syn*CaK functions as a potassium channel when expressed in CHO cells.

A) Representative current traces recorded under symmetrical ionic conditions (150 mM K gluconate on both sides, plus 2 mM $CaCl_2$ in the bath) in the inside-out excised patch configuration. The voltage ramp protocol shown in the upper panel was used to elicit channel activity. Representative, two consecutive current traces are shown. The lower panel shows activity recorded at -170 mV on an extended time scale. Under these conditions reversal potential is at 0 mV. **B)** Upper panel: Representative current trace recorded under asymmetrical ionic conditions (150 mM K gluconate solution with 2 mM $CaCl_2$ in the bath, 150 mM Na gluconate solution in the pipette). Middle panel: current recording on extended time scale from the indicated part of the upper panel. Lower panel: Representative trace recorded under the same ionic condition from CHO cells transfected with mutant *Syn*CaK. No activity can be recorded, the observed current is due to leak. **C)** Upper panel: Current trace recorded under the same ionic conditions except that bath, i.e. the intracellular side contained 10 mM $CaCl_2$. Lower traces show activity on extended time scale from the indicated region and at +100 mV.

Figure 3. Localization of *Syn*CaK in Cyanobacteria.
A) Plasma membrane (PM), soluble (S), thylakoid membrane (TH) and outer membrane (OM) fractions were isolated from *Synechocystis* (2 µg of proteins/lane). The channel protein was detected using anti-*Syn*CaK antibody at the expected molecular weight of 41 kDa. **B)** The purity of PM and TH fractions were checked by using antibodies against the plasma membrane marker NrtA, and the thylakoid marker CP43 (2 µg of proteins/lane).

Figure 4. Construction of a *Syn*CaK-deficient *Synechocystis* strain.
A) Schematic diagram of construction of the mutant organism. Δ*Syn*CaK was obtained by inserting a kanamycin-resistance cassette into the *Synechocystis* genome. Forward and reverse primers, introducing mutagenic sites, were used to generate a PCR product containing the *Syn*CaK gene in the central position and two flanking regions (see Experimental Procedures section for details). **B)** PCR analyses indicated lack of WT gene and correct insertion of the Kan^R gene in the mutant organism. Agarose gel electrophoresis of analytical PCR amplifications, performed on genomic DNAs from kanamycin-resistant control and Δ*Syn*CaK strains [1: Molecular Mass marker (1 Kb ladder, Promega); 2: wild-type DNA amplified with VC9 and CV10 primers; 3: Δ*Syn*CaK DNA amplified with VC9 primers: 4: wild-type DNA amplified with VC9 and DISP2 primers; 5: Δ*Syn*CaK DNA with VC9 and DISP2 primers; 6: wild-type DNA with DISP3 and CV10 primers; 7: Δ*Syn*CaK DNA with DISP3 and CV10 primers; 8: wild-type DNA amplified with DISP2 and DISP3 primers; 9: Δ*Syn*CaK DNA with DISP2 and DISP3 primers]. **C)** Western-blotting of protein extracts (0.3 OD_{730}) using the anti-*Syn*CaK antibody, showing no detection of *Syn*CaK channel (41 kDa, see arrow) in the mutant strain. Aspecific recognition of two other bands indicate equal loading.

Figure 5. Membrane potential analysis in wild-type and *Syn*CaK-deficient *Synechocystis* strain.
The JC-1 (5,5',6,6'-tetrachloro-1,1',3,3'-tetraethylbenzimidazolylcarbocyanine iodide) cationic carbocyanine dye has been used to highlight membrane potential differences between wild type and mutant *Synechocystis* strains. **A)** Confocal microscope analysis of the JC-1 fluorescence. The green fluorescence belongs to the monomer form of the dye; the red fluorescence is due to the J-aggregates that form at high dye concentration, i.e. high membrane potential; chlorophyll is pseudo-coloured in blue. Two series of images are shown for each strain. **B)** Green/red fluorescence ratio of the dye in mutants is higher than in wild-type bacteria (three independent experiments, N = 20). Difference is statistically significant ($p<0.05$).

Figure 6. *Syn*CaK-deficient *Synechocystis* strain is more resistant to Zn^{2+} than wild-type.
A) Growth of wild-type (W) and mutant (M) cells on agar BG11 medium with 5 mM glucose, at the indicated concentrations of $ZnCl_2$. Duplicates are shown. Photos were taken at day 5. Optical densities (at 730 nm) at 0 time point are indicated. At the two highest concentrations of Zn^{2+} (corresponding to 22 and 44 µM Zn^{2+}, respectively), spots obtained at 0.01 starting OD were omitted, due to lack of spots under these conditions characterized by lack of growth. Spot tests repeated other 3 times gave the same results. **B)** OD of liquid culture measured after 24 hours of growth in the absence or presence of 2 µM or 4 µM Zn^{2+} added to BG11. Values are normalized to OD under control condition.

SUPPLEMENTARY FIGURE LEGENDS

Figure S1. Bioinformatic analysis of *Syn*CaK.
A) Domains of *Syn*CaK (http://blast.ncbi.nlm.nih.gov/Blast.cgi). **B)** Hydropathy plot highlighting the presence of two predicted transmembrane domains. C) Different functional regions can be distinguished in the primary sequence: **TM1** (QELMAGAITLAGLFVVGTAWYRY); **PORE** (TLATVGFGE); **TM2** (SRLFTILLILMGLLTIGYMVN); **TrkA_N** (YILC**GYGRTG**QQIAFEFAVENIPFVVIDASPEVIIQAKLRDYAVLQGDATLDEILLAAHIERAI CIVSALSSDAENLYTVLSAKTLNPKIRAIARASSEEAVQKLKRAGADE); **GLICINE DOMAIN**, typical of TrkA N**_____(GYGRTG);_____TrkA C**_____(EEFRIGAEDCPYIGQTLREAQLRA QSGALILAIRRQDRKLIVGPMGDTHLLDADS LICLGTVEQL RALNQL).

Figure S2. Expression of *Syn*CaK in CHO cells.
*Syn*CaK-EGFP fusion expression in CHO cell plasma membrane as revealed by confocal microscopy. Co-localization of fusion proteins and plasma membrane-specific dye, FM 4-64 was observed. Overlapping is indicated by analysis of ROIs (Regions of interest). Images were analyzed using ImageJ (http://rsb.info.nih.gov/ij/index.html), in green EGFP and in red the PM dye. Representative images are shown.

Figure S3. Expression of single point pore mutant of *Syn*CaK in CHO cells.
As in Fig. S2.

Figure S4. Anti-*Syn*CaK specifically recognizes *Syn*CaK protein expressed in CD41(DE3) *E. coli* cells.
Induction at T = 0 with 0.7 mM IPTG. **(A)** PVDF membrane decorated with His tag antibody (1:2000), **(B)** PVDF membrane decorated with *Syn*CaK antibody (1:2500). Control cells were transformed using the empty pET28a vector. T, whole cells; P, pellet; S, supernatant fractions.

Figure S5. wild-type and mutant organisms do not differ in potassium content.
The potassium concentration was determined by atomic absorption spectroscopy. The amount of K^+ was normalized to the chlorophyll concentration of the respective cultures.

Figure S6. Growth of mutant cells is not altered at various light intensities.
Growth of wild-type and *Syn*CaK-less cells were grown on solid BG11 medium supplemented with 5 mM glucose (except when indicated No Glc: without glucose) at the indicated light intensities. Photos were taken at day 4. The experiment was repeated other two times giving similar results.

Figure S7. Growth of mutant cells is not altered under osmotic and salt stress.
Results are shown as in Fig. S6.

REFERENCES

Barrán-Berdón A.L., Rodea-Palomares I., Leganés F., Fernández-Piñas F. (2011) Free Ca^{2+} as an early intracellular biomarker of exposure of Cyanobacteria to environmental pollution. *Anal. Bioanal. Chem. 400, 1015-1029*

Bergantino E., Segalla A., Brunetta A., Teardo E., Rigoni F., Giacometti G.M., Szabò I. (2003) Light- and pH-dependent structural changes in the PsbS subunit of photosystem II. *Proc. Natl. Acad. Sci. USA 100, 15265-15270*

Berrier C., Coulombe A., Szabo I., Zoratti M., Ghazi A. (1992) Gadolinium ion inhibits loss of metabolites induced by osmotic shock and large stretch-activated channels in bacteria. *Eur. J. Biochem. 206, 559-565*

Checchetto V., Segalla A., Allorent G., La Rocca N., Leanza L., Giacometti G.M., Uozumi N., Finazzi G., Bergantino E., Szabò I. (2012) Thylakoid potassium channel is required for efficient photosynthesis in Cyanobacteria. *Proc. Natl. Acad. Sci. USA 109, 11043-11048*

Durell S.R., Hao Y., Nakamura T., Bakker E.P., Guy H.R. (1999) Evolutionary relationship between K^+ channels and symporters. *Biophysical. J. 77, 775-788*

Gobert A., Isayenkov S., Voelker C., Czempinski K., Maathuis F.J. (2007) The two-pore channel TPK1 gene encodes the vacuolar K^+ conductance and plays a role in K^+ homeostasis. *Proc. Natl. Acad. Sci. USA 19(104), 10726-10731*

Grass G., Fan B., Rosen B., Franke S., Nies D., Rensing C. (2001) ZitB (YbgR), a member of the cation diffusion facilitator family, is an additional zinc transporter in *Escherichia coli*. *J. Bacteriol. 183, 4664-4667*

Guffanti A., Wei Y., Rood S., Krulwich T. (2002) An antiport mechanism for a member of the cation diffusion facilitator family: divalent cations efflux in exchange for K^+ and H^+. *Mol. Microbiol. 45, 145-153*

Hassler C.S., Behra R., Wilkinson K.J. (2005) Impact of zinc acclimation on bioaccumulation and homeostasis in *Chlorella kesslerii*. *Aquatic Toxicology 74, 139-149*

Heginbotham L., Lu Z., Abramson T., MacKinnon R. (1994) Mutations in the K^+ channel signature sequence. *Biophysical J. 66, 1061-1067*

Iyer R., Iverson T.M., Accardi A., Miller C.A. (2002) Biological role for prokaryotic ClC chloride channels. *Nature 419, 715-718*

Jiang Y., Lee A., Chen J., Cadene M., Chait B.T., MacKinnon R. (2002) Crystal structure and mechanism of a calcium-gated potassium channel. *Nature 417, 515-522*

Jiang Y., Pico A., Cadene M., Chait B.T., MacKinnon R. (2001) Structure of the RCK domain from the *E. coli* K channel and demonstration of its presence in the human BK channel. *Neuron 29, 593-601*

Kuo M.M., Saimi Y., Kung C. (2003) Gain-of-function mutations indicate that *Escherichia coli* Kch forms a functional K conduit *in vivo*. *EMBO J. 22, 4049-4058*

Kuo M.M., Haynes W.J., Loukin S.H., Kung C., Saimi Y. (2005) Prokaryotic K^+ channels: from crystal structures to diversity. *FEMS Microbiol. Rev. 29, 961-985*

Kuo M.M., Saimi Y., Kung C., Choe S. (2007) Patch clamp and phenotypic analyses of a prokaryotic cyclic nucleotide-gated K^+ channel using *Escherichia coli* as a host. *J. Biol. Chem 282, 24294-24301*

Kuo M.M., Baker K.A., Wong L., Choe S. (2007) Dynamic oligomeric conversions of the cytoplasmic RCK domains mediate *Mt*hK potassium channel activity. *Proc. Natl. Acad. Sci. USA 104, 2151-2156*

Lin W., Chai J., Love J., Fu D. (2010) Selective electrodiffusion of zinc ions in a Zrt-, Irt-like protein, ZIPB. *J. Biol. Chem. 285, 39013-39020*

Martinac B., Saimi Y., Kung C. (2008) Ion channels in microbes. *Physiol. Rev. 88, 1449-1490*

Matsuda N., Uozumi N. (2006) Ktr-mediated potassium transport, a major pathway for potassium uptake, is coupled to a proton gradient across the membrane in *Synechocystis* sp. PCC 6803. *Biosci. Biotechnol. Biochem. 70, 273-275*

Nazarenko L.V., Andreev I.M., Lyukevich A.A., Pisareva T.V., Los D.A. (2003) Calcium release from Synechocystis cells induced by depolarization of the plasma membrane: MscL as an outward Ca^{2+} channel. *Microbiology 149, 1147-1153*

Nies D.H. (2003) Efflux-mediated heavy metal resistance in prokaryotes. *FEMS Microbiol. Rev. 27, 313-339*

Nouet C., Motte P., Hanikenne M. (2011) Chloroplastic and mitochondrial metal homeostasis. *Trends Plant Sci. 16, 395-404*

Novo D., Perlmutter N.G., Hunt R.H., Shapiro H.M. (1999) Accurate flow cytometric membrane potential measurement in bacteria using diethyloxacarbocyanine and a ratiometric technique. *Cytometry 35, 55-63*

Parfenova L.V., Abarca-Heidemann K., Crane B.M., Rothberg B.S. (2007) Molecular architecture and divalent cation activation of TvoK, a prokaryotic potassium channel. *J. Biol. Chem. 282, 24302-24309*

Paynter J.J., Andres-Enguix I., Fowler P.W., Tottey S., Cheng W., Enkvetchakul D., Bavro V.N., Kusakabe Y., Sansom M.S., Robinson N.J., Nichols C.G., Tucker S.J. (2012) Functional complementation and genetic deletion studies of KirBac channels: activatory mutations highlight gating-sensitive domains. *J. Biol. Chem. 285, 40754-40761*

Roosild T.P., Miller S., Booth I.R., Choe S. (2002) A mechanism of regulating transmembrane potassium flux through a ligand-mediated conformational switch. *Cell 109, 781-791*

Sagardoy R., Vázquez S., Florez-Sarasa I.D., Albacete A., Ribas-Carbó M., Flexas J., Abadía J., Morales F. (2010) Stomatal and mesophyll conductances to CO_2 are the main limitations to photosynthesis in sugar beet (*Beta vulgaris*) plants grown with excess zinc. *New Phytol. 187, 145-158*

Simeonova E., Garstka M., Kozioł-Lipińska J., Mostowska A. (2004) Monitoring the mitochondrial transmembrane potential with the JC-1 fluorochrome in programmed cell death during mesophyll leaf senescence. *Protoplasma 223, 143-153*

Stingl K., Brandt S., Uhlemann E.M., Schmid R., Altendorf K., Zeilinger C., Ecobichon C., Labigne A., Bakker E.P., De Reuse H. (2007) Channel-mediated potassium uptake in *Helicobacter pylori* is essential for gastric colonization. *EMBO J. 26, 232-241*

Szabò I., Negro A., Downey P.M., Zoratti M., Lo Schiavo F., Giacometti G.M. (2000) Temperature-dependent functional expression of a plant K^+ channel in mammalian cells. *Biochem. Biophys. Res. Commun. 274, 130-135*

Turner J.S., Robinson N.J. (1995) Cyanobacterial metallothioneins: biochemistry and molecular genetics. *Journal of Industrial Microbiology 14, 119-125*

Veley K.M., Marshburn S., Clure C.E., Haswell E.S. (2012) Mechanosensitive channels protect plastids from hypoosmotic stress during normal plant growth. *Curr. Biol. 22, 408-413*

Wang W.X., Rainbow P.S. (2004) Subcellular partitioning and the prediction of cadmium toxicity to aquatic organisms. *Environmental Chemistry 3, 395-399*

Zadek B., Nimigean C.M. (2006) Calcium-dependent gating of *Mt*hK, a prokaryotic potassium channel. *J. Gen. Physiol. 127, 673-85*

Zanetti M., Teardo E., La Rocca N., Zulkifli L., Checchetto V., Shijuku T., Sato Y., Giacometti G.M., Uozumi N., Bergantino E., Szabò I. (2010) A novel potassium channel in photosynthetic Cyanobacteria. *PLoS One 109, 11043-11048*

Zeng J., Yang L., Wang W.X. (2009) Cadmium and zinc uptake and toxicity in two strains of *Microcystis aeruginosa* predicted by metal free ion activity and intracellular concentration. *Aquatic Toxicology 91, 212-220*

Zeng J., Wang W.X. (2011) Temperature and irradiance influences on cadmium and zinc uptake and toxicity in a freshwater cyanobacterium, *Microcystis aeruginosa*. *J. Hazard Mater. 190, 922-929*

SynCaK project figures

Figure 1

```
SynCaK          MGLGSSSQENLLNLIDRQGRRLRQELMAGAI--TLAGLFVVGTAWYRYVE
MthK            MVLV-------IEIIRKHLPRVLK-VPATRILLLVLAVIIYGTAGFHFIE
                * *         :::* ::  *: : : *  *   : .::: *** ::::*

SynCaK          DWTWLDAFYMTTITLATVGFGETHPLSPASRLFTILLILMGLLTIGYMVN
MthK            GESWTVSLYWTFVTIATVGYGDYSPSTPLGMYFTVTLIVLGIGTFAVAVE
                . :*  ::* * :*:****:*:  * :* .  **: **::*: *:.  *:

SynCaK          RFTEAFIQGYFQDSLRRRQEQKVIE----RLADHYILCGYGRTGQQIAFE
MthK            RLLEFLIN---------REQMKLMGLIDVAKSRHVVICGWSESTLECLRE
                *: * :*:          *:: *::       : * ::**:..:  :   *

SynCaK          FAVENIPFVVIDASPEVIIQAKLRDYA-VLQGDATLDEILLAAHIERAIC
MthK            LRGSEV---FVLAEDENVRKKVLRSGANFVHGDPTRVSDLEKANVRGARA
                :  .::   .: *. * : :  **. * .::**.*  . *  *::. * .

SynCaK          IVSALSSDAENLYTVLSAKTLNPKIRAIARASSEEAVQKLKRAGADEVVS
MthK            VIVDLESDSETIHCILGIRKIDESVRIIAEAERYENIEQLRMAGADQVIS
                ::  *.**:*.:: :*. :.:: .:* **.*.  * :::*: ****:*:*

SynCaK          PYITGGKRLAAAALRPQVVSFVDGILTGADRSFYMEEFRIGAEDCPYIGQ
MthK            PFVISGRLMSRSIDDGYEAMFVQDVLAE-ESTRRMVEVPI-PEGSKLEGV
                *:: .*: :: :      . **:.:*:  : :  * *. * .*..   *

SynCaK          TLREAQLRAQSGALILAIRRQDRKLIVGPMGDTHLLDADSLICLGTVEQL
MthK            SVLDADIHDVTGVIIIGVGRGD-ELIIDPPRDYSFRAGDIILGIGKPEEI
                :: :*:::  :*.:*:.: * * :**:.*  *  :  .* :: :*. *::

SynCaK          RALNQLLCPLNPARVRLPKNHR
MthK            ERLKNYIS-------------A
                . *:: :.
```

Figure 2

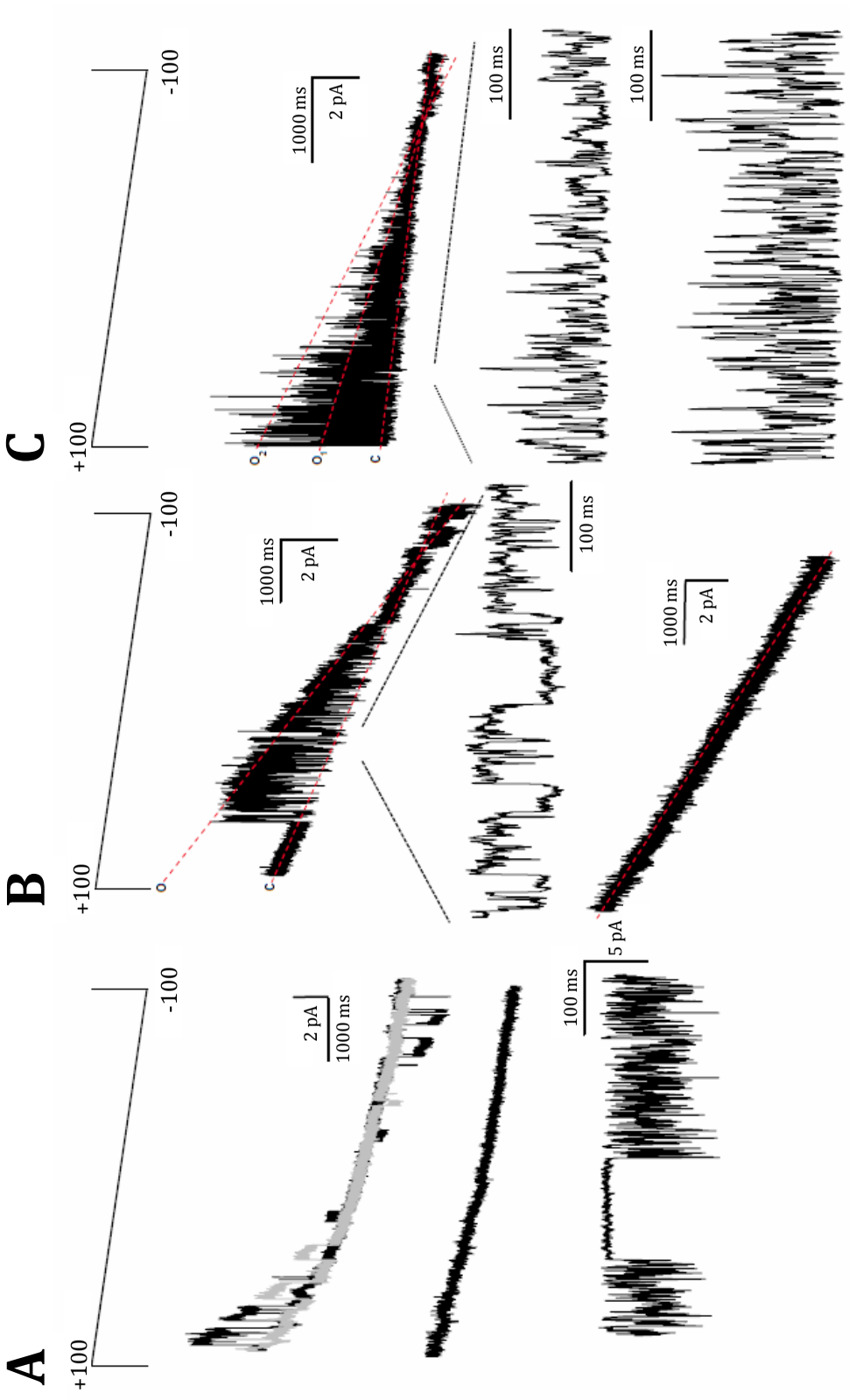

Figure 3

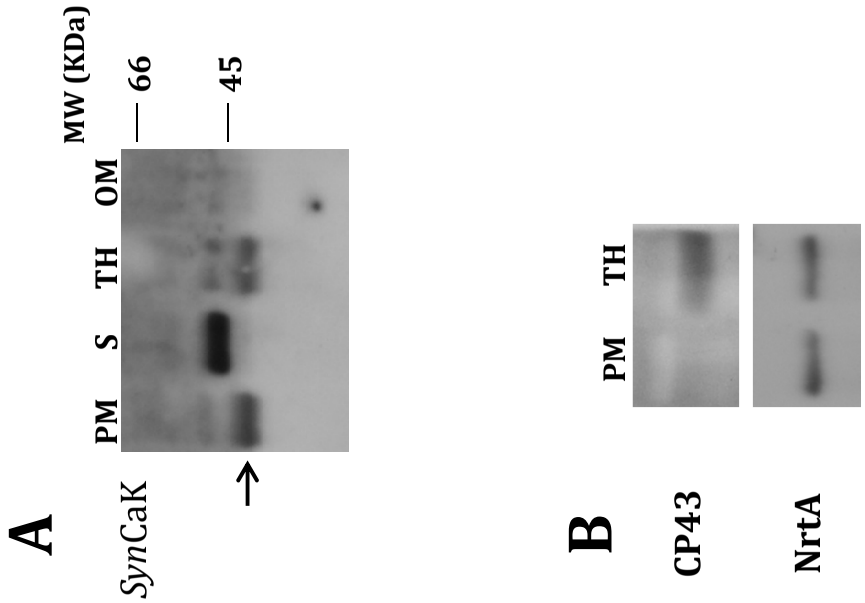

Figure 4

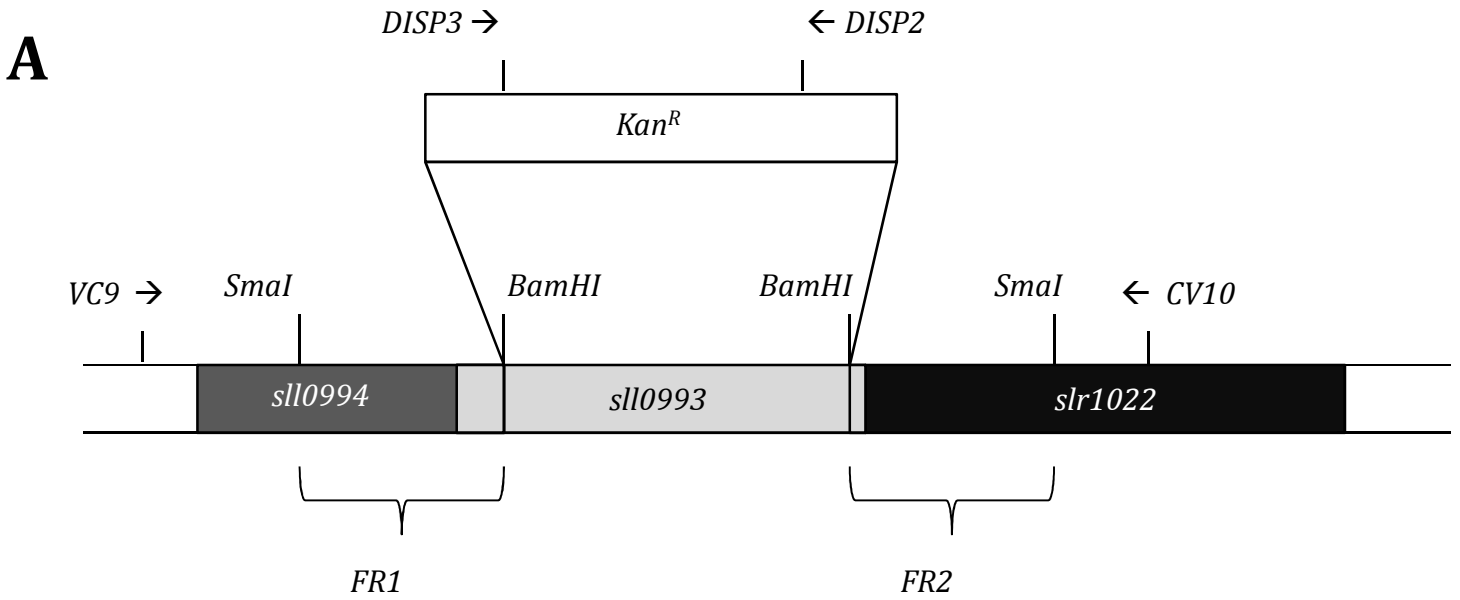
A
DISP3 →
← DISP2
Kan^R
VC9 →
SmaI
BamHI
BamHI
SmaI
← CV10
sll0994
sll0993
slr1022
FR1
FR2

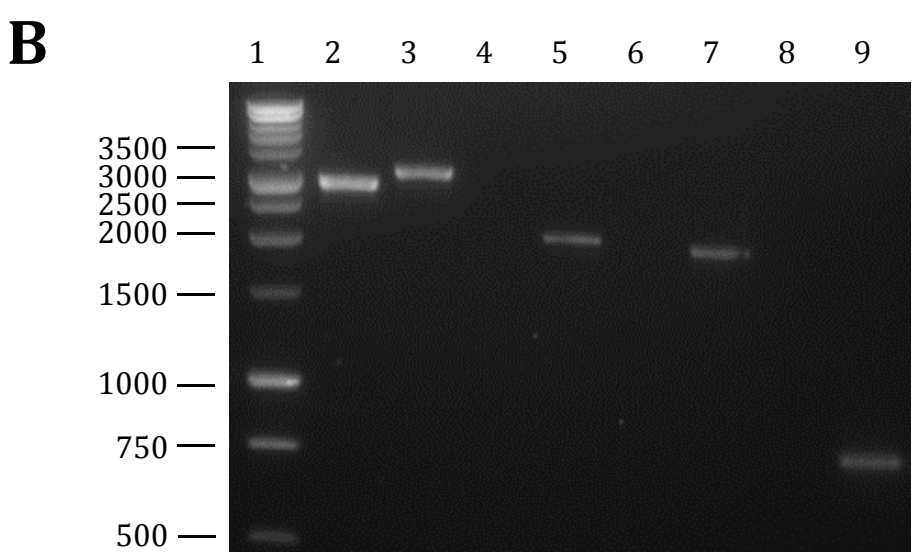
B
1 2 3 4 5 6 7 8 9
3500
3000
2500
2000
1500
1000
750
500

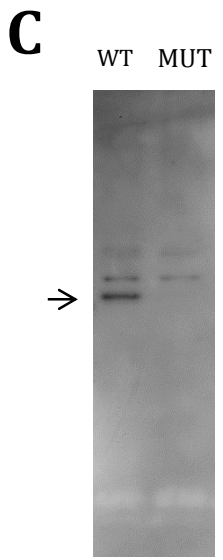
C
WT MUT

Figure 5

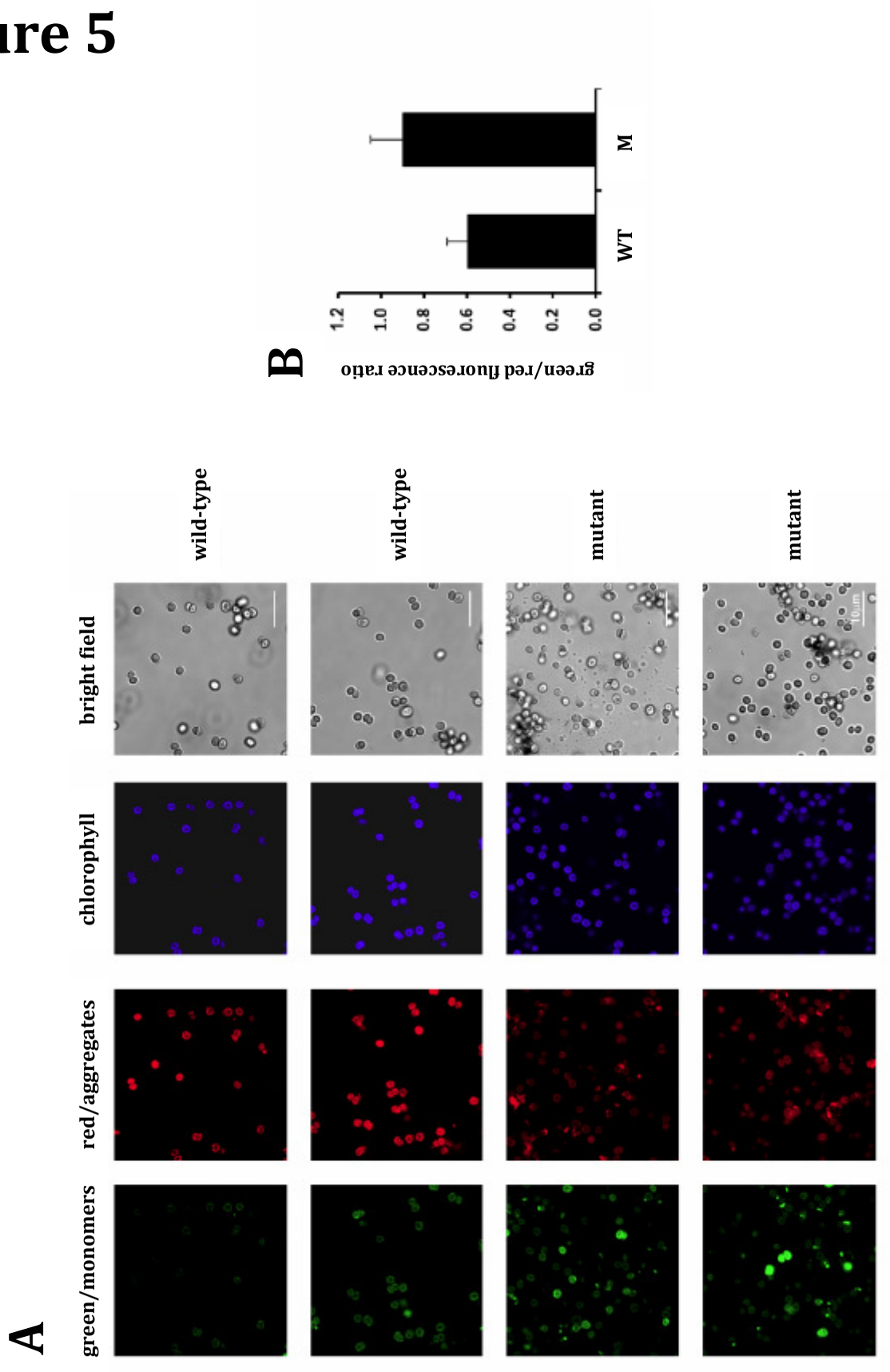
A
green/monomers
red/aggregates
chlorophyll
bright field
wild-type
wild-type
mutant
mutant
B
green/red fluorescence ratio
1.2
1.0
0.8
0.6
0.4
0.2
0.0
WT
M

Figure 6

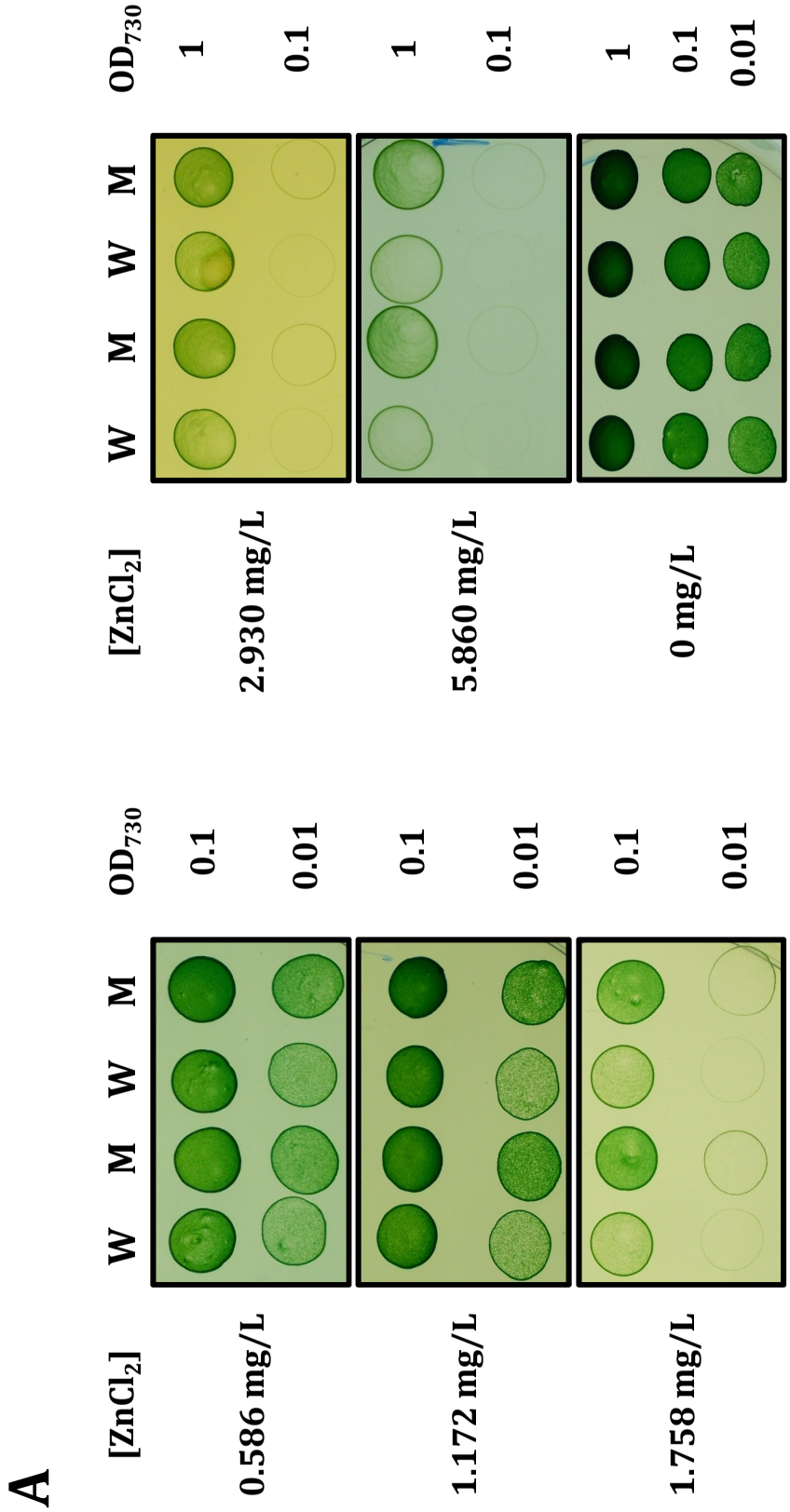
A
[ZnCl2]
OD730
W M W M
0.586 mg/L
0.1
0.01
1.172 mg/L
0.1
0.01
1.758 mg/L
0.1
0.01
[ZnCl2]
OD730
W M W M
2.930 mg/L
1
0.1
5.860 mg/L
1
0.1
0 mg/L
1
0.1
0.01

Figure 6

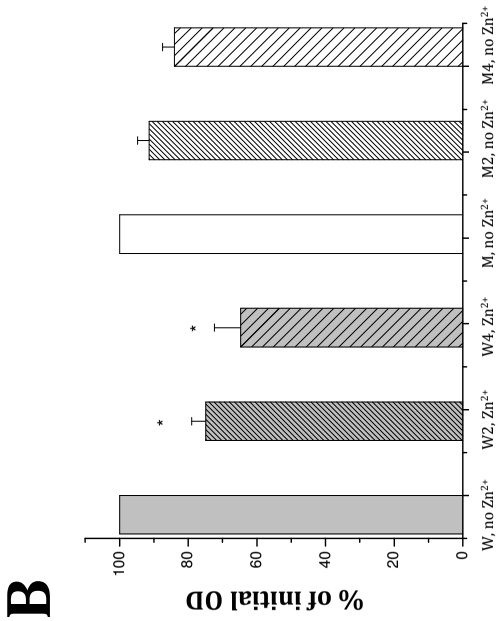
B
% of initial OD
0
20
40
60
80
100
W, no Zn2+
W2, Zn2+
W4, Zn2+
M, no Zn2+
M2, no Zn2+
M4, no Zn2+
*
*

Supplementary figures

Figure S1

A

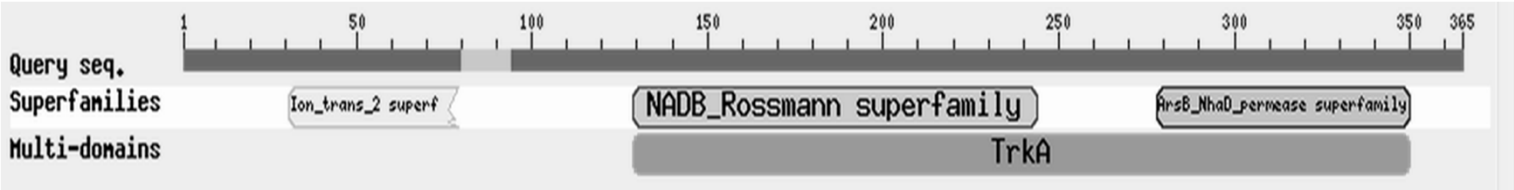

B

No.	N terminal	transmembrane region	C terminal	type	length
1	24	QELMAGAITLAGLFVVGTAWYRY	46	SECONDARY	23
2	75	SPASRLFTILLILMGLLTIGYMV	97	PRIMARY	23

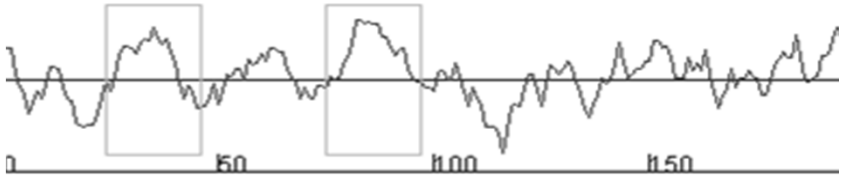

C

>gi|16329750|ref|NP_440478.1| potassium channel [*Synechocystis* sp. PCC 6803]

MGLGSSSQENLLNLIDRQGRRLRQELMAGAITLAGLFVVGTAWYRYVEDWTWLDAFYMTTI**TLATVGFGE**THPLS
PASRLFTILLILMGLLTIGYMVNRFTEAFIQGYFQDSLRRRQEQKVIERLADHYILCGYGRTGQQIAFELFAVENIPFVVI
DASPEVIQAKLRDYAVLQGDATLDEILLAAHIERAICIVSALSSDAENLYTVLSAKTLNPKIRAIARASSEEAVQKLKRA
GADEVVSPYITGGKRLAAAALRPQVVSFVDGILTGADRSFYMEEFRIGAEDCPYIGQTLREAQLRAQSGALILAIRRQD
RKLIVGPMGDTHLLDADSLICLGTVEQLRALNQLLCPLNPARVRLPKNHR

Figure S2

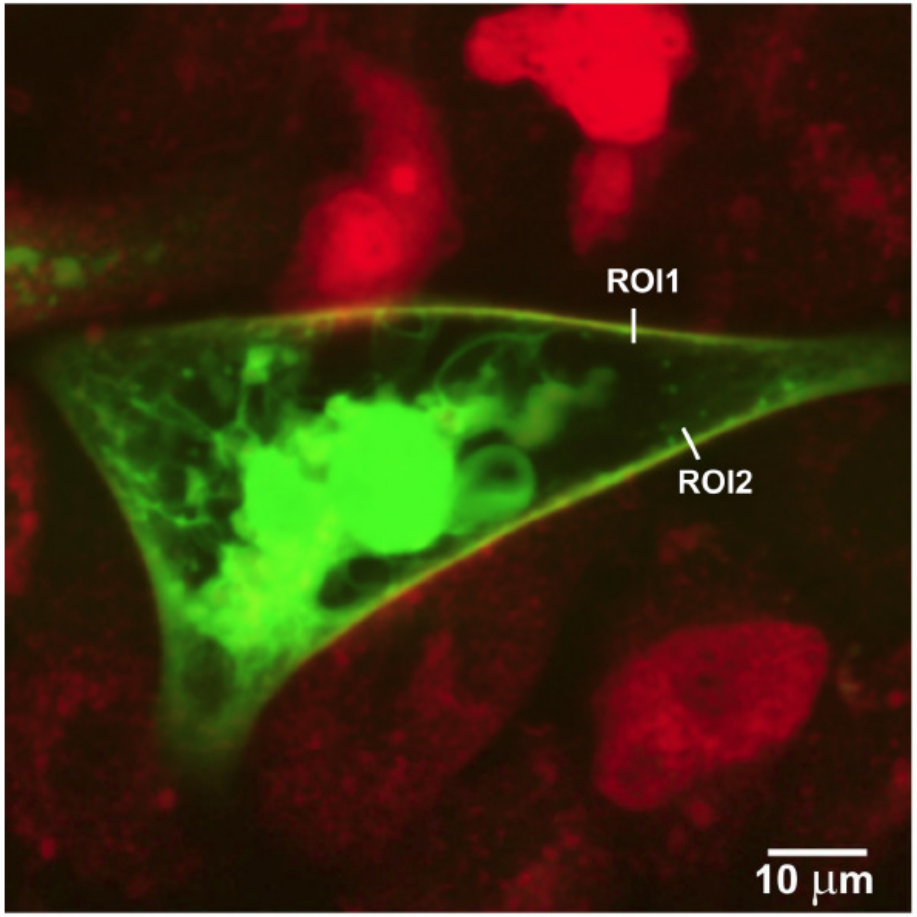
ROI1
ROI2
10 μm

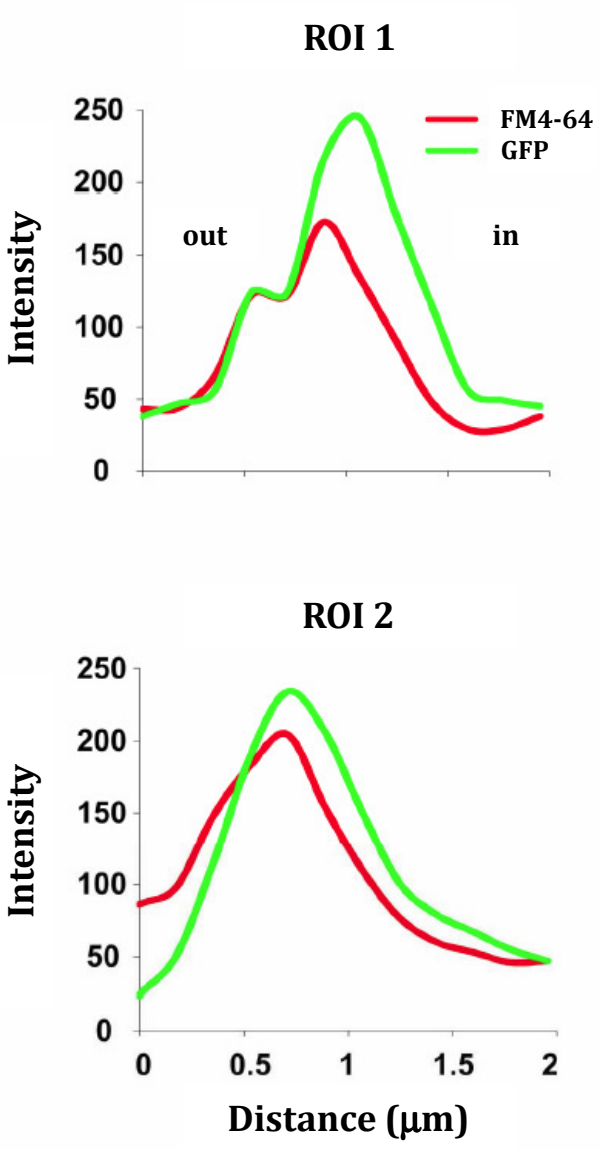
ROI 1
FM4-64
GFP
out
in
Intensity
250
200
150
100
50
0
ROI 2
Intensity
250
200
150
100
50
0
0
0.5
1
1.5
2
Distance (μm)

Figure S3

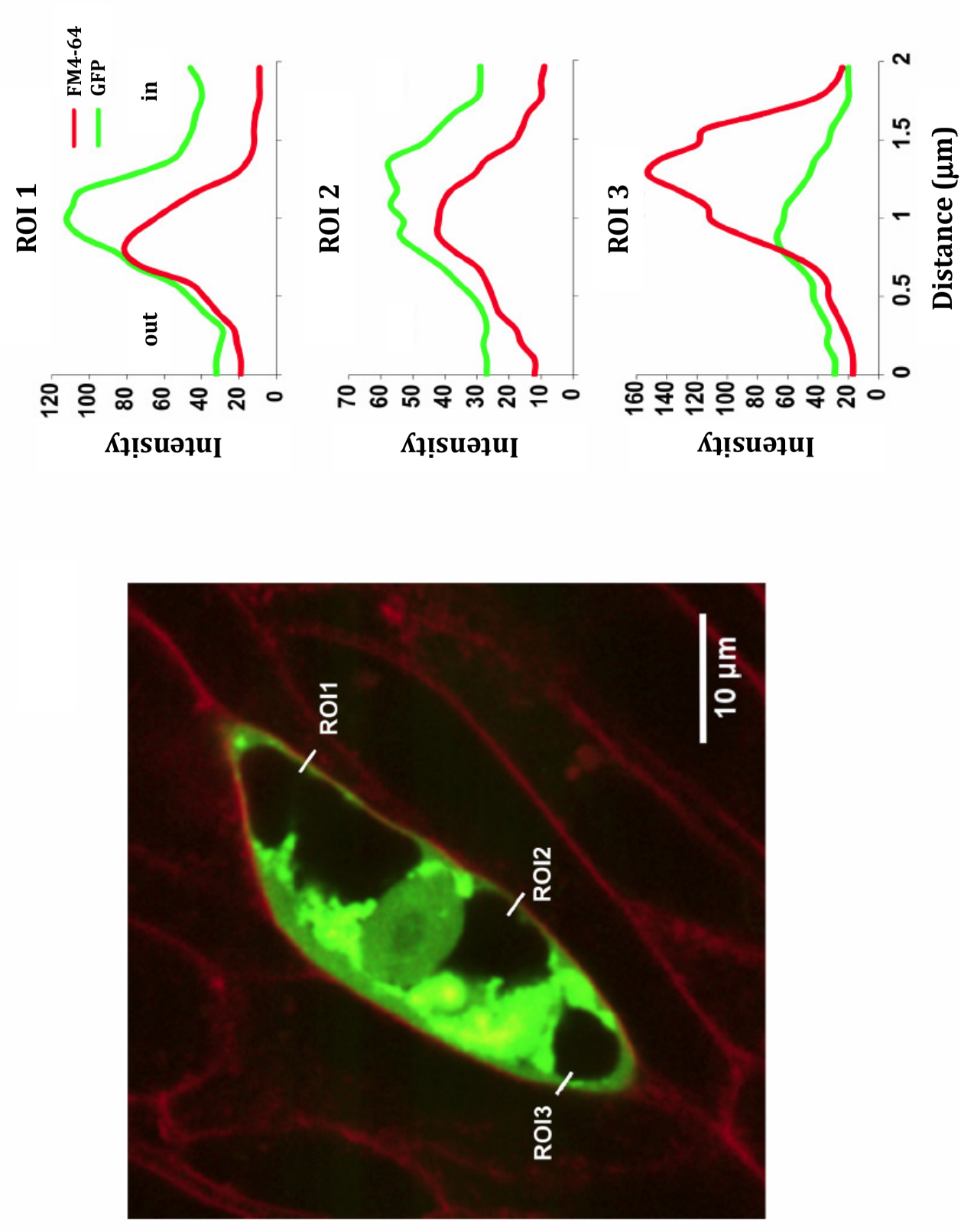
ROI 1
ROI 2
ROI 3
FM4-64
GFP
in
out
Intensity
Distance (µm)
ROI1
ROI2
ROI3
10 µm

Figure S4

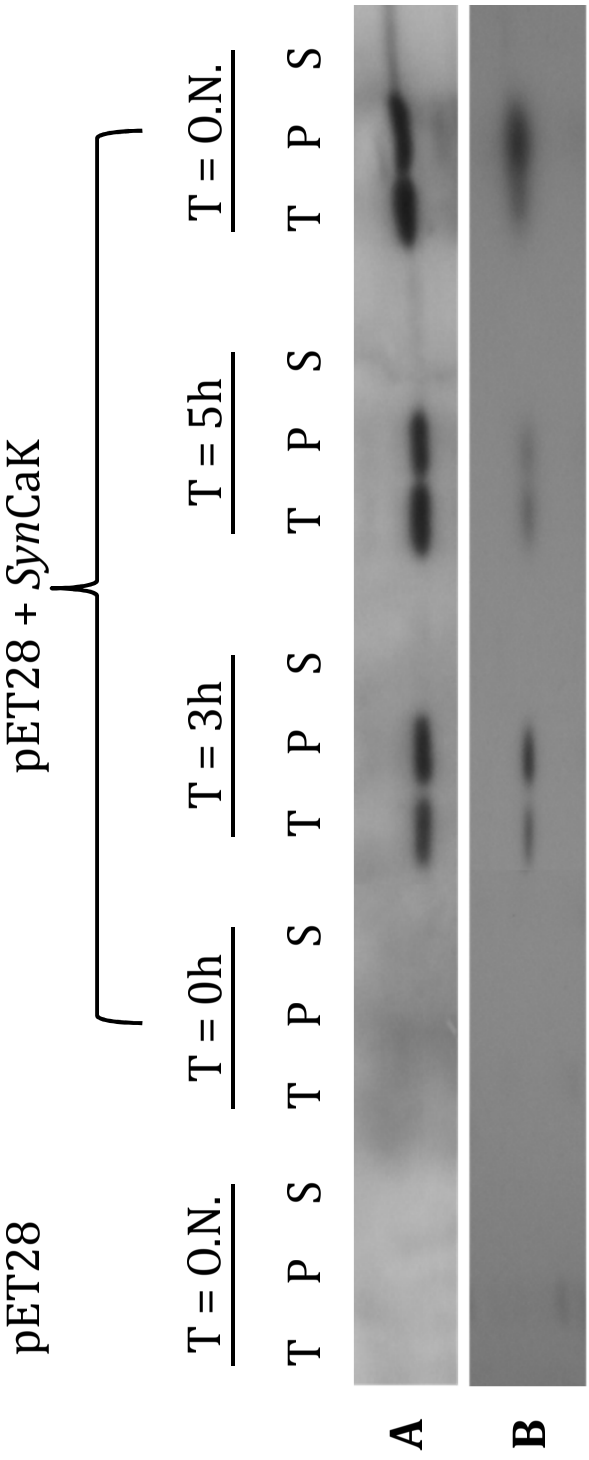

Figure S5

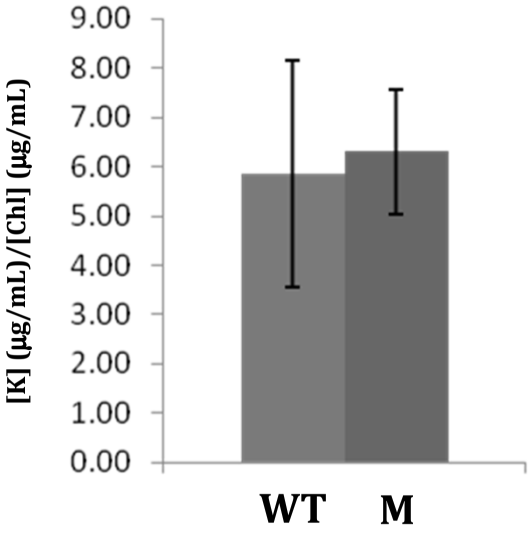

Figure S6

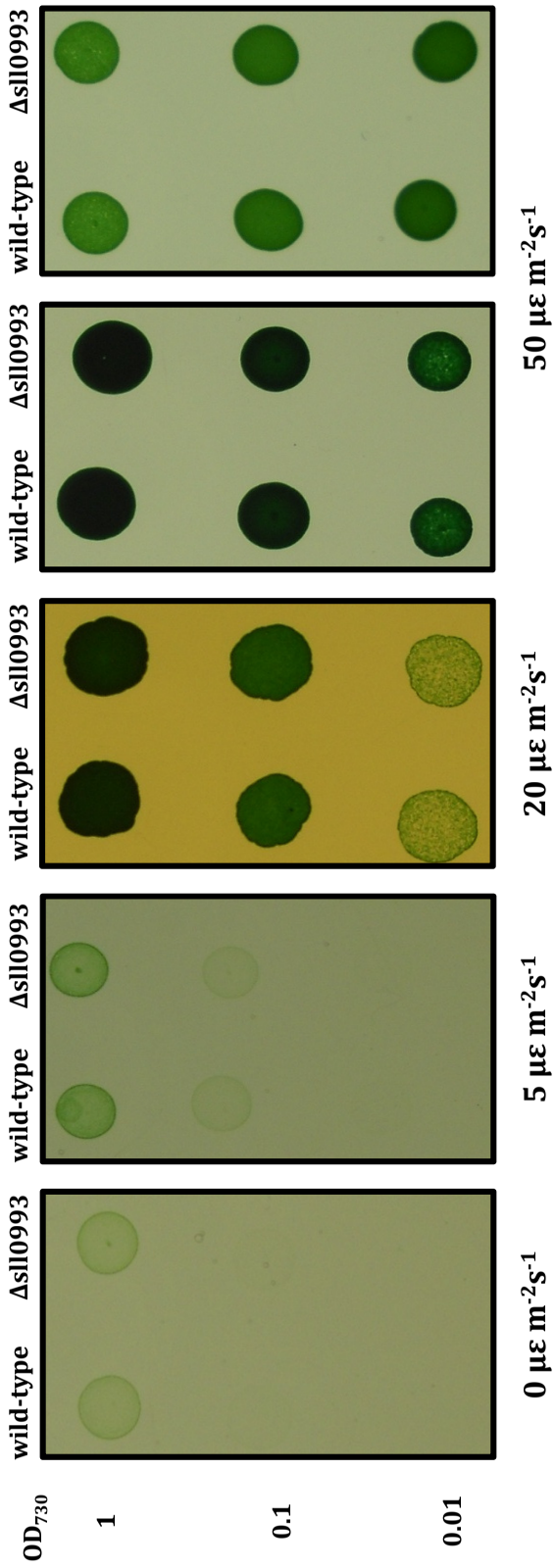
OD730
1
0.1
0.01
5 mM Glc
wild-type
Δsll0993
0 µε m-2s-1
5 µε m-2s-1
20 µε m-2s-1
50 µε m-2s-1
NO Glc

Figure S7

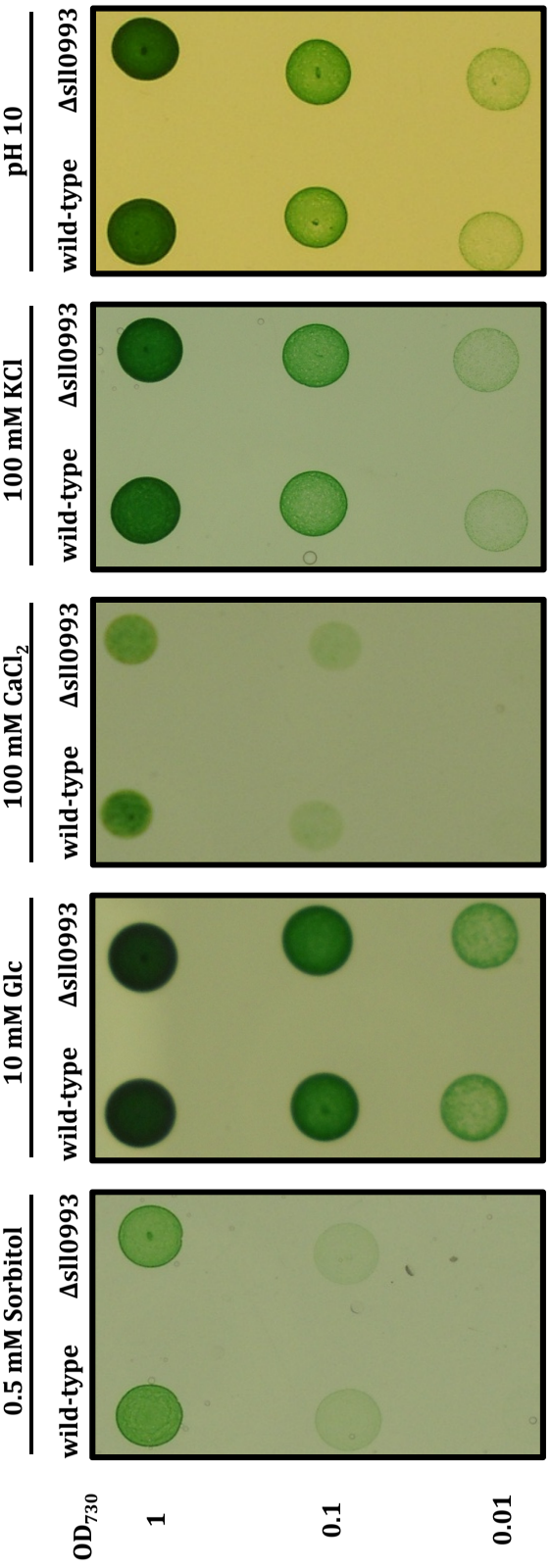
0.5 mM Sorbitol
10 mM Glc
100 mM CaCl2
100 mM KCl
pH 10
wild-type
Δsll0993
OD730
1
0.1
0.01

*At*MCU project

Localization and functional characterization of two homologues of the mammalian mitochondrial calcium uniporter in *Arabidopsis thaliana*.

Enrico Teardo*[1], Luca Carraretto*[1], Giorgio Mario Giacometti[1], Rosario Rizzuto[2], Ildikò Szabò[1]

[1]Department of Biology, University of Padua
[2]Department of Biomedical Sciences, University of Padua

*These authors share first authorship

Correspondence should be sent to:
I.S. e-mail: ildi@civ.bio.unipd.it

ABSTRACT

The mitochondrial calcium uniporter (MCU) has been identified from molecular point of view only very recently, in the mammalian system. A 40-kDa protein that works as Ca^{2+} channel was identified as MCU. Thus far, no information is available on Ca^{2+} uniporters in higher plants. Arabidopsis thaliana genome harbors 6 different genes, codifying for as many proteins, with significant sequence homology to the mammalian mcu gene. We started to investigate the properties of two AtMCU channels, with predicted mitochondrial or plastidial localization. First, to prove the subcellular localization, A. thaliana were transformed with vectors containing two different mcu genes in frame with EGFP. A clear mitochondrial or plastidial location was observed respectively using confocal microscopy. In vitro-expressed and solubilized proteins were also studied in planar lipid bilayer experiments, to examine their electrophysiological activity, showing a conductance of 85 pS in 150 mM Na gluconate and Gd^{3+} sensitivity, in accordance with data published for animal channels.

Work in progress

INTRODUCTION

Plants respond to environmental changes, to quickly adapt their metabolism to the new external conditions. The ability of a plant to react appropriately to a given stimulus is of vital importance. They react through different signal transduction pathways, but the most used for this purpose is the one involving Ca^{2+} as a second messenger. The main question is: how can a plant use a single second messenger, like Ca^{2+}, to discriminate on a big variety of external stimuli? The hypothesis has been proposed that this kind of signalling is based on a "Ca^{2+}-signature", meaning a different Ca^{2+}-elevation, intensity and duration profile to decode a specific information (McAinsh & Pittman, 2009; Dodd *et al*., 2010). For example, Ca^{2+} is subjected to circadian oscillations to specify cell timing processes (Love *et al*., 2004).
In the cytoplasm of the cell, the Ca^{2+} concentration is maintained at levels much lower than the extra-cytoplasmic compartments (about 10000-fold difference) in order not to interfere with the phosphate metabolism; for this reason, ions must be compartmentalized. The compartmentalization occurs at the level

of different organelles in plant cells and the maintenance of this difference in concentration leads to the generation of signals mediated by Ca^{2+}, in response to biotic and/or abiotic *stimuli* or stresses, thanks to the use of Ca^{2+} carriers or channels situated on cell membranes. In plant cells, as in those of animals, the compartments for the storage of Ca^{2+} ions are the endoplasmic reticulum and mitochondria; moreover, plant cell has the apoplast (the space between the cell walls) and the vacuole, the main retention compartment for Ca^{2+} in plants and has been shown to accumulate calcium in their chloroplasts as well.
In animal cells, the mitochondrial Ca^{2+} uptake and release has a fundamental role in the control of physiological processes; among these are the Ca^{2+} signaling in the entire cell. Furthermore, deregulation of mitochondrial Ca^{2+} fluxes starts the cascade of events that lead to cell death. Ca^{2+} homeostasis mechanisms have been already studied and recognized, but the identity of channels responsible for Ca^{2+} uptake and release was mysterious until recent time.
Recently, in two separate works (Baughman *et al*., 2011; De Stefani *et al*., 2011), the identification of a protein, called MCU was reported, that seems to be the Ca^{2+} uniporter of the inner mitochondrial membrane.
MCU is a 40-kDa protein, composed of two transmembrane domains, its down-regulation by siRNA reduces mitochondrial Ca^{2+} uptake in living HeLa cells and in isolated mitochondria, whereas its over-expression increased Ca^{2+} accumulation in mitochondria (De Stefani *et al*., 2011). MCU protein showed channel activity in planar lipid bilayers, with electrophysiological properties and inhibitor sensitivity of the uniporter (to ruthenium red and La^{3+}), previously identified as a calcium-selective ion channel in patch clamp experiments on mitoplasts (Kirichok *et al*., 2004). An MCU mutant, with two negatively charged residues in the putative pore-forming region replaced, had no channel activity.
In the *Arabidopsis thaliana* genome six genes are present which can be identified as putative MCU channels, since they are homologues of human MCU counterparts sharing the transmembrane domains, the pore-loop domain and the conserved DVME signature sequence. According to bioinformatics prediction, *Arabidopsis* MCU isoforms are localized at the level of mitochondria, except for *At*5g66650, which seems to have a double, mitochondrial and plastidial localization (Schwacke *et al*., 2003). The possibility that this isoform has plastidial localization is suggested by the observation that light-mediated Ca^{2+} influx into chloroplasts takes place, which can be strongly inhibited by ruthenium red (Kreimer *et al*., 1985), and displays kinetics and properties similar to those observed for mammalian MCU in bioenergetics experiments.

RESULTS AND DISCUSSION

Subcellular localization of two putative MCUs

The subcellular localization of two of the six MCU isoforms in *Arabidopsis thaliana*, called "mito-MCU" (*At*1g09575) for its purely mitochondrial prediction, and "CHL-MCU" (*At*5g66650), for its plastidial localization prediction was determined. These proteins show high sequence similarity to that of the two transmembrane segments and the pore region of mammalian MCU (Fig. 1). Furthermore, according to the Aramemnon database (aramemnon.botanik.uni-koeln.de), they both have two predicted transmembrane segments and clear mitochondrial targeting (for *At*1g09575) and possible dual targeting for *At*5g66650)(see Fig. S1 and S2). Leaves of 4-weeks-old *wt Col0* plants were transformed with *Agrobacterium*, carrying the pGREAT*::mcu::*EGFP construct by agroinfiltration and were observed after 2 days in confocal microscopy. As shown in Fig. 2A, the EGFP fluorescent

protein localized in small organelles close to the plasma membrane due to the presence of the large central vacuole, which were identified as mitochondria.
The evidence that these organelles were indeed mitochondria derives from a second transformation with the pBIN20*::mito-mCherry* CD3-991 construct (ABRC, http://www.arabidopsis.org/servlets/TairObject?type=stock&id=3001623330) by agroinfiltration (Fig. 1B), in which the mCherry red fluorescent protein presents, at the N-terminus, the sequence for mitochondrial translocation. Leaves transformed with this construct shown, in confocal microscopy, a signal that was of identical dimension and shape to that previously seen with the EGFP. In addition, the velocity of movement of organelles registered with the microscope in both experiments, was comparable.
A subsequent localization study, carried out by transforming *Arabidopsis* leaves with both constructs (Fig. 2C, D and E) showed perfect co-localization between mCherry and *At*MCU-EGFP, confirming the mitochondrial site for this isoform.
The same approach was applied for the plastidial-predicted isoform of MCU (*At*5g66650), that is the only MCU isoform that seems to have a potential double localization to both mitochondria and plastids.
As observable in Fig. 2F, G and H there is a perfect signal overlay between *At*MCU-EGFP and chlorophyll in chloroplasts, confirming the chloroplast targeting for the *At*5g66650 isoform. In contrast with the bioinformatics prediction, no EGFP signals in mitochondria were detected.

In vitro-expression of plastidial and mitochondrial *At*MCUs

Both CHL- and mito-*At*MCUs were succesfully expressed in an *in vitro* system, as described in the "Material and methods" section. The same procedure was already applied with success in the case of the mammalian MCU (De Stefani *et al*., 2011).
Reaction mixtures (indicated as RM) were treated with seven different detergents to test their capability to solubilize *At*MCU proteins. We wanted to verify which of these detergents solubilize better both *At*MCUs, to obtain a large amount of protein to be used then in planar lipid bilayer experiments.
In Fig. 3A Western blot and immunodetection with anti-His_6 TAG antibody of all the fractions collected from the solubilization process are shown. For both isoforms we observed a good solubilization with LysoPC, SDS and β-DM, whereas the other detergents used didn't provide a sufficient or complete solubilization of the proteins. LysoPC and SDS are unfortunately strong detergents and do not assure the native conformation of the protein. Furthermore, the use of these detergents is not compatible with the electrophysiological experiments, given their membrane-destabilizing effect.
Instead, β-DM gave an optimal result in solubilization and being this a weak-denaturing detergent, we can presume that the major part of the channel is in the correct and active tridimensional structure. For these reasons, β-DM was selected as the best detergent for our purposes.

Planar lipid bilayer experiments

When mammalian MCU currents were recorded in a sodium-gluconate low divalent solution (10 pM calculated $[Ca^{2+}]$, 100 mM Na gluconate), channel activity with a conductance of 55 pS (*vs* 6.2 pS as previously reported in De Stefani *et al*., 2011) could be observed at negative voltage ranges applied to the *cis* compartment, in accordance with the known characteristic of calcium channels to allow the passage of Na^+ upon removal of Ca^{2+} (e.g. Talavera and Nilius, 2006). Indeed, in both voltage-gated and CRAC calcium channels, selection against monovalents is due to binding of Ca^{2+} to sites within the ion conduction pathway with micromolar affinity (Hess and Tsien, 1984; Lepple-Wienhues and Cahalan, 1996). In

accordance with results on MCU studied in mitoplasts (Kirichok *et al*., 2004), the conductance of the channel was significantly higher in the low-divalent solution than in 100 mM calcium (De Stefani *et al*., 2011), and even a small increase of calcium concentration resulted in decrease of the unitary sodium current (Szabò I., personal communication, unpublished result). In light of these data with mammalian MCU; we decided to study activity of the plant MCUs in low divalent solution. Preliminary experiments show an activity recorded in two different experiments at -60 and -40 mV, respectively (shown in Fig. 4A and Fig. 4B) when the mitochondria-targeted isoform was incorporated into the asolectine membrane. The conductance was approximately 85 pS in both cases. Future experiments will be performed in order to prove that this protein allows the passage of calcium, however the ability of Gd^{3+} to block activity in both experiments (Fig. 4A-C) strongly suggests that the protein we are studying has characteristics compatible with those of the mammalian MCU activity. Our attempts to reveal channel activity by the CHL-MCU under the same conditions was unsuccessful by far.

CONCLUSIONS

In summary, in this work we present the first experimental evidence for the effective localization of two isoforms of putative MCU proteins within the plant cells and show experiments suggesting that also these proteins might indeed work as ion channels. Further study is necessary to confirm these data and to access the regulation of plant MCUs. In the animal system, MCU activity measured as calcium uptake into mitochondria has been shown be regulated by MICU1 (Mallilankaraman *et al*., 2012), an EF hand protein and the coiled-coiled protein cdc90a (Mallilankaraman *et al*., 2012). Interestingly, proteins showing homology with MICU1 can be identified in the Arabidopsis genome with predicted targeting to both chloroplasts and mitochondria. If this prediction was correct, it would further point to the chloroplast observed localization of one MCU isoform. While the role for MCU in mitochondrial calcium uptake has been extensively studied in the mammalian system (Rizzuto *et al*., 2012), no information is available on this point for plant cells. A recent methodological advance using mitochondria-targeted Cameleon fluorescence probe (Loro *et al*., 2012) should permit to measure calcium uptake in plants lacking *At*MCU isoforms. To this end, we have already obtained homozygous knock-out plants for both isoforms and started a collaboration with the group of Dr. Costa in Milan. Crossing of knockout plants with those expressing mitochondrial Cameleon is under way and hopefully would reveal an important physiological role for plant MCUs as well.
In light of the determination of the possible physiological roles of these proteins, it is worthwhile to look up databases concerning their expression in various tissues and phases of development. While little information is available on the mito-MCU, for CHL-MCU a clear tissue-dependent expression can be observed (at least at the *m*RNA level) according to Genvestigator site (https://www.genevestigator.com/gv) (Fig. S3).

MATERIALS AND METHODS

Agrobacterium tumefaciens strain and transformation of plants

For transformation of plants *A*. *tumefaciens* GV3101 strain, carrying the pSoup vector, was used. This strain was transformed with a pGreen-derived vector containing *mcu* (mitochondrial and plastidial-predicted) genes *in frame* with EGFP sequence, used for the infiltration of *A*. *thaliana* 4-weeks-old plants leaves.

A. tumefaciens was transformed using the freeze-thaw method as described in Jyothishwaran *et al*., (2007), and then plated in LB agar medium (10 g/L Tryptone, 5 g/L yeast extract, 10 g/L NaCl, 15 g/L Bacto-agar) with antibiotics.
Two days before infiltration, a single colony of transformed *A. tumefaciens* grown on agar plates was inoculated in 5 mL of YEP liquid medium (10 g/L Bacto-Tryptone, 10 g/L yeast extract, 5 g/L NaCl, pH 7.0) supplemented with specific antibiotics. Bacterial culture was incubated for 2 days at 30°C at 180 rpm on an orbital shaker.
After 48 hours, 2 mL of culture were transferred to Eppendorf tubes and pelleted by centrifugation at 3000 *g* for 5 min at room temperature. Bacterial pellet was resuspended in 1 mL of induction medium (10.5 g/L K_2HPO_4, 4.5 g/L KH_2PO_4, 1 g/L $(NH_4)_2SO_4$, 0.5 g/L Na citrate, 1 g/L glucose, 4 g/L glycerol, 1 mM $MgSO_4$, 10 mM MES, pH 5.6) and then transferred in 3 mL of induction medium supplemented with 100 μM acetosyringone (Sigma-Aldrich®) and grown for 6 hours at 30°C. Bacteria were pelleted at 3000 *g* for 5 minutes at room temperature, resuspended in infiltration medium (10 mM $MgSO_4$, 10 mM MES, pH 5.6) to a final OD_{600} of 0.400 and supplemented with 200 μM acetosyringone. This suspension was used for infiltration.

Confocal microscopy on leaves
Infiltrated leaves were observed after 2 days with the confocal microscope Leica TCS SP5 II (Leica Microsystems) mounted on a Leica DMI6000 CS inverted microscope with automated programmable scanning stage and motorized lens turret.
The images and videos were collected with the Leica Application Suite software (LAS AF, Leica Microsystems). For the excitation of EGFP and chlorophyll was used an Ar laser (wavelength: 488 nm); for fluorescence emission were used Leica pre-setted filters ("Leica EGFP", 500-520 nm; "Chlorophyll", 680-720 nm).

***In vitro*-expression of *At*MCU**
mcu genes for plastidial and mitochondrial-predicted proteins cloned in pIVEX 1.4 vector (5 Prime) were expressed in an *in vitro* system based on the continuous exchange cell-free (CECF) technique, using the RTS 100 Wheat Germ CECF Kit (Roche). Synthesis was conducted as described by Roche protocol for 24 hours at 24°C in continuous agitation (900 rpm) on a Thermomixer comfort unit (Eppendorf).
The resulting proteins in the reaction mixture were then solubilized with 7 different detergents (LysoPC, Triton X-100, SDS, decyl-β-D-maltopyranoside or β-DM, dodecyl-maltosyde or DM, OG and CHAPS) added at final concentration of 2%. Fractions of solubilized proteins selected for electrophysiological characterization were diluted 10 times in HEPES 10 mM, pH 7,4 and then used in planar lipid bilayer experiments.

SDS-PAGE and Western blot analysis
To test the solubilization process, we performed an SDS-PAGE protein separation followed by a *Western blot* and immunodetection with anti-His_6 TAG antibody (Sigma-Aldrich®). Reaction mixtures from *in vitro*-expression (indicated as "RM") and supernatants from solubilization treatment (named "S") were solubilized in SB buffer (300 mM TRIS/HCl pH 6.8, 11,5% w/v SDS, 50% w/v glycerol, 500 mM DTT, 0,1% w/v blue bromophenol) and loaded in a 10% acrylammide-6 M urea gel. After separation, proteins were transferred overnight on a PVDF membrane (BioTrace® PVDF Membrane, VWR).
Immunodetection of His_6-TPK3 was performed as reported: membrane was blocked in 10% milk solution in TBS buffer (10 mM TRIS pH 7.4, 150 mM NaCl), incubated for 2 hours with anti-His_6 TAG antibody diluted 1:1000 in TTBS buffer (10 mM TRIS pH 7.4, 150 mM NaCl, 0.05% v/v Tween 20), washed 6 times for 5 minutes each with TTBS buffer, incubated with

HRP-conjugated secondary antibody (diluted 1:10000 in TTBS buffer), washed 6 times for 5 minutes each with TTBS buffer and then exposed to HRP substrate (SuperSignal® West Pico, Thermo Scientific) for 5 minutes in agitation. Signal was detected with autoradiography films (Amersham Hyperfilm ECL™, GE Healthcare).

Bilayer experiments

Planar lipid bilayer experiments were carried out to determine electrophysiological activity of mitochondrial and plastidial-predicted *At*MCU from the *in vitro*-expression. An asolecitin solution in decane/chloroform with a 100:1 ratio *per* mg of lipids was used for artificial membrane construction. A membrane of 100 mV/pF was constructed between 2 compartments (*cis*/*trans*) and 3 mL of Na gluconate (150 mM Na gluconate, 10 mM HEPES, pH 7.4) were added in *cis* and *trans* compartments.
Defined volumes of 100 mM $GdCl_3$ were added alternatively in both compartments to test channel sensitivity.

FIGURE LEGENDS

Figure 1. Sequence alignment between mammalian and two plant MCU proteins.
TM1 and TM2 are shown in yellow, the region between the two transmembrane segments contains the pore loop. Alignment was obtained with ClustalW, * : identical amino acids; : conservative substitutions.

Figure 2. Localization of two isoforms of plant MCU by confocal microscopy.
*At*1g09575 and *At*4g66650 isoforms of MCU were expressed in fusion with EGFP in *Arabidopsis thaliana*. **A** and **B**: signals for EGFP and mCherry fluorescent proteins, respectively, in separated leaves transformation experiments shown an identical dimension and shape, suggesting a real mitochondrial localization for the *At*1g09575 isoform. In **C** and **D** are shown the signals of *At*MCU-EGFP (At1g09575) and *mito*-mCherry in a co-transformation experiments; in **E** there is the overlay of the previous images. Signals are perfectly overlapped, confirming the mitochondrial site for this isoform. The representative image shown was obtained in a cell where mobility of mitochondria was low for unknown reason.
In **F** is shown *At*MCU-EGFP (*At*4g66650) signal in a single-agroinfiltration experiment, in **G** is shown the chlorophyll in chloroplast, used as fluorochrome for co-localization. Signals overlaid in **H**, suggesting a plastidial localization of *At*4g66650 MCU isoform. No signals in mitochondria were detected for this double-located predicted MCU.

Figure 3. *In vitro*-expression and solubilization of putative MCU proteins.
Western blot and immunodetection with α-His_6 TAG antibody for *At*1g09575 and *At*4g66650 isoforms of MCU in *Arabidopsis thaliana*.
Please see text and "Materials and methods" section for detailed description.

Figure 4. Electrophysiological activity of *in vitro*-expressed mito-targeted plant MCU.
Representative current traces recorded at -60 **(A)** or -40 **(B)** mV are shown from two different experiments. **C)** shows amplitude histograms obtained from experiment shown in **A)** beofe and after addition of 100 microM Gadolinium to the cis side. Histograms were fitted using the Origin6.1 program set. Single channel current is approximately 5 pA at -60 mV, yielding a conductance value of 83 pS.

SUPPLEMENTARY FIGURE LEGENDS

Figure S1. Predicted membrane topology and organellar targeting of *At*1g09575. Source: Aramemnon database.

Figure S2. Predicted membrane topology and organellar targeting of *At*5g66650. Source: Aramemnon database.

Figure S3. Expression profile of *At*5g66650 transcripts.
Source: Genvestigator database.

REFERENCES

Baughman J.M., Perocchi F., Girgis H.S., Plovanich, M., Belcher-Timme C.A., Sancak Y., Bao X.R., Strittmatter L., Goldberger O., Bogorad R.L., Koteliansky V., Mootha VK. (2011) Integrative genomics identifies MCU as an essential component of the mitochondrial calcium uniporter. Nature 476, 341-345

De Stefani D., Raffaello A., Teardo E., Szabò I., Rizzuto R. (2011) A forty-kilodalton protein of the inner membrane is the mitochondrial calcium uniporter. *Nature 476, 336-340*

Dodd A.N., Kudla J., Sanders D. (2010) The language of calcium signaling. *Annu. Rev. Plant Biol. 61, 593-620*

Hess P., Tsien R.W. (1984) Mechanism of ion permeation through calcium channels. *Nature 309, 453-456*

Jyothishwaran G., Kotresha D., Selvaraj T., Srideshikan S.M., Rajvanshi P.K., Jayabaskaran C. (2007) A modified freeze–thaw method for efficient transformation of *Agrobacterium tumefaciens. Curr. Sci. 93, 770-772*

Kirichok Y., Krapivinsky G., Clapham, D.E. (2004) The mitochondrial calcium uniporter is a highly selective ion channel. *Nature 427, 360-364*

Kreimer G., Melkonian M., Holtum J.A.M., Latzko E. (1985) Characterization of calcium fluxes across the envelope of intact spinach chloroplasts. *Planta 166, 515-523*

Lepple-Wienhues A., Cahalan M.D. (1996) Conductance and permeation of monovalent cations through depletion-activated Ca^{2+} channels (ICRAC) in Jurkat T cells. *Biophys. J. 71, 787-794*

Loro G., Drago I., Pozzan T., Lo Schiavo F., Zottini M., Costa A. (2012) Targeting of Cameleons to various subcellular compartments reveals a strict cytoplasmic/mitochondrial Ca^{2+} handlingrelationship in plant cells. *Plant Journal 71(1), 1-13*

Love J., Dodd A.N., Webb A.A. (2004) Circadian and diurnal calcium oscillations encode photoperiodic information in *Arabidopsis*. *Plant Cell 16(4), 956-966*

Mallilankaraman K., Càrdenas C., Doonan P., Chandramoorthy H.C., Irrinki K.M., Golenàr T., Csordàs G., Madireddi P., Yang J., Müller M., Miller R., Kolesar J.E., Molgò J., Kaufman B., Hajnòczky G., Foskett J.K., Madesh M. (2012[1]) MCUR1 is an essential component of mitochondrial Ca^{2+} uptake that regulates cell metabolism. *Nat. Cell Biol. 14(12), 1336-1343*

Mallilankaraman K., Doonan P., Càrdenas C., Chandramoorthy H.C., Müller M., Miller R., Hoffman N.E., Gandhirajan R.K., Molgò J., Birnbaum M.J., Rothberg B.S., Mak D.D., Foskett J.K., Madesh M. (2012[2]) MICU1 is an essential gatekeeper for MCU-mediated mitochondrial Ca^{2+} uptake that regulates cell survival. *Cell 151, 630-644*

McAinsh M.R., Pittman J.K. (2009) Shaping the calcium signature. *New Phytol. 181(2), 275-294*

Rizzuto R., De Stefani D., Raffaello A., Mammucari C. (2012) Mitochondria as sensors and regulators of calcium signalling. *Nat. Rev.Mol. Cell Biol. 13(9), 566-578*

Schwacke R., Schneider A., Van der Graaff E., Fischer K., Catoni E., Desimone M., Frommer WB, Flugge UI, Kunze R. (2003) – ARAMEMNON, a novel database for *Arabidopsis* integral membrane proteins. *Plant Physiology vol. 131, 16-26*

Talavera K., Nilius, B. (2006) Biophysics and structure-function relationship of T-type Ca^{2+} channels. *Cell Calcium 40, 97-114*

*At*MCU project figures

Figure 1

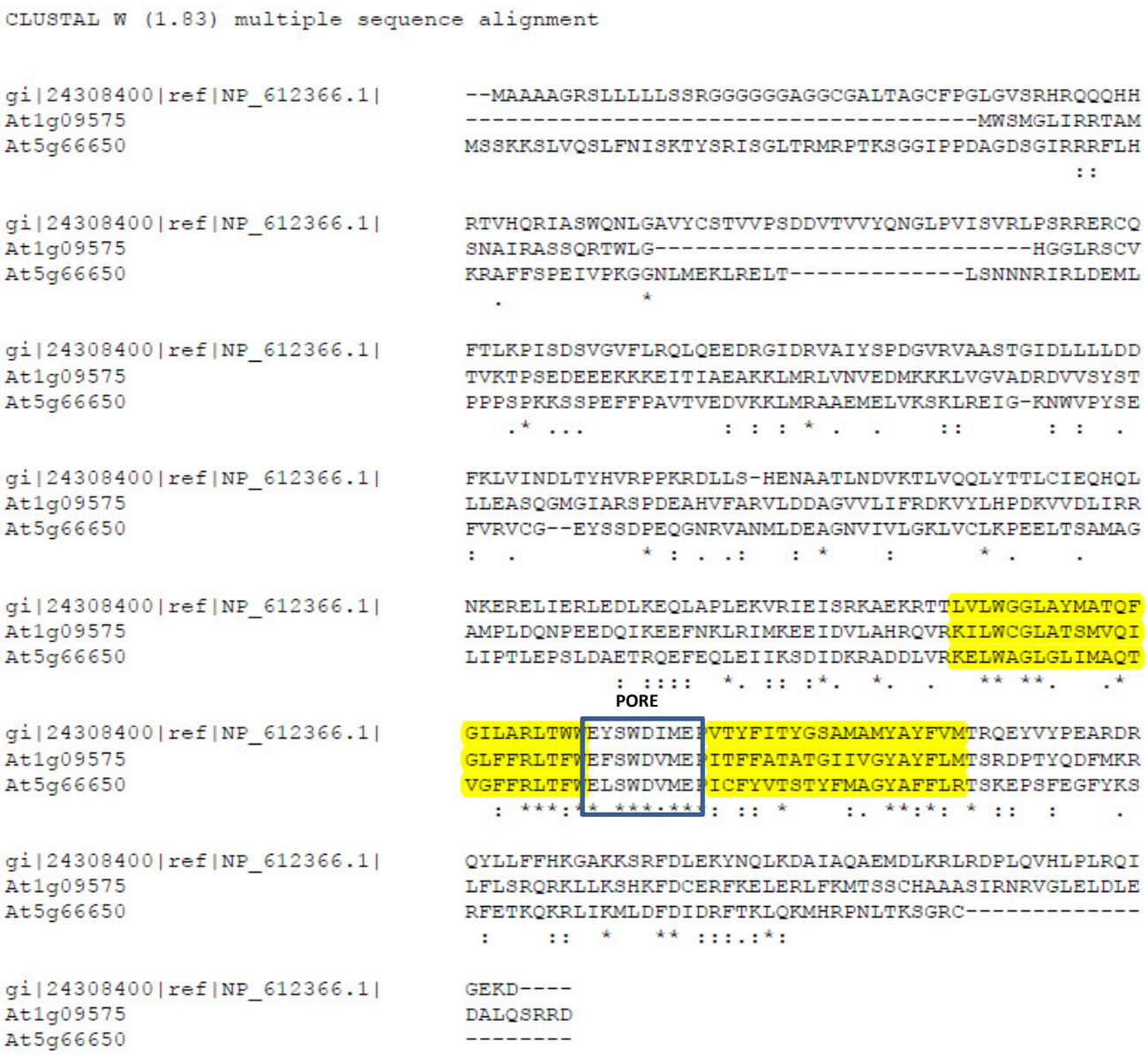
CLUSTAL W (1.83) multiple sequence alignment
gi|24308400|ref|NP_612366.1|
At1g09575
At5g66650
PORE

Figure 2

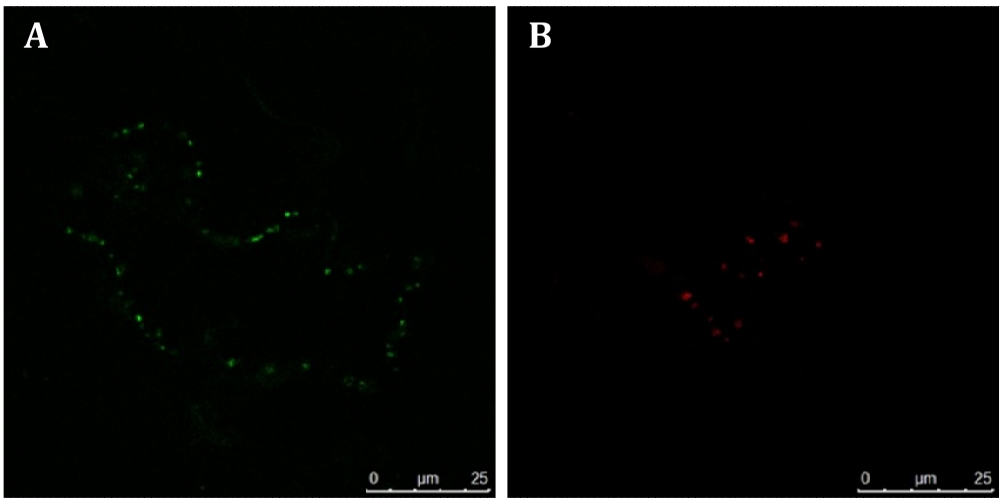

pGREAT*::mcu::*EGFP (*At1g09575*)

pBIN20*::mito-mCherry CD3-991*

Figure 2

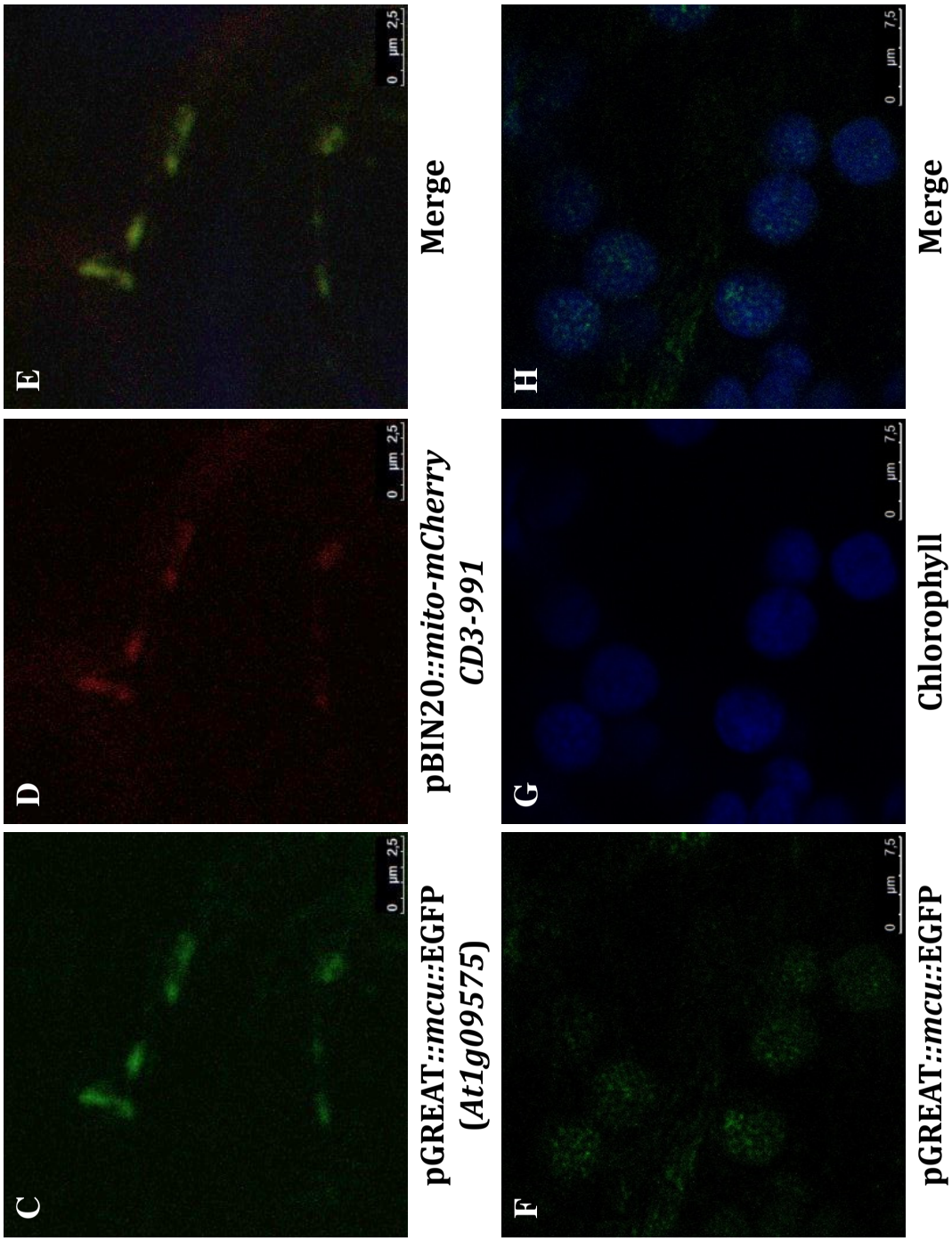
C
D
E
F
G
H
pGREAT::mcu::EGFP (At1g09575)
pBIN20::mito-mCherry CD3-991
Merge
pGREAT::mcu::EGFP (At4g66650)
Chlorophyll
Merge

Figure 3

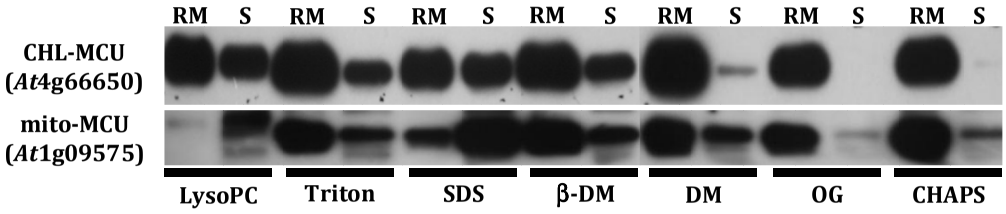
RM S RM S RM S RM S RM S RM S RM S
CHL-MCU
(At4g66650)
mito-MCU
(At1g09575)
LysoPC
Triton
SDS
β-DM
DM
OG
CHAPS

Figure 4

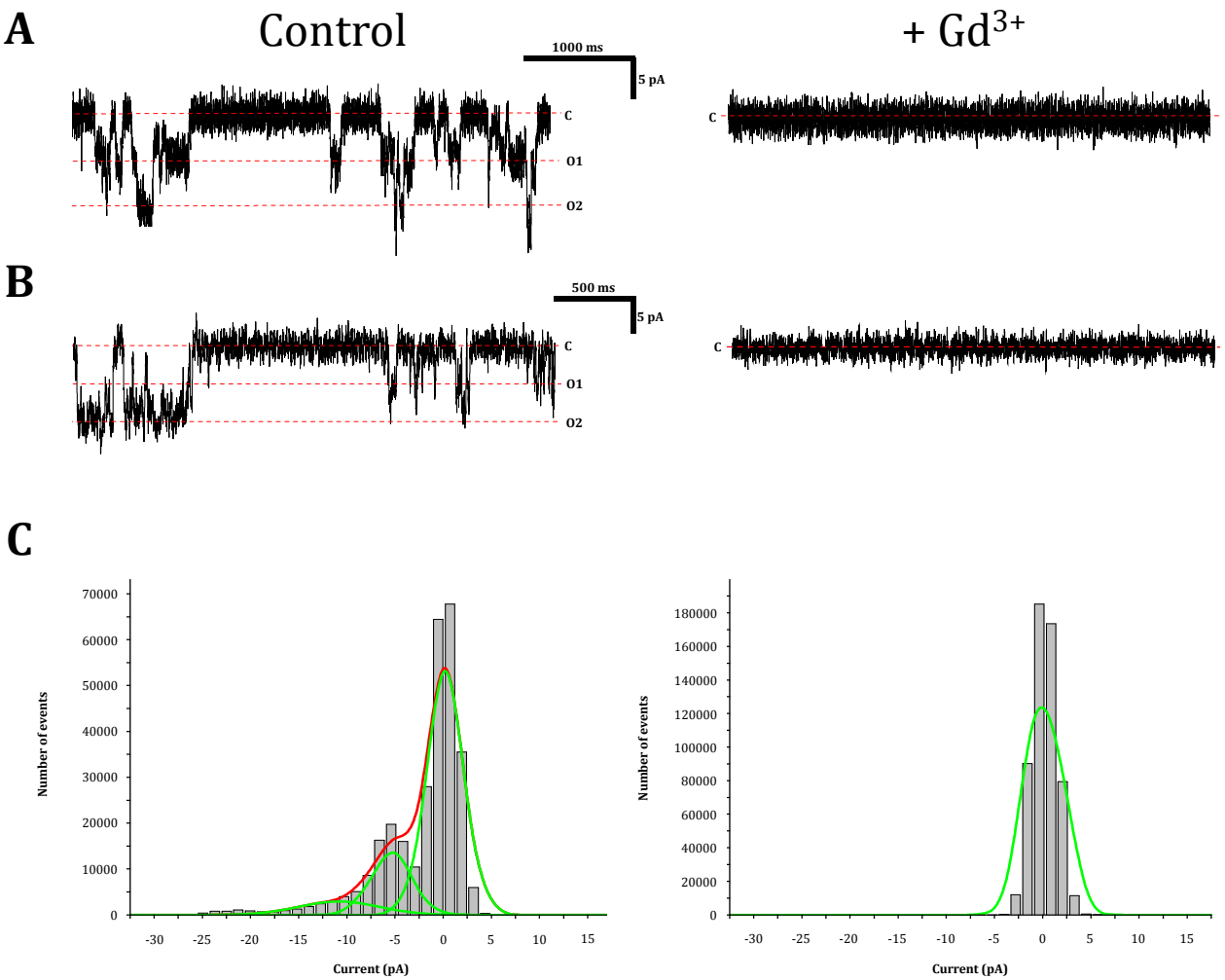
A
Control
+ Gd3+
1000 ms
5 pA
C
O1
O2
B
500 ms
5 pA
C
O1
O2
C
Number of events
Current (pA)
Number of events
Current (pA)

Supplementary figures

Figure S1

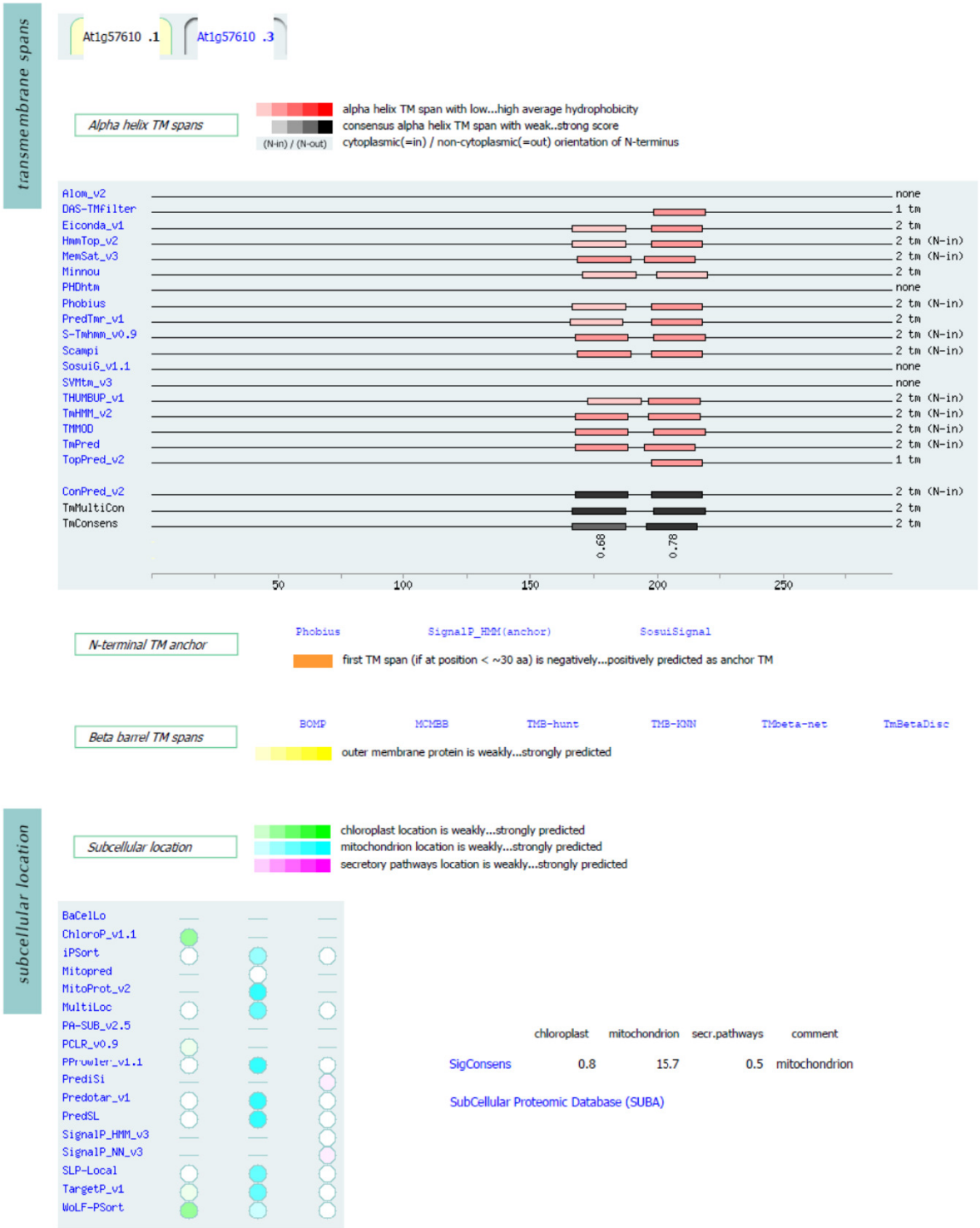
transmembrane spans
At1g57610 .1
At1g57610 .3
Alpha helix TM spans
alpha helix TM span with low...high average hydrophobicity
consensus alpha helix TM span with weak..strong score
(N-in) / (N-out)
cytoplasmic(=in) / non-cytoplasmic(=out) orientation of N-terminus
Alom_v2
DAS-TMfilter
Eiconda_v1
HmmTop_v2
MemSat_v3
Minnou
PHDhtm
Phobius
PredTmr_v1
S-Tmhmm_v0.9
Scampi
SosuiG_v1.1
SVMtm_v3
THUMBUP_v1
TmHMM_v2
TMMOD
TmPred
TopPred_v2
ConPred_v2
TmMultiCon
TmConsens
none
1 tm
2 tm
2 tm (N-in)
2 tm (N-in)
2 tm
none
2 tm (N-in)
2 tm
2 tm (N-in)
2 tm (N-in)
none
none
2 tm (N-in)
2 tm (N-in)
2 tm (N-in)
2 tm (N-in)
1 tm
2 tm (N-in)
2 tm
2 tm
0.68
0.78
50
100
150
200
250
N-terminal TM anchor
Phobius
SignalP_HMM(anchor)
SosuiSignal
first TM span (if at position < ~30 aa) is negatively...positively predicted as anchor TM
Beta barrel TM spans
BOMP
MCMBB
TMB-hunt
TMB-KNN
TMbeta-net
TmBetaDisc
outer membrane protein is weakly...strongly predicted
subcellular location
Subcellular location
chloroplast location is weakly...strongly predicted
mitochondrion location is weakly...strongly predicted
secretory pathways location is weakly...strongly predicted
BaCelLo
ChloroP_v1.1
iPSort
Mitopred
MitoProt_v2
MultiLoc
PA-SUB_v2.5
PCLR_v0.9
PProwler_v1.1
PrediSi
Predotar_v1
PredSL
SignalP_HMM_v3
SignalP_NN_v3
SLP-Local
TargetP_v1
WoLF-PSort
chloroplast
mitochondrion
secr.pathways
comment
SigConsens
0.8
15.7
0.5
mitochondrion
SubCellular Proteomic Database (SUBA)

Figure S2

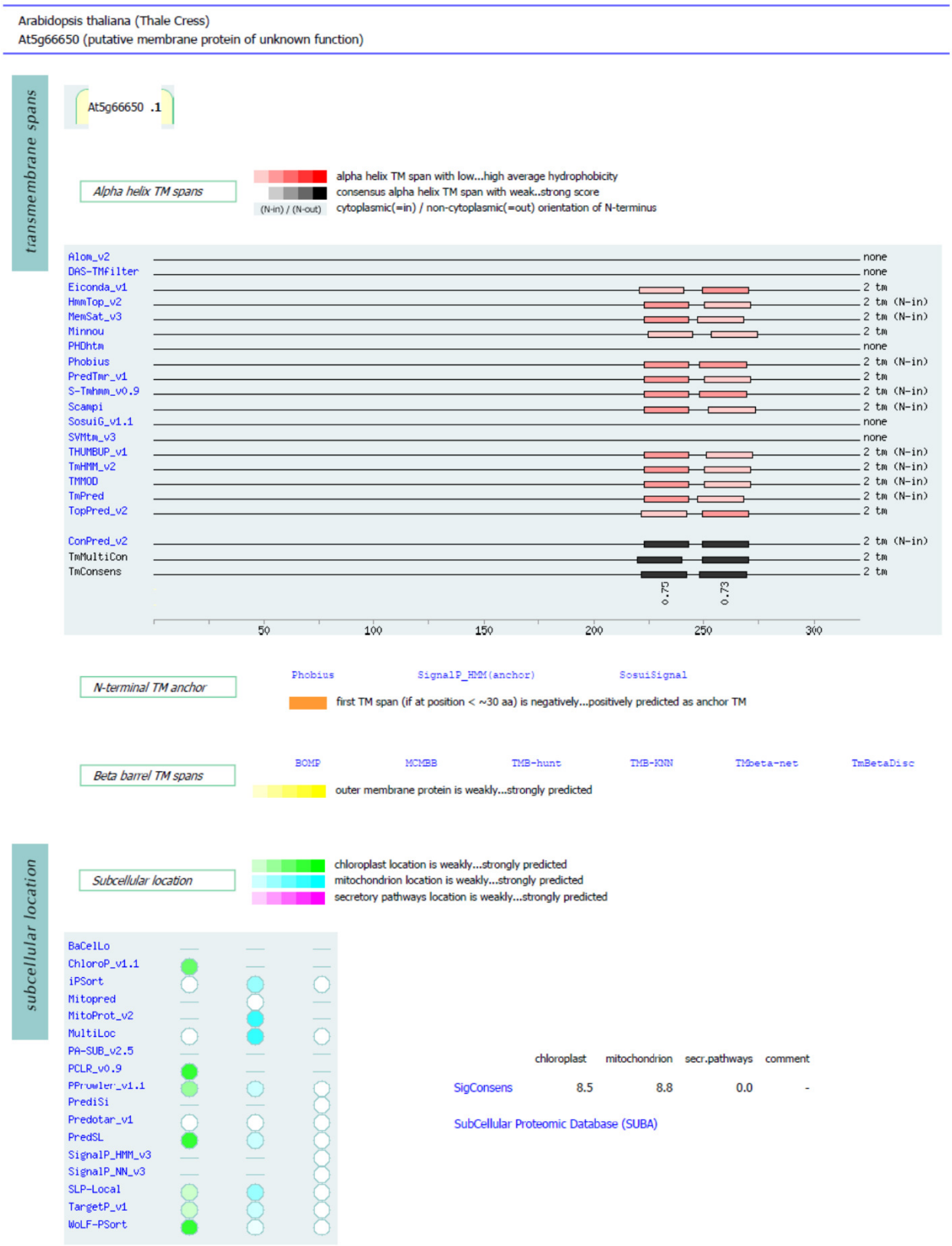
Arabidopsis thaliana (Thale Cress)
At5g66650 (putative membrane protein of unknown function)
transmembrane spans
At5g66650 .1
Alpha helix TM spans
alpha helix TM span with low...high average hydrophobicity
consensus alpha helix TM span with weak..strong score
(N-in) / (N-out)
cytoplasmic(=in) / non-cytoplasmic(=out) orientation of N-terminus
Alom_v2 none
DAS-TMFilter none
Eiconda_v1 2 tm
HmmTop_v2 2 tm (N-in)
MemSat_v3 2 tm (N-in)
Minnou 2 tm
PHDhtm none
Phobius 2 tm (N-in)
PredTmr_v1 2 tm
S-Tmhmm_v0.9 2 tm (N-in)
Scampi 2 tm (N-in)
SosuiG_v1.1 none
SVMtm_v3 none
THUMBUP_v1 2 tm (N-in)
TmHMM_v2 2 tm (N-in)
TMMOD 2 tm (N-in)
TmPred 2 tm (N-in)
TopPred_v2 2 tm
ConPred_v2 2 tm (N-in)
TmMultiCon 2 tm
TmConsens 2 tm
0.75
0.73
50
100
150
200
250
300
N-terminal TM anchor
Phobius
SignalP_HMM(anchor)
SosuiSignal
first TM span (if at position < ~30 aa) is negatively...positively predicted as anchor TM
Beta barrel TM spans
BOMP
MCMBB
TMB-hunt
TMB-KNN
TMbeta-net
TmBetaDisc
outer membrane protein is weakly...strongly predicted
subcellular location
Subcellular location
chloroplast location is weakly...strongly predicted
mitochondrion location is weakly...strongly predicted
secretory pathways location is weakly...strongly predicted
BaCelLo
ChloroP_v1.1
iPSort
Mitopred
MitoProt_v2
MultiLoc
PA-SUB_v2.5
PCLR_v0.9
PProwler_v1.1
PrediSi
Predotar_v1
PredSL
SignalP_HMM_v3
SignalP_NN_v3
SLP-Local
TargetP_v1
WoLF-PSort
chloroplast mitochondrion secr.pathways comment
SigConsens 8.5 8.8 0.0 -
SubCellular Proteomic Database (SUBA)

Figure S3

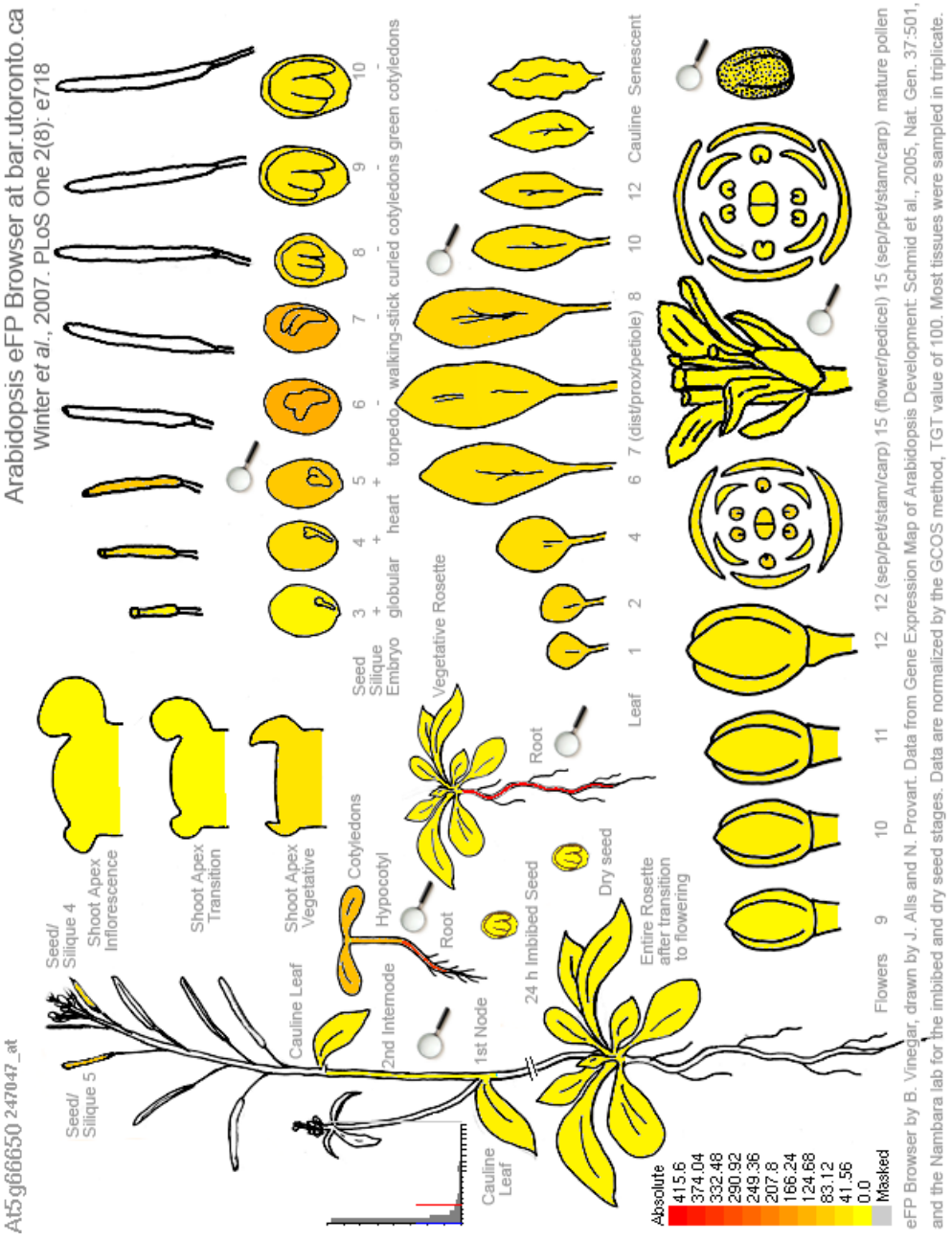
Arabidopsis eFP Browser at bar.utoronto.ca
Winter et al., 2007. PLoS One 2(8): e718
At5g66650 247047_at
Seed/ Silique 5
Seed/ Silique 4
Shoot Apex Inflorescence
Shoot Apex Transition
Shoot Apex Vegetative
Cauline Leaf
Cotyledons
Hypocotyl
2nd Internode
1st Node
Root
Cauline Leaf
24 h Imbibed Seed
Dry seed
Root
Vegetative Rosette
Entire Rosette after transition to flowering
Seed 3 4 5 6 7 8 9 10
Silique + + + - - - - -
Embryo globular heart torpedo walking-stick curled cotyledons green cotyledons
Leaf 1 2 4 6 7 (dist/prox/petiole) 8 10 12 Cauline Senescent
Flowers 9 10 11 12 12 (sep/pet/stam/carp) 15 (flower/pedicel) 15 (sep/pet/stam/carp) mature pollen
Absolute
415.6
374.04
332.48
290.92
249.36
207.8
166.24
124.68
83.12
41.56
0.0
Masked
eFP Browser by B. Vinegar, drawn by J. Alls and N. Provart. Data from Gene Expression Map of Arabidopsis Development: Schmid et al., 2005, Nat. Gen. 37:501, and the Nambara lab for the imbibed and dry seed stages. Data are normalized by the GCOS method, TGT value of 100. Most tissues were sampled in triplicate.

Figure S3

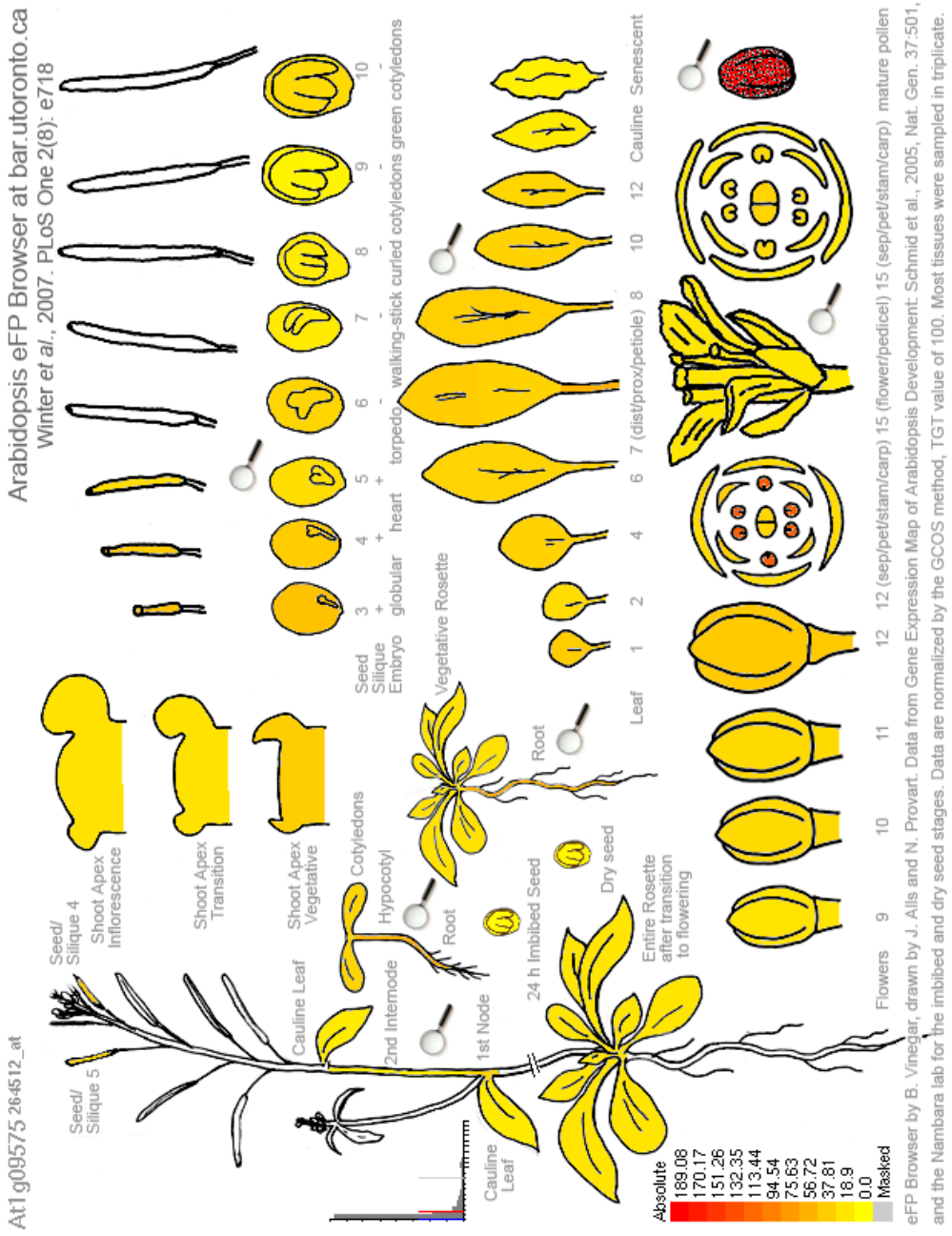
Arabidopsis eFP Browser at bar.utoronto.ca
Winter et al., 2007. PLoS One 2(8): e718
At1g09575 26-512_at
Seed/ Silique 5
Seed/ Silique 4
Shoot Apex Inflorescence
Shoot Apex Transition
Shoot Apex Vegetative
Cauline Leaf
Cotyledons
Hypocotyl
2nd Internode
1st Node
Root
Cauline Leaf
24 h Imbibed Seed
Dry seed
Root
Vegetative Rosette
Entire Rosette after transition to flowering
Seed 3 4 5 6 7 8 9 10
Silique + + + - - - - -
Embryo globular heart torpedo walking-stick curled cotyledons green cotyledons -
Leaf 1 2 4 6 7 (dist/prox/petiole) 8 10 12 Cauline Senescent
Flowers 9 10 11 12 12 (sep/pet/stam/carp) 15 (flower/pedicel) 15 (sep/pet/stam/carp) mature pollen
Absolute
189.08
170.17
151.26
132.35
113.44
94.54
75.63
56.72
37.81
18.9
0.0
Masked
eFP Browser by B. Vinegar, drawn by J. Alls and N. Provart. Data from Gene Expression Map of Arabidopsis Development: Schmid et al., 2005, Nat. Gen. 37:501, and the Nambara lab for the imbibed and dry seed stages. Data are normalized by the GCOS method, TGT value of 100. Most tissues were sampled in triplicate.

RINGRAZIAMENTI

E a conclusione di questa lunga tesi e di questo mio altrettanto lungo percorso di formazione, il quale mi ha permesso di arricchire le mie conoscenze e la mia professionalità in ambito biochimico e biofisico, giunge il momento di manifestare i miei più sentiti ringraziamenti, innanzitutto alla Prof.ssa Ildikò Szabò, per avermi offerto l'opportunità di svolgere il dottorato nel Suo laboratorio, nel "Gruppo Fotosintesi" del Prof. Giorgio Mario Giacometti, e per avermi costantemente seguito, consigliato e supportato in ogni singola fase dell'intero progetto.
Un ringraziamento non meno importante è rivolto al Dott. Enrico Teardo ed alla Dott.ssa Elide Formentin, i quali mi hanno materialmente introdotto ed addestrato a tutte le tecniche necessarie, affinché potessi portare a termine con successo il mio lavoro.
Ringrazio inoltre tutte le altre straordinarie persone del gruppo Giacometti, con cui ho stretto un ottimo rapporto di amicizia e di collaborazione e che in questo triennio mi hanno sempre sostenuto e, soprattutto, sopportato.